

# **IDENTIFYING URBAN DESIGNS AND TRAFFIC MANAGEMENT STRATEGIES FOR SOUTHERN CALIFORNIA THAT REDUCE AIR POLLUTION EXPOSURE**

Contract #12-308  
Final Report

February 27, 2017

Principal Investigator:  
Suzanne E. Paulson<sup>1</sup>

Co-Principal Investigators:  
J.R. DeShazo<sup>2</sup>, A.M. Winer<sup>3</sup> and A. Venkatram<sup>4</sup>

Researchers:  
Wonsik Choi<sup>1</sup>, Dilhara Ranasinghe<sup>1</sup>, Nico Schulte<sup>4</sup>, Lisa Wu<sup>2</sup>,  
Karen Bunavage<sup>1</sup>, Rodrigo Seguel<sup>1</sup>, Si Tan<sup>4</sup>

Collaborators:  
Jae-Jin Kim<sup>5</sup>

<sup>1</sup>University of California, Los Angeles, Department of Atmospheric and Oceanic Sciences, 405 Hilgard Ave., Los Angeles, California

<sup>2</sup>University of California, Los Angeles, Luskin Center for Innovation, Luskin School of Public Affairs, 3250 Public Affairs bldg., Los Angeles, California

<sup>3</sup>University of California, Los Angeles, Fielding School of Public Health, Environmental Health Sciences Department, 650 Charles Young Dr., Los Angeles, California

<sup>4</sup>University of California, Riverside, California, USA

<sup>5</sup>Pukyong National University, Department of Environmental Atmospheric Science, Busan, Korea

## i. Abstract

This study attempts to explain explicitly the direct and quantitative effects of complicated urban built-environment on near-road dispersion and levels of on-road air pollution at scales from a few meters away from the center of the street to several city blocks. This was studied using ultrafine particle concentrations ([UFP]) as a surrogate for on-road air pollution, as it is an excellent proxy for motor vehicle emissions at short time scales. We emphasize built-environments that arise around transit, transportation mode shifting, and transit oriented developments (TODs); types of development that are needed to move California communities toward improved public health combined with SB 375 goals of sustainability. Transit oriented developments are a type of community development that combines is a type of mixed-use community development that includes housing, office, retail and/or other amenities integrated into a walkable neighborhood, located within a half-mile of quality public transportation.

Seven measurement sites in the greater Los Angeles area with different built-environments but similar mesoscale meteorology were explored. At the sub-block scale, the data was used to explore the decay of air pollution away from intersections to find the optimal location of transit stops relative to the intersection, which lies about 40 m away from the center of the intersection. We also developed a detailed statistical micro-dynamics model that is able to closely reproduce second-by-second observations of UFP, and can disentangle the contributions of on-coming and on-going traffic, light and heavy-duty vehicles, traffic movements, building heights and other related features that impact pedestrian exposure. Next, we developed an approach to address several of the challenges associated with making high-resolution maps from mobile air pollution concentration measurements, including the question of how many repeats of a mobile monitoring route are needed to determine representative concentrations.

We find that the largest impact of the built environment is at the scale of several blocks. On the scale of a small neighborhood (several large city blocks), we find that after controlling for traffic, for most sampling days and sites, [UFP] were higher in the morning than those in the afternoon due to limited dispersion capacity combined with a relatively stable surface layer. In the calm mornings, the areal aspect ratio ( $Ar_{area}$ ) developed in this study for real urban configurations showed a strong relationship with block-scale UFPs.  $Ar_{area}$  includes the building area-weighted building height (or effective building height), the amount of open space, and the building footprint. In the afternoon, however, when wind speeds were generally higher and turbulence was stronger, the standard deviation of vertical velocity fluctuations,  $\sigma_w$ , was the most effective factor controlling [UFP]. The surrounding built environment appears to play an indirect role in observed [UFP] by affecting surface-level micrometeorology. The effects are substantial; controlling for traffic, differences in  $Ar_{area}$ , and building heterogeneity were related to differences in [UFP] by factors of two to three among the five study sites. These results have significant implications for pedestrian exposure to motor vehicle emissions as well as transit-oriented urban planning.

Moving to the scale of a single street, part of the study focused on street canyon-like urban built-environments. This work suggests that for this specific configuration, street-level concentrations of vehicle-related air pollutants can be estimated with a model that assumes that vertical turbulent transport of emissions dominates the governing processes. We developed a semi-empirical Vertical Dispersion Model (VDM), to describe the data collected in street canyons located in Hannover, Germany and Los Angeles. VDM indicates that magnification of concentrations relative to those in the absence of buildings is most sensitive to the aspect ratio of the street (the ratio of the effective building height to the street width). VDM estimates also indicate that the presence of the buildings in a street canyon configuration can potentially magnify street-level concentrations by as much as a factor of 3.5 relative to those in the absence of buildings. We translated the VDM equations into an

easy to use spreadsheet tool and python code that allows city planners to use VDM to conduct sensitivity analysis, generate concentration estimates, and develop mitigation strategies that aim to reduce the pedestrian exposure to air pollution within TODs. This tool is made available through the California Air Resources Board.

## ii. Executive Summary

This report investigates the impact of the built environment on concentrations of roadway pollutants, specifically ultrafine particles. The report emphasizes the configurations that arise around transit, mode shifting and transit-oriented development, and types of development that are needed to move California communities toward improved public health combined with SB 375 goals of sustainability. As higher density communities and transit-oriented developments are built, there is potential to create situations that expose more people to more roadway emissions. We seek to understand features of the built environment that may be adjusted to avoid or mitigate potential unintended consequences. Built environment effects are considered on several different scales: (1) sub-street scale within few meter of a road, (2) street scale looking at entirety of a single street, and (3) multi-block scale that spans over several blocks. The analyses were based on extensive field measurements made in several communities in the Los Angeles area during 2013, 2014 and 2015, most of it at high spatial and temporal resolution. In some cases, other datasets were used either from a 2008 study, also in Downtown Los Angeles and also supported by CARB, or from a longer term study in Hanover, Germany performed by other investigators. The communities in the Los Angeles area included four sites in Downtown Los Angeles, and sites in Temple City, Beverly Hills and Koreatown.

Exposure to elevated levels of roadway pollutants has been associated with a wide range of adverse health outcomes. Freshly emitted vehicular pollution is a complex mixture of gases and particles, of which ultrafine particles (UFP) is a major component. While the components of fresh vehicle emissions that cause adverse health effects is not well established, UFP are both an excellent proxy for roadway emissions and may potentially be a significant contributor to roadway-related toxicity. The analyses presented below begin at the sub-street scale and conclude at the multi-block scale. A summary for urban planners and policymakers is also provided.

### ii.1. Sub Street-Scale Results

#### ii.1.1. Siting Transit Stops: Decay of Pollutants around Intersections

We investigated the characteristics of cross-intersection concentration profiles of ultrafine particles (UFP) with 5 m spatial resolution. This was performed using 1,744 profiles covering 90 m before and after the center of each intersection. Cross-intersection UFP profiles were measured with a mobile monitoring platform at 10 signalized intersections at six urban sites with distinct built environments during both mornings and afternoons. Measurements were made within 1.5 m of the sidewalk at breathing height (1.5 m above ground level) to approximate sidewalk exposures. UFP profiles were strongly influenced by high emission events from accelerating vehicles and showed elevated concentration peaks within 30 m of intersection centers followed by sharp decreases in concentrations with distance. The elevation of UFP near the intersection was accompanied by more frequent and larger transient concentration spikes. Thus, people that stay longer at the intersection have an increased chance of being exposed to these short-term extremely high concentrations. The concentrations decay to somewhat lower levels before the intersection (the ‘near’ side), than after the intersection (the ‘far’ side). However, as siting transit stops after intersections is preferred for smooth traffic flow, we focus on the ‘far’ side. Simple time-duration exposure calculations suggest moving a bus stop from 20 to 40 m to after the intersection reduces transit-users’ exposure levels to the total UFP inversely proportional to the elevation magnitude near the intersection, by an amount that varies widely, from hardly reducing exposure to cutting it by more than half.

### ii.1.2. Development of a Statistical Model to Explain Micro-dynamics of Pollutant Concentrations on Roadways

We developed a novel micro-modeling approach to quantify the impacts of the factors controlling concentrations of roadway pollutants at the time-scale of seconds and spatial scale of meters. The statistical model characterizes how UFP concentrations vary around a Mobile Measurement Platform (MMP) as it travels along an urban transect in downtown Los Angeles. The data we use to estimate our statistical model comes from 11 MMP sampling transects on Broadway Street in and near downtown Los Angeles in 2008. Our model includes factors such as the state of motion, speed and land position of the MMP, the number of on-going and on-coming light duty (light-duty vehicles and motor-cycles), heavy duty (trucks), and buses encountered by the MMP along the transect. We also characterize the built environment adjacent to the MMP, including adjacent building heights and the presence of intersections. When the MMP was stopped at intersections, we measured the queuing time and queue position as well as the number and type of vehicles crossing in front of the MMP on the perpendicular street. We further characterized the acceleration events for the platoons of vehicles traveling in the on-going and on-coming directions as well as those crossing the intersection from the left or right. Finally, our model includes wind direction and speed as well as the time of day when the transects occurred.

The model is designed to expressly provide valid attribution of UFP concentrations to specific factors in the presence of many other potentially confounding factors. For example, we are able to characterize the effect on UFP concentration of the number and type of passing vehicles in both an on-going or on-coming direction, while controlling other factors. This high-resolution modeling framework is especially helpful at intersections to decompose the respective multi-directional traffic events (stopping, queuing, and accelerations) on UFP concentrations. We also show how our model can be used to characterize free-flow traffic patterns versus the stop-and-go dynamics along a transect.

For each of the factors discussed above, we estimate the average effect (direction and size) of the traffic event on the UFP concentrations, decomposing these average effects into their temporal profile, which may include important sign and magnitude changes, resulting from opposing effects such as vehicle-induced turbulence and emissions, both of which often increase with increasing vehicle size. The model reproduces the data very well. The most important factors are the type of vehicle and its activity (on-coming, on-going accelerating, crossing etc.).

### ii.1.3. Mapping Pollutant Concentrations in Urban Areas

Mobile air pollution monitoring offers an opportunity to “map” pollutants with much higher spatial resolution than sparse stationary monitors, but the data they produce presents some unique challenges. They also raise the important question of how many repeats along a given route are needed to determine representative concentrations along the route. We develop a framework to address the challenges and constraints to developing higher spatial resolution maps from mobile data. The challenges include the non-uniform spatial resolution and distribution of the measurements; that measurements are made at slightly different locations in each pass of the mobile monitoring platform along a specific route (each “run”); in some cases, the poor precision of global positioning system coordinate data; potential for over/underweighting data; and varying urban background concentrations. We find that use of a reference grid and piecewise cubic Hermite spline interpolation between measurements to give equal weight to each sampling “run” at each grid reference point addresses many of the challenges effectively. A background correction was implemented to facilitate averaging over several sessions. For 1 s time resolution data collected at normal city driving speeds, we show that concentration maps of 5 m spatial resolution can be obtained by including up to 21% interpolated values. Finally, we use UFP concentrations to consider the minimum number of sampling runs needed to make a representative concentration map

with a specific spatial resolution, finding that generally between 15 to 21 repeats of a particular route under similar traffic and meteorological conditions is sufficient.

## ii.2. The Multi-Block Scale

The built environment at the multi-block scale has a markedly larger influence than it does at the street scale. In our multi-block scale study, we attempt to explain explicitly the direct and quantitative effects of complicated urban built-environment on near-road dispersion and levels of vehicular emissions at the scale of several city blocks (here, the “multi-block scale”, again based primarily on ultrafine particle concentrations. For this study, we used five measurement sites in the greater Los Angeles area, with different built environments but similar mesoscale meteorology. The built environments varied from one with all 1-story buildings, one with a clearly defined street canyon, and three sites with very heterogeneous morphology characterized by a mix of one or two very tall buildings and low developments (parking lots or parks). After controlling for traffic throughout the study area, for most sampling days and sites, morning UFPs were higher than those in the afternoon due to limited dispersion capacity combined with a relatively stable surface layer in the morning. In the calm mornings,  $Ar_{area}$  developed in this study for real urban configurations showed a strong relationship with multi-block-scale average UFP concentrations.  $Ar_{area}$  includes the building-area-weighted building height, the low development, and the building footprint. In the afternoon, however, when wind speeds were generally higher and turbulence was stronger, vertical turbulence intensity  $\sigma_w$  was the most effective factor controlling the concentrations of vehicular pollution. The surrounding built environment appears to play an indirect role in observed UFP concentrations by affecting surface-level micrometeorology. The effects are substantial; controlling for traffic, differences in  $Ar_{area}$ , and building heterogeneity were related to differences in UFP concentrations of factors of two to three among our five study sites.

## ii.3. Street Canyon Dispersion Modeling

We developed a semi-empirical dispersion, referred to as the Vertical Dispersion Model (VDM), to describe data collected in street canyons located in Hannover, Germany and Los Angeles, USA. The data collected in Hannover indicated that street-level concentrations of vehicle-related pollutants are governed by vertical turbulent transport of emissions. The analysis of measurements made in field studies conducted in Los Angeles showed that the effects of urban buildings on pollutant dispersion can be parameterized in terms of the effective aspect ratio of the street, which is the ratio of the frontal area weighted height of buildings facing the street to the width of the street. The dispersion model, VDM, relates roof-level concentrations to street-level concentrations using traffic flow rate, the effective aspect ratio of the street, and roof level turbulence as inputs. This formulation allows VDM to use outputs from commonly used models such as AERMOD to estimate street-level concentrations in urban areas. Thus, this model can be used by urban planners to examine the impact of alternate TOD designs on street level concentrations associated with near surface emissions. We illustrate the application of VDM by estimating street-level concentrations of ultra-fine particles at the locations in Los Angeles where we conducted field studies. VDM estimates indicate that the presence of the buildings can potentially magnify street-level concentrations by as much as a factor of 3.5 relative to those in the absence of buildings.

We translated the VDM equations into a spreadsheet tool and python code that allows city planners to use VDM to conduct sensitivity analysis and generate concentration estimates. The spreadsheet tool is useful for development of mitigation strategies that aim to reduce the effective street aspect ratio or reduce emissions within the TOD through traffic management. The tool is made available through the California Air Resources Board.

## ii.4. Summary for Planners

Results from this study that are relevant to urban planning around transit and transit oriented development are summarized in a table below. These measures are not exclusive and should be considered in concert with other measures supported by related research and established guidelines, such as those requiring siting of sensitive population at least 500 feet from freeways, and statewide goals to reduce greenhouse gas emissions from transportation by reducing vehicle miles travelled and supporting development that will make it possible to replace car trips with bike, walking, and transit trips.

We emphasize that purpose of the table below is to assess the effects of specific features of the built-environment and what parameters should be considered when designing a TOD. This information should be considered in conjunction with other strategies not discussed here in planning decisions, including considerations of the vehicle emissions reduction, effective strategies to reduce vehicle miles traveled, and other factors.

In summary, this study suggests several strategies in developing a TOD to reduce exposure to pedestrians:

- Avoid development of high rises in close proximity
- Reduce building density (areal aspect ratio) by including open spaces, such as parks and parking lots, among the building environment
- Separate pedestrian walkway from streets and intersections expected to have substantial on-road traffic
- Develop transit systems to reduce on-road traffic during early mornings and late evenings
- Siting bus stops away from major on-road sources and intersections

Additionally, this study suggests several mitigation methods in existing TOD to reduce exposure to pollutants in urban areas:

- Develop a mitigation strategy to reduce vehicle traffic on streets with large aspect ratios
- Develop a mitigation strategy to divert pedestrians away from streets and intersections with heavy traffic
- Develop a mitigation strategy to divert pedestrians away from streets with large aspect ratios

Detailed information that provides evidences to these concluding statements can be found in the following report.

**Table for ii.4. General recommendations to reduce pedestrian and residential air pollution exposure in built environment.**

<b>Management</b>	<b>Suggested Direction</b>	<b>Approx. Size of Effect</b>	<b>Atmospheric Conditions &amp; Notes</b>
Areal aspect ratio ( $Ar_{area}$ ), which combines building area-weighted height, building footprint, and the amount of open space	Lower building volumes and more open space result in lower pollutant concentrations.	The difference between very dense and low density built environments is approximately a factor of three.	Important under calm conditions (in the mornings at our sites).
Building Heterogeneity	Isolated tall (high-rise) buildings result in lower concentrations than homogeneous shorter or many taller buildings with similar volume.	Highly heterogeneous built environments can decrease concentrations by up to approximately a factor of two relative to completely homogeneous built environments.	Important under unstable conditions with moderate winds (afternoons at our sites). Not critical when the atmosphere is stable.
Street Canyons (relatively contiguous walls of buildings)	Heterogeneous building forms avoid hotspots created by street canyons.	Tall street canyons (~50 m) can increase local traffic air pollution concentrations by up to about 50% relative to open space.	
Bus Stop Siting	Siting bus stops further from intersection will reduce exposures.	From no effect to more than a factor of two reduction from moving the site from 20 to 40 meters from the intersection on the “far” side.	Pollutant concentrations usually peak near the center of the intersection, although there is a high degree of variability.

### iii. Publication from this study

#### Published

---

- Choi, W., D. Ranasinghe, K. Bunavage, J.R. DeShazo, L. Wu, R. Seguel, A.M. Winer, and S.E. Paulson (2016) The effects of the built environment, traffic patterns, and micrometeorology on street level ultrafine particle concentrations at a block scale: Results from multiple urban sites. *Sci. Tot. Environ.* **15**;553: 474-85. doi: 10.1016/j.scitotenv.2016.02.083.
- Schulte, N., S. Tan, and A. Venkatram (2015) The ratio of effective building height to street width governs dispersion of local vehicle emissions. *Atmos. Environ.* 112: 54–63.
- Ranasinghe, D., W.S. Choi, A.M. Winer and S.E. Paulson (2016) Developing High Spatial Resolution Concentration Maps Using Mobile Air Quality Measurements. *Aerosol and Air Qual. Res.* **16** (8), 1841-1853.

#### In Preparation

---

- Choi et al. (2017) Cross-Intersection Profiles of ultrafine particles in various environments: Implications for Pedestrian Exposure and Transit Stop Siting.
- DeShazo, et al. (2017) Modeling the Micro-dynamics of Ultrafine Particle Concentrations Caused by Traffic Events at Street Intersections.

## Table of Contents

i. Abstract.....	2
ii. Executive Summary.....	4
ii.1. Sub Street-Scale Results .....	4
ii.1.1. Siting Transit Stops: Decay of Pollutants around Intersections .....	4
ii.1.2. Development of a Statistical Model to Explain Micro-dynamics of Pollutant Concentrations on Roadways .....	5
ii.1.3. Mapping Pollutant Concentrations in Urban Areas.....	5
ii.2. The Multi-Block Scale .....	6
ii.3. Street Canyon Dispersion Modeling .....	6
ii.4. Summary for Planners.....	7
iii. Publication from this study.....	9
Table of Contents.....	10
List of Tables .....	13
List of Figures .....	14
List of Abbreviations .....	18
iv. Introduction.....	19
v. Field Measurements and Statistical Modeling.....	22
v.1. Introduction.....	22
v.2. Background and Related Work.....	23
v.2.1. Current research needs for TOD planners .....	23
v.2.2. Overview: mobile platform studies .....	24
v.2.3. Overview: Studies investigating air pollution gradients near freeways .....	25
v.2.4. Previous results from the Air Resources Board Mobile Platform in Southern California.....	25
v.2.5. Overview: Longitudinal studies .....	26
v.3. Methods.....	27
v.3.1. Sampling sites and built-environmental characteristics .....	27
v.3.2. Instrumentation and Sampling Design .....	32
v.3.3. Collecting meteorological data using MMP.....	35
v.3.4. Site, built environment, and traffic characteristics .....	35
v.4. Results and Discussion.....	38
v.4.1. The effects of the traffic patterns, micro-meteorology, and built environment on street level UFP concentrations at a block scale .....	38

v.4.1.1. Characteristics of traffic patterns, micro-meteorology, and built environments .....	38
v.4.1.2. General Features of UFP concentrations .....	42
v.4.1.3. Elevated emissions at the intersections .....	44
v.4.1.4. Factors controlling near-roadway UFP concentrations.....	46
v.4.1.4.1. Calm morning conditions .....	46
v.4.1.4.2. Unstable afternoon conditions.....	48
v.4.2. Developing high spatial resolution concentration maps using mobile air quality measurements .....	50
v.4.2.1. High spatial resolution concentration maps .....	50
v.4.2.2. High Estimation of the minimum number of runs needed for representative concentration values.....	52
v.4.3. Statistical modeling of the micro-dynamics of UFP concentrations caused by traffic at street intersections.....	55
v.4.3.1. Statistical model development .....	55
v.4.3.1.1. Statistical model specification.....	56
v.4.3.2. Out of sample model prediction: assessing accuracy.....	62
v.4.3.3. Model development and general results.....	63
v.4.3.4. Temporal profiles of traffic events.....	66
v.4.3.5. Simulating changes in traffic composition.....	68
v.4.4. Cross-intersection profiles of UFP in various environments: implications for pedestrian exposure and transit stop siting.....	71
v.4.4.1. Data analysis and cross-intersection concentration profiles .....	71
v.4.4.2. Highly resolved UFP profiles around intersections .....	72
v.4.4.3. Implications to pedestrian exposure and transit-oriented development.....	79
vi. Dispersion Modeling .....	81
vi.1. Introduction.....	81
vi.2. Background and related work .....	82
vi.3. Methods.....	83
vi.3.1. Operational street pollution model (OSPM).....	83
vi.4. Results and Discussion.....	85
vi.4.1. Operational Analysis of long term measurements of near road concentrations of vehicle emissions to determine the primary variables governing dispersion in urban streets .....	85
vi.4.2. Development of a model to understand the impact of buildings on near-road concentrations using field measurements in Los Angeles .....	89
vi.4.2.1. Design of field measurements in Los Angeles.....	89
vi.4.2.2. Instrumentation .....	90
vi.4.2.3. Vertical dispersion model .....	91

vi.4.2.4. Evaluation of VDM with the local contribution .....	95
vi.4.2.5. Micro-meteorology .....	98
vi.4.2.6. Using VDM to Assess Exposure to Traffic Emissions in TODs .....	100
vi.4.2.7. Implications to pedestrian exposure and transit-oriented development.....	103
vii. Conclusions.....	104
vii.1.General Recommendations for TOD Design.....	105
vii.1.1. Built Environment Considerations .....	105
vii.1.1.1. Single street scale.....	105
vii.1.1.2. Multi-block scale.....	106
vii.1.2. Street design and land use considerations .....	106
vii.1.3. Other features of the built environment and other topics for future research .....	107
viii. Acknowledgement and References.....	108
viii.1. Acknowledgements .....	108
viii.2. References .....	108
viii.2.1. References for Section II.....	108
viii.2.2. References for Section III .....	113
ix. Appendix: Supporting information for Section vi.4.....	116

## List of Tables

Table 1. Description of field measurements including built-environments, measurement dates, instrumentation, and sampling design.....	27
Table 2. Built environments (Sites1-5) in the mobile sampling areas.....	28
Table 3. Characteristic traffic patterns observed for each site during the measurement periods. Values in parentheses are standard deviations.....	29
Table 4. Monitoring instruments on the mobile monitoring platform.....	33
Table 5. Measurement periods and surface meteorology at BW-7th.....	35
Table 6. Variable Definitions.....	36
Table 7. Summary Statistics of Variables.....	37
Table 8. Surface micro-meteorological conditions observed during sampling periods. Values in parentheses represent standard deviations of the respective parameters.....	39
Table 9. Average surface meteorology at Broadway and 7 <sup>th</sup> (Site1). Here, $u_*$ is the friction velocity, $\sigma_w$ is the variance of vertical wind velocity and TKE is the turbulent kinetic energy*.....	52
Table 10. Model estimated UFP concentrations.....	57
Table 11. Cumulative Impacts of Traffic Events.....	63
Table 12. Sampling dates and information of the intersections investigated in this study.....	72
Table 13. Basic statistics of the intersection UFP profiles of each direction for each site.....	74
Table 14. Basic statistics of intersection [UFP] profiles for each site. The values in parentheses are averages from all profiles of each traffic direction for each site.....	75
Table 15. Overview of measurement locations.....	90
Table 16. Summary of area weighted building height, street width, and aspect ratio of all sites.....	94
Table 17. General recommendations to reduce pedestrian and residential air pollution exposure in built environment.....	107

## List of Figures

- Figure 1. Map of measurements sites in the South Coast Air Basin. Red stars denote the sampling sites that cover 2-by-2 (or 2-by-3) blocks centered by the main intersection where traffic recording and stationary measurements were conducted in 2013. ....27
- Figure 2. (a) Map of building heights and morphology in DTLA. Color bar represents the building heights in feet. (b) The street view on Broadway St. captured in Google Earth. The building distributions and street views for the other sites are presented in the Supplementary Information. ....30
- Figure 3. Built environments of sampling sites: (a) *Site 2* (Olive & 12<sup>th</sup> St.), (b) *Site 3* (Vermont & 7<sup>th</sup> St.), (c) *Site 4* (Wilshire & Carondelet St.) in Los Angeles, and (d) *Site 5* (Temple City & Las Tunas) in Temple City. Top plots represent building distributions and heights (by colors in feet). The dashed line shows the sampling area. Bottom photos show the street view of the streets around the intersections. Color bar represents building height in meters. ....31
- Figure 4. Map of the Beverly Hills sampling route. Red line represents the mobile monitoring platform route and blue stars denote the locations of signalized intersections. ....32
- Figure 5. A schematic of the intersection sampling design. Green circles denote the location of a DiSCmini pair (across the street) for 5-minute stationary measurements. Red stars represent the location of surface and roof-top (only when roof-top access was possible) sonic towers. The actual positions and spatial scales are different from this illustration. 34
- Figure 6. The sampling route of the mobile monitoring platform (MMP) in downtown Los Angeles. BW denotes Broadway and EB, WB, NB, and SB represent eastbound, westbound, northbound and southbound, respectively. Map source: Google Earth. ....34
- Figure 7. Map of the Broadway Transect. ....35
- Figure 8. Micro-meteorological characteristics for sampling sites on individual days (specified by colors): (a) temperature, (b) mean wind speed, (c) vertical fluctuation of winds, (d) turbulence kinetic energy, and (e) friction velocity in the ground level. The shaded areas represent diurnal variations of data obtained at *Site5*, and squares, triangles, asterisks, and stars denote representative values for the *Site1*, *Site2*, *Site3*, and *Site4*, respectively. ....41
- Figure 9. Daily averaged [UFP] in the (a) morning and (b) afternoon sampling events at site. ....42
- Figure 10. The mean [UFP] of the transient high-spikes-removed time-series over the sampling areas in the morning vs. afternoon. Site 5 showed significant increases in [UFP] in the afternoon compared to the morning values despite comparable traffic volumes and more favorable atmospheric dispersive capacity. ....44
- Figure 11. The mean intersection vs. area-wide [UFP] distributions (a) in the morning and (b) in the afternoon sampling events at each sampling site. Vertical and horizontal bars denote standard deviations. ....45
- Figure 12. Comparisons of [UFP] variations in baseline time-series at the intersections and over the sampling area at (a) in the morning and (b) in the afternoon. Horizontal and vertical bars denote  $1\sigma$  variations. ....45

Figure 13. Daily [UFP] as a function of traffic flow rates (vehicles·min <sup>-1</sup> ) (a) in the morning and (b) in the afternoon sampling events. Ovals show a group of sampling site. ....	46
Figure 14. Comparisons of traffic corrected [UFP] vs. building area weighted building heights ( $H_{area}$ ) and the ratio of open space to sampling area ( $A_{open}/A_{site}$ ) for the morning sampling events. ....	47
Figure 15. Relationship between area aspect ratio ( $Ar_{area}$ ) and [UFP] normalized to traffic flow rates in the morning ( $R^2=0.67$ ). ....	47
Figure 16. Relationship between [UFP] and $\sigma_w$ for afternoonsampling events. (a) [UFP] vs $\sigma_w$ and (b) [UFP] normalized by observed traffic flows vs. $\sigma_w$ . The grey area represents the range of best fit curves as described in the text. The values for <i>Site2</i> are removed from the analysis due to very low traffic counts on the street and subsequent likely contributions from nearby streets and other sources (see text.) ....	49
Figure 17. Afternoon relationships between building heterogeneity vs. turbulence intensities: (a) vertical fluctuation of winds and (b) total turbulence kinetic energy (TKE) defined as $TKE = 1/2 \sqrt{\sigma_u^2 + \sigma_v^2 + \sigma_w^2}$ . Dotted and solid lines in (b) represent the best fits in linear ( $R^2=0.60$ ) and exponential ( $R^2=0.60$ ) forms, respectively, for illustration of the increase trends of TKE with building heterogeneity. ....	50
Figure 18. Spatial variation of background corrected UFP concentrations averaged over (a, b) morning and (c, d) afternoon sampling events over three days for (a, c) data including HEV-related spikes and (b, d) data excluding HEV-related spikes. The spatial resolution of the maps is 5 m. The heights of the buildings in the nearby area is shown in gray scale. ....	51
Figure 19. (a) The relative error of repeated calculations of mean concentration of HEV "spike removed" data, for different numbers of averaged afternoon runs included in the averaging (x-axis), at each line reference points along a single example street (BW SB) (y-axis.) (b, c) The variation of maximum relative error along different street segments vs. the number of averaged runs for morning (AM) and afternoon (PM) sampling events (b) for HEV "spikes removed" data and (c) for HEV "spikes retained" data. The green and yellow symbols denote the points at which the relative error is at or below 0.15. The spatial resolution of the maps considered is 5 m. ....	53
Figure 20. Actual versus Predicted UPF Concentrations for AM and PM Transects. ....	62
Figure 21. Time Profiles of Selected Traffic Events. ....	67
Figure 22. Baseline Free-flow Simulation and Simulation of Stop-start events at an intersection. ...	70
Figure 23. The mean UFP profiles across the intersection for each direction of the site (broken lines with symbols) and the mean profile of all directions for each site (black solid lines). N denotes the number of the total profiles obtained for the site. Left and right panels show the results for AM and PM sampling events, respectively. The % values in parentheses represent UFP elevation at the peak relative to the base value. ....	73
Figure 24. Same as Figure 23 but for (a) the entire A.M., (b) the P.M., and (c) the entire periods. Dark gray rectangles denote the location of the peak concentration and gray dashed rectangle indicate the base location. See text for the vertical gray dotted lines. ....	76
Figure 25. Cumulative [UFP] distribution plot at the peak (pink area) and base locations (gray area) indicated as black and gray dashed rectangles in Fig. (2c). Data are from the mean [UFP]	

profile for the entire sampling periods (N=1744). Red and black dotted lines show a linear fit for data between lower 20 to 70% (pink crosses and gray asterisks) for the peak and base location, respectively. Red Star and the white denote the mean values at the peak and base location, respectively. .... 77

- Figure 26. Relationships of relative (%) and absolute (particles·cm<sup>-3</sup>) elevations of UFP at the peak location with traffic parameters (traffic flow rate, queue length, and HEV considered queue length). The left panel (a, c, e) is for relative [UFP] elevation and the right panel for absolute concentration increase at the peak locations. Queue length is defined as the number of vehicles waiting for the green signal at the moment when traffic signal changes from red to green. .... 79
- Figure 27. Street Canyon Schematic (Source: <http://envs.au.dk/en/knowledge/air/Models/OSPM/>)82
- Figure 28. Map of Göttinger Strasse showing locations of concentration and micro meteorology stations and building heights. .... 86
- Figure 29. Comparison of equation (2) with observations during 2003. Top left shows scatter plot. Top right shows variation of observations (blue) and model (green) with wind speed. Bottom left shows variation with  $1/\sigma_w$ . Bottom right shows variation with wind direction. Wind directions parallel to the street are 163 and 343 degrees. .... 87
- Figure 30. Comparison of estimates from equation (2) without explicit wind speed dependence with corresponding observations during 2003. Top left shows scatter plot. Top right shows variation of observations (blue) and model (green) with wind speed. Bottom left shows variation with  $1/\sigma_w$ . Bottom right shows variation with wind direction. .... 88
- Figure 31. Field study locations in Los Angeles County. Map Data: Google. .... 90
- Figure 32. Instruments used in Los Angeles filed measurements. Left - Campbell scientific CSAT3 sonic anemometer. Center - Condensation particle counter. Right - AQMesh concentration monitor (at top of photo). .... 91
- Figure 33: Evaluation of the VDM with 30 minute average data from the building section of 8<sup>th</sup> Street (LA). Left panel: the emission rate is taken to be the 30 minute average value. Right panel: the emission rate is the daily average value. Surface concentrations are averages of both sides of the street. .... 94
- Figure 34. Evaluation of VDM model with data collected in the Los Angeles field studies. The concentration has been normalized by the daily average emission rate assuming an emission factor of  $2 \times 10^{14} \text{ veh}^{-1} \text{ km}^{-1}$ . .... 95
- Figure 35. Baseline and total concentration. .... 96
- Figure 36. Sensitivity of calculated baseline to window size (left) and cutoff percentile (right). .... 96
- Figure 37. Comparison of estimates from VDM with 30-minute averaged local contributions. Concentration is normalized by daily average emission rate, assuming an emission factor of  $10^{14} \text{ veh}^{-1} \text{ km}^{-1}$ . Left – The 8<sup>th</sup> St open section building height is zero. Right - The building height of the 8th St open section has been set equal to that of the 8th St building section. .... 97
- Figure 38. Micrometeorology measured at Los Angeles 8<sup>th</sup> St. site. Micrometeorology is determined from the 8<sup>th</sup> St. “building” and “roof” sonic anemometers. .... 98

Figure 39. Estimates of vertical velocity fluctuations measured at street level compared with measured values at several sites in Los Angeles. The black line is the 1 to 1 line. .... 99

Figure 40. Relationship between vertical velocity fluctuations measured at LAX and those at roof level on 8<sup>th</sup> St. - Data filtered so the roof site is downwind of the LAX site. (Wind direction at LAX within 20 degrees of the heading from LAX to 8<sup>th</sup> St.) - All other data. .... 100

Figure 41: Sensitivity of magnification (ratio of concentration with buildings to that with no buildings) to the area-weighted building height. The street width is 30 m. .... 102

Figure 42: Variation of PM2.5 concentration with hour of day predicted by the VDM spreadsheet. The area-weighted building height is 28 m and street width is 30 m. Traffic is typical of “arterial” roads. .... 102

## List of Abbreviations

ARB/CARB	California Air Resources Board
AGL	above ground level
BW	Broadway
CPBM	Canyon Plume Box Model
CPC	condensation particle counter
DTLA	Downtown Los Angeles
HEV	high emitting vehicle
IBL	internal boundary layer
LA	Los Angeles
MMP	Mobile Monitoring Platform
OSPM	Operational Street Pollution Model
SB375	Senate Bill 375, the Sustainable Communities and Climate Protection Act of 2008
TC	Temple City
TOD	transit oriented development
UBL	urban boundary layer
UCL	urban canopy layer
UFP	ultrafine particles
VDM	Vertical Dispersion Model

## iv. Introduction

Air pollution emissions from motor vehicles are spatially-heterogeneous in urban areas. A large fraction of an individual's exposure to air pollutants can be attributed to relatively short periods of time spent on and near roadways, which often have highly elevated air pollutant concentrations compared to areas even at moderate distances away from roadways (Behrentz et al. 2005; Fruin et al. 2004; Marshall et al. 2005). However, because of the lack of adequate air pollutant measurement data near local roadways, studies of health effects attributed to transportation-related air pollutants have generally used proximity to freeways or arterial roadways as a surrogate for vehicle-related air pollution (Brugge et al. 2007; Ren et al. 2008; Volk et al. 2011; Zhou and Levy 2007). Despite this generalization, near roadway air pollution studies have shown moderate increases in a long list of adverse health outcomes, including increased incidence of cancer (Pearson et al. 2000), asthma (Janssen et al. 2003), general mortality (Hoek et al. 2002), heart attacks (Tonne et al. 2007), autism (Volk et al. 2011), pre-term birth (Ren et al. 2008) and other adverse outcomes associated with air pollution exposure near roadways.

While California has made tremendous progress in reducing vehicular emissions, evidence of the dangers of roadway air pollutant exposure is growing, highlighting the need to ensure that implementation of regional and local sustainability strategies under programs like Senate Bill 375 (SB 375) are consistent with ARB's criteria and toxic pollution exposure reduction policy goals. SB 375 requires Metropolitan Planning Organizations (MPOs) to develop Sustainable Community Strategies (SCS) as part of their Regional Transportation Plan to demonstrate how they will achieve regional greenhouse gas reduction (GHG) targets. Many MPOs are adopting Sustainable Communities Strategies that seek to direct new development and population growth to transit corridors. For example, the Southern California Association of Governments has adopted its first Sustainable Communities Strategy in compliance with SB 375 in which they propose placing more than 50 percent of new growth in High Quality Transit areas or transit oriented development.

Transit oriented developments (TODs) are built environments in which high density residential developments are located close to public transportation and local businesses. TODs have the potential of improving environmental sustainability by reducing emissions associated with transportation, and promoting healthy activities such as walking and cycling (Boarnet and Crane, 2007). TODs are being promoted to reduce GHGs and air pollutant emissions associated with transportation because these environments are associated with reduced use of personal cars. TODs are also expected to reduce concentrations of air pollutants averaged over city scales. However, there is concern that high-density development will instead increase exposure of pedestrians, residents and other users of TODs due to increased densities of vehicle emissions and building morphologies associated with higher density development. Therefore, policies to encourage greater residential density around transit corridors may lead to the unintended effect of greater pedestrian exposure to roadway air pollutants. This problem may be especially acute at public transit stops deliberately located on high-volume arterial roadways to increase the passenger connectivity, accessibility, and multi-modal travel. As a result, the traditional policy response has been to move pedestrians and residents away from roadway emissions, a less feasible approach within many transit environments.

Moreover, actual exposure of pedestrians within such transit environments depends upon several factors including air pollution dispersion dynamics that vary with site-specific street-building morphologies, transit-stop locations, wind speed, temperature, and spatial proximity and intensity of emissions, traffic management, as well as, potentially, pedestrian enclosures, vegetation, and other features of the built environment. Transportation and urban planners routinely make an array of decisions that may affect pedestrian and residential air quality. With respect to local emissions

sources, transportation planners implement local traffic controls (such as signals, stoplights, and maximum speeds) on the transit arterial roadways that determine spatially where vehicles accelerate and how fast they travel. At the neighborhood scale, these planners make routing decisions that influence local traffic volume and composition on these same transit arterial roadways. These decisions together determine the precise location and timing of air pollutant emissions within a transit-stop environment. Despite the growing literature on near-roadway exposures, little is known about how to proactively design and plan for these transit environments to minimize air pollution exposures. In addition, models currently being used by air quality planners at regional levels have undergone limited evaluation with data under stable atmospheric conditions that typically represents urban built environments. To effectively evaluate future TODs, there is a need to develop a tool that can help planners better understand and evaluate how California's building morphologies affect pedestrian exposures, and a need to develop a guideline that can help the planners design the most optimal TODs to reduce pedestrian exposure to harmful air pollution emissions. To address these concerns, this study was constructed to address the following objectives:

- 1) Develop a guideline for TOD planners to reduce pedestrian exposure to air pollution in urban built environments by extending the qualitative understanding of the influence of the built environments on street level air pollution concentration through field measurements and statistical modeling
- 2) Develop a dispersion model that can be used to provide TOD planners quantitative links among the variables that control dispersion in complex urban environments and how best to reduce air pollution exposures in said environment

Our study seeks to help develop tools to minimize these exposures by advancing the understanding of factors controlling spatially-variable pollutant concentrations around roadways. The products include a rich measurements data set, and a refined predictive atmospheric dispersion model for the complex urban landscape. Further, these are used together with available literature to provide decision-support tools and information for transportation and urban planners to protect public health, pursuant to ARB's mission and goals of protecting the public from harmful exposure to air pollution and reducing GHGs. Specifically, the report disseminates evaluative and remedial decision-support tools for planners that focus on more effectively siting transit stops, managing intersection traffic flow, and shaping new TODs to reduce pedestrian air pollution exposure.

This study focuses on design and operational features that may both play a major role in determining pedestrian air pollution exposure and could be modified through local planning and transportation decisions. These meta-features include: 1) traffic volume, composition, and traffic calming strategies, 2) building heights around the arterial roadway, and 3) building set-backs from the arterial roadway. The result are summarized as tools and guidelines that transportation and urban planning decision makers can use to guide everyday decisions that impact the exposure of pedestrians in TODs.

The project uses a three-pronged approach combining extensive real-time measurements of air pollutants such as ultrafine particles, statistical analysis of real-time data and its relation to the morphology of the built environment and traffic management strategies, and development of a dispersion model for evaluating the impact of built-environment design features. Measurement data were collected with a mobile measurement platform, which provided a rich data set by repeatedly sampling for brief stationary periods in a dense matrix of locations on three-to-four approximately mile-long "transects". These measurements were augmented by additional instrumentation to characterize micro-meteorology and pollutant levels aloft.

The data were also combined with existing street-level pollutants measured using mobile measurement platform, and was used to explore relationships between building morphology, traffic

management strategies, and pollutant concentrations on length scales of several meters away from the roadway. To provide predictive ability and explore the potential improvements to pollutant levels that may be anticipated from potential land use changes, a semi-empirical model was developed. The Operational Street Pollution Model (OSPM) developed by the Danish National Environmental Research Institute (Berkowicz et al., 2000) was used as the starting point for this modeling exercise. OSPM incorporates the main features of our current understanding of dispersion in street canyons, and has undergone evaluation with real-world observations made in European cities (Berkowicz et al., 1997, Doring et al., 2011). However, this study indicated that OSPM did not account for the inhomogeneous building environments of typical U.S. cities, such as Los Angeles, in which tall buildings are interspersed among two or three story buildings and open spaces. This necessitated the development of a model specific for California conditions. Collectively, this research will identify and quantify the impacts of alternative policy solutions that have been less recognized but promises to reduce pedestrian air pollutant exposures in transit environments.

The report is presented in two sections that describe the methodology, and the results from the two different analytical approaches used to explain the complex data:

- Field Measurements and Statistical Modeling
- Dispersion Modeling

The results from the two approaches reinforce each other. The results from the statistical approach provide semi-quantitative guidance on the design of built environments to reduce exposure to vehicle related pollutants. The dispersion model translates the data from the field studies into a practical tool that can be used by planners to estimate the quantitative impact of strategies to reduce exposure to these pollutants.

## v. Field Measurements and Statistical Modeling

### v.1. Introduction

Fresh vehicular emissions contain a wide range of particle- and gas-phase species, including carbon monoxide, nitric oxide, a variety of volatile and semi-volatile organics, and ultrafine particles. Because such emissions are emitted and diluted together, their individual impacts are difficult to separate. In general, the best tracer of near roadway air pollution is ultrafine particles (UFP) as it is most prominently produced during burning of fuels in internal combustion engines. UFP can be measured reliably with 1 second time resolution with wide dynamic concentration ranges (5 – 6 orders of magnitude). As dispersion near intersections and in city blocks takes place in seconds rather than minutes, the high time resolution is essential in understanding pedestrian exposure to air pollution emissions. Additionally, because UFP are incorporated into larger particle sizes on relatively short time scales under dynamic nucleation events, in urban areas UFP tend to have steady background concentrations upon which the impact of local sources (such as motor vehicles) are extremely clear. Actual exposure of pedestrians in transit-served environments depends upon several factors including air pollution dispersion dynamics that vary with site-specific street-building morphologies, transit stop locations, wind speed, temperature, spatial proximity and intensity of emissions, and traffic management, as well as pedestrian enclosures, vegetation, and other features of the built environment. Despite a growing literature on near-roadway exposure, little is known about how to proactively design and plan for these transit-served environments in order to minimize air pollution exposure.<sup>1</sup>

Transportation and urban planners routinely make an array of decisions that may impact pedestrian and residential air pollutant exposures.<sup>2</sup> With respect to local emissions sources, transportation planners implement local traffic controls (such as signals, stop lights and maximum speeds) on the arterial roadways that determine spatially where vehicles accelerate and how fast they travel. At the multi-block scale, these planners make routing decisions that influence local traffic volume and composition on these same transit arterial roadways. These decisions together determine the precise location and timing of air pollutant emissions within a transit-stop environment. Through building, zoning, and street design ordinances, urban planners' decisions influence the height and spacing of buildings as well as how far setback they are from the arterial roadway. The resulting street-building morphology around a transit stop then interacts with the prevailing winds (and other meteorological conditions) to determine whether, and how quickly, emissions are dispersed.

It is, therefore, desirable to develop a set of comprehensive recommendations on how to reduce pedestrian and residential air pollution exposures that transportation and urban planners can reference when making future development plans. These may include traffic controls and urban building configuration, which impact emissions and dispersion, respectively. Within the transit environment, urban planners also decide where pedestrian density will be greatest through decisions about where to site transit stops, sidewalks, and parks.

Several studies investigating the influence of the built environment on street level concentrations have been published, mostly focusing on deep street canyons. Three recent studies have taken the

---

<sup>1</sup> We recognize there are best design practices such as enclosed/covered bus stops, closed canopy pedestrian byways, pedestrian byways below or above ground, and urban forest canopy parks, but these practices were not evaluated in this study. See Zhou and Levy, 2007; Brugge, et al., 2007; Karner et al., 2010 for a meta-analysis of this literature as it relates to near-roadway exposure.

<sup>2</sup> We focus here on exposures to pedestrians, but the findings of our research will also inform exposure to residents in transit-adjacent housing (Marshall, et al., 2005; Zhu, et al., 2005).

first step toward understanding dispersion of traffic-related pollutants in urban areas with inhomogeneous building morphology, which is consistent with the focus of this study (Boarnet et al. 2011; Buonanno et al. 2011; Karra et al. 2011). Buonanno et al. (2011) focused on particles, including UFP, measured in a town in central Italy; Karra et al. (2011) studied dispersion of CO in Nicosia, Cyprus; and Boarnet et al. (2011) examined PM<sub>2.5</sub> in downtown Los Angeles, California. Boarnet et al. (2011) further examined the factors governing PM<sub>2.5</sub> concentrations measured on sidewalks next to arterial roadways in five cities in southern California. The measurements indicated that the most effective controlling factors for sidewalk PM<sub>2.5</sub> concentrations are daily variations, time of day, wind speed and direction, and temperature. They also found that traffic and built environment variables, while statistically significant, accounted for only a small amount of the observed variation; however, it should be noted that their built environment variables were classified rather than quantified. After accounting for these most effective controlling factors, they concluded that street canyons with higher than 5-story buildings are related to high PM<sub>2.5</sub> concentrations, and adjacent paved lots were negatively associated with PM<sub>2.5</sub> concentrations. Boogard et al. (2011) conducted an extensive study in the Netherlands in which five species, including particle number concentrations and black carbon, were measured over 6 weeks at 8 urban roadside locations in five cities. Although their results did not discern the roles of meteorology and emissions, the two streets with buildings lining one or both sides of the street showed the largest road contributions.

While these studies provide insight into air pollution in built environments, the measurements lack the spatial resolution and completeness to discern contributions of detailed urban morphology and traffic control at a level that could inform highly-local planning decisions about the built environment and traffic flow. Minimizing exposure to transportation-related air pollution is not fully considered currently in the process of planning for TODs (Haughey and Sherriff 2010).

There are several relevant spatial scales that must be investigated to fully understand the impact of the built environment on near-road pollutant concentrations. Here, we focus on a spatial scales ranging from a few meters away from the roadway to several city blocks that span over a network of local roads. We develop quantitative links among the variables that control dispersion in complex urban environments, including building morphology, traffic flow rates, and micrometeorology using field measurements and statistical modeling. We consider data from five sites in the greater Los Angeles area, each with similar vehicle fleet composition and similar meteorology, but markedly different built environments and traffic flow patterns. Ambient air measurements were performed both in the early morning and in the mid-afternoon, which have significantly different atmospheric stability and wind profiles.

## v.2. Background and Related Work

### v.2.1. Current research needs for TOD planners

A growing number of studies are focusing on exposures to vehicle-related air pollutants in urban areas from various perspectives (Boarnet et al. 2011; Chan et al. 2002; Hagler et al. 2012; Kaur et al. 2007; Kinney et al. 2000; Ryan et al. 2008; Steffens et al. 2012; Tong et al. 2012). Several focus on exposure experienced by pedestrians, cyclists and automobile occupants (Adams et al. 2001a; Adams et al. 2001b; Kaur et al. 2007), and others examine the difference in air pollution exposure experienced on minor versus major thoroughfares (Boogaard et al. 2011). Researchers are also investigating the influence of barriers, including vegetation (Hagler et al. 2012; Steffens et al. 2012) and sound walls, on air pollution exposure (Baldauf et al. 2008; Bowker et al. 2007; Finn et al. 2010; Hagler et al. 2012; Ning et al. 2010). Most of these studies have focused on air pollutants that are not strongly correlated to freshly emitted roadway pollutants (such as PM<sub>2.5</sub>). Instead, studies using roadway air pollutants that are strongly associated to fresh motor vehicle emissions, such as

UFPs, are becoming more common (Hagler et al. 2012; Kaur et al. 2007; Ning et al. 2010). Land use regression models, an alternative to dispersion models, have also been utilized to relate these field measurement data of roadway air pollutants to exposures in different micro-environments (Rivera et al. 2012; Ryan et al. 2008). These models are valuable in several applications, including epidemiological studies, as they are easier to relate to geo-coded health data. However, they do not have predictive capability to inform block-level building and traffic design decisions.

Nevertheless, the importance of the detailed characteristics of buildings along streets on air pollutant concentrations is clear. For example, Tong et al. (2012) conducted a modeling study using ambient air monitoring data (Patel et al. 2009) focusing on black carbon, an excellent tracer for diesel traffic, to perform an analysis of the influence of buildings surrounding a school located in close proximity to a highway. The authors concluded that exposure to black carbon would have been about half if the buildings located between the school and the highway had not been there. Additional studies by Boogaard et al. (2011) and Boarnet et al. (2011), as presented previously, also provide insight into the importance of roadside building characteristics on air pollution concentrations.

While these studies provide information on air quality in built environments, the measurements lack the spatial resolution and completeness to refine and valid dispersion models for realistic urban landscapes. In addition, these studies have not been designed to inform highly-local planning decisions based on the morphology of built environment and local traffic flow regimes. Minimizing exposure to transportation-related air pollution is currently overlooked in the process of planning for TODs (e.g., (Haughey and Sherriff 2010)). Furthermore, no design tools are available for urban planners and transportation planners that incorporate the goals of minimizing air pollution exposures for residents and pedestrians in TODs.

### v.2.2. Overview: mobile platform studies

Instrumented vehicles, or mobile platforms, was first used in the 1980s and have been more widely implemented in the early twenty first century. They have been used for several research goals: (a) to measure air pollutant levels on-board vehicles (i.e., “in-cabin” concentrations) under realistic driving conditions; (b) measure air pollutant concentrations on roadways (rather than taking measurements alongside roadways from fixed sites); (c) to collect stationary ambient air measurements at a set of locations in close proximity to either a source (e.g., airports) or receptor of interest; (d) to characterize the decay of air pollutant levels with increasing distances away from roadways and other concentrated sources; (e) to look for “hot spots” and areas of anomalously elevated air pollutant concentrations in residential and other areas; and (f) to directly sample in-situ motor vehicle plumes (“chase” studies). Within the past five decades, there has been intense focus on measurement of UFPs because of its toxicity and its potential to affect human health. One of the direct antecedents for the present project, Westerdahl et al. (Westerdahl et al. 2005) and Fruin et al. (Fruin et al. 2008) utilized the California Air Resources Board’s (ARB’s) non-polluting (electric) mobile platform together with multiple scanning mobility particle sizers to measure UFP and associated air pollutant concentrations on freeways and residential streets in Los Angeles, California. These studies showed freeway on-road UFP concentrations to be largely driven by truck emissions while hard accelerations of gasoline-powered vehicles appeared to be the most common source of high UFP concentrations on arterials. In other in-vehicle studies of UFP, Miguel and co-workers (Zhu et al. 2007) conducted mobile monitoring in Los Angeles using a passenger car equipped with a high-efficiency particle arrestance (HEPA) filter system, including measurement of in-cabin and on-road measurements for both freeways and surface streets. Hitchins et al. (2000) and Kittelson et al. (2004b) also measured high concentrations of UFP on and near roadways. Several mobile monitoring studies that included UFP measurements have been conducted in Europe (Pirjola et al. 2004; Weijers et al. 2004) and in the eastern United States (Canagaratna et al. 2004; Kittelson

et al. 2004a). All of these studies demonstrate the usefulness of mobile platforms while supporting the notion that UFPs are useful tracer for motor vehicle activities.

### v.2.3. Overview: Studies investigating air pollution gradients near freeways

The existence of strong air pollution gradients near freeways have been recognized at least since the 1980s, with early studies focusing on gas phase pollutants (Rodes and Holland 1981). Hitchins et al. (2000) measured concentrations of fine and ultra-fine particles at a distance of 15 to 375 m away from a major roadway. They found that particle concentrations decayed to about half of the peak value (at the closest point to the roadway) at approximately 100-150 m downwind away from the roadway (Hitchins et al. 2000), which provides evidences of a sharp gradient of fine and ultrafine particles. Similar studies were also conducted by Zhu et al. (Zhu et al. 2002; Zhu et al. 2002a), who measured UFP, CO, and black carbon (BC) along the upwind (200 m) and downwind (300 m) sides of a freeway in Los Angeles during the daytime. Peak concentrations were observed immediately adjacent to the freeway, with concentrations of air pollutants returning to upwind background levels about approximately 300 m downwind of the freeway.

The few near-roadway studies conducted at nighttime indicated larger areas of impact than during the daytime. Nighttime UFP concentrations were reported by Zhu et al. (Zhu et al. 2006), who conducted measurements upwind (300 m) and downwind (500 m) of a freeway from 22:30 - 04:00. Although traffic volumes were much lower at night, particle number concentrations were about 80% higher 30 m downwind of the freeway compared with the daytime, with UFP concentrations of  $\sim 50,000 \text{ cm}^{-3}$  approximately 500 m downwind of I-405, a major Los Angeles freeway. Fruin and Isakov (Fruin and Isakov 2006) measured UFP concentrations in Sacramento, California, near the US Highway-50 freeway between 23:00 and 01:00 and found 30-80% of maximum centerline concentrations (measured on a freeway overpass) 800 m downwind. These differences suggests that air pollution gradients near freeways can vary not only based on the on-road traffic densities, but also based on meteorology that affects mixing and dynamic nucleation events downwind of the source.

### v.2.4. Previous results from the Air Resources Board Mobile Platform in Southern California

A steady stream of recent results have been produced by researchers at ARB, UCLA and a handful of additional institutions using the same ARB-maintained mobile platform (Choi et al. 2013b; Choi et al. 2016; Choi et al. 2012b; Choi et al. 2014; Fruin et al. 2008; Hu et al. 2009a; Hu et al. 2009b; Kozawa et al. 2008; 2009; Paulson et al. 2012; Quiros et al. 2012; Westerdahl et al. 2005; Westerdahl et al. 2008).

In a study published by Kozawa et al. (2009), researchers at ARB and UCLA investigated into the impact of goods movement in the communities of Wilmington and West Long Beach, California. The researchers analyzed residential multi-block measurements taken in a reference zone between 160 and 600 m away from (and to the west of) the I-710 freeway into the adjacent communities. The community level concentrations for BC, UFP, and NO were compared to concentrations measured within 150 m of the I-710 freeway. Data were analyzed for the morning and afternoon in both the winter and summer seasons.

In the summer season, the mean concentrations of BC, UFP and NO within the residential multi-block (away from the freeway or heavily-traveled surface streets), were approximately  $2.5 \mu\text{g m}^{-3}$ ,  $15,000 \text{ cm}^{-3}$  and 25 ppb, respectively, during morning monitoring period, and  $1 \mu\text{g m}^{-3}$ ,  $20,000 \text{ cm}^{-3}$  and 12 ppb, respectively, during the afternoon monitoring period. The comparable means for BC, UFP and NO in the winter were  $3 \mu\text{g m}^{-3}$ ,  $25,000 \text{ cm}^{-3}$  and 35 ppb, respectively, in the morning, and  $1.5 \mu\text{g m}^{-3}$ ,  $23,000 \text{ cm}^{-3}$  and 12 ppb, respectively, in the afternoon. In summary, the mean BC concentrations at the Wilmington community were comparable to the basin-wide mean

concentrations of 1-2  $\mu\text{g m}^{-3}$ . In addition, the mean UFP and NO concentrations ranged between 15,000 and 25,000  $\text{cm}^{-3}$  and between 10 and 35 ppb, respectively, as a function of time of day and season.

Ratios of BC, UFP and NO concentrations for measurements made within 150 m or less of the I-710 freeway divided by the residential multi-block concentrations for the same monitoring periods ranged between approximately 1 and 7 depending on the air pollutant, the time of day, the season, and the wind direction. When both areas were downwind of the I-710 freeway, the mean ratios for the near-roadway micro-environment divided by the residential multi-block micro-environment were approximately 2, 2 and 3 for BC, UFP and NO, respectively.

#### v.2.5. Overview: Longitudinal studies

Only few mobile platform studies of on-road or near-road air pollutant concentrations have been performed before the year 2000 due to limitations that involve instrument power and space constraints, so available longitudinal comparisons are limited. The earliest comprehensive on-road and in-vehicle measurements were conducted by Shikiya et al. (1989b) in Los Angeles in 1987/1988. The next major on-road study in California was conducted in 1997 (Rodes 1998) and allowed comparison of VOC concentrations in Los Angeles. The Los Angeles VOC results, when compared to the in-vehicle study conducted in 1987 (Shikiya et al. 1989a), reflected the significant reductions in vehicle emissions that occurred in the intervening decade. The in-vehicle aromatic VOC and CO concentrations measured in Rodes et al. (1998) were equal to or lower than the ambient concentrations measured by Shikiya et al. (1989a).

Mobile platform measurements of particles are more recent. Initial studies relied on optical counters, and comparisons are difficult across instrument types. Integrated mass measurements inside vehicles have been few due to the difficulty in obtaining sufficient mass over the time scale of hours. Rodes et al., (Rodes 1998) made some of the first measurements of on-road black carbon (BC), using an Aethalometer, thus providing one of the earliest potential “baselines” of on-road BC concentrations available for comparison for Los Angeles and Sacramento. They also sampled integrated  $\text{PM}_{2.5}$  and  $\text{PM}_{10}$  with filters and analyzed for metals. However, due to the study design of Rodes in which diesel vehicles were targeted, direct comparisons of BC concentrations require the adjustments described by Fruin et al. (Fruin et al. 2004). With these adjustments, comparisons of BC concentrations can be made back to 1997 if driving the same route at the same time of day. Available locations include arterial roadway and freeway routes in Sacramento and Los Angeles.

UFPs, generally measured by condensation particle counters (CPCs) have until recently been difficult to use in moving vehicles due to their sensitivity to motion. The first available measures of on-road UFP number in California are the studies of Westerdahl et al. (2005). They drove fixed freeway and arterial roadway routes in 2003 that have periodically re-driven these routes several times per year since then. Measurements also included NO,  $\text{NO}_2$ , BC, particle-bound PAH, CO,  $\text{CO}_2$ , and  $\text{PM}_{2.5}$ . These studies found fairly good day-to-day repeatability in the relationship between things like diesel truck volume and concentrations of BC, NO, and UFP. While day-to-day differences in absolute concentrations depend strongly on meteorology (and therefore time of day as well), their dependence on traffic conditions is more stable, thus lending itself to longitudinal comparisons and trend analysis.

## v.3. Methods

### v.3.1. Sampling sites and built-environmental characteristics

Extensive field experiments, including mobile and stationary measurements of vehicular pollutants and traffic, were conducted at four sites in and around downtown Los Angeles (DTLA) and at a site in Temple City, located 20 km east of DTLA, for 16 days between July and November 2013 (Figure 1, Table 1). Each sampling site represents a distinct urban built environment with a different building morphology (e.g., building heights and areas, intersection configurations, street widths, building densities, and overall homogeneity) and traffic patterns (e.g., traffic flow rates, traffic densities, fleet compositions, and traffic-light cycle periods). Each sampling site covered a 2-by-2 (or 2-by-3) block area centered on a main intersection where stationary sampling of pollutants and traffic monitoring were conducted, depending on availability of instruments. All sites were located more than 800 m from the nearest freeway, well outside the range of freeway influence during the daytime. As UFP are relatively short-lived and upwind areas for all sites consisted of similarly developed urban areas for many kilometers, the influence of areas farther than the neighboring several streets are not expected to be discernible in this dataset.

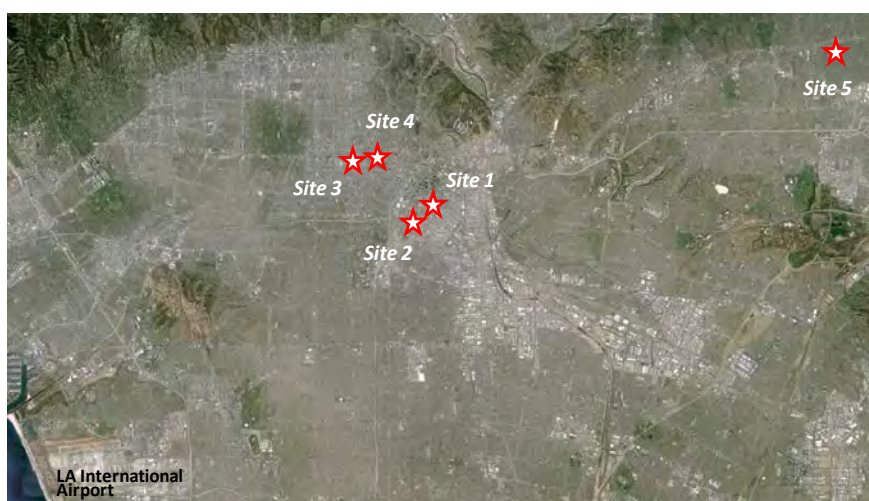


**Figure 1. Map of measurements sites in the South Coast Air Basin. Red stars denote the sampling sites that cover 2-by-2 (or 2-by-3) blocks centered by the main intersection where traffic recording and stationary measurements were conducted in 2013.**

**Table 1. Description of field measurements including built-environments, measurement dates, instrumentation, and sampling design.**

Sites	Built-Env.	Date	Instrumentation	Sampling strategy
Broadway & 7 <sup>th</sup> St. Site1	Street canyon with tall buildings (H>40m) at both side of the street. Highly trafficked on both streets.	7/1 7/2 7/3 7/5	[1] ARB-MMP; 2 DM; 2 sonic tower (roof & surface); 4 traffic recording cameras	[A] 2 DM were paired across the street, staying about 5 min. at mid-blocks and intersections (quasi-stationary)
		11/13	[2] Light-MMP; 3 DM; CPC; OPS; 2 surface sonic tower; 4 traffic cam	[B] 2 DM were stationary at the Intersections 1 CPC&OPS stayed at the sonic tower 1 DM stationary across the sonic tower
Temple City & Las Tunas Site5	All short buildings (H < 6 m) around the site Moderately trafficked (Las Tunas > Temple)	8/6	[1] but 1 sonic tower	[A]
		9/17 9/18	[3] Light-MMP; 1 DM; CPC; OPS; 2 sonic tower (roof &	[C] 1 DM at intersection (staying 5 light cycles at each corner) and CPC & OPS

			surface); 4 Traffic cameras	stayed next to sonic tower
Olive & 12 <sup>th</sup> St. Site2	One tall building at one corner of intersection + many open space Sparse traffic	9/24	[3]	[C]
		9/25		[C] but 1 DM was stationary across the sonic tower
Vermont & 7 <sup>th</sup> St. Site3	One tall building at intersection Large traffic on Vermont	10/7 10/14	[3]	[C]
		11/18	[2]	[B]
Wilshire & Carondelet Site4	Two tall buildings Modest traffic on Wilshire	11/1	[2]	[A] and additional DM was stationary across the sonic tower
		11/6	[2]	[B]
		11/20	[2]	[B]

*ARB-MMP*: California Air Resources Board mobile monitoring platform

*Light-MMP*: Electric vehicle equipped with a DiSCmini

*DM*: DiSCmini ultrafine particle counter, *CPC*: condensation particle counter, *OPS*: Optical particle sizer

The Broadway and 7<sup>th</sup> St. site (*Site1*) located in DTLA (34.04519°N / 118.25639°W) is a street canyon environment surrounded by tall commercial buildings on both sides of the streets. Building heights were > 40 m with little, if any, gaps between buildings. The block lengths/street widths (measured from building face to building face on the two sides of the street) of Broadway and 7<sup>th</sup> streets are 190 m/26 m and 100 m/22 m, respectively (see Table 2). The Olive and 12<sup>th</sup> St. site (*Site2*) is located 1 km southeast of *Site1* (34.03943°N / 118.26226°W). The intersection is occupied by a 130 m tall isolated skyscraper surrounded by large open spaces and low-story buildings. This site had low traffic flows and short queues (see Table 3). The block lengths/street widths of Olive and 12<sup>th</sup> St. are 180 m/28 m and 95 m/17 m, respectively. The Vermont and 7<sup>th</sup> St. site (*Site3*) located 4 km northwest of *Site1* (34.05976°N / 118.29164°W) is similar to *Site2*, but surrounding buildings are more densely patched and open spaces are smaller. In addition, Vermont Ave. in *Site3* is one of the busiest arterials in Los Angeles. The block lengths/street widths of Vermont Ave. and 7<sup>th</sup> St. are 190 m/30 m and 95 m/25 m, respectively. The Wilshire and Carondelet St. site (medium-sized buildings on one side, *Site4*) is located 3 km northwest from *Site1* and 1 km east from *Site3* (34.06012°N / 118.28054°W). *Site4* represents a typical city environment in the Los Angeles area, consisting of a mixture of open space and moderately-sized buildings. The whole block of the south side of Wilshire Blvd. is occupied by 30 m and 50 m tall buildings while the north side is open or occupied by 5 to 10 m tall buildings. The block lengths/street widths of *Site4* are 75 m/37 m (Wilshire) and 160 m/17 m (Carondelet). Finally, the Temple City and Las Tunas Blvd. site (a low and flat residential site, *Site5*) in Temple City (34.10669°N / 118.06090°W) is surrounded mostly by one-story single family homes and small commercial buildings (< 6 m in height). The block lengths/street widths of Temple City and Las Tunas Blvd. are 175 m/24 m and 115 m/30 m, respectively. Table 3 presents the height of urban canopy (mean building area-weighted building heights), where lower numbers indicate higher building morphology (e.g., *Site1* has a street canyon and tall buildings while *Site5* has a low/flat urban configuration). The distributions of buildings and building morphology around sampling sites are presented in Figure 2, Figure 3, and Table 2 presented below.

**Table 2. Built environments (Sites1-5) in the mobile sampling areas.**

	Broadway & 7th (Site1)	Olive St. & 12 <sup>th</sup> St. (Site2)	Vermont & 7 <sup>th</sup> St. (Site3)	Wilshire & Carondelet (Site4)	Temple City & Las Tunas (Site5)
# of buildings	59	34	90	44	143
Max. building height (m)	58	129	80	57	8
Mean building height, H <sub>bdg</sub> (m)	34	21	11	18	5

Bldg. area weighted height, $H_{area}$ (m)	40	42	25	24	6
Bldg. homogeneity, $H_{area}/H_{bldg}$ (dimensionless) (1=perfectly homogeneous)	1.16	2.01	2.21	1.39	1.09
Mean building ground area (m <sup>2</sup> )	1,030	1,395	585	992	225
Street width (m)	26 (BW) / 22 (7 <sup>th</sup> )	28 (Olive) / 17 (12 <sup>th</sup> )	30 (Ver) / 25 (7 <sup>th</sup> )	17 (Car) / 37 (Wil)	24 (TC) / 30 (LT)
Simple Aspect ratio ( $H_{area}/W_{street}$ )	1.7	1.9	0.9	0.9	0.2
Block length (m)	190 (BW) / 100 (7 <sup>th</sup> )	180 (Olive) / 95 (12 <sup>th</sup> )	190 (Ver) / 95 (7 <sup>th</sup> )	160 (Car) / 75 (Wil)	175 (TC) / 115 (LT)
Ratio occupied by bldg.	0.72	0.42	0.33	0.46	0.30

**Table 3. Characteristic traffic patterns observed for each site during the measurement periods. Values in parentheses are standard deviations.**

Date	Morning					Afternoon				
	Light cycle sec	Traffic rate #·min <sup>-1</sup>	HDV/MDV #/cycle	Queue length #/cycle	Traffic Ratio	Light cycle sec	Traffic rate #·min <sup>-1</sup>	HDV/MDV #/cycle	Queue length #/cycle	Traffic Ratio
Site1 (Street Canyon)										
7/1	69(4)	29(2)	1.4(1.2)	20(5)	0.47					
7/2						89(4)	41(8)	0.9(0.9)	31(8)	0.51
7/3	69(5)	29(6)	1.0(1.2)	18(5)	0.44	89(3)	43(8)	0.9(0.9)	29(5)	0.52
7/5	70(4)	22(5)	0.9(1.1)	12(4)	0.48	89(4)	35(5)	0.5(0.9)	29(6)	0.49
11/13	69(2)	34(5)	0.9(1.0)	21(5)	0.56	69(1)	28(5)	1.4(1.2)	20(5)	0.47
Site2 (Isolated skyscraper with low traffic rates)										
9/24	69(2)	22(7)	0.6(0.8)	3(2)	0.81	77(10)	12(3)	0.6(0.6)	2(1)	0.75
9/25	69(3)	27(7)	0.9(0.9)	6(3)	0.87	69(1)	10(3)	1.0(0.7)	3(2)	0.75
Site3 (Isolate skyscrapers with high traffic rates)										
10/7	89(3)	47(6)	2.0(1.2)	22(6)	0.81	89(1)	51(7)	1.4(1.1)	28(6)	0.75
10/14	91(12)	47(7)	1.4(1.1)	27(7)	0.81	90(11)	47(6)	1.2(1.0)	27(7)	0.77
11/18	89(1)	54(7)	1.6(1.1)	33(7)	0.77	89(2)	51(6)	1.1(1.0)	29(6)	0.76
Site4 (One-side medium height buildings)										
11/1	110(44)	30(5)	1.2(1.3)	4(2)	0.95	98(34)	29(9)	1.0(0.9)	5(2)	0.94
11/6	100(30)	35(6)	0.8(0.9)	4(2)	0.93	107(36)	29(4)	0.8(0.9)	6(3)	0.92
11/20	100(30)	35(6)	0.9(0.9)	5(3)	0.91	97(23)	30(5)	1.1(1.0)	6(2)	0.89
Site5 (Low and Flat)										
8/6	71(6)	45(7)	1.7(1.9)	24(9)	0.44	79(9)	64(10)	1.2(1.1)	50(15)	0.48
9/17						70(8)	49(10)	1.6(1.5)	27(8)	0.46
9/18	81(8)	61(10)	1.8(1.6)	41(13)	0.49	69(1)	55(9)	1.4(1.1)	33(10)	0.48

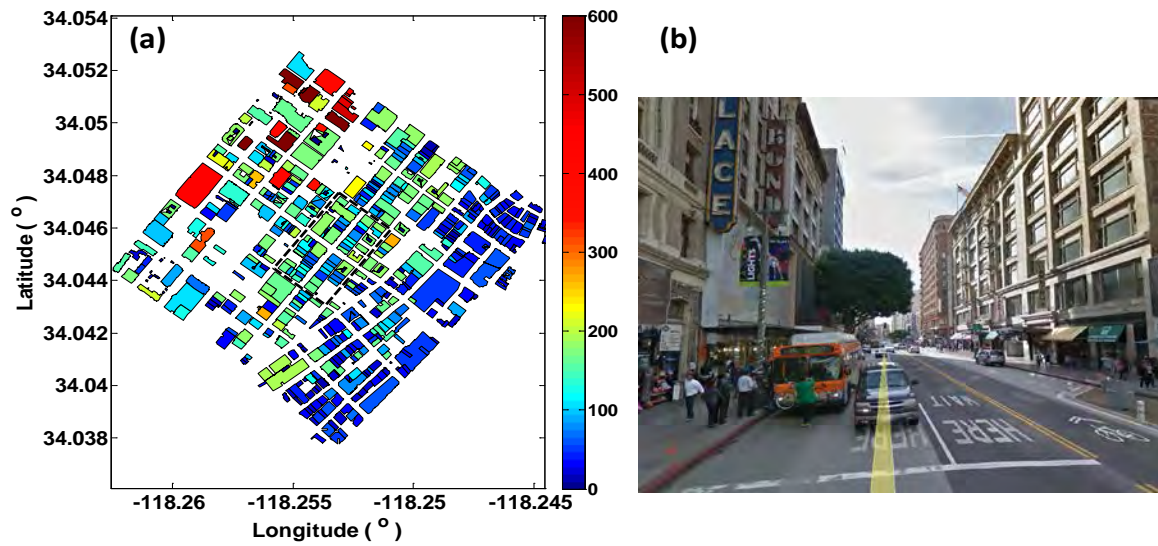


**Figure 2. (a) Map of building heights and morphology in DTLA. Color bar represents the building heights in feet. (b) The street view on Broadway St. captured in Google Earth. The building distributions and street views for the other sites are presented in the Supplementary Information.**

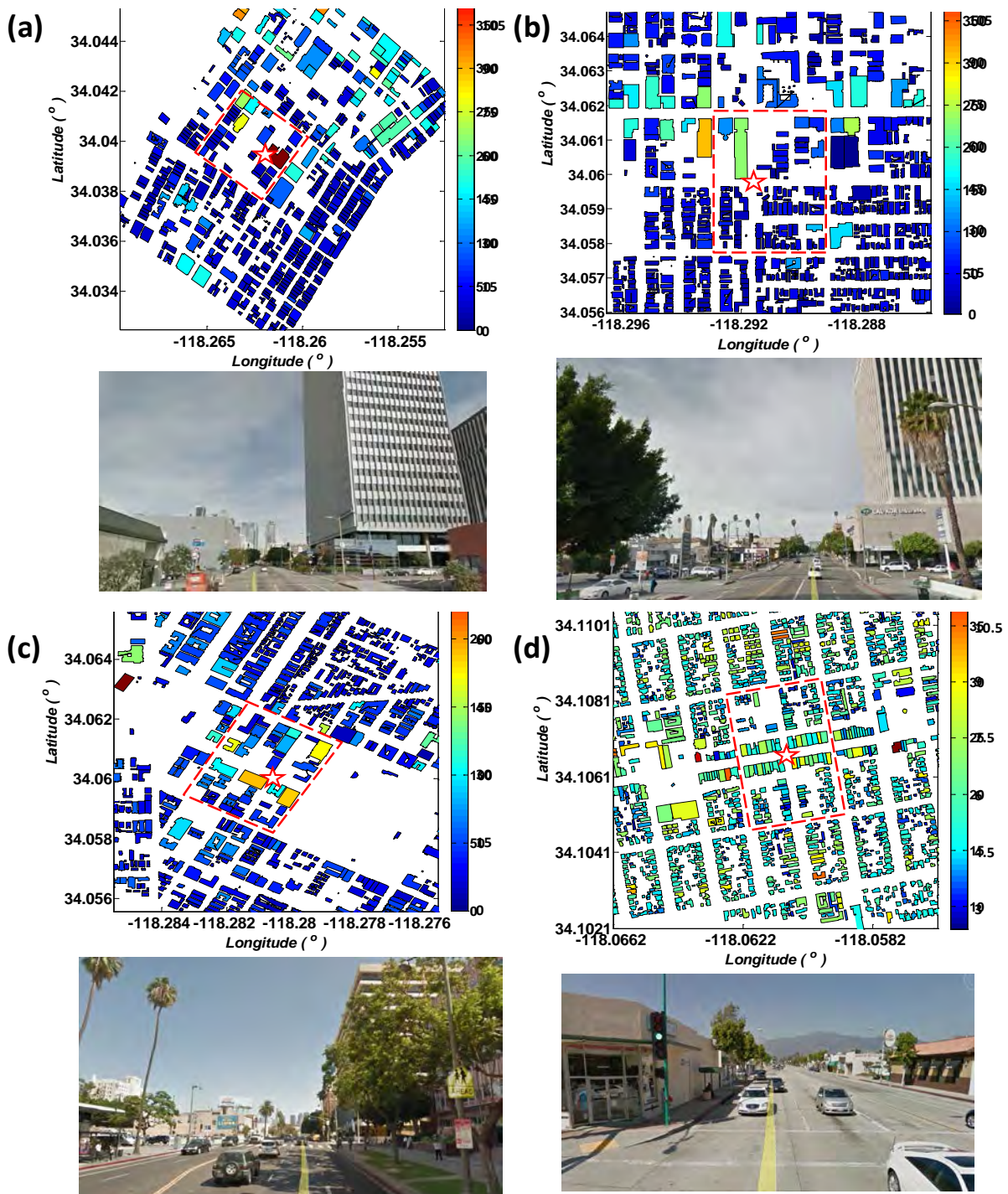
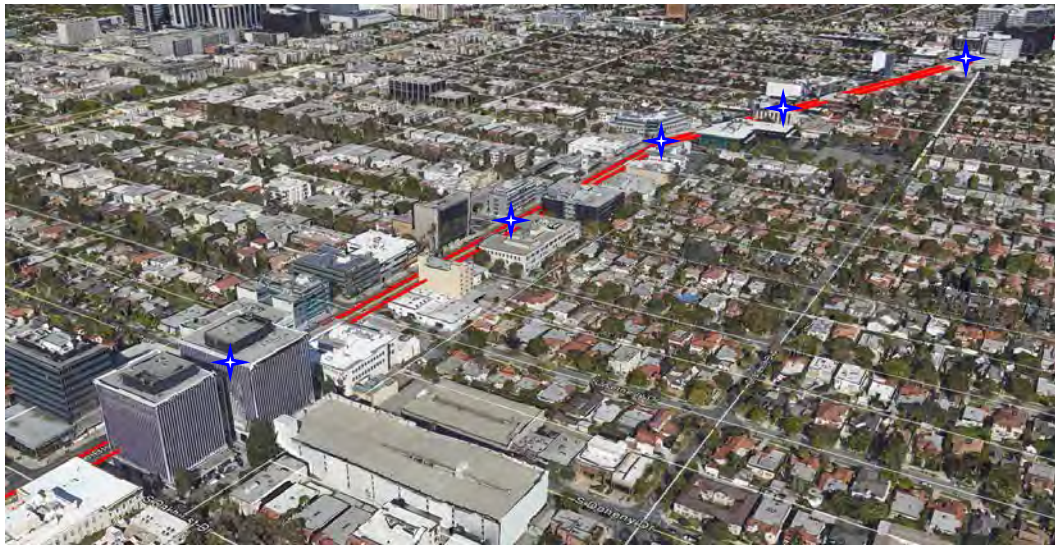


Figure 3. Built environments of sampling sites: (a) *Site 2* (Olive & 12<sup>th</sup> St.), (b) *Site 3* (Vermont & 7<sup>th</sup> St.), (c) *Site 4* (Wilshire & Carondelet St.) in Los Angeles, and (d) *Site 5* (Temple City & Las Tunas) in Temple City. Top plots represent building distributions and heights (by colors in feet). The dashed line shows the sampling area. Bottom photos show the street view of the streets around the intersections. Color bar represents building height in meters.

The 2014 summer sampling site was a 2 km-long section of Wilshire Blvd. located in Beverly Hills, CA (Figure 4). This site includes 5 signalized intersections and is surrounded by a variety of building configurations, with different traffic flow rates on the cross streets. Traffic was recorded at the two largest intersections, Doheney and La Cienega Blvd. that crossed Wilshire Blvd. Other sites were single intersections at which traffic was recorded in all four directions. The data from this site are discussed in the latter sections.



**Figure 4. Map of the Beverly Hills sampling route. Red line represents the mobile monitoring platform route and blue stars denote the locations of signaled intersections.**

### v.3.2. Instrumentation and Sampling Design

A fully-equipped Toyota RAV4 electric sub-SUV, maintained by ARB, served as a mobile monitoring platform (ARB-MMP). A suite of fast response instruments in the ARB-MMP measures various air pollutants, including UFP number concentrations and size distributions, nitrogen oxides (NO<sub>x</sub>), carbon monoxide (CO), carbon dioxide (CO<sub>2</sub>), particle-bound polycyclic aromatic hydrocarbons (PB-PAH), particulate matter with aerodynamic diameters less than 2.5 μm (PM<sub>2.5</sub>), and black carbon (BC) and have been used in a series of near-/on-road air quality studies (Choi et al. 2012a; Choi et al. 2013a; Hu et al. 2012; Kozawa et al. 2009, and others). When the ARB-MMP was not available due to maintenance, an electric vehicle (Chevrolet Volt or Nissan Leaf) equipped with a DiSCmini was used instead. The DiSCmini is a fast diffusion size classifier that measures UFP number concentration (20-700 nm size range) and the mean size of UFP collected every second. Many of the measurements were performed with a DiSCmini hand held particle counter (Matter Aerosol AG). As this instrument is relatively new, evaluations are only available for laboratory-generated nanoparticles under controlled indoor conditions (Bau et al. 2015; Mills et al. 2013).

A global positioning system, or GPS (GPSMAP 76CS, Garmin or BT-Q1000XT, Qstarz International Co., Ltd., depending on availability), was employed to record MMP positions every second, and the corrections of the GPS data were made using a line reference technique as described in detail in a companion paper (Ranasinghe et al. 2015). In this study, however, site-by-site comparisons are the main focus, and thus the highly spatially resolved data of the MMP were not used.

In general, the instruments in the MMP have different response times due to the characteristics of the instruments and differences in inlet length and flow rates. Air was drawn through a 6" diameter galvanized steel manifold installed through a window of the rear passenger space located 1.5 m above ground level. Sampling ports for each instrument were located in the middle of the manifold with short (0.5–2 m) sampling tubing (1/4" Teflon for gases and 1/4" conductive tubing for particles and 1/2" conductive tubing for FMPS). For each instrument, flow and zero checks were performed before and after each measurement session. To account for any slight day-to-day differences in response time, a time-lag correlation method was used in post-data processing to synchronize the response time of the instruments (Choi et al., 2012). Concentration data and MMP position data were recorded at 1 s time resolution. Table 5 below summarizes information on the time-response of the individual instruments employed in this study. A complete description of the MMP calibration procedures is available in Hu et al. (2009b).

**Table 4. Monitoring instruments on the mobile monitoring platform.**

Instrument	Measurement Parameter	Response time <sup>a</sup> (Inlet to record)
TSI Portable CPC, Model 3007	Sub-micrometer particle number count (10 nm–1 μm)	4 s
TSI FMPS, Model 3091	Size-segregated particle count (5.6–560 nm)	9 s
TSI DustTrak, Model 8520	PM <sub>2.5</sub> mass	5 s
EcoChem PAS 2000	Particle-bound PAH	10 s
Teledyne API Model 300E	CO	21 s
LI-COR, Model LI-820	CO <sub>2</sub>	7 s
Teledyne-API Model 200E	NO	22 s
Magee Scientific Aethalometer AE42	Black carbon	21 s
Vaisala Sonic Anemometer and Temperature/RH Sensor	Surface winds, temperature, and relative humidity	-
Garmin GPSMAP 76CS	Location and speed	-
Eurotherm Chessell Graphic DAQ Recorder	Data-logger	-

<sup>a</sup> Response time is an averaged value for smoke test results (Choi *et al.*, 2013).

In all cases, the inlet for instruments was located on the passenger side of the vehicle near the roofline, in as close proximity to the sidewalk as practical. The same post-data processes described in Choi *et al.* (2012a) were performed to synchronize instruments and precisely account for the response time (a time-lag correlation method on a twice-daily basis).

A combination of mobile and stationary measurements was conducted depending on the availability of instruments (see Table 1). Intensive measurements were conducted for ~ 2 hrs twice a day, once in the early morning (06:00 - 09:00) and once in mid-afternoon (13:00 - 17:00). These periods represent two distinct meteorological conditions: limited mixing in the mornings vs. vigorous vertical mixing due to surface heating in the afternoons. A schematic of the sampling design is shown in Figure 5. For the entire sampling period, the MMP drove four-leaf clover shaped routes around the main intersection, typically completing 7 to 12 repeats of the route for each morning or afternoon. To supplement mobile measurements, a pair of DiSCminis were deployed on pedestrian sidewalks to measure UFP number concentration. The DiSCmini pair, being positioned across the street from one another, sampled for 5 to 10 minutes at the mid-blocks and intersections on one street and then moved to other mid-block or intersection locations (see Figure 5 and Figure 6). The objective of mobile sampling was to obtain highly resolved spatial distributions of pollutant concentrations, whereas paired measurements of UFP are useful for investigating street canyon and other effects caused by in-canopy circulation in different built environments. Also, paired DiSCmini measurements were taken in the immediate location of pedestrians at a height near breathing zones and therefore acted as a surrogate for direct pedestrian exposure to vehicular emissions.

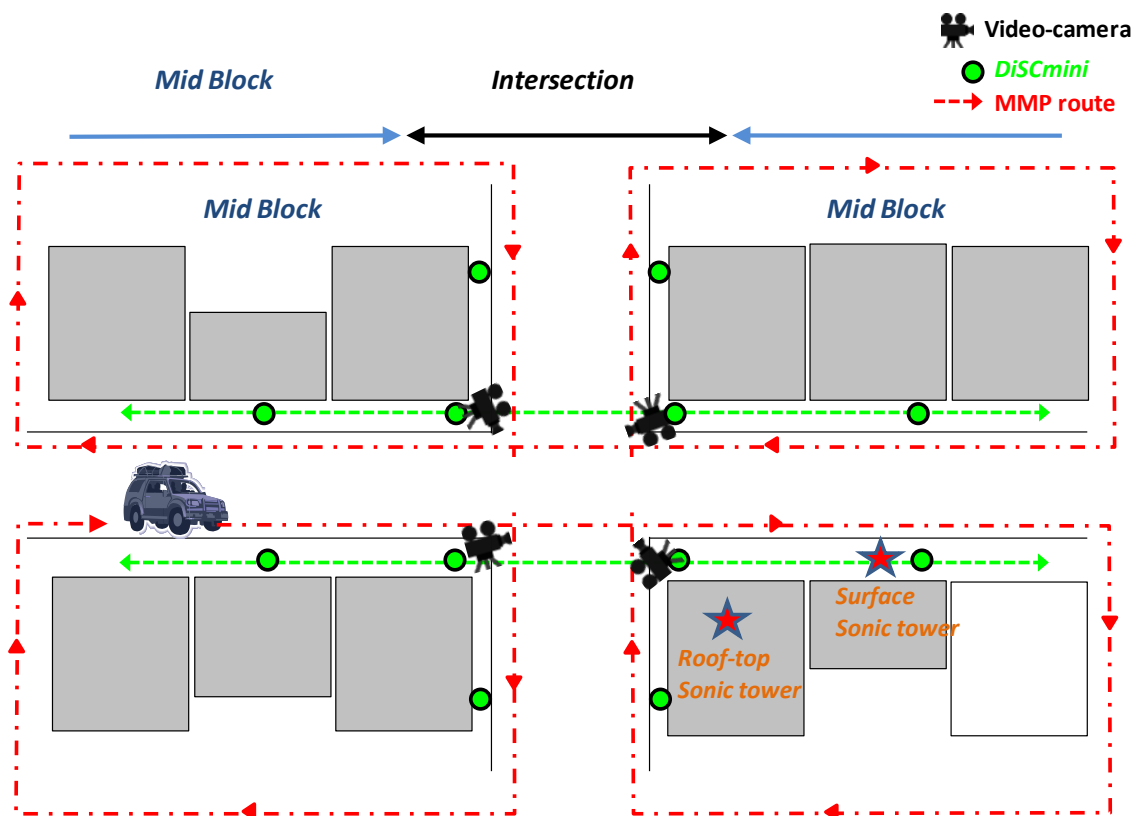


Figure 5. A schematic of the intersection sampling design. Green circles denote the location of a DiSCmini pair (across the street) for 5-minute stationary measurements. Red stars represent the location of surface and roof-top (only when roof-top access was possible) sonic towers. The actual positions and spatial scales are different from this illustration.

Systematic in-field inter-comparison between DiSCmini, Condensation Particle Counter (CPC, TSI 3007), and Scanning Mobility Particle Sizer (SMPS, TSI 3080) verified that the results from the DiSCmini for both particle number and size were in good agreement with conventional particle instruments. In this study, all DiSCmini data were converted to corresponding CPC values to be compared directly, because the CPC has more widely and conventionally been used in UFP air quality studies.

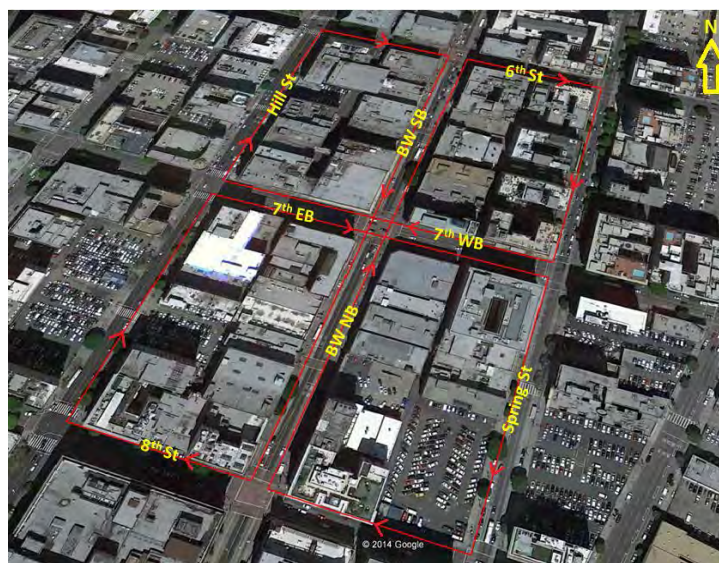


Figure 6. The sampling route of the mobile monitoring platform (MMP) in downtown Los Angeles. BW denotes Broadway and EB, WB, NB, and SB represent eastbound, westbound, northbound and southbound, respectively. Map source: Google Earth.

### v.3.3. Collecting meteorological data using MMP

The MMP was parked intermittently at various locations for 5 min periods to collect meteorological data from its sonic anemometer mounted on the roof of the MMP. In each measurement session, video recordings of the traffic were made at the central intersection using cameras mounted at each of the four corners of the intersection. Detailed information on the traffic signal light changes and the traffic counts for all four traffic flow directions were obtained manually by reviewing the video records. All data processing was done in MATLAB R2012a (The Mathworks, Inc.). Table 6 below summarizes the meteorological information that was collected at Site1 (Broadway and 7th).

**Table 5. Measurement periods and surface meteorology at BW-7th.**

Date	Measurement Period	BW			7 <sup>th</sup>		
		Wind speed (m s <sup>-1</sup> )	Wind direction <sup>#</sup>	Traffic flow (vehicles s <sup>-1</sup> )	Wind speed (m s <sup>-1</sup> )	Wind direction <sup>#</sup>	Traffic flow (vehicles s <sup>-1</sup> )
7/1/2013	09:15–11:45	0.96	SW	0.09	1.08	ESE-NE*	0.15
	15:30–18:00	0.91	SW	+	+	+	+
7/3/2013	08:15–11:00	1.34	SSE–SW*	0.10	1.06	ESE–NE*	0.13
	16:00–18:00	1.80	SW–S*	0.18	1.45	NE	0.18
7/5/2013	08:45–11:00	1.23	*	0.95	0.94	ESE–NW*	0.08
	15:30–18:15	1.13	SSW–NW*	0.14	1.48	NE	0.14

<sup>#</sup> NE (northeasterly), ESE (east-southeasterly), SSE (south-southeasterly), S (southerly), SSW (south-southwesterly), SW (southwesterly), NW (northwesterly).

\* variable wind (wind direction was spread over two or more quadrants).

+ data not available.

### v.3.4. Site, built environment, and traffic characteristics

The site, the built environment, and the traffic characteristics all play a role in the variability of UFP concentrations on and near a roadway. Figure 7 presents an aerial view of the Broadway transect that was examined in this study. In addition, Table 7 below provides definitions to many of the variables on Broadway transect (and any other transects) that can potentially impact the UFP concentration measurements while using MMP and semi-stationary monitoring. Table 8 provides information and summary of the statistics on the key variables described in Table 7 and how variant each of these variable parameters are on Broadway transect. This provides additional insight into the resulting data and how they may affect the ambient air measurements.



**Figure 7. Map of the Broadway Transect.**

**Table 6. Variable Definitions.**

All variables are continuous unless otherwise indicated	
Variable	Definition
Ultrafine particle concentration	Number of particles less than 100 nanometers in diameter measured in thousands per cubic centimeter of sampled air
Idle-to-moving	Binary variable indicating whether MMP is in queue
Speed	Measured speed of MMP measured in meters per second
Lane number	Lane position of MMP relative to right-hand curb.
Light-duty	Observed number of light-duty vehicles in visual range of MMP
Medium & Heavy-duty	Observed number of medium- or heavy-duty vehicles in visual range of MMP
Buses	Observed number of buses in visual range of MMP
Acceleration event	Binary variable indicating whether an acceleration event occurred in visual range of MMP
On-going Traffic	Indicates traffic conditions observed heading in same direction as MMP
On-coming Traffic	Indicates traffic condition observed heading in opposite direction as MMP
Crossing from the left traffic	Indicates traffic condition observed crossing direction of MMP from left
Crossing from the right traffic	Indicates traffic condition observed crossing direction of MMP from right
Intersection	Binary variable indicating no neighboring buildings to MMP (indicates MMP was in an intersection)
Average building height (m)	Observed average height of buildings directly neighboring MMP
Building height differential (m)	Height of building to the east relative to building to the west
North-south wind component	Wind speed in meters per second; positive if prevailing wind is from north, negative if from south
East-west wind component	Wind speed in meters per second; positive if prevailing wind is from east, negative if from west
Position	Linear reference unit measured in meters

As shown in Table 7, the mean level and standard deviation of *UFP* was 10.40 and 0.79 thousand/cm<sup>3</sup> respectively with a minimum value of zero and maximum value of 14.14. Later in our study, the variable, *UFP*, will be lagged to explore the correlation of recently measured *UFP* concentrations and contemporaneous *UFP* concentrations. We will define these lagged variables as *UFP*-1, *UFP*-2, *UFP*-3, etc. to indicate that the *UFP* concentrations were 1, 2 and 3, seconds prior to the contemporaneous *UFP* measurement. These sensitivity analysis provides additional confidence in the results during detailed analysis of the MMP and stationary measurements.

**Table 7. Summary Statistics of Variables.**

	Mean	Std. Dev.	Min	Max
Ultrafine Particle Concentration (thousands/cm <sup>3</sup> )	10.4	0.79	0	14.14
<i>MMP State of Motion and Speed</i>				
Idle-to-moving	0.27	0.45	0	1
Speed (m/s)	7.53	8.52	0	174.83
Lane number	3.86	0.47	1	5
<i>On-going Traffic</i>				
Light-duty	0.054	0.33	0	9
Medium & heavy-duty	0.004	0.066	0	1
Buses	0.006	0.082	0	2
Acceleration event	0.014	0.118	0	1
<i>On-Coming Traffic</i>				
Light-duty	0.276	0.57	0	4
Medium & heavy-duty	0.012	0.109	0	1
Buses	0.028	0.165	0	2
Acceleration event	0.013	0.112	0	1
<i>Crossing from the Left Traffic</i>				
Light-duty	0.06	0.252	0	2
Medium & heavy-duty	0.003	0.054	0	1
Buses	0.003	0.052	0	1
Acceleration event	0.003	0.052	0	1
<i>Crossing from the Right Traffic</i>				
Light-duty	0.064	0.266	0	3
Medium & heavy-duty	0.005	0.073	0	1
Buses	0.001	0.037	0	1
Acceleration event	0.004	0.062	0	1
<i>Built Environment</i>				
Intersection	0.12	0.32	0	1
Average building height (m)	16.62	15.53	0	71.24
Building height differential (m) <sup>a</sup>	-3.88	20.51	-61.57	61
<i>Meteorology</i>				
North-south wind component (m/s) <sup>b</sup>	-1.89	2.01	-3.91	1.31
East-west wind component (m/s) <sup>b</sup>	-0.68	1.7	-2.99	1.79
<p><sup>a</sup> Difference in height of neighboring buildings is positive if the building to the east is taller, and negative if the building to the west is taller.</p> <p><sup>b</sup> North-south wind component is positive if the north-south component of the prevailing wind is northerly, negative if southerly. East-west wind component is positive if the east-west component of the prevailing wind is easterly, negative if westerly.</p>				

***MMP Street Position and Velocity.*** We collected a wide range of independent variables that may be correlated with changes in UFP concentrations. The variable *speed* indicates the velocity of the MMP measure in meters per second (m/s) with a mean of 7.53 m/s. The variable *idle-to-moving* indicates that the MMP is stationary in a queue of traffic, most frequently waiting to cross an intersection. *Lane number* indicates what street lane the MMP occupies, relatively to the right hand curb with the parking lane nearest the curb being 1 and middle left-hand turning lane being 5. The mean value for lane is 3.86 indicating that the MMP was most often traveling in lane 3, near-center travel lane. Later in our analysis we will employ a variable *position* which indicates the linear

coordinates of the MMP along a linear transect representing the entire transect. We will discuss the use of this locator variable in later analysis.

**Traffic Conditions.** Figure 2 may serve as a visual aid in understanding the definition of variables that includes i) traffic conditions around the MMP and ii) the adjacent built and transportation environment. As the MMP traveled along Broadway we characterized traffic that was a) on-going, for traffic traveling in the same southward direction as the MMP, b) on-coming traffic, for vehicles traveling northward on Broadway, approaching and then passing the MMP on its left side, c) when the MMP approached or was stopped before an intersection, d) as MMP crossed the intersection from the left, and e) traffic crossing the intersection from the right. For each of these traffic directions, we further characterized traffic in terms of i) acceleration events, indicating that traffic had transitioned from a stationary position at the traffic light to a state of motion as traffic accelerated. We also characterized the number of vehicles moving in each direction by type of vehicle, indicating the number of ii) light-duty vehicles, iii) medium and heavy-duty vehicles and iv) buses. Table 2 reveals that the on-going light-duty traffic counts are higher compared to on-coming traffic counts. For example, on-going light-duty vehicles exhibited a mean count of 0.330 per second while on-coming light-duty vehicles exhibited a mean of 0.109 per second. The traffic crossing the MMP from the left and from the right exhibited comparable counts of 0.252 and 0.266 per second, respectively for light-duty vehicles.

**Adjacent Built Environment.** As the MMP travelled southward we also characterized the built environment features immediately adjacent at the time scale of one second. We chose to characterize the adjacent *average building height*, mean of 16.62, with a minimum of zero for parking lots or vacant land and a maximum of 71 meters for tall buildings. We also characterized the *building height differential*, subtracting the height on the west side from the east side as measured in meters. While the mean of the building height differential was only -3.88 meters, the minimum was -61.57 meters while the maximum was 61 meters. The variable *intersection* indicated when the MMP was in an intersection. The variable's mean of 0.12 in Table 2 suggests that the MMP was in an intersection approximately 12% of the time spent traversing the transect.

## v.4. Results and Discussion

### v.4.1. The effects of the traffic patterns, micro-meteorology, and built environment on street level UFP concentrations at a block scale

#### v.4.1.1. Characteristics of traffic patterns, micro-meteorology, and built environments

Observed traffic characteristics at each of the sites are shown in Table 3. The basic traffic light stops were 69 or 89 seconds; these changed actively depending on traffic conditions. Traffic rates ( $vehicles \cdot min^{-1}$ ) were comparable or higher during the afternoon sampling compared to the morning sampling periods, except at *Site2*. The highest traffic rates were observed at *Site3* and *Site5* in both the mornings and the afternoons. Although the traffic rates were comparable between *Site3* and *Site5*, traffic density at *Site3* was significantly higher due to unequal distributions of traffic between the two streets and the denser arterial-street-network in this commercial/business district. Of the five sampling sites, *Site1* and *Site5* had equal traffic between north-south and east-west bound streets while *Site3* and *Site4* showed significant disparity in traffic rates. *Site2* also had unequal traffic distributions, but the overall traffic rate was comparatively small. Heavy- and medium-duty vehicles were encountered infrequently for all sampling sites ( $< 1.5 vehicle \cdot min^{-1}$ ).

Observed meteorology including detailed surface micrometeorology is summarized in Table 8 and Figure 8. Morning meteorology was generally calm for all sampling sites, with mean wind speeds below  $1.4 \text{ m}\cdot\text{s}^{-1}$  with  $1\sigma$  values within  $0.4 \text{ m}\cdot\text{s}^{-1}$ ; with the exception of 9/25/2013 at *Site2*, where the wind was exceptionally strong at  $1.9 (\pm 0.6) \text{ m}\cdot\text{s}^{-1}$ . Friction velocity ( $u_*$ ), vertical wind fluctuation ( $\sigma_w$ ), and turbulence kinetic energy (*TKE*) appeared to be similar among the sites in the morning (see Table 9). In the afternoon, wind speeds increased up to  $3.3 \text{ m}\cdot\text{s}^{-1}$  with  $1\sigma$  values within  $0.6 \text{ m}\cdot\text{s}^{-1}$ . Thus, meteorological conditions were not variable for the 2-hour sampling periods. Turbulence parameters for afternoon sampling periods varied more widely between sites. For instance, *Site1*, *Site4*, and *Site5* had less turbulent surface conditions than *Site2* and *Site3*. As noted earlier *Site2* and *Site3* have more heterogeneous building morphology with one or two isolated tall buildings together with large open areas and/or low building areas than other sampling sites. This heterogeneous building configuration may generate more intense turbulence near the intersections as discussed later.

**Table 8. Surface micro-meteorological conditions observed during sampling periods. Values in parentheses represent standard deviations of the respective parameters.**

	Morning					Afternoon				
Date	Temp. (°C)	<sup>a</sup> Wind speed m/s	$u_*$ m/s	$\sigma_w$ m/s	TKE $\text{m}^2 \text{s}^{-2}$	Temp. (°C)	<sup>a</sup> Wind speed m/s	$u_*$ m/s	$\sigma_w$ m/s	TKE $\text{m}^2 \text{s}^{-2}$
Site1 (Street canyon)										
7/1	25.9 ( $\pm 1.7$ )	1.0 ( $\pm 0.2$ )	0.23	0.37	0.47	32.2 ( $\pm 2.1$ )	1.1 ( $\pm 0.3$ )	0.23	0.40	0.46
7/2	26.1 ( $\pm 1.4$ )	1.2 ( $\pm 0.3$ )	0.27	0.40	0.61	23.5 ( $\pm 1.2$ )	1.7 ( $\pm 0.3$ )	0.29	0.52	1.02
7/3	23.0 ( $\pm 1.3$ )	1.2 ( $\pm 0.1$ )	0.17	0.35	0.47	22.5 ( $\pm 1.0$ )	1.7 ( $\pm 0.2$ )	0.36	0.57	0.97
7/5	20.6 ( $\pm 1.4$ )	0.9 ( $\pm 0.2$ )	0.19	0.30	0.47	24.0 ( $\pm 0.6$ )	1.6 ( $\pm 0.2$ )	0.15	0.48	1.21
11/13	24.2 ( $\pm 0.4$ )	0.8 ( $\pm 0.2$ )	0.20	0.27	0.18	29.9 ( $\pm 0.6$ )	0.5 ( $\pm 0.1$ )	0.12	0.19	0.08
Site2 (Isolated skyscraper with low traffic rates)										
9/24	26.6 ( $\pm 0.4$ )	0.8 ( $\pm 0.2$ )	0.15	0.24	0.23	28.3 ( $\pm 0.2$ )	2.1 ( $\pm 0.6$ )	0.72	0.73	1.90
9/25	21.7 ( $\pm 0.5$ )	1.9 ( $\pm 0.6$ )	0.88	0.97	1.83	24.9 ( $\pm 0.4$ )	3.3 ( $\pm 0.4$ )	0.48	0.59	1.84
Site3 (Isolated skyscrapers with high traffic rates)										
10/7	22.8 ( $\pm 0.5$ )	1.4 ( $\pm 0.4$ )	0.13	0.41	0.77	27.8 ( $\pm 0.7$ )	2.6 ( $\pm 0.5$ )	0.40	0.68	2.11
10/14	17.9 ( $\pm 1.4$ )	0.7 ( $\pm 0.1$ )	0.35	0.38	0.31	28.6 ( $\pm 0.4$ )	1.9 ( $\pm 0.3$ )	0.42	0.61	1.26
11/18	15.4 ( $\pm 0.4$ )	0.9 ( $\pm 0.2$ )	0.23	0.36	0.39	20.2 ( $\pm 0.4$ )	2.6 ( $\pm 0.3$ )	0.27	0.70	1.60
Site4 (One-side medium height buildings)										
11/1	17.2 ( $\pm 1.7$ )	1.2 ( $\pm 0.4$ )	0.16	0.39	0.54	29.1 ( $\pm 0.4$ )	0.9 ( $\pm 0.2$ )	0.43	0.56	0.51
11/6	15.1 ( $\pm 1.4$ )	0.9 ( $\pm 0.1$ )	0.20	0.37	0.35	26.3 ( $\pm 0.3$ )	0.6 ( $\pm 0.2$ )	0.27	0.27	0.25
11/20	16.0 ( $\pm 0.3$ )	0.5 ( $\pm 0.1$ )	0.19	0.23	0.17	19.1 ( $\pm 0.2$ )	1.7 ( $\pm 0.3$ )	0.13	0.38	0.74
Site5 (Low and flat)										
8/6						29.4 ( $\pm 0.6$ )	1.5 ( $\pm 0.1$ )	0.45	0.63	1.07
9/17	21.4 ( $\pm 0.5$ )	0.7 ( $\pm 0.1$ )	0.10	0.26	0.24	30.3 ( $\pm 1.1$ )	1.1 ( $\pm 0.2$ )	0.26	0.40	0.47
9/18	20.0 ( $\pm 0.6$ )	0.6 ( $\pm 0.1$ )	0.18	0.27	0.23	29.0 ( $\pm 0.8$ )	1.0 ( $\pm 0.2$ )	0.23	0.39	0.41

a. Wind speeds represent the ground level values obtained with sonic anemometer measurements. Thus wind direction is strongly influenced by localized built environment, and not shown in this table. Prevailing wind direction over the urban canopy obtained from nearby weather station is also presented.

	Morning			Afternoon		
Date	Temp. (°C)	Wind speed (m/s)	Wind direction (degree)	Temp. (°C)	Wind speed (m/s)	Wind direction (degree)
<i>Site1 (Street canyon)<sup>a</sup></i>						

7/1	27.7 ( $\pm 1.1$ )	1.0 ( $\pm 0.2$ )	178 ( $\pm 29$ )	33.9 ( $\pm 2.2$ )	1.1 ( $\pm 0.2$ )	199 ( $\pm 10$ )
7/2	N/A	N/A	N/A	26.3 ( $\pm 1.2$ )	1.6 ( $\pm 0.3$ )	189 ( $\pm 6$ )
7/3	N/A	N/A	N/A	N/A	N/A	N/A
7/5	23.3 ( $\pm 0.9$ )	1.1 ( $\pm 0.3$ )	121 ( $\pm 79$ )	26.0 ( $\pm 0.5$ )	2.3 ( $\pm 0.4$ )	250 ( $\pm 9$ )
11/13	N/A	N/A	N/A	N/A	N/A	N/A
<i>Site2 (Isolated skyscraper with low traffic rates)<sup>b</sup></i>						
9/24	23.9 ( $\pm 2.8$ )	0.7 ( $\pm 1.2$ )	30(-) <sup>c</sup>	27.4 ( $\pm 0.6$ )	2.1 ( $\pm 0.6$ )	270 (-)
9/25	20.0 ( $\pm 1.1$ )	1.9 ( $\pm 0.6$ )	100(-)	23.7 ( $\pm 0.3$ )	1.5 (-)	200 (-)
<i>Site3 (Isolated skyscrapers with high traffic rates)<sup>b</sup></i>						
10/7	25.2 ( $\pm 2.8$ )	Calm	Calm	26.5 ( $\pm 0.8$ )	1.7 ( $\pm 0.3$ )	260 (-)
10/14	17.2 ( $\pm 3.1$ )	Calm	Calm	26.7 ( $\pm 0.6$ )	1.5 (-)	290 (-)
11/18	15.5 ( $\pm 1.4$ )	Calm	Calm	19.2 ( $\pm 0.3$ )	1.8 ( $\pm 0.4$ )	280 (-)
<i>Site4 (One-side medium height buildings)<sup>b</sup></i>						
11/1	17.2 ( $\pm 4.2$ )	Calm	Calm	29.2 ( $\pm 0.3$ )	1.4 ( $\pm 1.3$ ) <sup>d</sup>	280 (-)
11/6	19.6 ( $\pm 3.3$ )	1.0 ( $\pm 0.9$ )	N/A	25.6 ( $\pm 1.6$ )	1.0 ( $\pm 0.9$ )	260 (-)
11/20	16.6 ( $\pm 0.7$ )	Calm	Calm	17.9 ( $\pm 0.1$ )	-	-
<i>Site5 (Low and flat)<sup>a</sup></i>						
8/6	N/A	N/A	N/A	N/A	N/A	N/A
9/17	N/A	N/A	N/A	29.1( $\pm 1.1$ )	2.0 ( $\pm 0.3$ )	186 ( $\pm 17$ )
9/18	20.1 ( $\pm 0.8$ )	1.0 ( $\pm 0.2$ )	40 ( $\pm 48$ )	28.2 ( $\pm 0.6$ )	2.3 ( $\pm 0.6$ )	199 ( $\pm 14$ )

a. Data from sonic anemometer installed on the roof of the building

b. Weather station data located at the University of Southern California (USC)

c. (-) denotes lack of data

d. Inferred from incomplete data from USC weather station

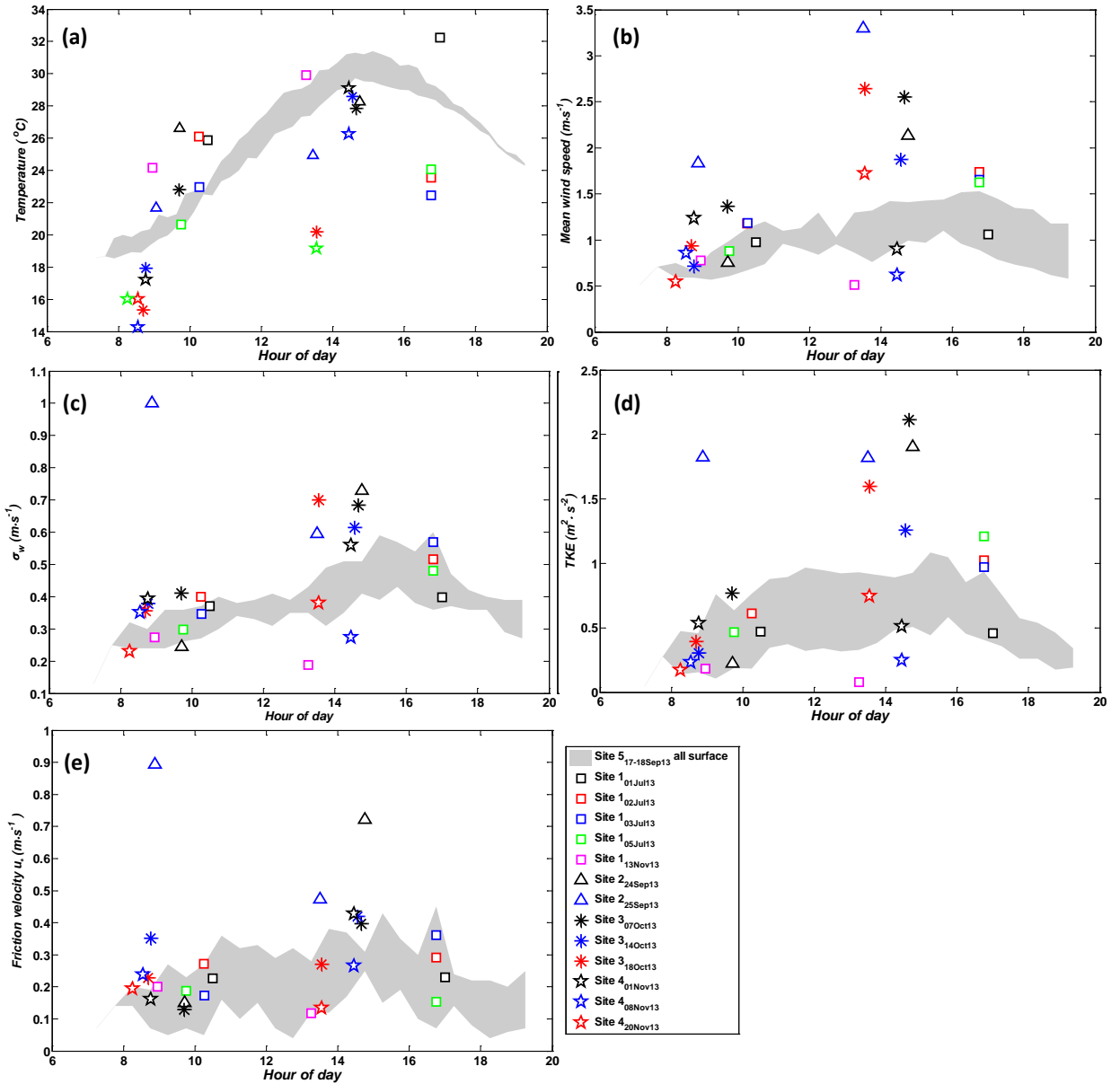


**Figure 8. Micro-meteorological characteristics for sampling sites on individual days (specified by colors): (a) temperature, (b) mean wind speed, (c) vertical fluctuation of winds, (d) turbulence kinetic energy, and (e) friction velocity in the ground level. The shaded areas represent diurnal variations of data obtained at *Site5*, and squares, triangles, asterisks, and stars denote representative values for the *Site1*, *Site2*, *Site3*, and *Site4*, respectively.**

To quantitatively investigate the built-environmental effects on street-level pollutant distributions, the key built-environmental factors were defined and calculated: the number of buildings in the sampling area; the mean building height (Eq. 1); building area-weighted height (Eq. 2); building heterogeneity (Eq. 3), street width, block length, and ratio of the area occupied by buildings to the total sampling area (building density; Eq. 4):

$$\text{Mean building height, } H_{\text{bldg}} = \frac{\sum_{i=1}^N H_i}{N} \quad (1)$$

$$\text{Building area-weighted building height, } H_{\text{area}} = \frac{\sum_{i=1}^N (S_i \times H_i)}{\sum_{i=1}^N S_i} \quad (2)$$

$$\text{Building heterogeneity} = H_{\text{area}} / H_{\text{bldg}} \quad (1 = \text{perfectly homogeneous}) \quad (3)$$

$$\text{Building density} = \frac{\sum_{i=1}^N S_i}{\text{sampling area}} \quad (1 = \text{entirely covered by buildings, } 0 = \text{open space}) \quad (4)$$

where,  $N$  is number of buildings in the sampling area,  $H_i$  and  $S_i$  are height and area of the  $i^{\text{th}}$  building, respectively. *Sampling area* is defined as the area of the rectangle covering the sampling area, as shown in Figure 2. We note that a simple arithmetic mean of  $H_{\text{bldg}}$  can be significantly lowered when a sampling area consists of one very large isolated skyscraper and many small short buildings such as in *Site2* and *Site3*. Thus, we use  $H_{\text{area}}$ , which is defined as the building area-weighted building height (Eq. 2). Consequently, the dimensionless ratio of  $H_{\text{area}}$  to  $H_{\text{bldg}}$  represents the building heterogeneity; this has a value of 1 for perfectly homogeneous building morphology and higher values for more heterogeneous building morphology. *Site1* and *Site5* have the most homogeneous built environments (heterogeneity of 1.16 and 1.09, respectively) but are very different: *Site1* has all tall buildings (>40m height street canyon) and *Site5* has all small one-story buildings (lowest building canopy of 6 m). Tall buildings on one side and small ones on the other side gave *Site4* an intermediate homogeneity of 1.39. *Site2* and *Site3* were the most heterogeneous (2.01 and 2.21, respectively). These quantitative parameters can be compared directly with our observed UFP concentrations to find the direct effects of built environments.

#### v.4.1.2. General Features of UFP concentrations

To compare the representative levels of pollutants due to roadway emissions in various built environments, concentrations obtained from mobile measurements within each sampling area were averaged. Due to significant differences in meteorology between early mornings and afternoons (e.g., boundary layer depth, vertical mixing capacity, prevailing winds, and possibly secondary formation of nucleation mode particles), the results from the morning and the afternoon sampling were analyzed and discussed separately.

Figure 9 shows the daily mean UFP concentrations ([UFP] hereafter) for each sampling site. In general, [UFP] were higher in the morning than in the afternoon due to lower boundary layer heights with less turbulence, which limit vertical dispersion of emissions and increase pollutant residence time in the surface layer. Exceptions were *Site5*, *Site2* on September 5th, and *Site1* on July 5th, which showed higher concentrations in the afternoon. This cannot be explained by either emissions or dispersion because traffic flow rates were comparable to morning sampling events and the near surface atmospheric condition was more turbulent with a deeper boundary layer in the afternoon. The estimated boundary layer heights from vertical temperature profiles observed at Los Angeles International Airport (18 km southwest from *Site1*) were at least two times greater in the afternoon than morning sampling events on the following days: 236 m vs. 798 m on 9/5/2013; 174 m vs. 361 m on 9/17/2013; and 298 m vs. 486 m on 9/18/2013 (data on 7/5/2013 are not available).

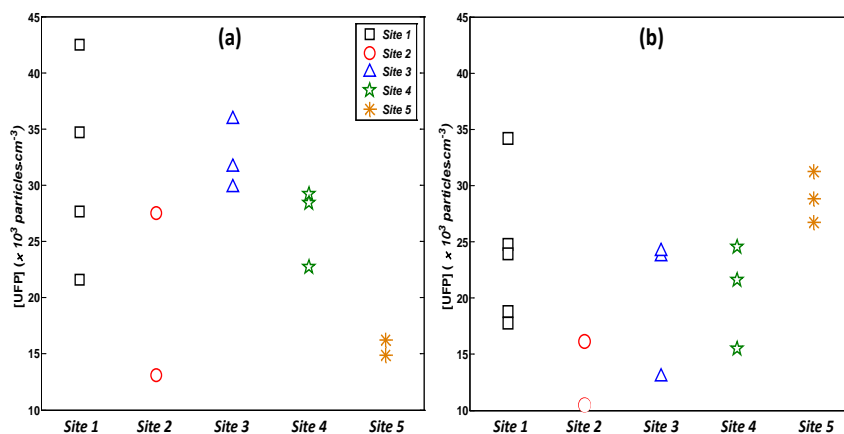


Figure 9. Daily averaged [UFP] in the (a) morning and (b) afternoon sampling events at site.

We hypothesize that enhanced afternoon concentrations were caused by photochemical secondary production of UFP (Hu et al. 2012; Ning et al. 2007). The interesting feature is that the afternoon elevation in the transient high-spikes-removed [UFP] was observed only when the morning [UFP] were less than  $2 \times 10^4 \text{ particles} \cdot \text{cm}^{-3}$ . On the other days, morning and afternoon [UFP] were linearly related to one another (Figure 10). In the morning of July 5th at *Site1*, however,  $\text{PM}_{2.5}$  values were extraordinarily high (above the upper limit of DustTrak,  $> 1 \text{ mg/m}^3$ ), presumably due to Independence Day fireworks on the evening of July 4th. Thus, lower [UFP] in the morning could be due to lower traffic (24% lower) and/or an increased coagulation sink for fresh UFP from the dramatically increased  $\text{PM}_{2.5}$  (Choi and Paulson 2016). *Site1*, the street canyon site in DTLA, had the highest [UFP] in both morning and afternoon, likely due to limited mixing with upper ambient air. *Site1* has a fairly tall, homogeneous building height and large simple aspect ratio,  $A_r=1.7$  (defined as the ratio of  $H_{area}$  to the mean street width, Table 2). *Site5* had the lowest [UFP] in the morning presumably because the small  $H_{area}$  and  $A_r$  (Table 2) help enhance the vertical mixing. *Site2* also had low [UFP] compared to the other sites, even though the simple  $A_r$  at this site is highest ( $A_r=1.9$ ). This can be explained by relatively low traffic flow rates at this site, combined with a negligible number of motor vehicles in queues during red lights at intersections. We also note that the simple  $A_r$  does not account for open spaces (e.g. the gaps between buildings or large parking lots). The high  $A_r$  at *Site2* derives from two tall isolated skyscrapers but this sampling site also has vast open parking areas (Figure 3), as shown by the minimal number of buildings in the selected area (Table 2). Morning [UFP] at *Site3* were comparable to *Site1* but sharply decreased in the afternoon, reaching levels similar to *Site4* that is lower than *Site1*. The elevated concentrations in the morning at *Site3* were likely due to both the heavy traffic flows and traffic density (Table 3). However, given that traffic flow rate and traffic density at *Site3* were similar during both the morning and the afternoon and higher than those at *Site1* and *Site4*, lower afternoon [UFP] (relative to *Site1* and *Site4*) cannot be readily explained with only traffic parameters. Consequently, these observations strongly suggest that [UFP] for each site were controlled by different factors (discussed quantitatively in later sections) depending on meteorological and built-environmental conditions.

#### v.4.1.2.1. Identification and replacement of transient high-spikes from high-emitting or accelerating vehicles

The UFP time-series obtained with the MMP includes a significant portion of transient concentration spikes (ca. 10 to 15%) due to high emitting vehicles (HEV) encountered during measurements (Choi et al. 2013a). These short-lived spikes can be higher than the baseline by factors of  $\sim 3$  to 50 and affect the mean concentrations. Here we used an approach developed by Choi et al. (2013a) to separate the transient HEV spikes from the baseline variations.

The initial baseline variations were obtained from least squares quadratic polynomial fitting resistant to outliers as a smoothing function. Then, the standard deviation of initial baseline-subtracted UFP ( $\sigma_{\Delta UFP}$ ) was calculated. The initial threshold value ( $C_{T0}$ ) was defined as 3 times of initial  $\sigma_{\Delta UFP}$  and the new threshold value ( $C_{T1}$ ) was calculated using  $3 \times \sigma_{\Delta UFP < C_{T0}}$  for the dataset of  $\Delta UFP < C_{T0}$ . This step was repeated until the threshold values converged on the specific constant value. In general, the threshold values converged within 8 iterations. The UFP concentrations higher than the final  $C_T$  were flagged as transient spikes and replaced with corresponding baseline values if needed. Figure 10 below represents the morning and afternoon [UFP] comparisons after the removal of transient high-spikes from the time-series at each of the sampling sites.

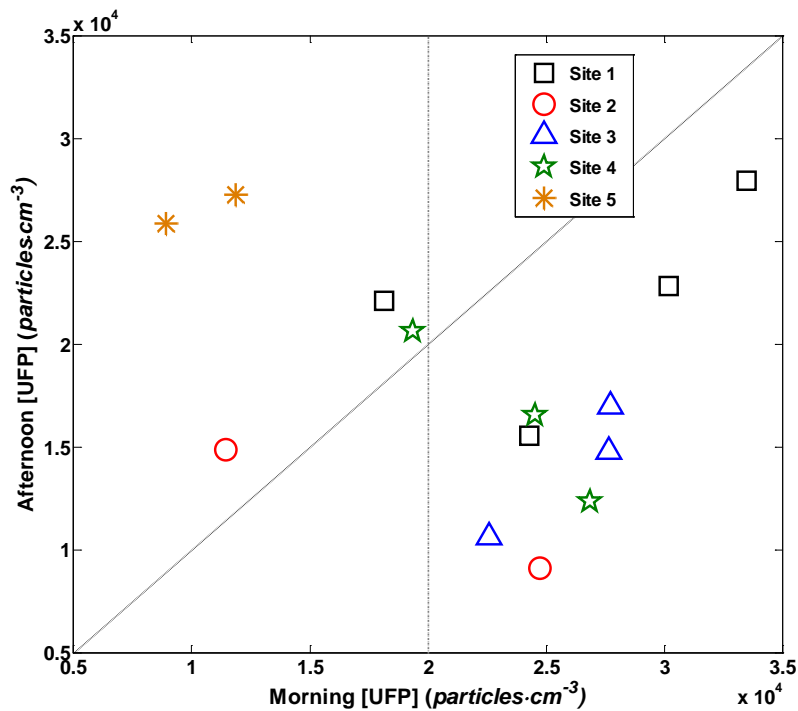


**Figure 10. The mean [UFP] of the transient high-spikes-removed time-series over the sampling areas in the morning vs. afternoon. Site 5 showed significant increases in [UFP] in the afternoon compared to the morning values despite comparable traffic volumes and more favorable atmospheric dispersive capacity.**

#### *v.4.1.3. Elevated emissions at the intersections*

One of the objectives of this field study was to investigate variations in pedestrian exposure to roadway emissions at different locations. In this respect, the study present general quantitative impacts of vehicle acceleration at intersections. Figure 11 shows the mean [UFP] at intersection corners (measured with stationary DiSCminis) vs. the average for the whole sampling area (measured with the MMP) at each of the sampling sites. The intersection averages were consistently higher than the whole sampling area average in both morning and afternoon sampling events for all sites except *Site3* afternoon. In the morning, [UFP] at the intersections was higher than the sampling area average by 24%, 10%, 5%, 11% and 55% at *Site1*, 2, 3, 4 and 5, respectively; in the afternoon, intersections corners were higher by 36%, 31%, -14%, 18% and 31%, respectively. Traffic at *Site3* was concentrated on Vermont Ave. and, due to a long queue that covered the entire sampling blocks, acceleration events occurred over the whole sampling section of Vermont Ave., likely causing less significant intersection impacts.

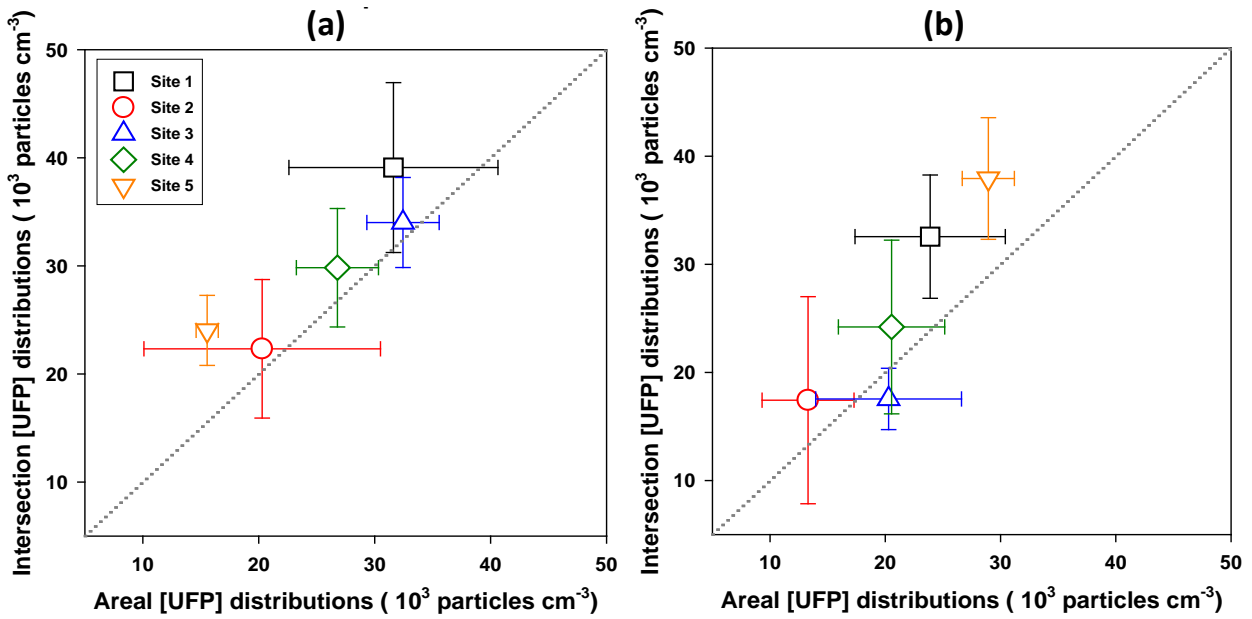


**Figure 11.** The mean intersection vs. area-wide [UFP] distributions (a) in the morning and (b) in the afternoon sampling events at each sampling site. Vertical and horizontal bars denote standard deviations.

Consistently higher [UFP] at the corners of intersections provides clear evidence that acceleration of vehicles at intersections increases pedestrian exposure to UFP. This is consistent with the argument in Klems et al. (2010) that the dominant period of transient spikes in UFP time-series matches traffic-light cycles. Although Klems et al. (2010) addressed only occurrences and periods of spikes from the intersection accelerations, this study, in addition, observed that the spike-removed baseline levels obtained with the same method in Choi et al. (2013a) were higher at intersection corners compared to the values over the sampling area: 29/33%, 15/38%, 2/3%, 7/18%, and 61/27% for *Sites 1, 2, 3, 4, and 5* in the morning/afternoon, respectively (Figure 12). This implies, perhaps unsurprisingly, that higher emissions from vehicle accelerations at intersections are quickly mixed with ambient air and, at steady-state, result in persistently higher [UFP] in the intersection areas.

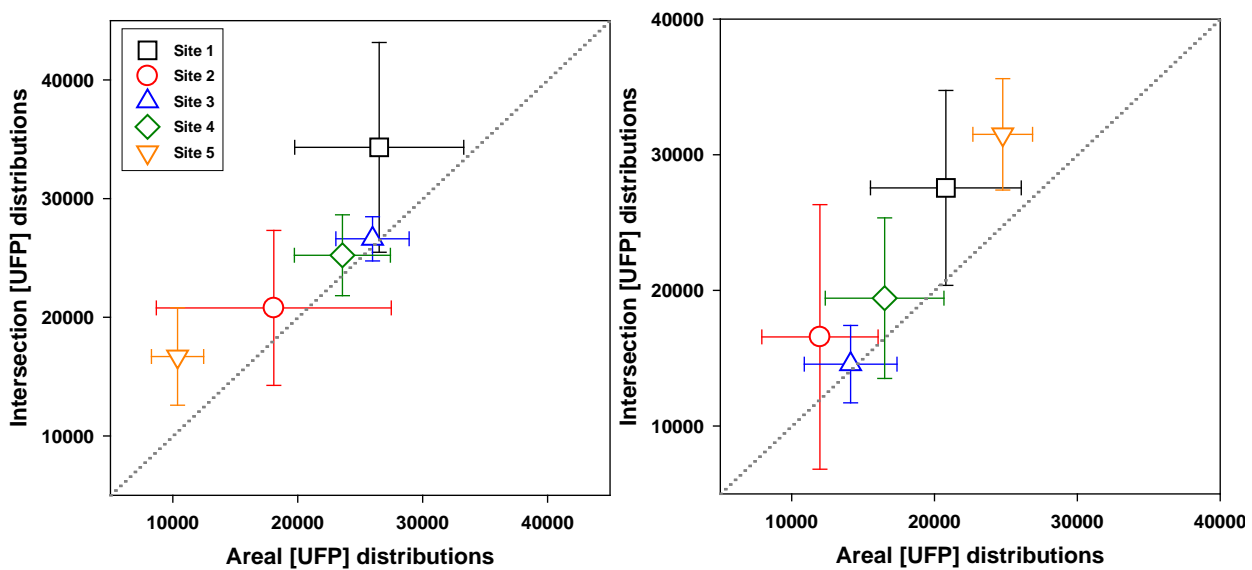


**Figure 12.** Comparisons of [UFP] variations in baseline time-series at the intersections and over the sampling area at (a) in the morning and (b) in the afternoon. Horizontal and vertical bars denote  $1\sigma$  variations.

Given that the MMP route includes intersection areas (Figure 2) and the peak concentrations due to acceleration do not necessarily appear exactly at the corners (they can instead appear before and/or after intersections) (Ranasinghe et al. 2015), the concentration difference at intersection vs. over the sampling area can be higher than the values presented above. More complete analyses for the intersection impacts (including the locations and shapes of intersection peaks) will be presented separately.

#### v.4.1.4. Factors controlling near-roadway UFP concentrations

##### v.4.1.4.1. Calm morning conditions

Most morning sampling events were calm, and meteorological variations between sites were not sufficient to explain the wide [UFP] variations among sampling sites (Figure 8). Traffic differences were noticeable between sites, but day-to-day variations at a single site were relatively insignificant. It appears that, in general, higher traffic rates led to higher levels of UFP, except at the two sites with extreme built-environments: the street canyon (*Site1*) and the low, flat canopy (*Site5*). The tall, homogeneous building canopy in the street canyon had higher [UFP] compared to observed traffic flow rates, and the opposite was true for the homogeneous built environment with the lowest building canopy (Figure 13).

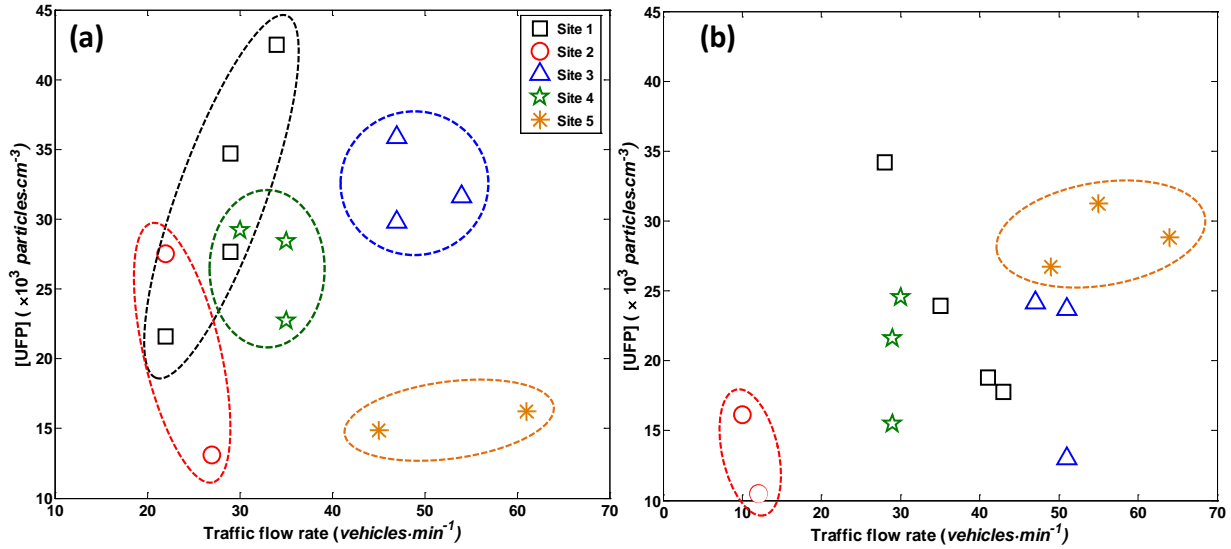


Figure 13. Daily [UFP] as a function of traffic flow rates (vehicles·min<sup>-1</sup>) (a) in the morning and (b) in the afternoon sampling events. Ovals show a group of sampling site.

A noticeable positive correlation was found between [UFP] and building area-weighted building height,  $H_{area}$ , particularly in the morning (Figure 14). *Site1* and *Site2* have similar  $H_{area}$  values of around 40 m, however, the high  $H_{area}$  at *Site2* results from few very tall buildings (~130 m) on a site with many large open parking lots around the intersection (Table 2 and Figure 3a), while *Site1* is largely surrounded by ~40 m buildings. To better capture the characteristics of different built-environment, a block-scale areal aspect ratio ( $Ar_{area}$ ) was developed (Eq. 5):

$$Ar_{area} = \frac{H_{area}}{L_{diag} \times \left(1 - \sum S_{bldg} / A_{site}\right)} = \frac{H_{area}}{L_{diag} \times \left(A_{open} / A_{site}\right)} = \frac{H_{area}}{L_{open}} \quad (5)$$

where  $\sum S_{bldg}$  is the sum of the building ground areas,  $A_{site}$  is the area of the sampling site,  $L_{diag}$  is the diagonal block length, and  $L_{open}$  and  $A_{open}$  are the length scale and area of open space, respectively.

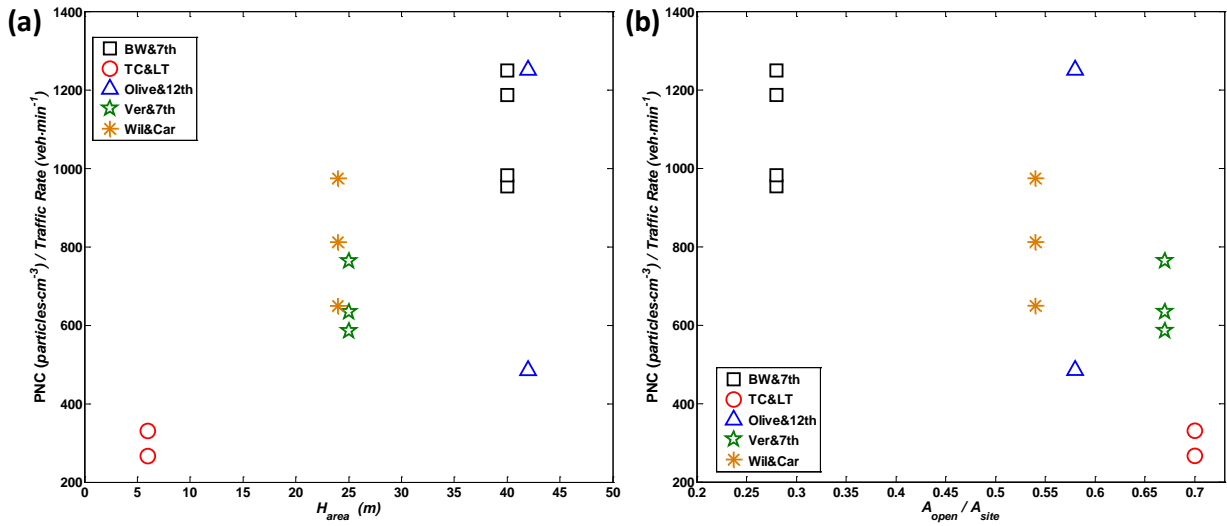


Figure 14. Comparisons of traffic corrected [UFP] vs. building area weighted building heights ( $H_{area}$ ) and the ratio of open space to sampling area ( $A_{open}/A_{site}$ ) for the morning sampling events.

The traffic-corrected [UFP], which is defined simply as observed [UFP] divided by observed traffic flow rate, showed a strong relationship with  $Ar_{area}$  (Figure 15 and Eq. 6):

$$\frac{[UFP]}{\text{Traffic flow rate}} = 286 \times \log(Ar_{area}) + 1193 \quad (R^2 = 0.67) \quad (6)$$

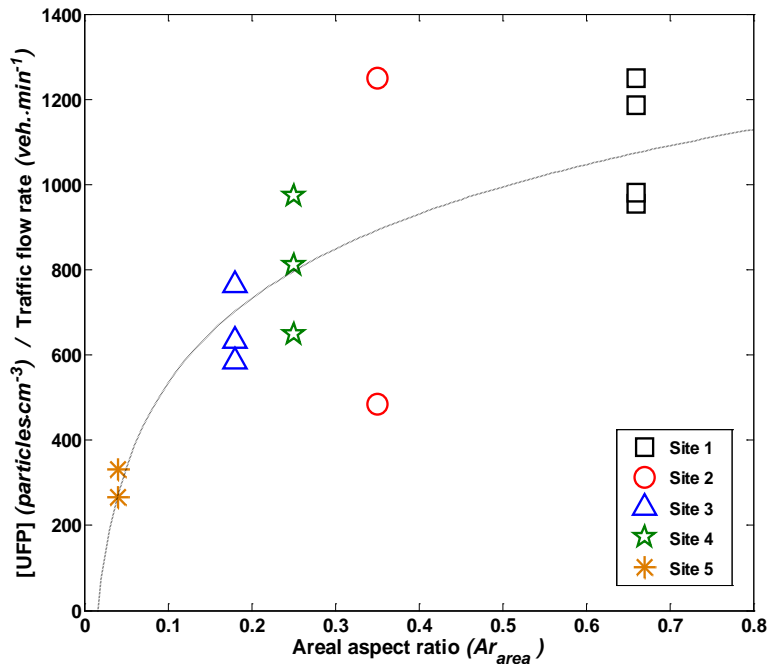


Figure 15. Relationship between area aspect ratio ( $Ar_{area}$ ) and [UFP] normalized to traffic flow rates in the morning ( $R^2=0.67$ ).

Due to a log form of the best fit curve, [UFP] increase sharply with  $Ar_{area}$  in a low  $Ar_{area}$  regime, but in a high  $Ar_{area}$  regime, the slope of [UFP] elevation with  $Ar_{area}$  is dampened. The log form of the best fit implies that once the aspect ratio is above a critical level, recirculation cells form in the lower part of building canopy (Liu et al. 2004). Once the in-canopy recirculation cells are a dominant feature, additional increases in aspect ratio have a weaker effect on ground-level vehicular pollutants because recirculation cells separate ground-level in-canopy air from upper ambient air. More details about air flow impacts on spatial distributions of air pollutants will be presented in a

separate study (Ranasinghe et al. 2015). Consequently, our results suggest that built environments, particularly the areal aspect ratio ( $Ar_{area}$ ) and traffic conditions, determine the spatial patterns of UFP levels under calm morning conditions.

#### **v.4.1.4.2. Unstable afternoon conditions**

In the afternoon, the areal aspect ratio does not explain the [UFP] between sampling sites as well as it does in the morning (Figure 14). This is not surprising given an increased meteorological influence due to more diverse meteorology between sampling sites/days in the afternoons. Differences in conditions such as deeper boundary layer depth, stronger turbulence intensities (Choi et al. 2011; Hussein et al. 2006; Seibert et al. 2000), and additional UFP source from photochemical secondary production may affect [UFP] (Hu et al. 2012; Ning et al. 2007).

In the afternoon, vertical fluctuations of winds ( $\sigma_w$ ) are the strongest factor in determining UFP levels, as shown by the straightforward relationships between [UFP] and  $\sigma_w$  ( $R^2=0.43$ , Figure 16). As the surface atmosphere becomes more turbulent (higher  $\sigma_w$ ), UFP levels decrease due to stronger atmospheric dispersion. The effect of  $\sigma_w$  on [UFP] becomes more evident when [UFP] are corrected for traffic flow rates;  $R^2$  values increase up to 0.83 (Figure 16b). Note that two data points obtained from *Site2* clearly departed from the trend and thus were excluded from the curve fitting analyses. *Site2* has very infrequent traffic with traffic flow rates of only 1/3 to 1/5 of other sampling sites (Table 2). Relatively high [UFP] despite minimal vehicular emissions at this site are likely caused by an influx from nearby busy streets combined with a contribution from secondary production. This implies that horizontal wind fields play a critical role in understanding the heterogeneous spatial distributions of pollutants, particularly on streets with little pollution of their own.

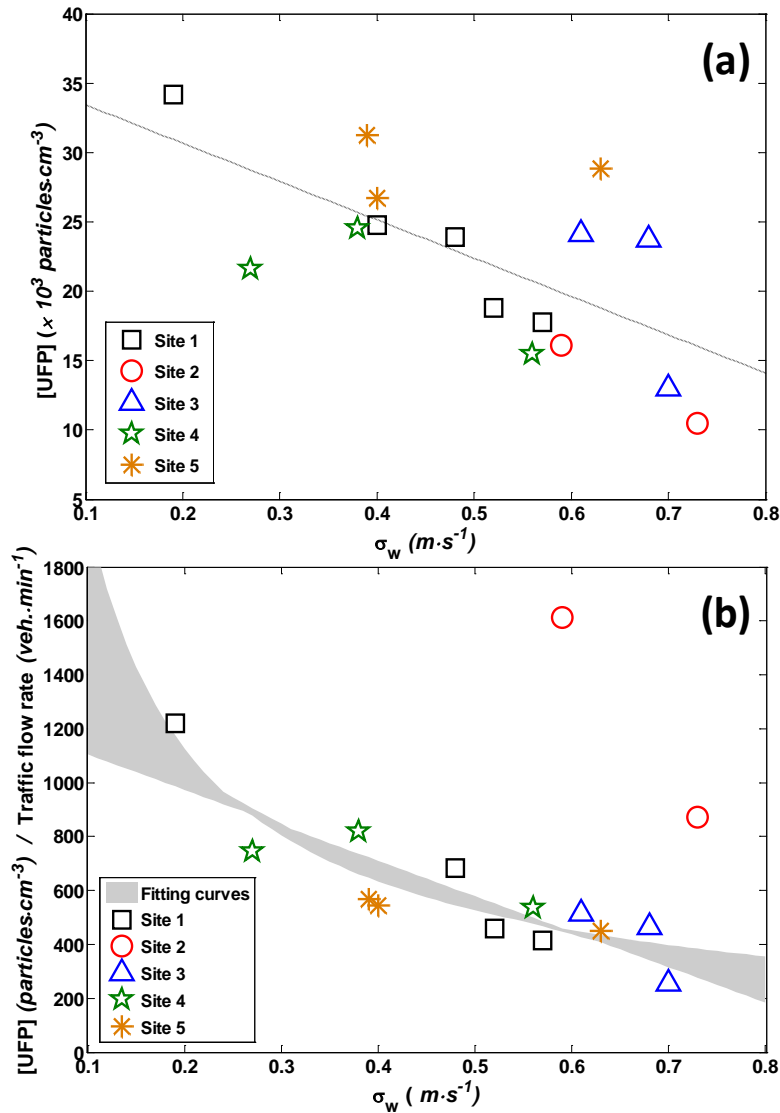


**Figure 16. Relationship between [UFP] and  $\sigma_w$  for afternoonsampling events. (a) [UFP] vs  $\sigma_w$  and (b) [UFP] normalized by observed traffic flows vs.  $\sigma_w$ . The grey area represents the range of best fit curves as described in the text. The values for *Site2* are removed from the analysis due to very low traffic counts on the street and subsequent likely contributions from nearby streets and other sources (see text.)**

There is not an obvious theoretical basis from which to derive a quantitative relationship between  $\sigma_w$  and traffic normalized [UFP], and our data do not span a large enough range to suggest the best form. Thus, several types of simple curve fits were applied: linear, exponential, logarithmic, and power (Eq. 7). The linear form resulted in slightly lower  $R^2$  value compared to others. Although the fitted values disperse widely at both ends, all fits showed a good agreement within observed  $\sigma_w$  range; the shaded area in Figure 16b shows the maximum and minimum values of the curve fits.

$$\begin{aligned}
 \frac{[UFP]}{\text{Traffic flow rate}} &= -1315 \cdot \sigma_w + 1236 & (R^2 = 0.74) \\
 &= 1645 \cdot \exp(-2.21 \cdot \sigma_w) & (R^2 = 0.80) \\
 &= -563 \cdot \log(0.76 \cdot \sigma_w) & (R^2 = 0.81) \\
 &= 296 \cdot \sigma_w^{-0.83} & (R^2 = 0.83)
 \end{aligned}
 \tag{7}$$

The strong relationships between traffic-normalized [UFP] and  $\sigma_w$  emphasize the role of surface micro-meteorology in determining afternoon air pollution levels. However, we hypothesize that

built environments also affect air pollutant distributions indirectly by altering the turbulence intensities. To support this hypothesis, the comparisons between heterogeneity of building morphology for each site and observed surface turbulence parameters are shown in Figure 17.

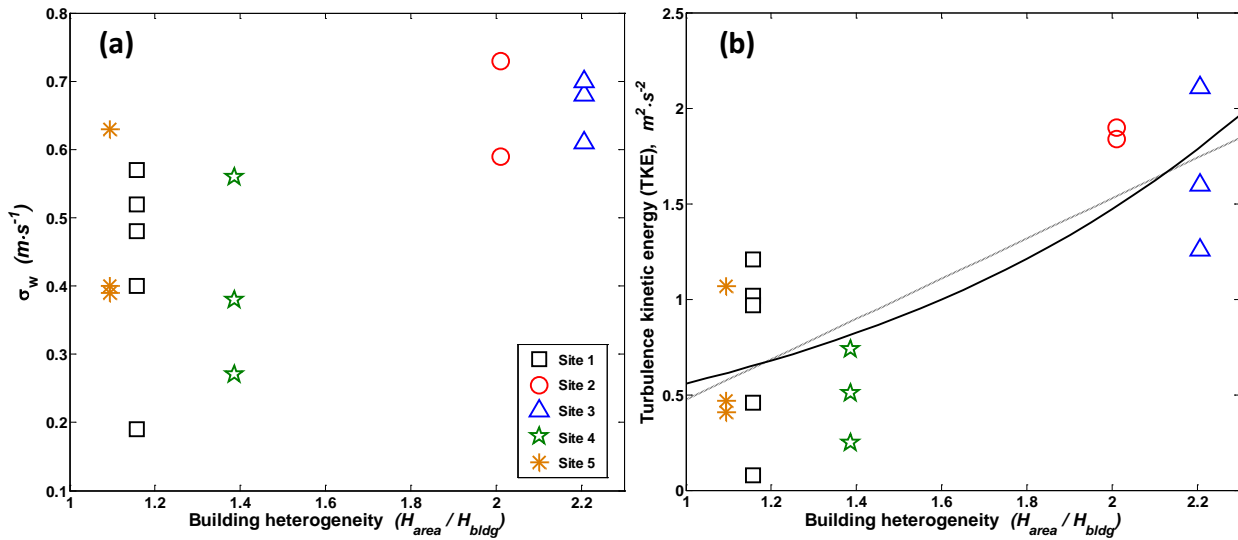


**Figure 17. Afternoon relationships between building heterogeneity vs. turbulence intensities: (a) vertical fluctuation of winds and (b) total turbulence kinetic energy (TKE) defined as  $TKE = 1/2 \sqrt{\sigma_u^2 + \sigma_v^2 + \sigma_w^2}$ . Dotted and solid lines in (b) represent the best fits in linear ( $R^2=0.60$ ) and exponential ( $R^2=0.60$ ) forms, respectively, for illustration of the increase trends of TKE with building heterogeneity.**

The fluctuations of vertical winds that showed the strongest relationships with the afternoon [UFP] appear to be somewhat related to building heterogeneity (Figure 17a). However, the daily variations of  $\sigma_w$  for each sampling site are so large compared to the magnitude of the observed range that the relationships are not strong. On the other hand, the most heterogeneous sites, *Site2* and *Site3*, had consistently stronger  $\sigma_w$  than other more homogeneous sites. As expected, the surface level turbulence kinetic energy for each site sharply increased with building heterogeneity (Figure 17b). This relationship implies that a heterogeneous building configuration enhances surface level turbulence, intensifying atmospheric dispersive capacity and reducing surface air pollutant levels under unstable daytime conditions.

#### v.4.2. Developing high spatial resolution concentration maps using mobile air quality measurements

##### v.4.2.1. High spatial resolution concentration maps

The 5 m spatial resolution maps shown in Figure 18 are the result of careful consideration of several underlying data processing issues of mobile monitoring data. With the use of a background correction, we were able to average data over sampling events on different days, and thus over a higher number of runs. After averaging the data over varying effects of micro-meteorology, traffic volume, traffic fleet composition, and background concentrations over different sampling events on different days, resulting UFP concentration maps retain the robust block and sub-block scale features of the concentration variation, making them a potentially useful tool in identifying pollution hot-spots at the block or the sub-block scale.

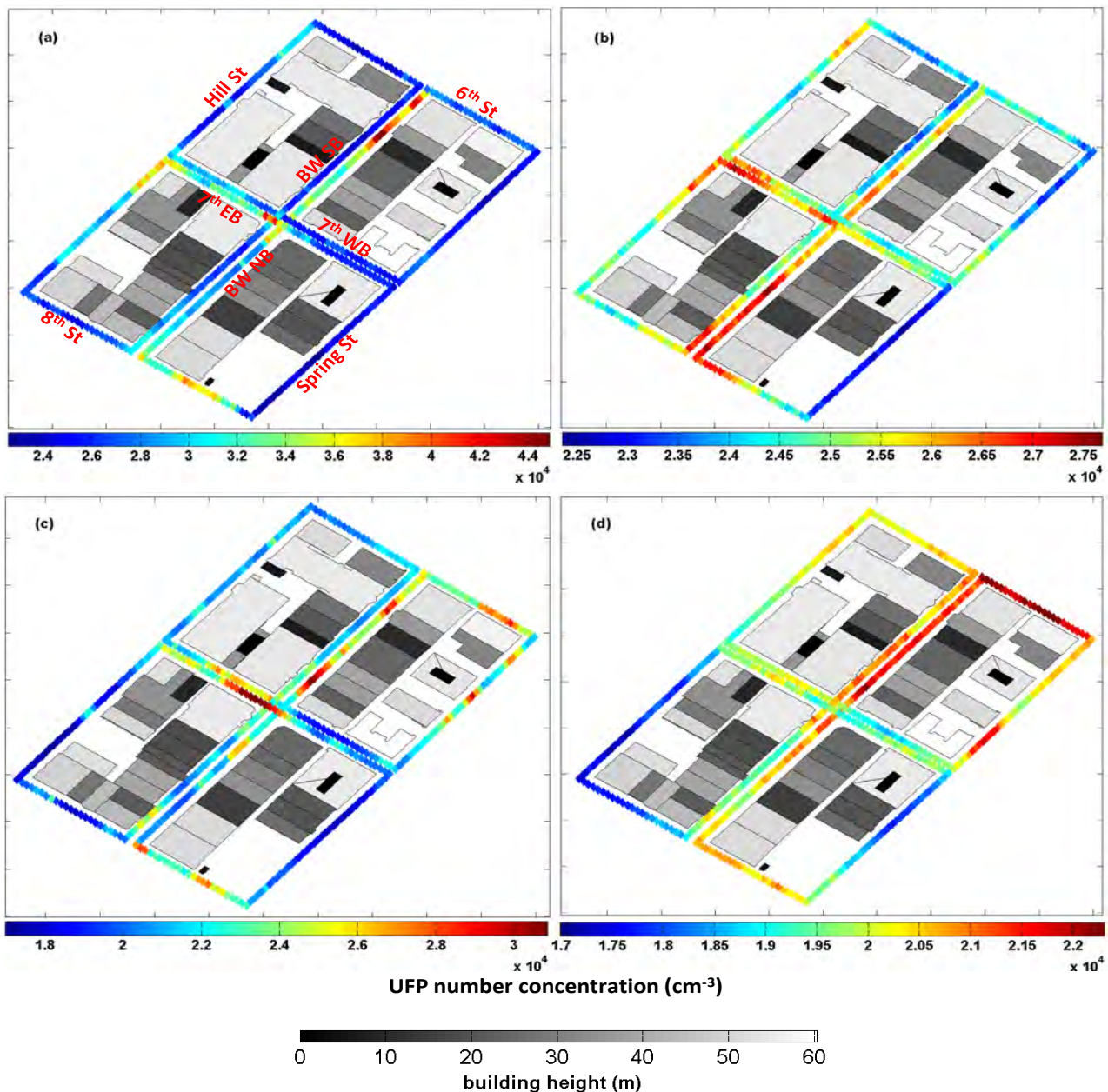


**Figure 18. Spatial variation of background corrected UFP concentrations averaged over (a, b) morning and (c, d) afternoon sampling events over three days for (a, c) data including HEV-related spikes and (b, d) data excluding HEV-related spikes. The spatial resolution of the maps is 5 m. The heights of the buildings in the nearby area is shown in gray scale.**

Figure 18 shows the UFP concentration maps at 5 m spatial resolution for the full data set including HEV-related spikes (“raw”, Figure 18(a) and Figure 18(c)) and also for the data with HEV-related spikes removed (“spikes removed”, Figure 18(b) and Figure 18(d)). The dominant feature of the “raw” concentration maps are the ‘hot-spots’ that appear at and near intersections, including both the area where queues form and where vehicles accelerate away from intersections. Once the HEV-related spikes are removed, features appear that reveal the influence of the built environment on street level UFP concentrations. While “raw” concentration maps are important in exposure analysis, maps with HEV spikes removed help understand various other factors influencing small spatial scale variations of the UFP concentration.

The “spikes removed” data reveal features at both the block- and the sub-block scales. Figure 18(d) shows that at the block-scale, 6th street in the afternoon shows the highest concentrations despite having low average traffic volume compared to other streets. On 7th street, in both morning and afternoon, there are generally higher concentrations on the east-bound side compared to the west-

bound side, despite having nearly the same traffic flow in both directions. Moreover, Figure 18(b) shows that at the sub-block scale, in the morning on Broadway north-bound near the intersection of 8th and BW, the south end of the block has elevated concentration in comparison to the queue forming at the north end. A similar situation can be noted on 8th street, just west of the intersection of BW and 8th, where the east end of the block shows elevated concentration in comparison to the queue forming at the west end. Many of these features can be explained by the surface level wind flow patterns that are heavily influenced by the local built environment, traffic patterns, and non-vehicle local sources. More detailed analyses of the effects of surrounding building morphology, micro-meteorological variations, and air flow patterns due to the built environment and traffic patterns on concentration distributions at different scales will be presented separately (Ranasinghe et al., in prep.).

*v.4.2.2. High Estimation of the minimum number of runs needed for representative concentration values*

Due to transient and small spatial scale variations in air pollution concentrations, a single run of mobile measurements is clearly unable to capture a representative concentration field of an area. This raises the question of how many repeated measurements are needed to estimate a representative concentration field. Clearly this question is dependent on variability in meteorological as well as traffic conditions; features that in some cases might require very large amounts of sampling. In this study, typical morning and afternoon conditions at *Site1* was investigated. The average wind speeds on BW were  $1.2 \pm 0.2 \text{ m s}^{-1}$  for mornings and  $1.3 \pm 0.5 \text{ m s}^{-1}$  for afternoons. The most prevalent wind direction on BW was SW in both morning and afternoon sampling events. On 7th, the average wind speeds were  $1.0 \pm 0.1 \text{ m s}^{-1}$  for mornings and  $1.5 \pm 0.1 \text{ m s}^{-1}$  for afternoons. The most prevalent wind directions on 7th were ESE in the mornings and NE in the afternoons (Table 9). To investigate this question, the following exercise was performed on the UFP number concentration data set.

**Table 9. Average surface meteorology at Broadway and 7<sup>th</sup> (*Site1*). Here,  $u_*$  is the friction velocity,  $\sigma_w$  is the variance of vertical wind velocity and TKE is the turbulent kinetic energy\*.**

Date	Temp. (°C)	$u_*$ (m s <sup>-1</sup> )	$\sigma_w$ (m s <sup>-1</sup> )	TKE (m <sup>2</sup> s <sup>-2</sup> )	Temp. (°C)	$u_*$ (m s <sup>-1</sup> )	$\sigma_w$ (m s <sup>-1</sup> )	TKE (m <sup>2</sup> s <sup>-2</sup> )
	Morning				Afternoon			
7/1/2013	25.9	0.23	0.37	0.47	32.2	0.23	0.40	0.46
7/3/2013	23.0	0.17	0.35	0.47	22.5	0.36	0.57	0.97
7/5/2013	20.6	0.19	0.30	0.47	24.0	0.15	0.48	1.21

First, all morning runs and all afternoon runs from the background-corrected concentration data set were collected separately. Each of these sets had runs spanning several days; many with fairly similar meteorological and traffic conditions (Table 5). For mornings, up to 22 runs were available for BW south-bound and 7th east-bound and 24 runs for BW north-bound and 7th west-bound. For afternoons, up to 19 runs were available for BW south-bound and 20 runs for other streets. For each street, at each line reference point, runs were selected at random (without replacement) and the mean concentration was calculated using an increasing number of runs, up to one less than the total number of runs available. This process was repeated 10 times for each street, choosing runs in different random order. For the sets of 10 repeated mean UFP concentration calculations at different reference points and for different number of averaged runs, the relative error (standard deviation normalized by mean) was calculated and plotted (Figure 19(a)). As shown in Figure 19(a), the rate of decrease in relative error varies among reference points along a given street. For simplicity, the maximum relative error along each street is considered and plotted against number of runs averaged for HEV "spikes removed" data (Figure 19(b)) and for HEV "spikes retained" data (Figure 19(c)). The minimum number of runs needed for the relative error to drop below 0.15 is calculated (the green or yellow symbols on each plot in Figure 19(b) and Figure 19(c)) and considered as the minimum number of runs needed for a representative UFP concentration value.

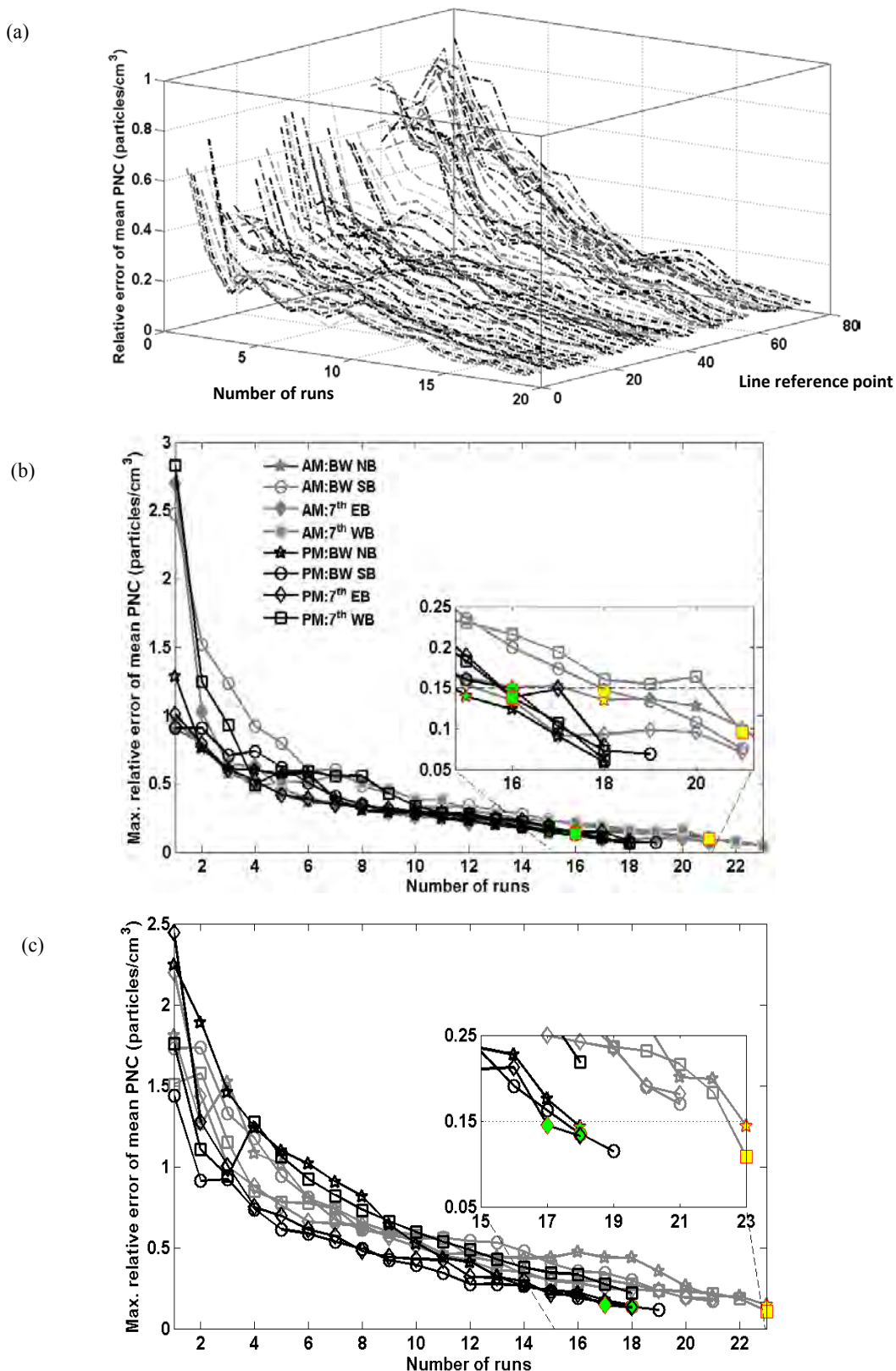


Figure 19. (a) The relative error of repeated calculations of mean concentration of HEV "spike removed" data, for different numbers of averaged afternoon runs included in the averaging (x-axis), at each line reference points along a single example street (BW SB) (y-axis.) (b, c) The variation of maximum relative error along different street segments vs. the number of averaged runs for morning (AM) and afternoon (PM) sampling events (b) for HEV "spikes removed" data and (c) for HEV "spikes retained" data. The green and yellow symbols denote the points at which the relative error is at or below 0.15. The spatial resolution of the maps considered is 5 m.

The estimate of the minimum number of runs needed for representative UFP concentration values at 5 m spatial resolution varies somewhat from street to street and is dependent on the data filters applied (Figure 19(b) and Figure 19(c)). For HEV "spikes removed" data, the maximum relative error along each street vs. number of averaged runs (Figure 19(b)) drops rapidly (in the first 2–7 runs). The maximum relative error along streets also drops rapidly, from the initial values of 282–90% to 50% at 4–9 runs, after which it decreases more slowly, reaching 15% at 15–21 runs. Hence the estimate of the minimum number of runs needed for representative concentrations at 5 m spatial resolution ranges between 16–21 runs for the mornings and between 15–16 runs for the afternoons (Figure 19(b)). For mornings when 16 runs are included, the average relative error considering all four streets is 11%. For afternoons when 15 runs are included, the average relative error considering all four streets is 9%. The morning sampling events usually have low wind speeds (Table 9). Consequently, the TKE and variance of  $\sigma_w$  are lower in the mornings in comparison to the afternoons (Table 9), denoting lower atmospheric turbulence and mixing rates. The need for more runs for the morning sessions can be attributed to the lower mixing rates, resulting in a stronger influence of local sources on pollutant concentrations.

The inclusion of transient and large HEV spikes generally increases the minimum number of runs needed for all the streets and for both AM and PM sampling events (Figure 19(c)). Similar to the HEV "spikes removed" data, morning sampling needs more runs compared to afternoon sampling. For HEV "spikes retained" data, the maximum relative error along each street vs. number of runs averaged drops slowly compared to HEV "spikes removed" data. The maximum relative error along streets also drops from the initial values of 244–143% to 50% at 8–14 runs and subsequently drops below 15% with additional runs. For all the streets, maximum relative error drops below 22% at 21–23 runs for the mornings and at 17–18 runs for the afternoons. Hence, we conclude that the minimum number of runs needed for representative UFP concentrations at 5 m spatial resolution is at least 21–23 runs for the mornings and at least 17–18 runs for the afternoons.

These results apply only to UFP concentrations because the minimum number of runs needed for representative concentration values depends on the magnitude of variance of the data set. Hence the results depend on the air pollutant considered. We also showed that the results depend on the data filters applied (Figure 19(c)). For both HEV "spikes removed" and "spikes retained" data sets, the initial values of the maximum relative error markedly decreased when spatial resolution was decreased to 10 m. The minimum number of runs needed for representative concentration values generally decreased for all the streets and for both AM and PM sampling events.

In their effort to assess the minimum number of runs needed for representative concentrations at the street-scale, Van Poppel et al. (2013) and Peters et al. (2013) used data from moderately sized sets of mobile monitoring runs (20–24 runs), selecting different numbers of runs at random (without replacement) and averaging them to calculate the street means or medians. They used 1 s time resolution data collected by a MMP travelling at an average speed  $2.7 \text{ m s}^{-1}$ . The minimum number of runs needed to obtain representative concentrations was defined as the point at which these mean/median values calculated using a sub-set of runs came within a certain percentage deviation (15%–25%) of their "representative values". They defined the "representative values" as the mean/median of all available runs. Peters et al. (2013) using a 15% deviation percentage concluded that for UFP concentrations the number of runs needed was 16 and 18 for the two sites considered. Van Poppel et al. (2013) used a portion of the data set used in Peters et al. (2013) study and concluded that for UFP concentrations, a 25% deviation could be achieved from 10–16 and 8–16 runs depending on the street, for analysis without and with background correction, respectively. In a continuation of this work, Van den Bossche et al. (2015) used a large dataset (96–256 runs) of BC measurements for a similar exercise. BC was measured at 1 s time resolution but as discussed earlier, the spatial resolution of these data is variable and complex due to the use of a post-data processing technique (ONA). Allowing replacement in the random selection of runs and employing

a background correction, trimmed mean, and 25% deviation, they concluded the number of runs needed is 14–61 depending on the street and also showed that the required number of runs rose to 108 when considering a spatial resolution of 20 m. Prior studies (Peters et al., 2013; Van Poppel et al., 2013) conducted with small UFP data sets are different from this study in terms of both the way in which the minimum number of required runs is defined and in the spatial scale considered. Despite these differences, our estimate of the minimum number of runs needed for representative UFP concentration values is also comparable with these two prior studies.

#### v.4.3. Statistical modeling of the micro-dynamics of UFP concentrations caused by traffic at street intersections

A statistical model was developed to understand the UFP concentrations being measured by MMP to determine how on-road sources and micro-dynamic parameters affect the measurements. By constructing a statistical model, it is possible to perform sensitivity tests in which it would produce UFP concentration results under various scenarios constructed to determine how best to reduce emission/exposure on- and near-roadways. The following sections of this report describes the fundamental of the statistical model and results that reflect the MMP measurements conducted in this study.

##### v.4.3.1. Statistical model development

The concentration of UFP at a point in time and space along the transect is assumed to be a function of both contemporaneous and past variations in emissions of UFPs and in environmental conditions influencing the dispersion thereof. If at every time,  $t$  :

- $y_t$  is the concentration of UFP
- $X_t$  is a vector of observed factors affecting the concentration of UFP
- $\epsilon_t$  is the cumulative effect of unobserved factors affecting the concentration of UFP

Then the concentration of UFP at time  $t$  may be written:

$$y_t = f(X_t, X_{t-1}, X_{t-2}, \dots, \epsilon_t)$$

Or, if  $f(\cdot)$  is assumed to be linear in terms (which may include higher order terms, such as quadratics or interactions of factors), we have the infinitely distributed lag model:

$$y_t = \alpha + \beta_t \cdot X_t + \beta_{t-1} \cdot X_{t-1} + \beta_{t-2} \cdot X_{t-2} + \dots + \epsilon_t$$

$$y_t = \alpha + \sum_{l=0}^{\infty} [\beta_{t-l}] \cdot X_{t-l} + \epsilon_t$$

where  $\alpha$  is the intercept term. This model may be estimated by ordinary least squares provided that the time series of UFP concentrations is stationary (and thus less prone to producing spurious results). With this formulation:

- $\beta_{t-l}^k$  is the “dynamic multiplier”—the effect of factor  $k$ , observed at lag length  $l$ , on contemporaneous UFP
- $\sum_{l=0}^{\infty} \beta_{t-l}^k$  is the “cumulative multiplier”—the cumulative effect of all past observations of factor  $k$  on contemporaneous UFP or, alternately, the cumulative effect of a single observation of factor  $k$  on contemporaneous and all future observations of UFP

Two issues remain, however. First, data on infinite lags of the factors affecting the concentration of UFP are unavailable. Second, the estimates of the coefficients will be biased if the unobserved effect,  $\epsilon_t$ , is correlated over time. This is likely, particularly with high frequency data. So rather than estimate the dynamic and cumulative multipliers directly, we conduct consistent ordinary least squares estimation by including lagged values of UFP (and, implicitly, lagged values of the unobserved effect) as additional regressors. This yields the autoregressive distributed lag model:

$$y_t = \delta + \sum_{i=1}^q (\theta_{t-i} \cdot y_{t-i}) + \sum_{i=0}^r (\phi_{t-i} \cdot X_{t-i}) + v_t$$

where  $q$  and  $r$  are the chosen lag lengths for lagged values of UFP and the observable factors affecting the concentration of UFP, respectively. (The optimal choice of  $q$  and  $r$  will vary depending on the application; we discuss our choices in this setting further below.)

Dynamic and cumulative multipliers of interest may then be recovered as functions of the estimated coefficients. This proceeds by transforming the estimated Eq. 3 into Eq. 2 in this sub-section through successive substitution of the estimated Eq. 3 for  $y_{t-i}$ . Standard errors for the multipliers may then be approximated using the delta method. Simulations of synthetic scenarios may then be conducted using the estimated Eq. 3 by setting all factors (other than those specified by the scenario) to their long-run means and forecasting the resulting evolution of the concentration of UFP. The above discussion suggests that estimation should be conducted using the autoregressive distributed lag model so long as  $y_t$  is stationary within runs, and  $\epsilon_t$  is serially correlated within runs.

#### v.4.3.1.1. Statistical model specification

Our preferred specification for the model is present in Table 10. The numbers of various lags are selected to maximize explanatory power, while minimizing concerns about collinearity and overfitting. An augmented Dickey-Fuller test rejects at the 1 percent significance level, for each of the twelve runs, the null hypothesis that the concentration of UFP is non-stationary. Moreover, the first-and second-order partial autocorrelations of the residuals of the infinitely distributed lag model are statistically different from zero at the 5 percent level for all runs (and at the 1 percent level for all but one run); consequently at least two lags of the concentration of UFP should be included as additional explanatory variables.

This specification of the autoregressive distributed lag model features fifteen lags of the concentration of UFP. It includes contemporaneous and two lags of the following variables: i) mobile monitoring platform (MMP) lane, ii) MMP idle status, iii) MMP speed, iv) building height (average), v) building height (east-west difference).

This model also contains contemporaneous and eight lags of the following variables: i) intersection status, ii) acceleration events (ongoing, oncoming, left-crossing or right-crossing traffic), iii) light-duty vehicle (ongoing, oncoming, left-crossing or right-crossing traffic), iv) heavy-duty vehicle (ongoing, oncoming, left-crossing or right-crossing traffic), and v) bus (ongoing, oncoming, left-crossing or right-crossing traffic). Finally, the model includes a fourth-order polynomial in position along the transect index. Because the Goldfeld-Quandt test rejects at the 1 percent significance level, for most combinations of runs, the null hypothesis that the unobserved effects have equal variances, heteroskedasticity-robust standard errors are used throughout.

**Table 10. Model estimated UFP concentrations**

	Coef.	Robust Std. Err.	t	95% Conf. Interval	
Ultrafine particles	-	-	-	-	-
<i>L1</i>	1.570023	(0.032944)	47.66	1.505429	1.634618
<i>L2</i>	-0.97724	(0.06129)	-15.94	-1.09742	-0.85707
<i>L3</i>	0.462292	(0.058039)	7.97	0.348494	0.576091
<i>L4</i>	-0.1962	(0.051342)	-3.82	-0.29687	-0.09553
<i>L5</i>	0.111163	(0.052347)	2.12	0.008525	0.213801
<i>L6</i>	-0.0746	(0.052223)	-1.43	-0.177	0.027793
<i>L7</i>	0.047506	(0.046826)	1.01	-0.04431	0.139319
<i>L8</i>	-0.01174	(0.044584)	-0.26	-0.09915	0.075682
<i>L9</i>	-0.02807	(0.046768)	-0.6	-0.11977	0.063625
<i>L10</i>	0.043222	(0.045103)	0.96	-0.04521	0.131656
<i>L11</i>	-0.00584	(0.047927)	-0.12	-0.09981	0.088138
<i>L12</i>	-0.06238	(0.052001)	-1.2	-0.16434	0.039584
<i>L13</i>	0.064465	(0.045479)	1.42	-0.02471	0.153637
<i>L14</i>	-0.00614	(0.037542)	-0.16	-0.07975	0.067465
<i>L15</i>	0.003634	(0.020206)	0.18	-0.03598	0.043253
MMP lane number	0.021661	(0.023973)	0.9	-0.02534	0.068665
<i>L1</i>	-0.03214	(0.038736)	-0.83	-0.10809	0.043809
<i>L2</i>	0.020199	(0.031948)	0.63	-0.04244	0.08284
MMP speed	-0.00108	(0.000974)	-1.11	-0.00299	0.000827
<i>L1</i>	-0.00027	(0.000519)	-0.52	-0.00128	0.00075
<i>L2</i>	0.001176	(0.000605)	1.95	-9.17E-06	0.002362
MMP speed <sup>2</sup>	9.63E-06	(9.14E-06)	1.05	-8.29E-06	2.76E-05
MMP speed × MMP speed [L1]	-2.41E-06	(2.33E-05)	-0.1	-4.80E-05	4.33E-05
MMP speed × MMP speed [L2]	-4.3E-05	(4.09E-05)	-1.05	-0.00012	3.74E-05
Light-duty (on-going)	-0.00498	(0.010035)	-0.5	-0.02466	0.014696
<i>L1</i>	0.009632	(0.012011)	0.8	-0.01392	0.033183
<i>L2</i>	0.002232	(0.010139)	0.22	-0.01765	0.02211
<i>L3</i>	-0.00399	(0.009377)	-0.43	-0.02237	0.014398
<i>L4</i>	0.004014	(0.008987)	0.45	-0.01361	0.021635
<i>L5</i>	0.03278	(0.019689)	1.66	-0.00583	0.071385
<i>L6</i>	-0.00351	(0.01187)	-0.3	-0.02678	0.019768
<i>L7</i>	-0.0252	(0.008029)	-3.14	-0.04095	-0.00946
<i>L8</i>	-0.01705	(0.010656)	-1.6	-0.03794	0.003844
Light-duty (on-coming)	0.008546	(0.008049)	1.06	-0.00724	0.024328
<i>L1</i>	0.006847	(0.008713)	0.79	-0.01024	0.02393
<i>L2</i>	-0.00211	(0.007518)	-0.28	-0.01685	0.012628
<i>L3</i>	-0.00817	(0.007961)	-1.03	-0.02378	0.007441
<i>L4</i>	-0.00085	(0.007741)	-0.11	-0.01602	0.014331
<i>L5</i>	0.016506	(0.007749)	2.13	0.001311	0.0317
<i>L6</i>	0.002587	(0.007536)	0.34	-0.01219	0.017363
<i>L7</i>	0.001244	(0.007086)	0.18	-0.01265	0.015137
<i>L8</i>	-0.00774	(0.006849)	-1.13	-0.02117	0.005689

	Coef.	Robust Std. Err.	t	95% Conf. Interval	
Light-duty (cross from left)	-0.01417	(0.009027)	-1.57	-0.03187	0.00353
<i>L1</i>	-0.00858	(0.00935)	-0.92	-0.02691	0.00975
<i>L2</i>	-0.00891	(0.010808)	-0.82	-0.0301	0.012282
<i>L3</i>	0.017274	(0.010686)	1.62	-0.00368	0.038227
<i>L4</i>	-0.00414	(0.011633)	-0.36	-0.02694	0.018673
<i>L5</i>	0.002213	(0.011937)	0.19	-0.02119	0.025617
<i>L6</i>	0.004934	(0.009314)	0.53	-0.01333	0.023196
<i>L7</i>	0.017519	(0.010199)	1.72	-0.00248	0.037518
<i>L8</i>	0.012175	(0.012117)	1	-0.01158	0.035933
Light-duty (cross from right)	0.001778	(0.00944)	0.19	-0.01673	0.020287
<i>L1</i>	-0.00587	(0.010189)	-0.58	-0.02585	0.014112
<i>L2</i>	-0.00602	(0.009618)	-0.63	-0.02488	0.012841
<i>L3</i>	-0.00683	(0.008405)	-0.81	-0.02331	0.009653
<i>L4</i>	-0.0074	(0.009283)	-0.8	-0.02561	0.010797
<i>L5</i>	0.005945	(0.009092)	0.65	-0.01188	0.023772
<i>L6</i>	0.005077	(0.013298)	0.38	-0.021	0.031152
<i>L7</i>	0.00422	(0.008896)	0.47	-0.01322	0.021662
<i>L8</i>	-0.00144	(0.013014)	-0.11	-0.02696	0.024073
Heavy/medium-duty (on-going)	-0.00531	(0.029522)	-0.18	-0.06319	0.052579
<i>L1</i>	0.027436	(0.065685)	0.42	-0.10135	0.156226
<i>L2</i>	0.004115	(0.031977)	0.13	-0.05858	0.066813
<i>L3</i>	-0.0637	(0.038713)	-1.65	-0.13961	0.012207
<i>L4</i>	0.027891	(0.034249)	0.81	-0.03926	0.095044
<i>L5</i>	-0.02322	(0.027525)	-0.84	-0.07719	0.030746
<i>L6</i>	0.059098	(0.026915)	2.2	0.006325	0.111871
<i>L7</i>	0.073935	(0.032116)	2.3	0.010964	0.136906
<i>L8</i>	0.018336	(0.032131)	0.57	-0.04466	0.081336
Heavy/medium-duty (on-coming)	-0.05056	(0.023199)	-2.18	-0.09605	-0.00507
<i>L1</i>	0.039984	(0.033778)	1.18	-0.02625	0.106212
<i>L2</i>	0.003812	(0.036426)	0.1	-0.06761	0.075233
<i>L3</i>	-0.03505	(0.031004)	-1.13	-0.09584	0.025739
<i>L4</i>	0.007392	(0.031211)	0.24	-0.0538	0.068587
<i>L5</i>	-0.04074	(0.031396)	-1.3	-0.1023	0.020822
<i>L6</i>	0.021185	(0.034177)	0.62	-0.04583	0.088197
<i>L7</i>	0.011189	(0.024192)	0.46	-0.03625	0.058624
<i>L8</i>	-0.00397	(0.023871)	-0.17	-0.05078	0.042833
Heavy/medium-duty (cross from left)	-0.04469	(0.024822)	-1.8	-0.09336	0.003982
<i>L1</i>	-0.04284	(0.036507)	-1.17	-0.11442	0.028737
<i>L2</i>	0.025378	(0.023068)	1.1	-0.01985	0.070608
<i>L3</i>	0.007655	(0.042993)	0.18	-0.07664	0.091952
<i>L4</i>	0.073666	(0.04015)	1.83	-0.00506	0.152388
<i>L5</i>	-0.00061	(0.024931)	-0.02	-0.04949	0.048272
<i>L6</i>	0.061759	(0.0572)	1.08	-0.05039	0.173912
<i>L7</i>	-0.01299	(0.029304)	-0.44	-0.07045	0.044471
<i>L8</i>	-0.01243	(0.027829)	-0.45	-0.06699	0.042139

	Coef.	Robust Std. Err.	t	95% Conf. Interval	
Heavy/medium-duty (cross from right)	-0.01111	(0.023332)	-0.48	-0.05686	0.034637
<i>L1</i>	-0.00384	(0.029673)	-0.13	-0.06202	0.054345
<i>L2</i>	-0.06229	(0.029217)	-2.13	-0.11958	-0.00501
<i>L3</i>	-0.00332	(0.030497)	-0.11	-0.06312	0.056471
<i>L4</i>	0.019426	(0.028825)	0.67	-0.03709	0.075944
<i>L5</i>	-0.0046	(0.031342)	-0.15	-0.06605	0.056858
<i>L6</i>	0.01017	(0.038304)	0.27	-0.06493	0.085273
<i>L7</i>	0.060909	(0.08433)	0.72	-0.10444	0.226257
<i>L8</i>	-0.01557	(0.02606)	-0.6	-0.06667	0.035528
Bus (on-going)	0.008687	(0.02706)	0.32	-0.04437	0.061745
<i>L1</i>	0.028092	(0.030012)	0.94	-0.03075	0.086938
<i>L2</i>	-0.04942	(0.029853)	-1.66	-0.10796	0.00911
<i>L3</i>	-0.00908	(0.035777)	-0.25	-0.07923	0.061065
<i>L4</i>	-0.01559	(0.031622)	-0.49	-0.07759	0.046415
<i>L5</i>	-0.02942	(0.047037)	-0.63	-0.12164	0.06281
<i>L6</i>	-0.01523	(0.030386)	-0.5	-0.07481	0.044351
<i>L7</i>	0.009399	(0.036993)	0.25	-0.06314	0.081933
<i>L8</i>	0.003148	(0.038153)	0.08	-0.07166	0.077955
Bus (on-coming)	0.042706	(0.029711)	1.44	-0.01555	0.100961
<i>L1</i>	-0.02875	(0.021672)	-1.33	-0.07125	0.013739
<i>L2</i>	0.031345	(0.026528)	1.18	-0.02067	0.083358
<i>L3</i>	0.030845	(0.0268)	1.15	-0.0217	0.083393
<i>L4</i>	-0.03489	(0.023118)	-1.51	-0.08022	0.010436
<i>L5</i>	-0.05048	(0.021203)	-2.38	-0.09206	-0.00891
<i>L6</i>	0.042297	(0.022479)	1.88	-0.00178	0.086372
<i>L7</i>	-0.01136	(0.022346)	-0.51	-0.05518	0.03245
<i>L8</i>	0.008167	(0.018929)	0.43	-0.02895	0.045281
Bus (cross from left)	0.03628	(0.051009)	0.71	-0.06373	0.136295
<i>L1</i>	0.01695	(0.056579)	0.3	-0.09399	0.127886
<i>L2</i>	-0.01409	(0.034951)	-0.4	-0.08262	0.054436
<i>L3</i>	0.006299	(0.052042)	0.12	-0.09574	0.10834
<i>L4</i>	0.052658	(0.036783)	1.43	-0.01946	0.12478
<i>L5</i>	0.040381	(0.038769)	1.04	-0.03563	0.116396
<i>L6</i>	0.077589	(0.061751)	1.26	-0.04349	0.198667
<i>L7</i>	0.087997	(0.059011)	1.49	-0.02771	0.2037
<i>L8</i>	-0.08822	(0.054626)	-1.62	-0.19533	0.018884
Bus (cross from right)	-0.11105	(0.109929)	-1.01	-0.32659	0.104489
<i>L1</i>	-0.00908	(0.037571)	-0.24	-0.08274	0.064588
<i>L2</i>	0.028099	(0.030309)	0.93	-0.03133	0.087527
<i>L3</i>	-0.01513	(0.023961)	-0.63	-0.06211	0.031852
<i>L4</i>	0.033668	(0.037116)	0.91	-0.03911	0.106443
<i>L5</i>	0.031641	(0.033618)	0.94	-0.03428	0.097557
<i>L6</i>	0.04424	(0.03808)	1.16	-0.03043	0.118906
<i>L7</i>	-0.00868	(0.028001)	-0.31	-0.06358	0.046227

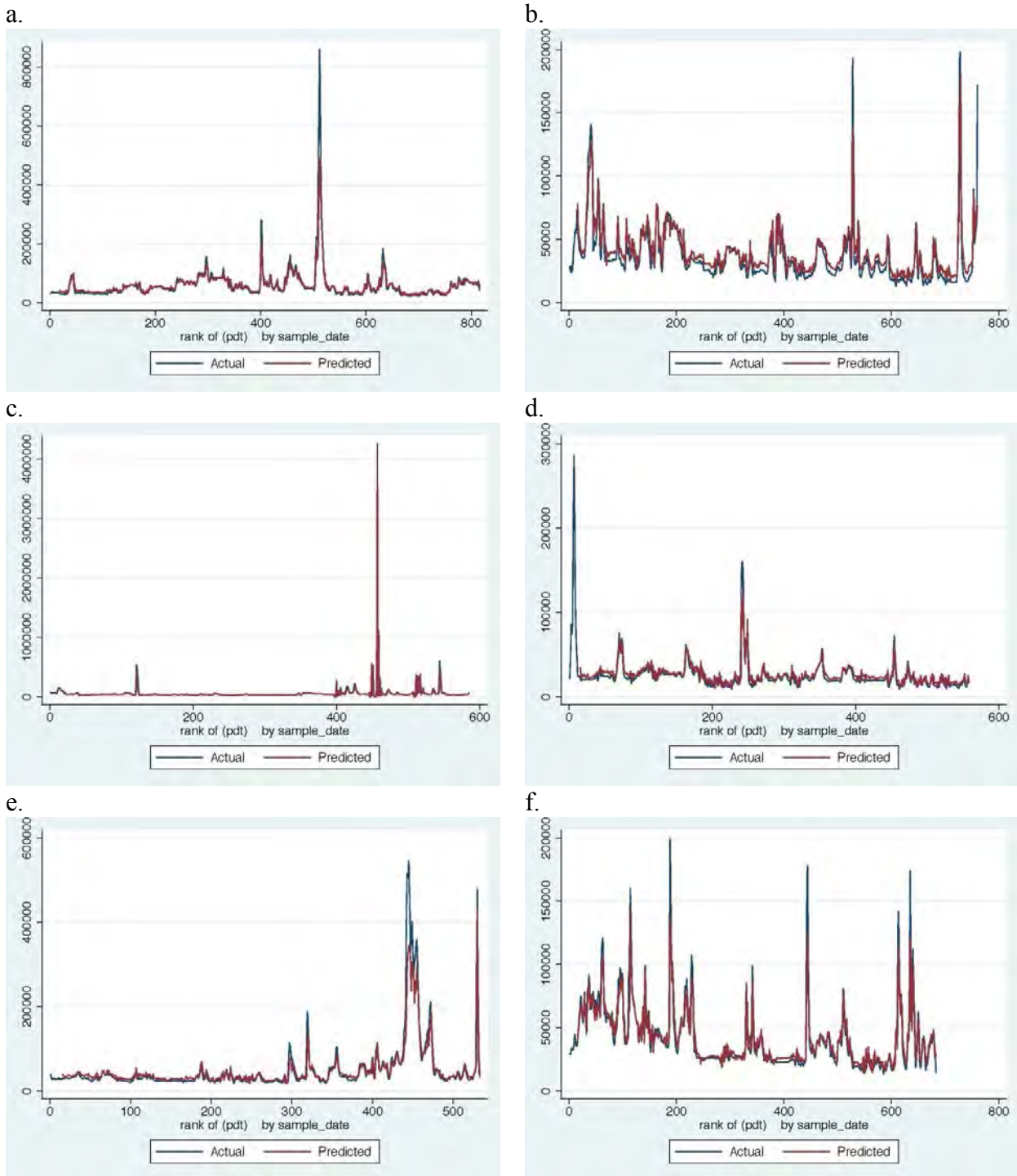
	Coef.	Robust Std. Err.	t	95% Conf. Interval	
<i>L8</i>	-0.00914	(0.024205)	-0.38	-0.0566	0.038321
Acceleration (on-going)	-0.01689	(0.038817)	-0.44	-0.093	0.05922
<i>L1</i>	0.110624	(0.046376)	2.39	0.019694	0.201553
<i>L2</i>	0.027547	(0.058163)	0.47	-0.0865	0.141589
<i>L3</i>	0.190339	(0.141579)	1.34	-0.08726	0.467938
<i>L4</i>	0.209642	(0.09996)	2.1	0.013648	0.405637
<i>L5</i>	0.077272	(0.055305)	1.4	-0.03117	0.18571
<i>L6</i>	0.042518	(0.036491)	1.17	-0.02903	0.114067
<i>L7</i>	0.075313	(0.041)	1.84	-0.00508	0.155703
<i>L8</i>	0.056461	(0.044719)	1.26	-0.03122	0.144143
Acceleration (on-coming)	0.02797	(0.039676)	0.7	-0.04983	0.105764
<i>L1</i>	-0.07029	(0.048921)	-1.44	-0.16621	0.02563
<i>L2</i>	-0.03298	(0.07294)	-0.45	-0.176	0.110035
<i>L3</i>	-0.14594	(0.142616)	-1.02	-0.42557	0.133691
<i>L4</i>	-0.22217	(0.088564)	-2.51	-0.39582	-0.04852
<i>L5</i>	-0.03385	(0.064731)	-0.52	-0.16077	0.093067
<i>L6</i>	-0.01779	(0.046737)	-0.38	-0.10943	0.073843
<i>L7</i>	-0.01851	(0.044124)	-0.42	-0.10503	0.068002
<i>L8</i>	0.019328	(0.052231)	0.37	-0.08308	0.121739
Acceleration (cross from left)	0.020756	(0.030988)	0.67	-0.04	0.081516
<i>L1</i>	-0.02112	(0.030586)	-0.69	-0.08109	0.038854
<i>L2</i>	0.050372	(0.06047)	0.83	-0.06819	0.168937
<i>L3</i>	0.049612	(0.033572)	1.48	-0.01621	0.115438
<i>L4</i>	0.131799	(0.224735)	0.59	-0.30885	0.572444
<i>L5</i>	-0.05979	(0.054833)	-1.09	-0.1673	0.04772
<i>L6</i>	0.124471	(0.107919)	1.15	-0.08713	0.336069
<i>L7</i>	-0.0268	(0.031938)	-0.84	-0.08942	0.035826
<i>L8</i>	0.025801	(0.030489)	0.85	-0.03398	0.085582
Acceleration (cross from right)	-0.01862	(0.039225)	-0.47	-0.09553	0.058293
<i>L1</i>	-0.02311	(0.051862)	-0.45	-0.1248	0.078575
<i>L2</i>	-0.00725	(0.027757)	-0.26	-0.06168	0.047174
<i>L3</i>	-0.06603	(0.035083)	-1.88	-0.13482	0.002757
<i>L4</i>	0.188406	(0.149858)	1.26	-0.10543	0.482237
<i>L5</i>	-0.01735	(0.044845)	-0.39	-0.10528	0.070574
<i>L6</i>	0.055406	(0.036781)	1.51	-0.01671	0.127523
<i>L7</i>	0.023112	(0.025406)	0.91	-0.0267	0.072926
<i>L8</i>	-0.02465	(0.028053)	-0.88	-0.07965	0.030358
Intersection	-0.02876	(0.015911)	-1.81	-0.05996	0.002436
<i>L1</i>	0.015379	(0.01671)	0.92	-0.01738	0.048141
<i>L2</i>	-0.01167	(0.015824)	-0.74	-0.0427	0.019359
<i>L3</i>	0.013785	(0.01475)	0.93	-0.01514	0.042707
<i>L4</i>	-0.01144	(0.014643)	-0.78	-0.04015	0.017268
<i>L5</i>	0.012445	(0.013926)	0.89	-0.01486	0.03975
<i>L6</i>	-0.01066	(0.013016)	-0.82	-0.03618	0.014865
<i>L7</i>	0.038222	(0.014022)	2.73	0.010728	0.065716

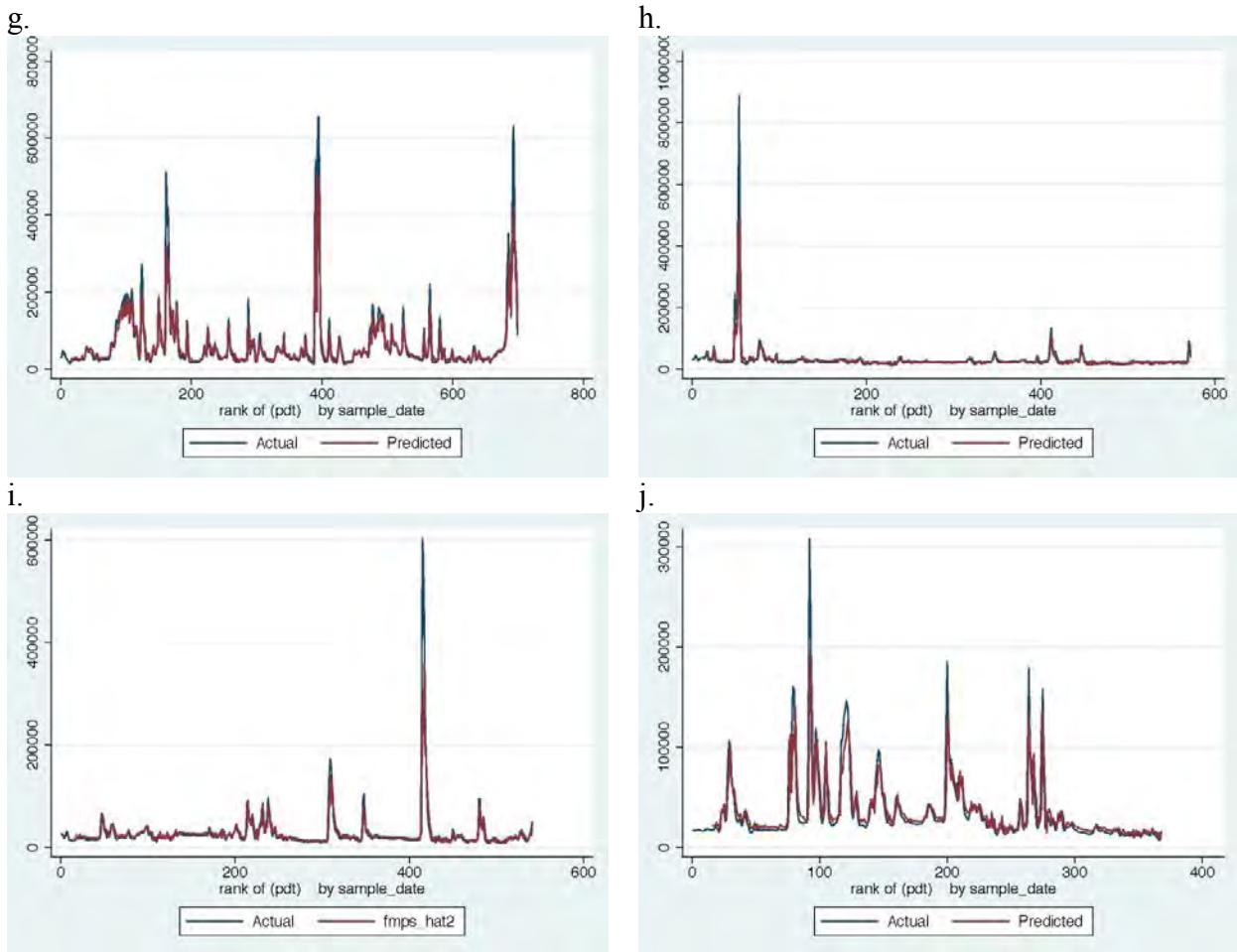
	Coef.	Robust Std. Err.	t	95% Conf. Interval	
<i>L8</i>	-0.00132	(0.012158)	-0.11	-0.02516	0.022518
Avg. building height	-0.00051	(0.00056)	-0.91	-0.00161	0.000587
<i>L1</i>	0.000082	(0.000693)	0.12	-0.00128	0.001441
<i>L2</i>	0.000438	(0.000523)	0.84	-0.00059	0.001463
Building height diff.	4.56E-05	(0.000376)	0.12	-0.00069	0.000783
<i>L1</i>	0.000312	(0.000375)	0.83	-0.00042	0.001047
<i>L2</i>	0.000363	(0.000294)	1.23	-0.00021	0.000938
North-south wind	-0.00656	(0.004016)	-1.63	-0.01443	0.001315
North-south wind × Avg. building height	0.000356	(0.000146)	2.43	6.91E-05	0.000642
East-west wind	0.004917	(0.004085)	1.2	-0.00309	0.012927
East-west Wind × Building height diff	-0.00029	(0.000231)	-1.28	-0.00075	0.000158
Linear position	-9.1E-05	(0.000101)	-0.9	-0.00029	0.000106
Linear position <sup>2</sup>	7.44E-08	(7.87E-08)	0.94	-8.00E-08	2.29E-07
Linear position <sup>3</sup>	-2.36E-11	(2.34E-11)	-1.01	-6.94E-11	2.23E-11
Linear position <sup>4</sup>	2.53E-15	(2.35E-15)	1.08	-2.08E-15	7.13E-15
Constant	0.617515	(0.091564)	6.74	0.437983	0.797046

v.4.3.2. *Out of sample model prediction: assessing accuracy*

To test for overfitting of our model, we perform 12-fold cross validation of the model iteratively leaving out each run, and using the remaining runs to predict the concentration of UFP for the withheld run. The resulting correlations of the actual and predicted concentrations range from 0.68 to 0.95, suggesting that the model predicts quite well out-of-sample.

**Figure 20. Actual versus Predicted UPF Concentrations for AM and PM Transects.**





*v.4.3.3. Model development and general results*

Our empirical model presented in Table 10 contains over a hundred estimated parameters, several of which involved lagged variables as well as interaction effects between numerous variables. To ease the interpretation of this model we present the estimated cumulative effects on UFP of focal variables in Table 11. We estimate the cumulative effect of a given variable on UFP, e.g., the number of on-going light-duty vehicles in front of the MMP, by placing all the other parameters at their mean values. We then estimate the predicted concentration of UFP when the variable of interest is set to zero, e.g., no on-going light-duty vehicles, and compared that with predicted UFP concentration when the variable of interest is set to its mean level, e.g., on-going light-duty vehicles. In addition, we bound these mean cumulative effects by estimating their 95% confidence intervals.

**Table 11. Cumulative Impacts of Traffic Events.**

All effects are in thousands of particles per cm <sup>3</sup> .				
	Impact	Std. Error	95% Conf. Interval	
<i>MMP State of Motion and Speed</i>				
Idle-to-moving	-28.65	(-11.4)	-50.99	-6.31
Speed (m/s)	-15.32	(-5.74)	-26.56	-4.07
Lane number	15.73	(-4.47)	6.97	24.49
<i>On-going Traffic</i>				
Light-duty	9.78	(-14.01)	-17.69	37.24
Medium & Heavy-duty	142.76	(-90.31)	-34.26	319.78

All effects are in thousands of particles per cm <sup>3</sup> .				
	Impact	Std. Error	95% Conf. Interval	
Buses	-25.66	(-155.91)	-331.25	279.92
Acceleration event	-58.7	(-122.98)	-299.74	182.34
<i>On-Coming Traffic</i>				
Light-duty	-0.99	(-16.77)	-33.85	31.87
Medium & heavy-duty	-18.8	(-57.18)	-130.88	93.28
Buses	-21.31	(-71.44)	-161.34	118.72
Acceleration event	-158.72	(-127.01)	-407.66	90.22
<i>Crossing from the Left Traffic</i>				
Light-duty	30.05	(-34.74)	-38.04	98.15
Medium & heavy-duty	80.79	(-76.07)	-68.31	229.89
Buses	92.64	(-111.96)	-126.8	312.08
Acceleration event	26.96	(-98.47)	-166.05	219.97
<i>Crossing from the Right Traffic</i>				
Light-duty	-10.94	(-58.6)	-125.8	103.92
Medium & heavy-duty	-30.58	(-162.81)	-349.68	288.53
Buses	54.04	(-59.01)	-61.61	169.69
Acceleration event	52.59	(-50.29)	-45.98	151.17
<i>Built Environment</i>				
Intersection	320.15	(-120.69)	83.6	556.7
Average building height (m)	1.7	(-4.5)	-7.13	10.52
Building height differential (m) <sup>a</sup>	233.06	(-270.62)	-297.36	763.48
<sup>a</sup> Difference in height of neighboring buildings is positive if the building to the east is taller, and negative if the building to the west is taller.				

As narrative strategy, we begin by describing variables that would become apparent as the MMP begins its transect sampling run. Thus, we started with variables associated with the i) MMP's state of motion and speed, ii) the on-going and on-coming traffic, iii) dynamics as it approaches and passes through an intersection, and finally, iv) the effects of the built environment and its interactions with meteorology.

***MMP State of Motion and Speed.*** As the MMP commences its transect sampling run, our model predicts that as it moves from *idle to moving* that the UFP concentrations will decline by -29 thousand/cm<sup>3</sup> with 95% intervals of -51 and -6. Notice that both confidence intervals are negative, indicating with a high degree of confidence that this change produces consistently lower UFP concentration. Similarly, as the *MMP speed* increases an additional meter per second, the measured UFP decline by 15 thousand/cm<sup>3</sup> with confidence intervals of -27 and -4. Both declines in UFP associated with changes in forward motion of the MMP may arise either by mixing or a partial vortex forming around the intake opening. As the MMP encounters slower moving traffic, causing it to *change lanes*, this is associated with an increase in UFP on the order of 16 thousand/cm<sup>3</sup> and are consistently positive (95% CI: 7 to 25 thousand/cm<sup>3</sup>).

**On-going Vehicles.** As the MMP travels along Broadway, it will encounter on-going traffic in immediately adjacent lanes and in front of it. The effect of adding the mean number of *on-going light-duty vehicles* is to increase the predicted UFP by 10 thousand/cm<sup>3</sup> with a 95% confidence interval of -18 and 37 thousand/cm<sup>3</sup>. The predicted effect of adding the mean number of *on-going heavy and medium vehicles* was to increase UFP by over 142 thousand/cm<sup>3</sup> with a confidence interval of -34 and 320 thousand/cm<sup>3</sup>. Notice that effect of adding on-going heavy duty vehicles as compared to light-duty vehicles is to increase UFP concentrations by more than a factor of 10. In contrast, the predicted effect increasing the mean number of *on-going buses* is to decrease UFP to -26 thousand/cm<sup>3</sup>, with wide 95% confidence intervals of -331 and 280 thousand/cm<sup>3</sup>. Thus, is likely due to both the high fraction of natural gas buses and their ability to entrain a larger volume of cleaner air from aloft into their wakes.

**On-coming Vehicles.** The MMP also passes on-coming traffic in the opposite two lanes. For on-coming vehicles we anticipate two potentially countervailing effects. On-coming traffic releases fresh emissions which would increase UFP concentration, albeit very briefly as these vehicles pass by the MMP. This rapid passing of these on-coming vehicles is also associated with increased turbulence and mixing of air which may dilute UFP concentrations around the MMP leading to a lowering of UFP concentrations.

The cumulative impacts (Table 11) suggest that the mean effect of all types of on-coming vehicles is associated with lower UFP. However, while the upper 95% confidence interval for each type of vehicle includes positive values but at concentrations that are lower than those associated with comparable on-going vehicles. For example, the effect of adding the mean number of *on-coming light-duty vehicles* was to decrease the predicted UFP by 1 thousand/cm<sup>3</sup> with a 95% confidence interval of -34 and 32 thousand/cm<sup>3</sup>. The predicted effect of adding the mean value of *on-coming heavy and medium vehicles* was to decrease UFP by over 19 thousand/cm<sup>3</sup> with a confidence interval of -131 and 93 thousand/cm<sup>3</sup>. The predicted effect for the mean number of *on-coming buses* is a -22 thousand/cm<sup>3</sup> with 95% confidence intervals of -116 and 119 thousand/cm<sup>3</sup>. Notice that size of these effects increases progressively with the body size of vehicles (light-duty vehicle, mid to large truck, bus) which may be associated with increasingly larger induced turbulence effects.

**Dynamics at Intersections.** The emission and dispersion dynamics at intersections are complex, as vehicles approach, enter and leave the intersection from four directions. From each direction, some vehicles will queue and idle at a red stop light before accelerating from that stationary position through the intersection as part of a platoon of vehicles. We find that measured UFP concentrations are highest while the MMP is in intersections as compared to when it is traveling along streets bounded by buildings. When entering an *intersection*, our model predictions UFP will increase by mean amount of 320 thousand/cm<sup>3</sup> with 95% confidence intervals of 84 and 557.

Our model enables us to explore several questions related to the UFP concentrations measured by the MMP while it is both i) stopped at an intersection and ii) as it traverses the intersection. For context, consider the MMP as it approaches an intersection from an on-going direction as in Figure 2. Our model enables us to consider a setting in which the MMP first comes to a stop in a queue at a red light. Traffic is waiting to cross into the intersection from the left, which will pass closest to the queuing MMP. Traffic is also waiting to cross into the intersection from the right in lanes that are relatively further away. Recall that the prevailing wind direction is from the southwest. Thus, when vehicles crossing from the right accelerate from a stopped position, the wind will tend to move their fresh emissions toward the queuing MMP. However, when vehicles crossing from the left accelerate from a stopped position, these fresh emissions are generally released downwind of the MMP. In keeping with these predictions, acceleration events for traffic crossing from the right are

associated with UFP increase of 58 thousand/cm<sup>3</sup> when vehicles crossing from the left accelerate, the associated UFP increase is much smaller 27 thousand/cm<sup>3</sup>.

These queuing vehicles also crossed in front of the queuing MMP. Light-duty vehicles crossing from the left were associated with an increase of 30 thousand/cm<sup>3</sup> while heavy duty vehicles were associated with an increase of 81 thousand/cm<sup>3</sup>. Buses crossing from the left were associated with an UFP concentration increase of 92 thousand/cm<sup>3</sup>. There is no agreement whether these increases in UFP are contributions from these specific vehicles or whether these types of vehicles created different turbulence patterns that spread local emissions that had accumulated previously.

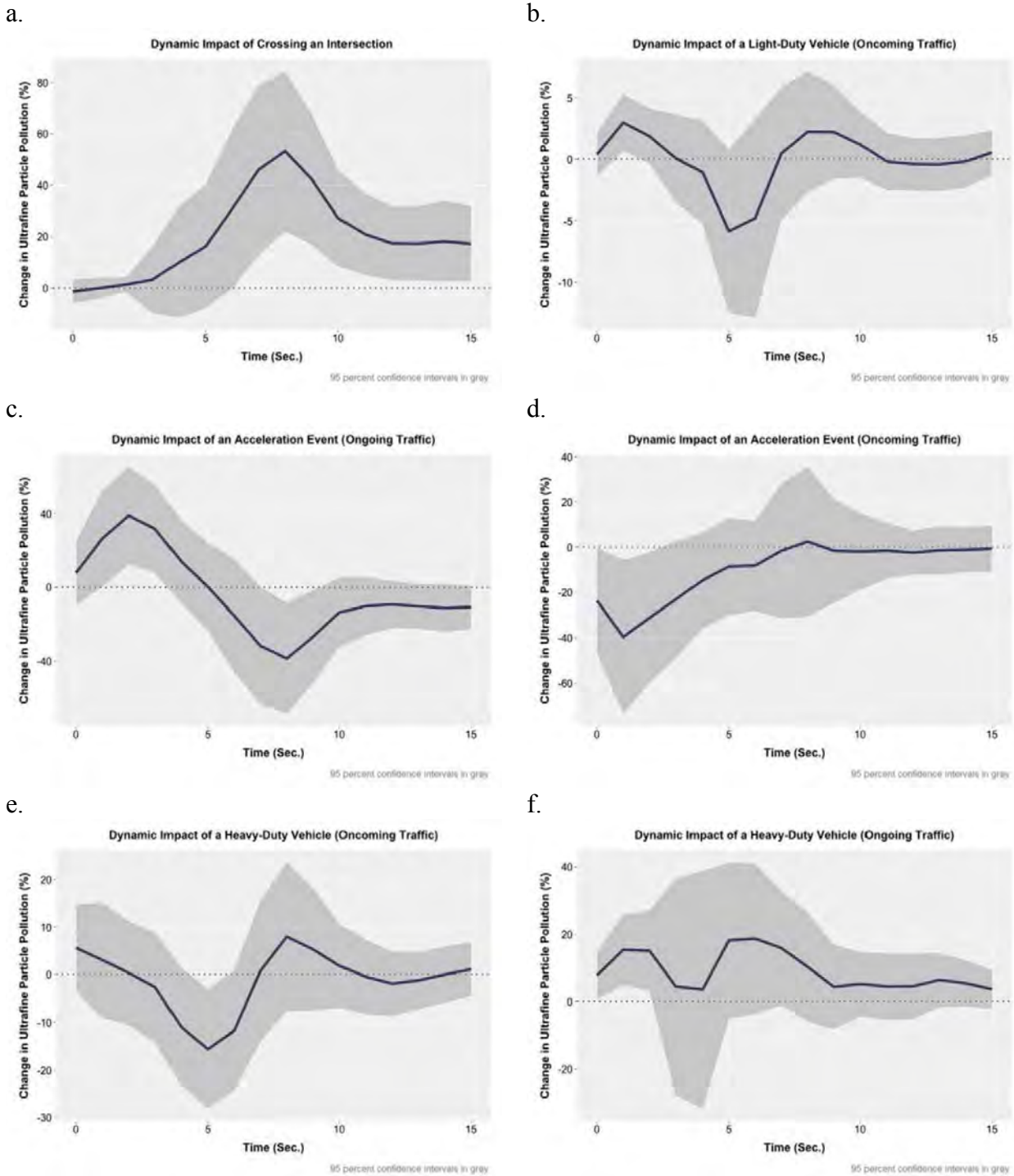
What it is curious, is that some types of vehicles crossing from the right produce different effects. Light-duty vehicles and heavy duty vehicles crossing from the right were associated with lower (not higher) UFP concentrations in the queuing MMP. When crossing from the right, light-duty vehicles and heavy-duty vehicles were associated with -11 thousand/cm<sup>3</sup> and -31 thousand/cm<sup>3</sup> respectively. Right-crossing buses, as with left-crossing buses, were associated with increase in UFP concentration of 53 thousand/cm<sup>3</sup>. Especially for variables associated with intersection dynamics, it is important to notice how large the confidence intervals are.

#### *v.4.3.4. Temporal profiles of traffic events*

In the previous section, we summarized the effects of various traffic impacts as simple averages, while in reality each event transpired over a period of time. Including higher temporal resolution within our model enables us to describe for each of these events how the UFP concentration varies over time. In the forgoing analysis, we examine the temporal profile of selected events over 15 second intervals by setting all the variables at their mean levels before re-setting the relevant event from zero to its mean level. Below we have chosen a few events to illustrate how valuable this type of analysis may be.

**Intersections.** We begin with Figure 21, which describes the UFP impacts of the MMP crossing an intersection. The y-axis represents the percentage change from the UFP mean prior to the MMP entering an intersection. The solid line represents the means UFP level while the shaded area indicates the 95% confidence intervals. Using the estimated model to simulate the effects of MMP passing through the intersection, we observed that UFP concentrations peaks at over 50% of their pre-event mean between 5 and 10 seconds after entering the intersection. Even after 15 seconds, the simulations reveal the UFP concentrations are 20% above their pre-event, and statistically-significantly so. This suggests a longer time period is needed to fully characterize the time profile of intersection effects, which we will explore in the following section.

**Figure 21. Time Profiles of Selected Traffic Events.**



***On-coming traffic: Heavy and Light Duty.*** In the previous section, recall that the cumulative impact of all types of on-coming vehicles was associated with a decrease UFP. However, we identified two countervailing effects of coming traffic: i) an increase in fresh emission and ii) an increase vehicle induced turbulence which might entrain cleaner air and reduce UFP concentrations. Below we compare the time profiles of heavy and light duty vehicles. Heavy duty vehicles are likely to travel more slowly and be larger than light duty vehicles, thus presenting different patterns of vehicle induced turbulence.

The cumulative impact on UFP concentration from an *on-coming heavy duty vehicle* was a -19 thousand/cm<sup>3</sup> with a 95% confidence interval of -131 and 93 thousand/cm<sup>3</sup> (Table 11). However, Figure 5e reveals significant systematic temporal variation in UFP concentrations for on-coming heavy duty vehicles. Within the first second of the on-coming heavy duty vehicles being visually identified the UFP concentrations decreased, reaching its lowest point at the 5th second before increasing to about 8% above pre-event concentrations. By the 10th second, concentrations levels have returned to their pre-event level.

The UFP concentration for an *on-coming light duty vehicle* was a -1 thousand/cm<sup>3</sup> with a 95% confidence interval of -34 and 32 thousand/cm<sup>3</sup> (Table 11). Figure 21 shows a systematic m-shaped temporal variation in UFP concentrations for on-coming light duty vehicles. Within the first second of the on-coming light duty vehicles being visually identified, a small (2-3%) but statistically significant increase in the UFP concentration was observed. At about the 4 second mark, on-coming light duty vehicles are then associated with a drop of over 5% in UFP concentration, and this persists until second 7. After this, concentrations rebound, and positive correlation up to 2-3% concentration level until they level off at second 7 to prior background levels. While small in magnitude, the aggregate effect of numerous on-coming light duty vehicles may prove to be significant.

***Acceleration events for On-going and Oncoming Traffic.*** Acceleration events, which includes all vehicle types, occurs when traffic that was stopped at a red light accelerates. As shown in Table 11, the cumulative impacts of on-going acceleration events were -59 thousand/cm<sup>3</sup>. Figure 21 presents the dynamic impacts of an acceleration event for on-going traffic. For the first 5 seconds, UFP concentrations are strongly correlated with acceleration, with the peak mean level rising to 40% of pre-event levels before falling and are statistically different from zero at the 95% level. Between the 5th and 10th second, UFP concentrations decreased by 40%; again this difference is statistically different from zero at the 95% level. Focusing only on the simple mean of -59 thousand/cm<sup>3</sup> for on-going traffic masks this consistent and significant lateral s-pattern in UFP concentrations.

As shown in Table 11, the cumulative impacts of on-coming acceleration events were -159 thousand/cm<sup>3</sup>. This impact is one directional; Figure 5d shows a time profile in which UFP concentrations drop immediately (within 1 second) to a low of 40% but with the 95% confidence interval including -70%. The concentration then increases steadily until approximately the 7th second where it stabilizes at pre-event levels, suggesting vehicle-induced entrainment of cleaner air dominates an increase in UFP from the vehicle plume.

#### *v.4.3.5. Simulating changes in traffic composition*

The estimated model from Table 10 can also be used to characterize larger scale travel-patterns and traffic composition scenarios and their associated UPF concentration transect profile. We begin with a baseline scenario in which the MMP travels 400 m through an intersection without stopping and starting again. We then add a stop-start scenario at the intersection to this same 400 m transect. This simulation enables us to characterize the predicted UFP concentration profile distinctly in terms of time (per second) versus distance (per meter) revealing important differences. Finally, we use the estimated model to consider how the stop-start scenario differs if there is a significant increase in the number of light duty vehicles.

***Our Baseline assumptions and UFP Predictions.*** The baseline simulation is over a 400 meter transect representative of the broader Broadway environment. It contains a 12-meter intersection from meter 103 to 115. This case represents a rational scenario in which a vehicle is not required to stop at an intersection. The MMP cruises for 225 m/30 s. at constant speed (7.5 m/s) across an intersection. No acceleration instances occur, no cross-traffic is encountered, and all neighboring buildings are 15 m high. Wind variables and location fixed effects (building height and differences)

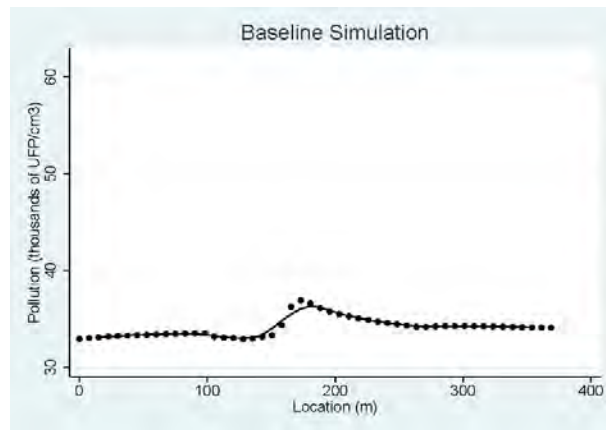
are set to long-run averages. On-going and on-coming traffic are also set to long-run averages. The resulting UFP concentration profile is presented in Figure 22a. The starting UFP concentration is approximately 32 thousand/cm<sup>3</sup>. Shortly after passing through the intersection UFP concentrations increase slightly to approximately 37 thousand/cm<sup>3</sup> before returning to the starting baseline.

**“Stop-and-start” Simulation.** The MMP travels for 10 seconds at 7.5 m/s, then decelerates for 10 seconds, before stopping at the intersection for 30 seconds. As soon as the MMP comes to a complete stop, cross-traffic accelerates into the intersection. On-coming, on-going, left- and right-cross-traffic (when occurring) are set to long-run averages. As soon as the MMP starts accelerating, on-going and on-coming traffic accelerate into the intersection. It then accelerates through the intersection for 10 seconds and cruises for 10 seconds returning to a velocity of 7.5 m/s.

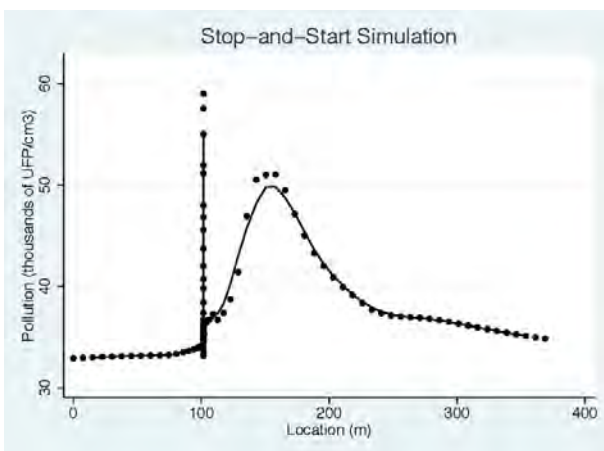
The UFP concentration profile associated with this simulation may be expressed in terms of location (or distance such meters) as shown in Figure 22b. Figure 22b shows a marked increase of almost 60 thousand/cm<sup>3</sup> in measured UFP concentrations at 103 m, when the MMP is stopped for 30 s in front of the red light (and cross traffic). Notice that in this stopped position, the measured UFP are nearly twice the baseline concentration of 32 thousand/cm<sup>3</sup>. The simulation reveals a significant second spike of UFP concentrations for the next 85 m as the MMP accelerates with a platoon of other vehicles passing through the fresh emissions of the crossing traffic. This second peak of UFP rises in concentration to almost 50 thousand/cm<sup>3</sup>. This simulation illustrates the spatial structure and origins of the more aggregate intersection plume of emissions shown earlier in Figure 21.

**Figure 22. Baseline Free-flow Simulation and Simulation of Stop-start events at an intersection.**

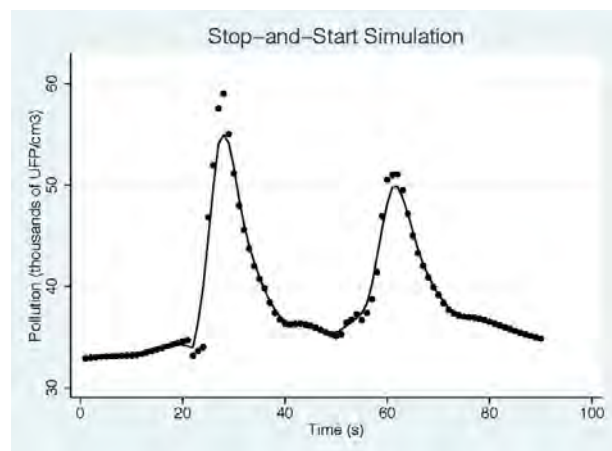
a.



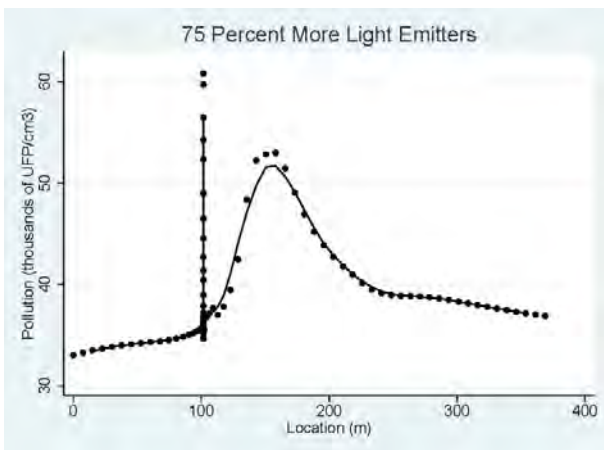
b.



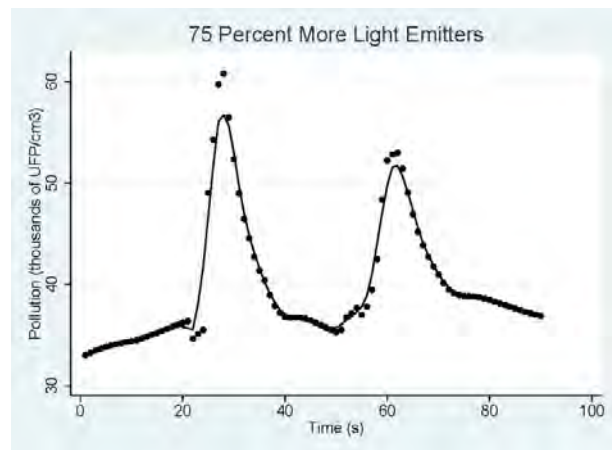
c.



d.



e.



The UFP concentration profile can also be characterized in terms of time (i.e., seconds) as shown in Figure 22c. This time-denominated profile also shows a bi-modal distribution of UFP but unlike the location-denominated profile, this distribution is smoother. What we learn from this presentation of the data is that UFP emission spikes sharply just after the 20 s mark as soon as the MMP has come to full stop. What is obscured by the distance-denominated profiles, but is revealed here is that UFP concentrations then steadily decline over the next 30 s the MMP is stationary at the stop light. As the MMP accelerated over the next 10 s and moved across the intersection UFP concentrations steadily increased. The second emission plume peaks just as the MMP is exiting the intersection (at the 60 s mark) and then steadily declines.

In principle, this model should also be able to simulate changes in UFP associated with changes in the composition of traffic around the MMP. In our last simulation, we evaluate the effects on an increase of 75% in light duty vehicles. This is shown in Figure 22d and Figure 22e, which represents both the distance- and time-denominated UFP profiles. The levels of concentrations can be directly compared to the Figures 6B and 6C which have the average number of the light duty vehicles. The increase in UFP appears small: The peaks in both profiles increase by about 3 thousand/cm<sup>3</sup> which is about a 10 percent increase. Given that number of light duty vehicles increase by 75% this seems like a small increase. We also explore increasing the number of heavy duty vehicle by a comparable amount. Because heavy duty vehicles were very infrequently encountered, and thus represented a very small base, even doubling them did not significantly alter the UFP profiles in our simulations.

#### v.4.4. Cross-intersection profiles of UFP in various environments: implications for pedestrian exposure and transit stop siting

##### v.4.4.1. *Data analysis and cross-intersection concentration profiles*

Producing representative profiles from MMP data presents a few challenges associated with over/underweighting data and dealing with day-to-day variations in background concentrations. The acquisition of correct positioning information of the MMP is critical in obtaining highly resolved concentration profiles. Handheld GPS units have approximately 3 to 5 m accuracy with a wide area augmentation system (WAAS). Nonetheless, under specific conditions such as street canyons shadowing effects can result in poor reception of satellite signals (Birmili et al. 2013; Misra and Enge 2006; Ranasinghe et al. 2016). These wandering GPS position data were corrected with a line referencing technique developed by Ranasinghe et al. (2016). Briefly, a reference line consisting of evenly spaced points was assigned for each direction of the streets. Five-meter spatial resolution for the points on the reference line was chosen, based on the mean MMP speed driven for all sessions (3.0 m·s<sup>-1</sup> with  $1\sigma = 2.9$  and 3.4 m·s<sup>-1</sup> for the morning and afternoon sampling periods, respectively). Each GPS data point was assigned to the closest reference point. When multiple data points are assigned to one reference point (e.g., when the MMP stopped or was moving slowly), these data were averaged. This avoids the problem of overweighting a run with many data points compared to a run when the MMP passed by a reference point without stopping. The other overweighting problem occurs when some runs have no data assigned to a particular reference point, due to a fast-moving MMP. To avoid this problem, the concentration profile for each individual run was interpolated using Piecewise-Cubic-Hermite-Interpolation scheme (PCHIP) (Fritsch and Carlson 1980). PCHIP was successfully applied to interpolate data points while faithfully preserving the concentration profiles (Ranasinghe et al. 2016).

To obtain representative concentration profiles for intersections many concentration profiles were collected in different built- and traffic-environments. In addition, to avoid the distortions from daily concentration variations on averaging the profiles, the minimum value of each profile was subtracted from the profile before averaging. Then, to put the data back on a meaningful scale, the mean of the minimum values from all collected profiles was added to obtain mean concentration profiles. In the figures, the MMP driving direction is represented by a (-) sign when it approaches the intersection, zero at the center of intersections, and (+) signs after passing by the intersection. Thus, distance in the averaged profiles consistently represents the traffic direction in which the MMP was headed, and not the direction relative to the compass. The distance covers 90 m on either side of the intersection, which was chosen because the average block length is 180±64 m (Table 12) and earlier work has suggested this range captures most of the variability around intersections (Goel and Kumar 2015). Sampling sites are shown in Figure 2, Figure 3, and Figure 4 in Section 2.1.

**Table 12. Sampling dates and information of the intersections investigated in this study.**

	Bev	BW&7th	Olv&12th	Ver&7th	Wil&Car	TC&LT
Street	(1) varying (2) Wilshire Blvd.	(1) Broadway St. (2) 7th St.	(1) Olive St. (2) 12th St.	(1) Vermont Ave. (2) 7th St.	(1) Carondelet St. (2) Wilshire Blvd.	(1) Temple City Blvd. (2) Las Tunas Blvd.
Street width	(1) varying (2) 30-38 m	(1) 26 m (2) 22 m	(1) 28 m (2) 17 m	(1) 30 m (2) 25 m	(1) 17 m (2) 37 m	(1) 24 m (2) 30 m
Traffic flow rates (A.M.)	(1) varying (2) 24	(1) 12 (2) 15	(1) 21 (2) 4	(1) 39 (2) 10	(1) 2 (2) 31	(1) 25 (2) 28
Traffic flow rates (P.M.)	(1) varying (2) 47	(1) 20 (2) 20	(1) 8 (2) 3	(1) 38 (2) 12	(1) 2 (2) 27	(1) 26 (2) 29
Traffic density (qualified)	Long queue length in one direction (WB in A.M. and EB in P.M.)	Medium queue lengths but slow vehicle speeds	Minimal queue lengths	Long Queue lengths covered the whole block particularly in NB	Low queue lengths	Long queue lengths but rapidly dissipated due to effective traffic flow
Distance between traffic lights	(1) varying <sup>a</sup> (2) 330 m <sup>b</sup>	(1) 200 m (2) 125 m	(1) 180 m (2) 125 m	(1) 224 m (2) 174 m <sup>c</sup>	(1) 190 m (2) 100 m	(1) 200 m (2) 135 m
Number of profiles obtained for each run	2 (east-, west-bound) × 5 intersections = 10	4 (north-, south-, east-west-bound)	3 (north-, south-, east-bound)	4 (north-, south-, east-west-bound)	4 (north-, south-, east-west-bound)	4 (north-, south-, east-west-bound)
Sampling dates	6/17/2014 6/19/2014 6/24/2014 6/36/2014	7/1/2013 7/2/2013 7/3/2013 7/5/2013	9/24/2013 9/24/2013	10/7/2013 10/14/2013 11/18/2013	11/1/2013 11/6/2013 11/20/2013	8/6/2013 9/17/2013 9/18/2013

*v.4.4.2. Highly resolved UFP profiles around intersections*

In this section, we show [UFP] profiles around signalized intersections obtained by averaging individual profiles that were collected for varying traffic, spatial, and temporal spans. The averaging spans expanded from each traffic direction for each site into the entire traffic directions for each site and into the entire sites for the morning and afternoon sampling events.

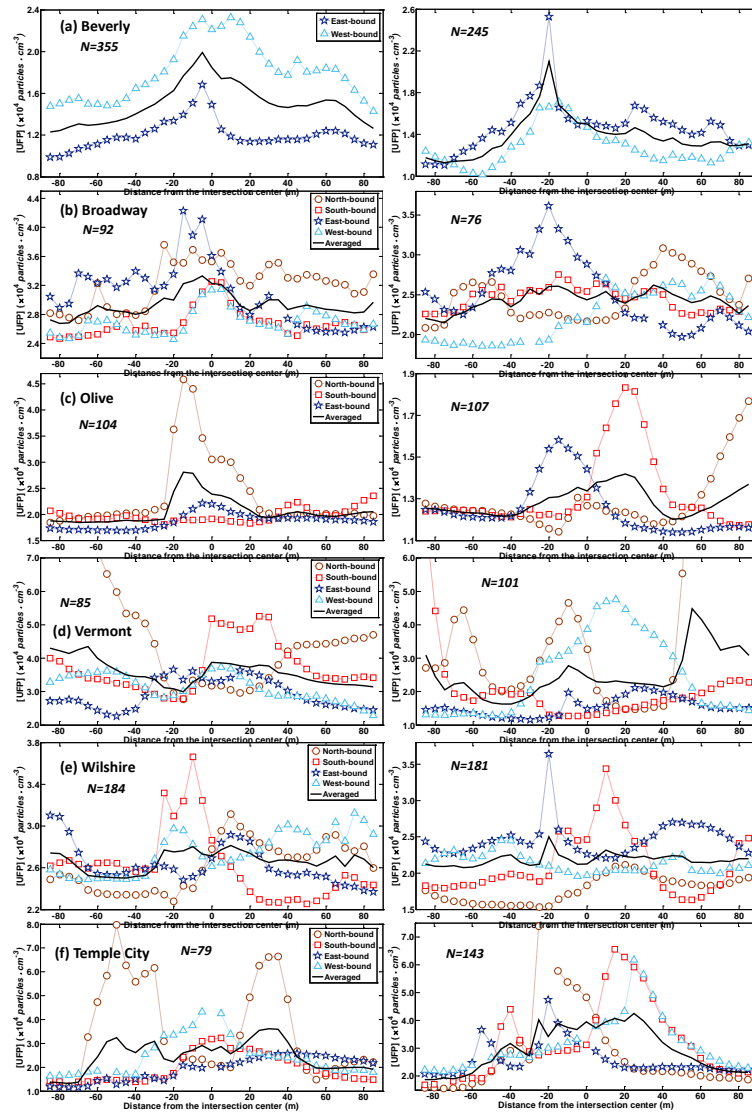


**Figure 23.** The mean UFP profiles across the intersection for each direction of the site (broken lines with symbols) and the mean profile of all directions for each site (black solid lines). N denotes the number of the total profiles obtained for the site. Left and right panels show the results for AM and PM sampling events, respectively. The % values in parentheses represent UFP elevation at the peak relative to the base value.

Figure 23 and Table 13 show the statistical results of averaging [UFP] profiles of each direction for each site. The first striking feature of the mean [UFP] profiles of each traffic direction for each site is that highly elevated [UFP] occurs commonly near the intersections but at varying locations (mostly < 30 m from the intersection center) within a relatively short distance range (roughly less than 60 m of peak width) (Figure 23). The only exception was Vermont & 7<sup>th</sup> site, at which the profiles showed more complicated shapes. Vermont Ave. is one of the busiest arterial streets in Los Angeles, and for both morning and afternoon sampling events, the road experienced traffic congestion along the entire sampling block (particularly for the north-bound). Thus, vehicles repeatedly stopped and accelerated throughout, likely causing higher [UFP] all along the roadway. In this respect, we confined the distance range to identify the intersection peak within  $\pm 50$  m from the intersection center.

**Table 13. Basic statistics of the intersection UFP profiles of each direction for each site.**

Site	Direction	Morning			Afternoon		
		Peak position (m)	Base position (m)	Conc. Diff. between peak and base (%) <sup>a</sup>	Peak position (m)	Base position (m)	Conc. Diff. between peak and base (%) <sup>a</sup>
Beverly	EB	-5	-85	70.4	-20	-75	128.4
	WB	10	-55	62.9	-15	-55	69.0
Broadway	EB	-15	60	65.3	-20	50	84.0
	WB	5	-75	27.4	10	-55	45.8
	NB	-15	-70	38.3	40	-85	48.1
	SB	0	-80	31.8	-15	55	22.8
Olive	EB	-5	-45	31.0	-15	50	38.8
	NB	-15	35	137.9	-5	-15	14.3
	SB	0	-25	5.8	20	75	55.8
Vermont	EB	-20	-50	62.0	25	-30	83.2
	WB	5	85	63.0	15	-50	270.0
	NB	-50	-15	217.5	-10	30	215.8
	SB	25	-20	88.4	-30	-5	60.6
Wilshire	EB	10	85	23.0	-20	15	65.2
	WB	-20	-45	19.4	-45	-5	25.3
	NB	10	-20	36.8	20	-25	38.0
	SB	-10	50	62.4	10	50	110.2
eTemple City	EB	40	-70	122.7	-20	-75	90.3
	WB	-5	-45	154.7	25	-75	127.0
	NB	30	-75	447.3	-25	-65	226.6
	SB	5	-40	132.6	15	-85	181.6
Mean <sup>b</sup> (std)		15 (15)	54 (23)	86 (93)	20 (10) <sup>b</sup>	46 (26)	95 (72)

The mean relative elevations of the peak [UFP] near the intersection was 86% ( $1\sigma = 93\%$ ) and 95% ( $1\sigma = 72\%$ ) compared to the profile minima for the morning and afternoon session, respectively (Table 13), although they ranged widely (6 ~ 447% for the morning and 23 ~ 270% for the afternoon session). The mean position of the concentration peaks is 15 ( $\pm 15$ ) m and 20 ( $\pm 10$ ) m from the center of the intersection for the morning and afternoon sampling events, respectively. The mean location of the minimum concentrations occurred 54 ( $\pm 23$ ) m and 46 ( $\pm 26$ ) m from the center of the intersection for the morning and afternoon sampling events, respectively. It should be noted that the peak distance is the absolute value, although the peak and minimum concentrations occurred in both far and near sides of the intersection. Peaks appeared equally before or after the intersection; 57% were on the near side on the morning, and 50% in the afternoon. The minimum position, however, appeared more on the near side of the intersections; 76 and 66% appearing on the near side in the morning and afternoon, respectively. This implies that there would be a reduction in exposure, were bus stops sited before the intersection. However, we also acknowledge that there are several other factors that favour the far side for placing traffic stops, including better traffic flow and shorter stop times for transit vehicles, both of which tend to lower air pollutant emissions and/or exposure of transit users.

The varying location and magnitude of [UFP] peak resulted from complex interactions between the built environment, traffic (as well as vehicle composition), drivers' behavior, winds, and other meteorological conditions. This complicated feature of intersection peak locations and magnitudes should be noted when stationary measurements for pedestrian exposure to vehicular emissions are conducted near the intersection.

The black solid lines in Figure 23 represent the results of averaging all of the directions for each site together. Averaging more profiles together (beyond the first 10 or 20, which have a lot of variance)

results in progressively smaller differences between the peak and minimum concentrations, due to variations in the location of the peak concentration. As a result, while averaging more data together results in more generalized profiles, it underestimates potential exposures around the intersection. For example, the elevation of [UFP] (concentration difference between the peak and minimum values relative to the minimum,  $\Delta$ [UFP]) is significantly increased when  $\Delta$ [UFP] was obtained from averaging all  $\Delta$ [UFP] for individual directions, compared to one obtained from the profile of averaging all of the directions for the entire sites. The mean increase in [UFP] near the intersection was 50 and 66% when  $\Delta$ [UFP] was calculated from the latter case in the morning and afternoon sampling events, respectively, while these values increased to 86 and 95% when we averaged  $\Delta$  [UFP] obtained from the profiles of each traffic directions (the former case). Nonetheless, the common feature of the mean concentration profiles for each sampling site is similar to those for individual traffic directions that [UFP] were higher near the intersections and had larger variations than locations about 40 m or more from the intersections (Figure 23 and Table 14).

**Table 14. Basic statistics of intersection [UFP] profiles for each site. The values in parentheses are averages from all profiles of each traffic direction for each site.**

		Bev	BW&7 <sup>th</sup>	Oliv&12 <sup>th</sup>	Ver&7 <sup>th</sup>	Wil&Car	TP&LT	AVG
A.M.	Peak conc.	19,910	33,311	28,062	38,792	28,145	36,115	30,723
	Min. conc.	12,292	26,760	18,455	29,923	25,017	13,218	20,944
	Mean. conc.	14,815	29,316	20,605	35,869	26,626	24,777	25,366
	Conc. Difference between peak and min. conc.	7,618 (7,967)	6,551 (10,474)	9,607 (12,711)	8,869 (21,306)	3,128 (9,030)	22,897 (31,780)	9,779 (16,401)
	Conc. difference relative to min. conc.	62% (67%)	24% (41%)	52% (58%)	45% (82%)	13% (35%)	173% (214%)	50% (86%)
	Peak conc. location	-10 m <sup>a</sup>	-10 m	-15 m	0 m	10 / -10 m	30 m <sup>b</sup>	
	Baseline location	-85 m	-80 m	-70 m	-15 m	-45 m	-75 m	
P.M.	Peak conc.	20,989	26,224	14,193	29,430	24,990	52,469	28,049
	Min. conc.	11,280	21,455	12,013	16,278	20,776	28,714	18,419
	Mean conc.	13,815	24,256	12,865	25,010	21,848	39,646	22,907
	Conc. Difference between peak and min. conc.	9,709 (10,602)	4,769 (10,098)	2,180 (5,759)	11,493 (23,164)	4,214 (10,793)	23,756 (43,582)	9,353 (18,103)
	Conc. difference relative to min. conc.	86% (99%)	22% (50%)	18% (36%)	71% (158%)	20% (60%)	83% (155%)	66% (95%)
	Peak conc. location	-20 m	35 / -20 m	20 m	-10 m	-20 m	25 / -25 m	
	Baseline location	-75 m	-75 m	-45 m	-40 m	-65 m	-70 m	

a. Positive length denotes the distance after the intersection center

b. Negative length means the distance before the intersection center

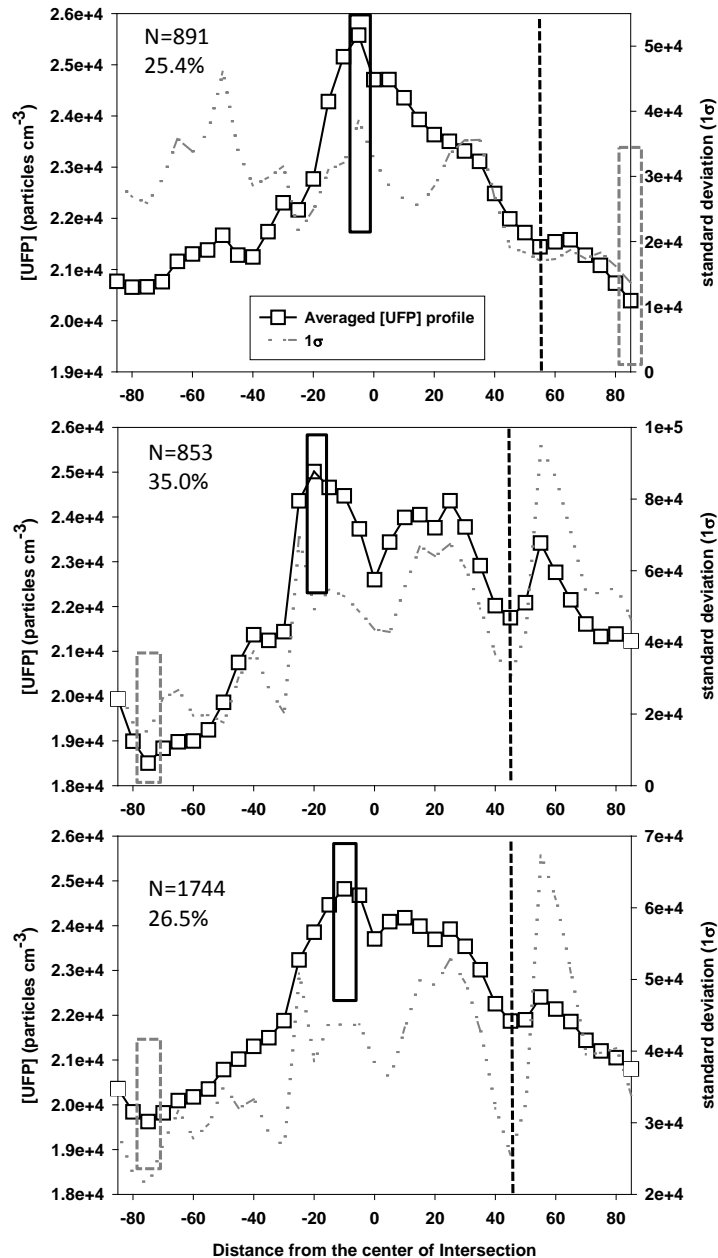


**Figure 24.** Same as Figure 23 but for (a) the entire A.M., (b) the P.M., and (c) the entire periods. Dark gray rectangles denote the location of the peak concentration and gray dashed rectangle indicate the base location. See text for the vertical gray dotted lines.

While more optimized values could potentially be developed for more specific situations, we produced several averages to produce simplified, general results. In this respect, the averaged cross-intersection profiles for the mornings (891 profiles) and afternoons (853 profiles) of the all sites were calculated (Figure 24a, b). Similar to the mean profiles for each site and each traffic direction, the peak concentrations occurred within 30 m before and after the center of intersection and sharply decreased by 45~55 m from the intersection. The peak concentrations near the intersections were 25% and 35% higher than the baseline values for the mornings and afternoons, respectively. Given that the magnitude of morning and afternoon averaged profiles were similar, all transect data (1744 individual profiles) were also averaged to produce a single mean intersection profile. Considering the large number of conditions represented, the mean profile is expected to show the general pattern of cross-intersection pollutant concentration variations regardless of time and location at least for the Los Angeles area. The peak concentration occurred 10 m before the intersection, and was 27% higher than the baseline value at 75 m before the intersection. Shoulder peaks occurred at 10 m and

25 m after the center of intersection and had higher standard deviations and sharply decreased with distance from the intersection up to 45 m, although [UFP] kept decreasing more slowly with farther distance.

**Variability in the profiles.** The common feature of the mean cross-intersection [UFP] profiles was that larger variability was observed at and around the intersection peak locations than at distances farther away from the intersection (grey dashed lines in Figure 24). Thus, although the mean peak concentration was about 27% higher than that at 75 m away from the intersection center, the concentrations at some moments much higher than the mean value; the  $1\sigma$  standard deviation at the peak is about double the mean concentration.

This section discusses the concentration distributions at two extreme cases: at the intersection peak and the baseline where the lowest concentration occurred in the mean profile. For the overall [UFP] average profile (Figure 24c), the peak concentration was recorded at 10 m before the center of intersection (indicated with a black rectangle) and the baseline value was set about 75 m before the intersection (indicated with a grey dotted rectangle), each of which includes 1,744 data points ( $N=1,744$ ). Using the collected data for two locations, cumulative distribution plots were obtained (Figure 25). The linear fit obtained with observation data between lower 25% and 75% of the dataset was considered as a baseline of cumulative distribution (red and black dotted lines) because in this range data distribute quasi-linearly ( $R^2 > 0.99$  for both the peak and base locations). In this way, the transient [UFP] spikes above the baseline that likely originated from excessive emissions events can be quantified. In addition, the baseline fit provides the information with respect to [UFP] variations in lower concentration part. The baseline for the peak location (a red dotted line in Figure 25) was slightly higher (slope =  $2.80 \pm 0.01 \times 10^4$ ) than that for the base location (slope =  $2.51 \pm 0.01 \times 10^4$ ). The difference in the interceptions between two baselines was negligible (4,603 vs. 4,233 for the peak and base locations, respectively). Overall, the baseline difference between two cases was only 10% relative to the base case (calculated by integrating the baseline fits from lower 25% through 75% of data).

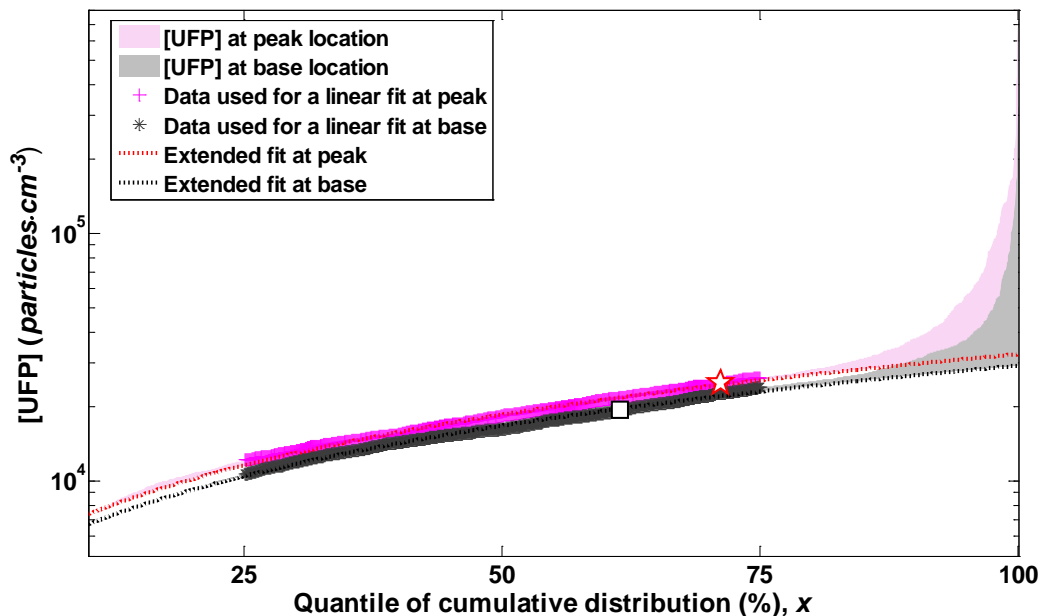


**Figure 25.** Cumulative [UFP] distribution plot at the peak (pink area) and base locations (gray area) indicated as black and gray dashed rectangles in Fig. (2c). Data are from the mean [UFP] profile for the entire sampling periods ( $N=1744$ ). Red and black dotted lines show a linear fit for data between lower 20 to 70% (pink crosses and gray asterisks) for the peak and base location, respectively. Red Star and the white denote the mean values at the peak and base location, respectively.

The major differences between two cases occurred in the upper 15% of the dataset. The observations sharply shot over the fitted baseline around the upper 15% of data for both the peak and base locations, however, larger deviations were shown for the peak location than the base case. These large deviations from the fitted baseline were caused most likely by elevated emissions from high emitting vehicles or simultaneous accelerating of several more moderately polluting vehicles in a queue, because differences in traffic flow rates and fleet compositions between the two locations are negligible due to their close proximity (65 m from one another).

An accelerating effect in the upper quintile region at the peak location (Excessive Emission Impact, EEI) is defined as the ratio of the integration of difference between observed concentrations and fitted baseline at the peak to that at the base location:

$$EEI = \frac{\int [UFP]_{diff, peak} dr}{\int [UFP]_{diff, base} dr}$$

where  $[UFP]_{diff} = [UFP] - [UFP]_{fit(20\% - 70\%)}$  (shaded areas between fitted line and UFP distribution) and subscripts peak and base represent the peak and base location, respectively. The *EEI* value for the UFP profile averaged for the entire profiles was 2.2. Considering the magnitude of  $[UFP]$  at the peak is dampened in the averaged profile due to varying locations of intersection peaks, acute effects due to high emission events can also be underestimated in the above analysis. Indeed, the mean *EEI* from the profiles of individual directions significantly increased: 9.6 ( $\pm 8.0$ ) for morning and 16.3 ( $\pm 16.5$ ) for afternoon. This implies that under some conditions (e.g., when traffic signal changes), pedestrian can possibly be exposed to more intensive and frequent excessive vehicular emissions near the intersections than mid-blocks.

**Traffic effects on the magnitude of intersection UFP elevation.** We attempt to relate traffic patterns to the magnitude of UFP elevations at the peak locations, which varied widely by sites as well as by traffic directions at the same site. Variables for traffic patterns include (1) traffic flow rates per traffic-signal cycle (vehicles $\cdot$ min $^{-1}$ ), (2) vehicle number waiting for green light at the moment the signal changed from red to green (queue length; Q-length), and (3) the queue length considering the proportion of high emitting vehicles (HEV; defined as heavy and medium duty diesel vehicles in this study). The third variable (HEV-Q-length) was defined as:

$$HEV\text{-}Q\text{-length} = (Q - \text{length}) \times \frac{TFR_{tot} - TFR_{HEV}}{TFR_{tot}} + 20 \times (Q - \text{length}) \times TFR_{HEV}$$

where  $TFR_{tot}$  and  $TFR_{HEV}$  represent traffic flow rates of total vehicles and HEV, respectively. The weighting value of 20 for HEV was introduced based on re-construction of the literature review (Choi et al. 2013a; Kumar et al. 2011). HEV weighting on traffic flow rate did not change the results (not shown), thus this is not included in the discussion.

All three variables showed positive correlations with both relative and absolute UFP elevations at the intersection (relative UFP elevation is defined as the ratio of the concentration difference between the peak and minimum locations to the minimum concentration, and absolute elevation is simply the concentration difference between the peak and minimum locations) (Figure 26). However, *TFR* correlated (in an exponential form) less significantly with UFP elevations than the other traffic variables, and these correlations disappeared for the afternoon sampling events (Figure 26a, b). Whereas, Q-length was linearly correlated with UFP elevations better than *TFR*; the relationships were kept in the afternoon sampling events as well (Figure 26cd). The best correlations were obtained between HEV weighted Q-length and UFP elevations for the morning periods, although afternoon relationships were comparable to those of Q-length (Figure 26e, f). A wide scatter of these 1:1 plots was likely produced by a large variability of emissions from

individual vehicles due to different driving behaviour and vehicle maintenance as well as vehicle composition. A slight improvement in correlations by weighting HEV effects on Q-length is likely due to a small portion of HEV in a vehicle composition at the study sites ( $2.6\pm 1.0\%$  and  $2.5\pm 1.9\%$  of the total traffic for the morning and afternoon periods, respectively).

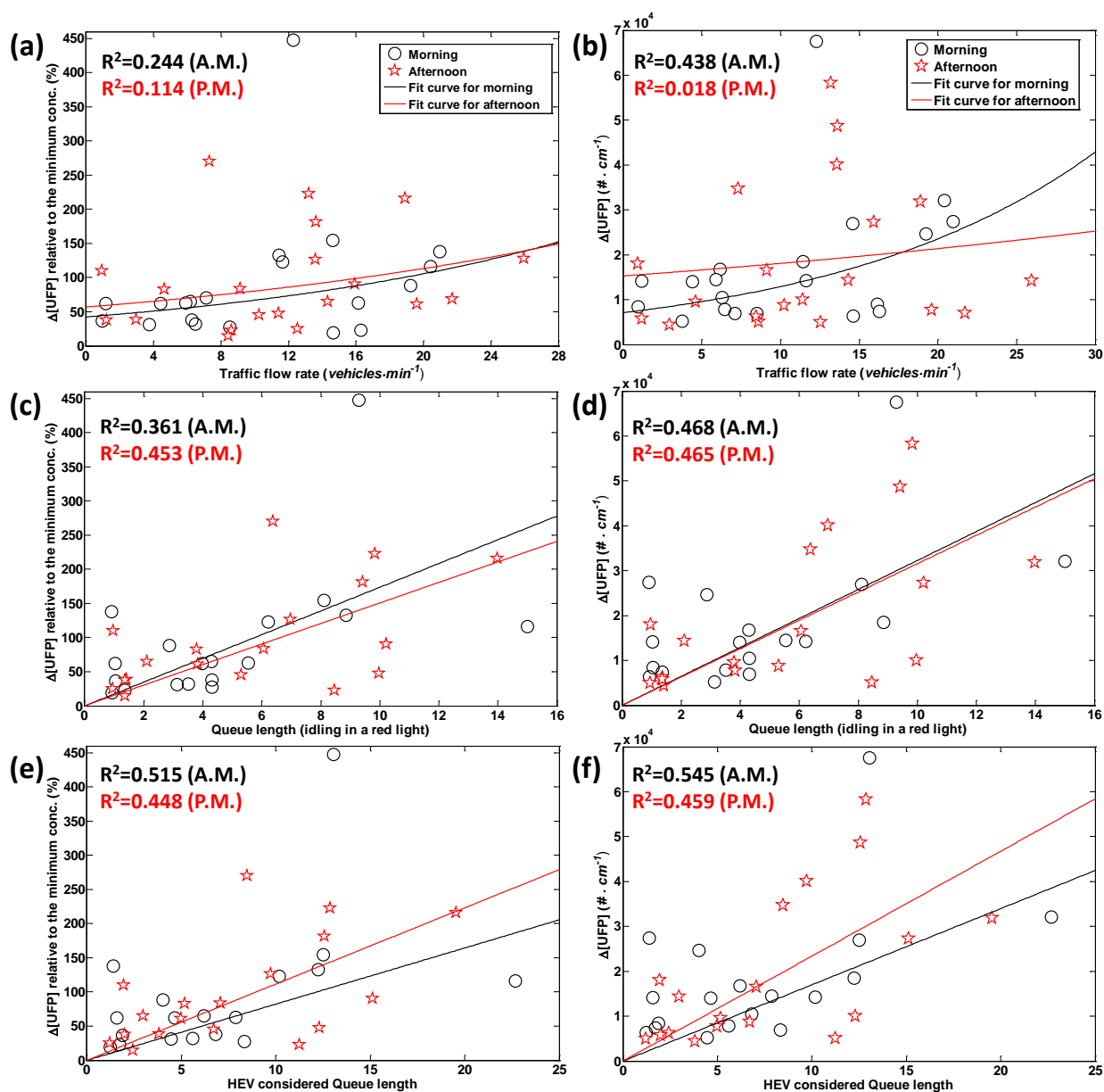


**Figure 26. Relationships of relative (%) and absolute (particles·cm<sup>-3</sup>) elevations of UFP at the peak location with traffic parameters (traffic flow rate, queue length, and HEV considered queue length). The left panel (a, c, e) is for relative [UFP] elevation and the right panel for absolute concentration increase at the peak locations. Queue length is defined as the number of vehicles waiting for the green signal at the moment when traffic signal changes from red to green.**

Consequently, we believe that HEV weighted Q-length is likely a more important factor controlling UFP elevations at the intersections, which is reasonable considering that heavy-duty diesel trucks emit much more UFP than gasoline-powered vehicles under certain conditions and a bigger group of vehicles accelerating simultaneously would emit more UFP.

#### v.4.4.3. Implications to pedestrian exposure and transit-oriented development

Here, for the case of bus stop siting taken alone, we estimate the exposure levels of transit users to elevated [UFP] around the intersections using a simple time-duration model of pedestrians moving through and/or waiting in the zones of low and high UFP concentrations for two cases: when bus

stops are located 40 m vs. 20 m after the center of intersection. The 'exposure level' is represented by the sum of [UFP] exposure for the period of activities ( $\sum[UFP]$ ). The 40 m distance was chosen based on the mean distance of the local minimum in the concentration profile and 20 m is based on the mean distance of the concentration peaks. A mean pedestrian walk speed of  $1.4 \text{ m}\cdot\text{s}^{-1}$  (Knoblauch et al. 1996; Parise et al. 2004) was assumed, and the UFP concentrations were set constant in both the affected zone (high UFP concentration was assumed within 20 m before and after the intersection) and beyond the affected zone (low UFP). The transit users' behaviour was assumed that (1) people spend 10 s for disembarkment, (2) walk to the intersection at constant speed, (3) spend 45 s (half of a traffic light cycle) to traverse a single crosswalk at the intersection, (4) walk to the bus stop for transfer, and (5) wait for a bus for 10 minutes at the bus stop.

The results suggest that pedestrian experiences more exposure in the case of 20 m bus-stop location compared to the 40 m case unless intersection [UFP] is not elevated. The extent of increased risk is also proportional to the extent of UFP elevation at the intersection. We note that absolute differences in concentrations are of less value than relative differences because the absolute UFP concentrations vary widely depending on location as well as in time, since vehicle fleets, maintenance, and fuels are continuously evolving, both within and between different countries and regions. Additionally, other directly emitted air pollutants such as  $\text{NO}_x$  or VOCs may be of interest. However, using the current data set as an example, in case the intersection  $[UFP] = 3.0 \times 10^4$  particles  $\text{cm}^{-3}$  and local minimum  $[UFP] = 2.0 \times 10^4$  particles  $\text{cm}^{-3}$  (50% lower at 40 m), the total exposure levels were  $1.4 \times 10^7$  particles  $\text{cm}^{-3}$  vs.  $2.0 \times 10^7$  particles  $\text{cm}^{-3}$  at the 40 m and 20 m bus stop location, respectively. This corresponds to 38% reduction in UFP exposure when the bus stop is located at 40 m from the intersection. This result indicates that locating bus stops around 40 m and farther away from the center of intersections reduces transit user's exposure to intersection emission events.

## vi. Dispersion Modeling

### vi.1. Introduction

Regional planning efforts indicate that TODs are expected to reduce regional air pollution (~10 km). However, there is concern that high building density can reduce dispersion of pollutants relative to that in terrain without buildings. Thus, TOD residents living or working in close proximity to urban streets may be exposed to elevated concentrations of vehicle emitted pollutants. This report describes the results of a research study designed to estimate the effect of building morphology on dispersion and hence air quality within a TOD.

Results from field studies (Hanna et al., 2014), laboratory experiments (Barlow and Belcher, 2002), and numerical simulations (Hang et al., 2012; Ketzler et al., 2000) have provided valuable insight into the mechanisms that govern dispersion of pollutants in the urban canopy. This information is the basis for semi-empirical dispersion models such as the Canyon Plume Box Model (CPBM) (Yamartino and Wiegand, 1986), and the Operational Street Pollution Model (OSPM) (Berkowicz et al., 1997). These models apply primarily to street canyons between relatively uniform buildings, which are common in Europe where these models originate. They are not applicable to the inhomogeneous building structures that characterize urban area cores in the United States, because the inhomogeneous environments produce complex flow structures inconsistent with the street canyon model formulation (Karra et al., 2011; Nelson et al., 2007).

Inhomogeneous built environments with tall buildings can induce flows that are significantly different from the idealized flows assumed in street canyon models. A wind tunnel study of an urban neighborhood with a single tall tower found enhanced vertical dispersion in the wake of the tower (Brixey et al., 2009). Another wind tunnel model of Manhattan found strong transport of contaminants up the lee sides of several of the tallest buildings (Heist et al., 2004). Results of the Joint Urban 2003 field study showed that the flow within an inhomogeneous street canyon was complex, with different flow structures resulting from slightly differing wind directions (Nelson et al., 2007). Large downdrafts and updrafts that could transport pollutants vertically were also observed.

Because of the complexity of the flows in such areas, the objective of the study reported here is limited to capturing the essential features of dispersion in the presence of buildings through a semi-empirical dispersion model. The model was developed through analysis of data from 1) a five year measurement program conducted in a street canyon in Hannover, Germany 2) field studies conducted in Los Angeles. The results of the analysis have been summarized in the form of a semi-empirical dispersion model that relates street-level pollutant concentrations to local emissions, building morphology, and micrometeorological variables.

The semi-empirical model used in this study can be contrasted with comprehensive models such as computational fluid dynamics (CFD) models. CFD models are designed to be general purpose because they solve the governing equations directly and can be adapted to a broad range of problems. However, they are numerically cumbersome and their results are difficult to interpret. Most importantly, they have not undergone adequate evaluation with real-world data (Di Sabatino et al., 2007). On the other hand, the relatively simple structure of the semi-empirical model allows calibration with field data to develop a practical tool that provides concentration estimates consistent with observed values.

The semi-empirical model described here seeks to explain first order effects of buildings on dispersion using only a small number of essential built environment and meteorological variables. It is designed to allow city planners and policymakers to support decisions related to the impact of TOD design on exposure to traffic emissions.

Here, we provide an overview of our knowledge of dispersion in urban environments, and describe the analysis of near road concentration data collected at an urban site in Hannover, Germany using several semi-empirical dispersion models. The analysis provides insight into the meteorological variables that govern dispersion in an urban built environment. This provides motivation for our study of dispersion in environments with non-uniform building height and spatial inhomogeneity, and also motivates the need for the field measurements that were conducted in Los Angeles. This is followed by a development and evaluation of the semi-empirical dispersion model with data collected in the field measurements conducted in Los Angeles.

Finally we provide the conclusions and the implications for the design of TODs. In this section, we present a method to estimate the impact of a planned TOD on street level concentrations of vehicle related emissions. This method can be readily used in combination with commonly used regulatory models, such as AERMOD (Cimorelli et al., 2005), to estimate the magnitude of concentration hotspots that can be created through the interaction between emissions and flow effects induced by urban buildings.

## vi.2. Background and related work

The impact of the built environment on dispersion of emissions in urban areas has been studied over the past 40 years using results from field, tracer, wind tunnels and numerical simulations. Models to estimate the magnitude of this impact have typically characterized urban morphology in terms of the “street canyon” shown in Figure 27. The street canyon is a long street with uniform buildings on both sides, forming a canyon. When the rooftop wind blows close to perpendicular to the canyon, one or multiple vortices form within the canyon. A single vortex results in the wind direction at street level pointing in the opposite direction to that at the rooftop, from the windward side to the leeward side. When the rooftop wind is at an angle, a helical vortex forms within the canyon.

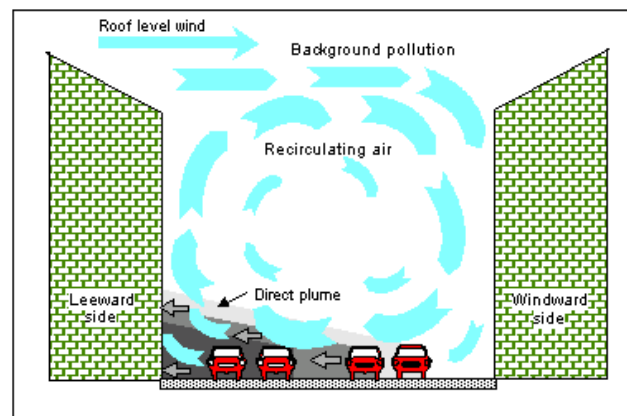


**Figure 27. Street Canyon Schematic (Source: <http://envs.au.dk/en/knowledge/air/Models/OSPM/>)**

The existence of a vortex within the street canyon depends on the aspect ratio, the ratio of building height to street width. When the aspect ratio is small, no consistent vortex forms within the canyon, and when the aspect ratio is large, multiple vortices may form. The widely used operational street pollution model (OSPM, Berkowicz, 2000) uses the vortex to divide the street canyon into two regions in modeling dispersion. This is discussed in more detail in a later section.

Some studies show the importance of the rooftop wind speed in determining dispersion in street canyons. Other studies indicate that vertical pollutant transport occurs due to an unstable shear layer that develops at the top of the canyon (Louka et al., 2000). The unsteady fluctuations of the shear layer cause intermittent recirculation in the canyon, thus intermittently flushing pollutants out of the canyon. Nakamura and Oke, (1988) measured temperatures within a 17 m tall street canyon. They found that the temperature difference between roof and canyon floor was usually less than 0.5 °C.

During the day the floor was warmer than the roof and during the night the floor was cooler. The temperature differences are very small, a fact that is attributed to rapid mixing within the canyon. The air is unstable or near neutral within the canyon, even during the night. During the day the vertical canyon surfaces provide large surface area to absorb solar radiation. The building material stores heat, with the result that during the night the canyon can remain warm. In the context of an entire urban area this is known as the urban heat island. The implication for dispersion is that the turbulence levels are likely to be larger within the urban area during nighttime than outside the urban area, and thus dispersion is also likely to be larger in the urban area than in a rural area at night.

The existing work on modeling street canyons is summarized by Vardoulakis et al., (2003). Existing models can be classified as: empirical regression models, semi-empirical box models, semi-empirical Gaussian plume models, Lagrangian particle models, unsteady Gaussian puff models, and CFD models. We are most interested in the semi-empirical box and Gaussian plume models because they require easily measured input variables and capture only the essential mechanisms of dispersion in cities. The Canyon Plume Box Model (CPBM) (Yamartino and Wiegand, 1986) was one of the first street canyon models that was evaluated with field data. The Operational Street Pollution Model (OSPM) (Berkowicz, 2000) borrowed the major ideas in CPBM and introduced simplifications that has made it more accessible to the non-expert user. Because OSPM is the most widely used street canyon model, we describe it next.

## vi.3. Methods

### vi.3.1. Operational street pollution model (OSPM)

Dispersion of pollutants in urban areas is governed by complex flows that result from the interaction of boundary-layer flow with buildings in the urban canopy. The flows can assume a number of forms even within the idealized street canyon shown in Figure 27. The street canyon refers to the structure formed by a long street lined on both sides by buildings of uniform height. The wind can be channeled along the street canyon if the upper level wind is at an angle to the axis of the canyon. When the rooftop wind is perpendicular to the street axis, the flow inside the canyon forms a vortex in which the wind direction at street level can be opposite to that at roof level. The length of the recirculating vortex at ground-level depends on the height of the upwind building. At oblique wind angles, the flow can also appear in the form of a helical vortex with its axis along the street. At intersections, the flow can separate at building edges and to give rise to vortices with vertical and horizontal axes (See Belcher, 2005 for a review of urban flows; Tiwary et al., 2011).

The foundation of OSPM is a model for dispersion in a street canyon. The model treats the road as a long area source with the emissions distributed evenly over the width of the road. Concentrations associated with emissions from vehicles in a street canyon are assumed to consist of two components: 1) a direct plume of emissions that is transported by the surface wind, and 2) a well-mixed region corresponding to the re-circulating flow in the canyon. The vortex divides the street into two regions; within the vortex, the surface wind blows towards the leeward side, and outside the vortex, the surface wind blows towards the windward side of the canyon. The direct plume contributions to the leeward and the windward side receptors depend on the fraction of road emissions within these two regions. If the vortex, whose length depends on the height of the upwind buildings and wind speed, covers the entire street width, there is no direct contribution to the windward receptor. Conversely, if the vortex length is small compared to the width of the road, the leeward receptor sees a small direct contribution, while the windward receptor is subject to most of the direct contribution. The second component of the concentration, the well mixed concentration within the vortex, depends on emissions into the vortex and the outflow from the top and the sides of the vortex, which is idealized as a trapezoid. In general, the total concentration,  $C$ , at a receptor is given by

$$C = C_d + C_m + C_b, \quad (1)$$

where  $C_d$  is the direct plume contribution,  $C_m$  is the well mixed concentration in the vortex, and  $C_b$  is the background concentration corresponding to sources outside the road. We can illustrate the structure of OSPM by considering the special case when the wind blows perpendicular to the road, and the canyon is deep enough that the vortex covers the entire width of the road. Then, the direct contribution,  $C_d$ , on the leeward side of the canyon is given by

$$C_d = \sqrt{\frac{2}{\pi}} \frac{Q}{\sigma_w W} \ln \left( 1 + \frac{\sigma_w W}{h_0 u_s} \right), \quad (2)$$

where  $Q$  is the emission per unit length of the road,  $\sigma_w$  is the standard deviation of the vertical velocity fluctuations at street level,  $W$  is the width of the road,  $h_0$  is the height over which the emissions are mixed next to the vehicle, and  $u_s$  is the wind speed at the height of emissions, which is taken to be 2 m. For this special case, the windward receptor is only affected by the well mixed concentration given by

$$C_m = \frac{Q}{\sigma_{wt} W}. \quad (3)$$

where  $\sigma_{wt}$  is the standard deviation of the vertical velocity fluctuations at the top of the canyon, which is related to the rooftop wind speed, and traffic induced turbulence at the base of the street canyon. The structure of the recirculating vortex in the street canyon is a function of the wind angle with respect to the street axis, and the height of the upwind building. The wind speed at emission level,  $u_s$ , is related to the rooftop wind speed,  $u_t$ , through an extension of the logarithmic profile to the emission height,

$$u_s = u_t \frac{\ln(h_0 / z_0)}{\ln(H / z_0)} (1 - 0.2 p \sin \Phi) \quad (4)$$

$$p = \max \left( \frac{H_{upwind}}{H}, 1 \right)$$

where  $H$  is the average height of the canyon,  $\Phi$  is the angle between the wind at roof top and the street canyon axis, and  $z_0$  is the urban roughness length. Notice that when  $H_{upwind} = 0$ , the building has no effect on the wind speed at emission height. Similarly, the wind is allowed to flow through the canyon when  $\Phi = 0$ . The standard deviation of vertical velocity fluctuations near ground-level is taken to consist of two components: 1) that related to wind speed at emission height, and 2) that generated by vehicle motion:

$$\sigma_w = \left( (\alpha u_s)^2 + \sigma_{wc}^2 \right)^{1/2}, \quad (5)$$

where  $\alpha = 0.1$  and  $\sigma_{wc}$  is associated with turbulence induced by vehicle motion. OSPM parameterizes this component in terms of vehicle speed and dimensions, width of the road, and traffic flow rate. The emission rate,  $Q$ , is taken to be a function of the traffic flow rate, the mix of vehicles, and the emission factors for each of the pollutants. For the simplest case of one type of vehicle with a flow rate of  $N$  (vehicles/s) and emission factor,  $e_f$  (g/(m.vehicle)), the emission rate is given by

$$Q = Ne_f \quad (6)$$

In OSPM,  $\sigma_w$ , the standard deviation of the vertical velocity fluctuation, is related to the surface wind speed,  $u_s$ , and traffic induced turbulence, and the surface wind speed, in turn, is related to the rooftop wind speed. The inputs to OSPM are: 1) average height and width of the street canyon; the upwind and downwind buildings can have different heights, 2) the orientation of the street canyon, 3) the rooftop wind speed and direction, 4) the emission rate, which can be calculated internally within OSPM given the mix of vehicles and traffic flow rates, 5) the traffic parameters required to estimate traffic induced turbulence, and 6) the background concentrations as a function of time.

The implicit assumption is that the mean wind speed is the primary meteorological variable determining the magnitude of the dispersion. As we show later, the rooftop and near surface vertical turbulent velocities or the average rooftop vertical velocity provided better explanations of near road concentrations. Additionally, the assumption of a constant turbulent intensity of 0.1, used to estimate the near surface turbulence from the wind speed, is questionable based on observations of much larger turbulent intensities made in this study as well as those in other field measurements in Oklahoma City and Manhattan (Hanna et al., 2007).

In the next section we describe the analysis of near road concentration data collected in Hannover, Germany. The data is used to evaluate several dispersion models in order to identify the meteorological variables that govern dispersion in Hannover. The results also guided the development of the model to describe the data collected in the field studies conducted in Los Angeles.

## vi.4. Results and Discussion

### vi.4.1. Operational Analysis of long term measurements of near road concentrations of vehicle emissions to determine the primary variables governing dispersion in urban streets

The German Niedersächsisches Ministerium für Umwelt, Energie und Klimaschutz operates an air quality monitoring network throughout Germany. We obtained data from two monitoring sites that record gaseous pollutants,  $PM_{2.5}$ , and  $PM_{10}$  concentrations as well as meteorological data. The two sites, HRSW and HRVS, are located in Hannover on Göttinger Strasse. Figure 28 presents a map of the buildings and site locations. The sites are positioned at two heights, one (HRVS) near ground level within the urban canopy and one (HRSW) on a building roof 34 m above the street site. Concentration measurements were made at 1.5 m AGL and 35.5 m AGL. The buildings adjacent to Göttinger Strasse are 20 m tall and have almost no gaps between them, thereby forming a 20 m tall, 25 m wide and 200 m long street canyon. Göttinger Strasse runs along a line that points 17 degrees west of north. The street level HRVS site was instrumented with a sonic anemometer at 10 m AGL to measure 30 minute average wind speed, temperature, turbulent fluxes of momentum and heat, and vertical and horizontal turbulent velocity. The roof level HRSW site measured 30-minute average wind speed, wind direction, solar radiation, temperature, humidity, pressure, and precipitation at 42 m AGL. Automatic traffic counts classified into passenger cars and trucks were made. Data was obtained from January 1, 2003 through December 31, 2007.

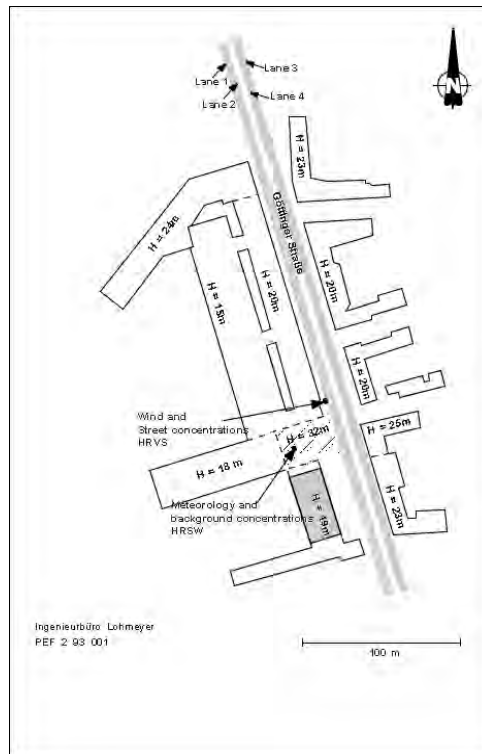


**Figure 28. Map of Göttinger Strasse showing locations of concentration and micro meteorology stations and building heights.**

We used the  $\text{NO}_x$  concentration measurements for model comparison because  $\text{NO}_x$  emission factors can be estimated within a factor of two. These emission factors were determined using the EPA Emfac 2007 emission model (CARB, 2015). We used the average emission factors for light and heavy duty trucks for the truck portion of the traffic and that of light duty vehicles for the passenger car portion. The emission resulting emission factors for the year 2003 are 0.465 g/km and 6.18 g/km for light duty vehicles and trucks respectively. Model performance was quantified through the geometric mean,  $m_g$  and standard deviation  $s_g$  of the ratio of the measured to the estimated concentrations, the correlation coefficient,  $r^2$  and the fraction of measurements within a factor of two of model estimates, *fact2*.

Figure 29 compares estimates from equation (2) using  $h_0 = 2 \text{ m}$  with corresponding observed concentrations. The scatter plot shows that the model overestimates measurements by a factor of two, and the correlation between model estimates and observations is 0.37. The other panels of Figure 29 show the variation of the modeled and observed concentrations, normalized by emission rate, with 10 m wind speed, standard deviation of vertical velocity fluctuations, and wind direction. The variation of the observations is generated by binning data based on the variables on the x-axes and computing the average value in each bin. Error bars show standard deviations of the data within each bin. These figures show that the model systematically overestimates observations when the wind speed is less than about 1 m/s. We see that the normalized measured concentration varies linearly with  $1/\sigma_w$ . The model shows similar sensitivity to  $1/\sigma_w$ , except for very small values of  $\sigma_w$  where the model underestimates concentrations.

The bottom right panel of Figure 29 shows that the model predicts the correct magnitude of concentrations when the wind direction is parallel to the street, and overestimates when the wind direction is perpendicular to the street. The model reproduces the observed variation of concentration with wind direction even though the model equations are independent of wind direction because the magnitude of the wind speed varies with direction. The model produces larger

concentrations when the wind direction is perpendicular to the street because the wind speed is smaller during these conditions.

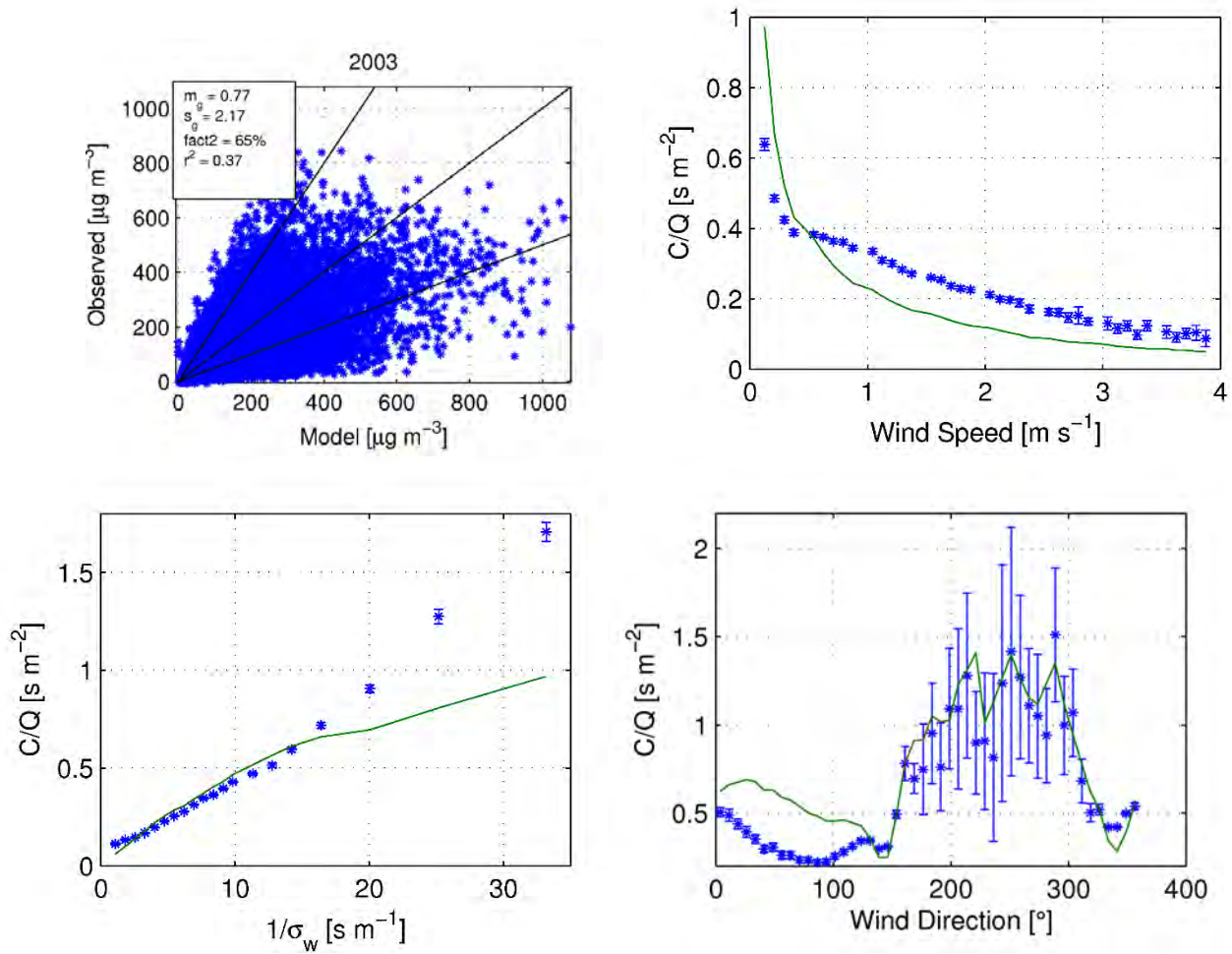


**Figure 29. Comparison of equation (2) with observations during 2003. Top left shows scatter plot. Top right shows variation of observations (blue) and model (green) with wind speed. Bottom left shows variation with  $1/\sigma_w$ . Bottom right shows variation with wind direction. Wind directions parallel to the street are 163 and 343 degrees.**

Figure 30 compares concentrations measured in 2003 with estimates from the model when the log term containing the explicit dependence on surface wind speed is neglected:

$$C_s = \alpha \frac{Q}{\sigma_w W} + C_r \quad (7)$$

where  $\alpha$  is a parameter whose value is determined empirically. The value of  $\alpha$  that best describes the data using the assumed emission factors is 0.9. Equation (7), which is the leading term of Equation (2), is similar to the OSPM recirculating contribution model (Berkowicz et al., 1997), although in OSPM, the rooftop value of  $\sigma_w$  is prescribed, and is determined from the rooftop wind speed through a constant turbulent intensity.

The model bias is smaller than that corresponding to equation (2), with an  $m_g$  of 1.02. The correlation coefficient of  $r^2 = 0.62$  is also better than that from equation (2). The fraction of data within a factor of two of the observations is 72%. The bottom left panel of Figure 30 shows that the model has the same sensitivity to  $\sigma_w$  as the observations, although it tends to underestimate while equation (2) is unbiased except for very small values of  $\sigma_w$ . The top right panel of Figure 30 shows

that model also has the correct sensitivity to wind speed, and has less bias than equation (2) when the wind speed is less than 1 m/s. We conclude that the model without the explicit wind speed dependence performs better than that given by equation (2) under low wind speed conditions. The improved performance under low wind speed conditions is also seen on the bottom right panel of Figure 8, which shows concentration plotted against wind direction. In the figure we see that model overestimates less than equation (2) during perpendicular flow conditions, when the wind speed is smallest.

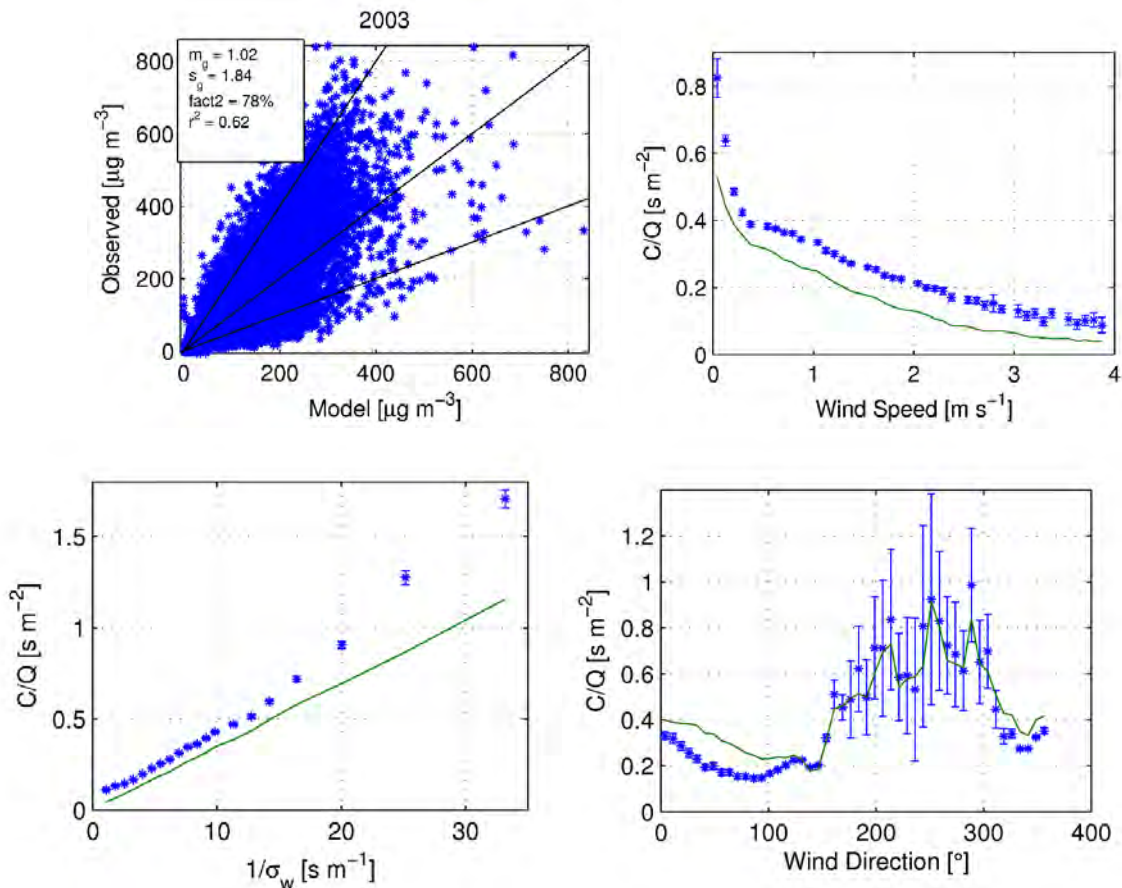


**Figure 30. Comparison of estimates from equation (2) without explicit wind speed dependence with corresponding observations during 2003. Top left shows scatter plot. Top right shows variation of observations (blue) and model (green) with wind speed. Bottom left shows variation with  $1/\sigma_w$ . Bottom right shows variation with wind direction.**

Based on this comparison we conclude that the vertical turbulent velocity explains most of the variance of the observed concentrations, while the explicit inclusion of wind speed does not improve predictions of near road concentrations. The importance of the vertical turbulent velocity and insensitivity to wind speed was observed previously in near road concentrations of vehicle emitted NO (Venkatram et al., 2007). It is surprising that the near road concentrations are not more strongly correlated with the street level wind speed because the standard deviation of vertical velocity fluctuations is normally strongly correlated with wind speed. However, in urban environments where mean wind speeds are small the horizontal turbulent velocities are usually very large relative to the mean wind speed, and the mean wind varies significantly depending on the presence of nearby buildings (Hanna et al., 2007). The result is that horizontal motion is better characterized as a turbulent dispersion rather than advection by a strong mean flow. Thus, the concentrations are primarily determined by turbulent transport in the vertical direction. This view of urban dispersion is somewhat inconsistent with the street canyon picture of a strong recirculating vortex flow.

This analysis of data from Hannover indicates that the street level vertical turbulent velocity is the dominant variable controlling dispersion within a street. The next section develops a model based on this result.

#### vi.4.2. Development of a model to understand the impact of buildings on near-road concentrations using field measurements in Los Angeles

The analysis of measurements of near road concentrations of vehicle emissions in Göttinger Strasse, Hannover, Germany determined the primary meteorological variables that govern dispersion of vehicle emissions in urban environments. The analysis could not examine the impact of building morphology on concentrations because the data was obtained at a single site where the buildings were relatively uniform in height. The field studies conducted in Los Angeles provided the information required to include the effects of building morphology on dispersion of street-level emissions.

##### *vi.4.2.1. Design of field measurements in Los Angeles*

The design of the Los Angeles field measurements is based on the knowledge gained from the analysis of data from Göttinger Strasse in Hannover. The analysis shows that the standard deviation of vertical velocity fluctuations measured at approximately half the building height is the primary variable governing near road concentrations. Thus, the Los Angeles field study included measurements of the near surface and rooftop turbulent velocities. The field study also included measurements of mean wind speed and wind direction in order to evaluate the performance of other dispersion models such as OSPM. OSPM estimates the near road concentration as the sum of the direct plume contribution from the road and the recirculating contribution, due to trapping of pollutants within the street canyon. The recirculating contribution is governed by the rooftop standard deviation of vertical velocity fluctuations. In OSPM (see section 2 for details), the rooftop turbulence and surface wind speed and turbulence levels are estimated from the rooftop mean wind speed. Thus, our field study included measurements of the turbulence and mean winds at the urban rooftop as well as at the surface.

For most practical applications, the rooftop wind speed and direction within the urban area have to be estimated from measurements of wind speed at a nearby local monitoring station, most likely located at a nearby airport. This is because 1) meteorological variables are not routinely measured in urban areas, and 2) it is difficult to make representative measurements in urban areas with tall buildings because flow around individual buildings can be significantly influenced by the wake effects of individual buildings. Thus, it is necessary to relate urban values that govern dispersion to upwind rural meteorology. The wind speed and turbulence from the upwind rural area are modified by the built environment as the air passes from an upwind monitoring station to the urban site of interest. The wind speed at the urban rooftop, and therefore the turbulence and near surface mean wind as well, are thus a function of the overall built environment characteristics between the rural reference location and the urban site. The modification of the meteorological variables between the reference and urban sites is modeled using the internal boundary layer (IBL) model described in a later section. The field studies conducted in Los Angeles were designed to evaluate the IBL model by including measurements of the mean wind and turbulent variables at a rural reference location upwind of the urban field sites.

We used ultrafine particles (UFP) as the tracer to evaluate the dispersion models. There are several reasons for this choice. First, UFP is associated with negative health effects (Knibbs et al., 2011). Second, at the time scales of interest, dispersion is the primary mechanism for reducing UFP particle number concentrations (Ketzler and Berkowicz, 2004). Third, we have access to several TSI3022A condensation particle counters that provide high resolution measurements of UFP.

Field measurements pose significant challenges to isolating the effects of the buildings on dispersion because variability in uncontrolled factors such as traffic emission rate can overwhelm the signal due to the presence of buildings. The evaluation of the dispersion model requires accurate estimates of the emission rates, which are difficult to determine in practice. During the typical congested driving conditions of urban environments, the local traffic within a street is often accelerating or idling, which increases the uncertainty in estimating emission rates (Smit et al., 2008). Emission models of gaseous pollutants and particle mass are usually accurate within a factor of two or three (Smit et al., 2010). Ultrafine particle number (UFP), which we use as the primary measured pollutant in the field study, has emission factors that vary by about an order of magnitude (Kumar et al., 2011). Because of the uncertainty in the emission estimates, UFP concentration measurements were made at two sections on the same street when possible: one section with tall buildings adjacent to the street, and another where there are no buildings or very short adjacent buildings. This design ensures that local vehicle emissions are similar at the two locations, allowing us to directly compare concentrations at the open and building sections to isolate the building effect. The experiment design conducted in practice has depended on availability of instruments, and the overall design has evolved as we gained knowledge from previous experiments. The measurements were made at various time periods between September 2013 and July 2014. Figure 31 shows the location of the field sites. Table 15 gives an overview of the dates during which measurements were made and summarizes the building morphology of the sites. Appendix A gives an overview of the building morphology of the various field locations in this campaign the details of each experiment and the instrumentation used at each of the field sites.

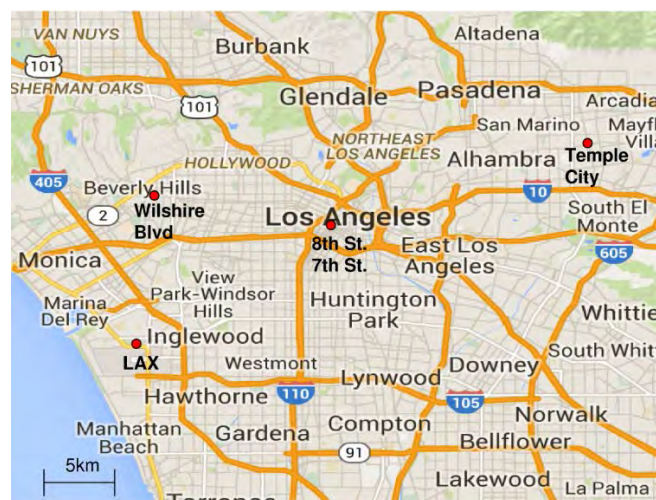


Figure 31. Field study locations in Los Angeles County. Map Data: Google.

Table 15. Overview of measurement locations

Location	Dates		Building Morphology
	Micrometeorology	UFP	
8 <sup>th</sup> St., Los Angeles	4/23/14 – 5/13/14	5/7/14, 5/9/14	Simultaneous open site and deep street canyon ( $H/W=2.0$ ).
Wilshire Blvd., Beverly Hills	5/19/14 – 7/1/14	5/30/14	Variable building heights up to 50 m
Temple City Blvd., Temple City	1/13/14 – 2/14/14	1/15/14 – 1/17/14	Uniform height shallow street canyon ( $H/W=0.2$ ).
7 <sup>th</sup> St./Broadway, Los Angeles	9/20/13	9/20/13	Deep street canyon. Two perpendicular streets.

vi.4.2.2. Instrumentation

We used Campbell Scientific CSAT3 3D sonic anemometers (Figure 31) to record the three components of wind speed and the sonic temperature at a sampling frequency of 10 Hz. The data were processed using the method described in (Kaimal and Finnigan, 1994) to yield the 30 or 60

minute averaged values of the turbulent heat flux, surface friction velocity, standard deviation of the vertical and horizontal turbulent velocities, wind speed, wind direction, temperature, and Monin-Obukhov Length.

TSI 3022A condensation particle counters (Figure 31) were used to record ultrafine particle number concentrations at a sampling rate of 1 Hz. Samples were drawn through a copper and Tygon tube with the tube sampling inlet set at 1 m above ground level. The instruments measured the concentration of particles with diameters greater than 10 nm (50% detection efficiency is 10 nm). The inlet flow rate is  $25 \text{ cm}^3\text{s}^{-1}$  and the flow rate through the detector is  $5 \text{ cm}^3\text{s}^{-1}$ . Power was supplied by **12 V 100 A hr** lead acid deep cycle batteries through **12 V to 120 V** AC power inverters. Data loggers were constructed to record data from the serial port and store it on SD cards. AQMesh five gas concentration monitors (Figure 31) were used to measure concentrations of carbon monoxide, nitrogen oxide, nitrogen dioxide, ozone, and sulfur dioxide at the 8th St and Temple City field sites.

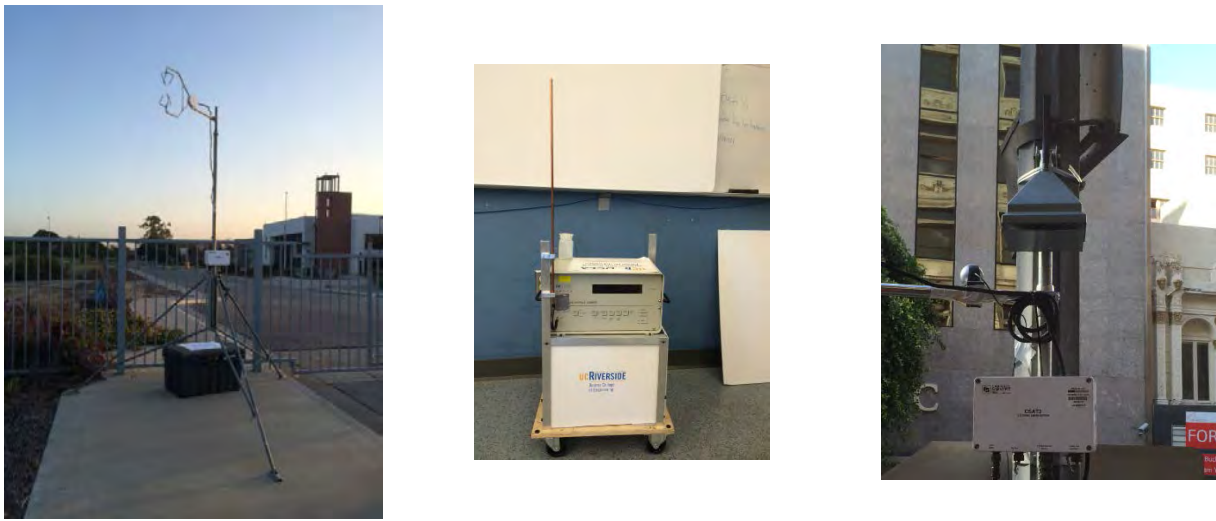


**Figure 32. Instruments used in Los Angeles field measurements. Left - Campbell scientific CSAT3 sonic anemometer. Center - Condensation particle counter. Right - AQMesh concentration monitor (at top of photo).**

#### *vi.4.2.3. Vertical dispersion model*

Based on the analysis of the data collected in Hannover, Germany, we formulated the Vertical Dispersion Model (VDM) by assuming the horizontally averaged concentration in the street canyon is governed primarily by vertical transport, so that the flux of pollutants at the surface is matched by vertical turbulent diffusion:

$$Q \sim KW \left( \frac{C_s - C_r}{H} \right) \quad (8)$$

where  $Q$  is the emission rate per unit length of the street canyon,  $W$  is the width of the canyon, and  $H$  is the equivalent height of the canyon. If we assume that the background makes similar contributions to  $C_s$  and  $C_r$ , we can evaluate Equation (8) with observations by using the difference between the observed  $C_s$  and  $C_r$ . The eddy diffusivity  $K$  is expressed as

$$K = \sigma_w l \quad (9)$$

where  $\sigma_w$  is the vertical average, between the surface and roof, of the standard deviation of vertical velocity fluctuations, and  $l$  is a mixing length. The vertically averaged  $\sigma_w$  is estimated from the measured surface,  $\sigma_{ws}$ , and roof,  $\sigma_{wr}$ , values from

$$\frac{1}{\sigma_w} = \frac{1}{2} \left( \frac{1}{\sigma_{wr}} + \frac{1}{\sigma_{ws}} \right) \quad (10)$$

If we assume that the size of the large turbulent eddies dominating vertical mixing is limited by the smaller of the street width and height,  $l$  is proportional to the smaller of  $W$  and  $H$ , so that

$$l \sim \left( \frac{WH}{W+H} + h_0 \right) \quad (11)$$

where  $h_0$  is a mixing length associated with the size of the source. Substituting Equations (9) and (11) into Equation (8) yields

$$C_s = \frac{Q}{\beta \sigma_w W} \frac{H(1+a_r)}{H+h_0(1+a_r)} + C_r \quad (12)$$

where the aspect ratio  $a_r = H/W$ . Equation (12) has the same form as Equation (4), except that it contains the aspect ratio,  $H/W$ . The value of  $\beta$  that is consistent with the aspect ratio of Göttinger Str. and the best fit value for  $\alpha = 0.9$  in Equation (4) is 1.7. However, we find that a value of 1.0 provides a better fit to the Los Angeles data. Note that the parameter  $\beta$  combines the proportionality constants implied in Equations (8) and (11). If measurements at roof level are not available, we can estimate  $C_r$  by assuming that the local emissions are matched by vertical transport at roof level:

$$Q = \gamma C_r \sigma_{wr} W \quad (13)$$

where the value of  $\gamma$  is determined by fitting the model to field measurements described in the next section. Substituting Equation (13) into (12) yields

$$C_s = \frac{Q}{\gamma \sigma_{wr} W} \left[ 1 + \frac{\gamma \sigma_{wr}}{\beta \sigma_w} \frac{H(1+a_r)}{H+h_0(1+a_r)} \right] \quad (14)$$

Equations (12) and (14) are referred to as the Vertical Dispersion Model (VDM). Equation (12) can be used if  $\sigma_w$  and  $C_r$  are known. In the field studies conducted in Los Angeles, information at roof level was not available at several of the sites, and it was necessary to estimate  $\sigma_{wr}$ . We can estimate  $\sigma_{wr}$  by assuming that turbulent kinetic energy produced at roof level, per unit length of street,  $u_{*r}^2 U_r W$ , is dissipated over the volume of the street:

$$u_{*r}^2 U_r W \sim \sigma_{wr}^3 W A \sim \frac{\sigma_w^3}{l} W H \quad (15)$$

where  $l$  is the length scale of the large turbulent eddies within the canyon, and  $u_{*r}^2$  and  $U_r$  are the shear stress and the mean wind speed at roof level, both of which are correlated with  $\sigma_{wr}$ . If  $l$  is similar to the form given by Equation (11), we can write the semi-empirical expression

$$\frac{\sigma_{wr}}{\sigma_w} = \left(1 + \eta \frac{H}{W}\right)^{1/3} \quad (16)$$

where  $\eta=0.4$  provides the best fit with the data as shown in a later section. The ratio of rooftop and average  $\sigma_w$  is nearly constant because the 1/3 power in Equation (16) results in low sensitivity to the aspect ratio.

The models described in this section were evaluated with data from field studies conducted at several locations in Los Angeles, California, the details of which are presented in in section 3. At most of these locations, the buildings lining these streets varied substantially in height. So the application of the dispersion model depended on defining an effective building height,  $H$ . We found that the following definition provided the best agreement between model estimates and observations:

$$H = \frac{1}{L} \sum_i H_i B_i \quad (17)$$

where  $L$  is the street length,  $H_i$  and  $B_i$  are the height and width (along the length of the street) of building  $i$ , and the sum is taken over all the buildings on one side the street. Equation (17) can be interpreted as the area-weighted building height: the sum of the frontal area of the buildings divided by the street length. Then, the equivalent building height used in Equation (11) is the average over both sides of the street.

We assume that the modeled concentration represents an average over the street canyon within one city block. For the effective building height to be consistent with the model, it is calculated from the geometry of all the buildings bordering the street canyon within one city block. The use of the block length for defining the scale for horizontal inhomogeneity is arbitrary, but the assumption of horizontal homogeneity within one city block has been used in models such as SIRANE (Soulhac et al., 2011), and comparisons with observations indicate that this is a useful assumption.

Figure 33 evaluates the leading term,  $1/(\sigma_w W)$ , of the VDM with observations made at the building section of 8<sup>th</sup> St. on May 9<sup>th</sup>, 2014. The surface concentration in the figure is the average of the concentration on both sides of the street. The vertical concentration differences shown on the left panel are 30 minute averages normalized by the emission rate calculated using the traffic flow rate and constant emission factor of  $10^{14} \text{ veh}^{-1} \text{ km}^{-1}$ . This emission factor is the same order of magnitude as that observed in an urban street canyon (Ketzler et al., 2003). We assumed that the background concentrations at the surface and the roof were the same, so that the concentration difference represented only the component associated with emissions from the street canyon.

The left panel shows that the observations are correlated with  $1/(\sigma_w W)$ , which is proportional to the predictions of the VDM. The right panel assumes that the emissions are constant, corresponding to the daily average traffic flow. Neglecting the variation of traffic flow surprisingly improves the correlation between model estimates and observations of  $(C_s - C_r)/Q$ . This illustrates the uncertainty in relating UFP emissions to the traffic flow rate and a constant emission factor, since variation in vehicle speed and acceleration can significantly affect the emission factor (Kittelson et al., 2004). It is clear from the analysis that the concentration difference between the surface and the

roof is governed by the standard deviation of the vertical velocity fluctuations. This is consistent with the assumption underlying the VDM.

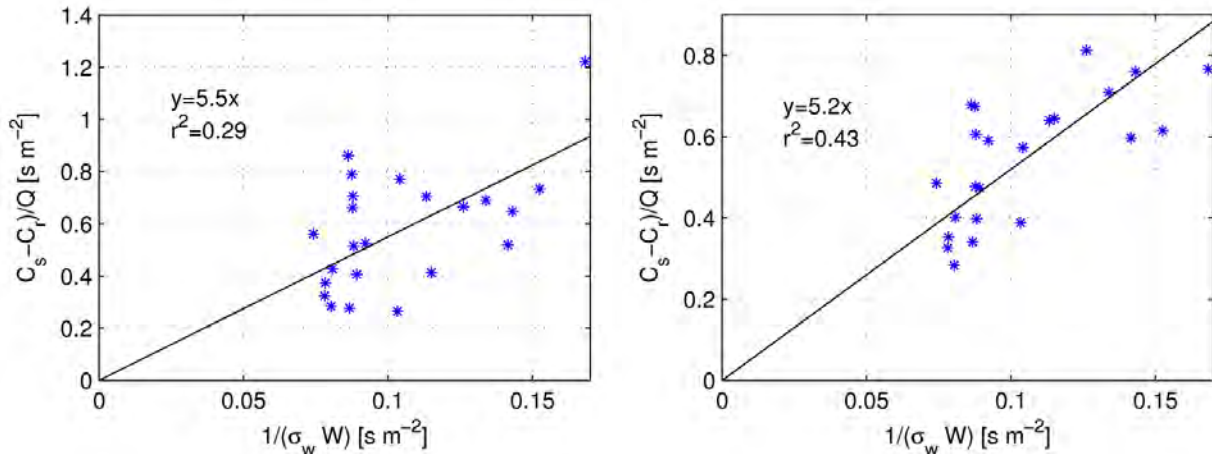


**Figure 33: Evaluation of the VDM with 30 minute average data from the building section of 8<sup>th</sup> Street (LA). Left panel: the emission rate is taken to be the 30 minute average value. Right panel: the emission rate is the daily average value. Surface concentrations are averages of both sides of the street.**

We next describe the evaluation of the VDM at the other sites in Los Angeles where the field studies were conducted. This required estimating the effective aspect ratio of the field study sites. We obtained building height and outline information from the Los Angeles County GIS data portal (Los Angeles County, 2008), which was used to calculate the built environment parameters shown in Table 16 for each site. The table also shows the average hourly traffic recorded during the field measurements.

**Table 16. Summary of area weighted building height, street width, and aspect ratio of all sites.**

Site	Area weighted building height (m)	Street width (m)	Aspect ratio	Average Traffic (veh/hr)
8th St Building Section	43.25	20.0	2.16	722
8th St Mid Section	34.5	20.0	1.73	722
Broadway	35.9	26.0	1.38	1013
7th St	45.8	25.0	1.83	1162
Temple City	6.00	30.0	0.20	1849
Wilshire Blvd Building	36.0	30	1.20	2772
Wilshire Blvd Open	8.25	30	0.28	2772

Figure 34 shows the evaluation of equation (12) with the vertical concentration differences at all the sites in the Los Angeles field study where rooftop concentration measurements were made. We have used a value of  $\beta = 1.0$  for the VDM model estimates. The slope of the line that fits the data is consistent with a UFP emission factor of  $2 \times 10^{14} \text{ veh}^{-1} \text{ km}^{-1}$ . This value is within the range reported in literature (Ketznel et al., 2003). The model underestimates the concentrations on Broadway, but most of the model estimates are within a factor of two of the observations.

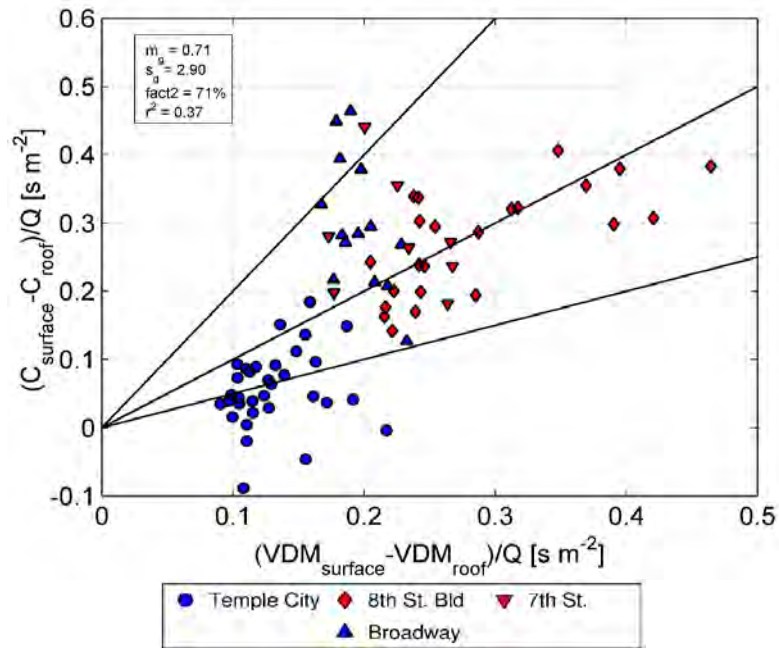


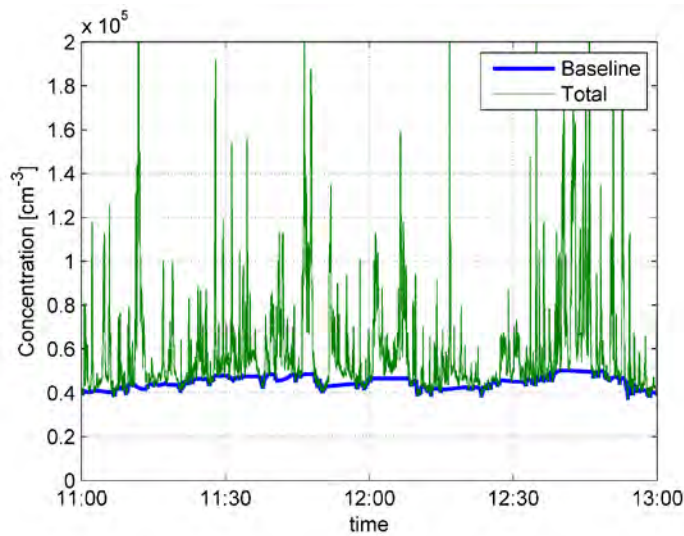
Figure 34. Evaluation of VDM model with data collected in the Los Angeles field studies. The concentration has been normalized by the daily average emission rate assuming an emission factor of  $2 \times 10^{14} \text{ veh}^{-1} \text{ km}^{-1}$ .

#### vi.4.2.4. Evaluation of VDM with the local contribution

At several of the field sites, we did not have access to the roof of a tall building to make the measurements required to eliminate the background concentration using the vertical difference in concentrations. A model for the background, such as that in Pournazeri et al., (2014) could be used to estimate the background; however, it is difficult to apply such a model because it requires a detailed particle emission inventory for the LA basin. This inventory is not yet available in view of the large uncertainty in estimating emissions of ultrafine particles. Moreover, the "open" sites have no well-defined rooftop concentration since there is no building height at which to measure the concentration. For this reason, we developed an alternative method to analyze the data that does not rely on measurements of the roof concentration. Instead of using the vertical concentration difference to evaluate equation (12), we determined the contribution of local emissions to the total concentration observed at the surface monitors, and compared only this "local contribution" with the estimates from equation (14).

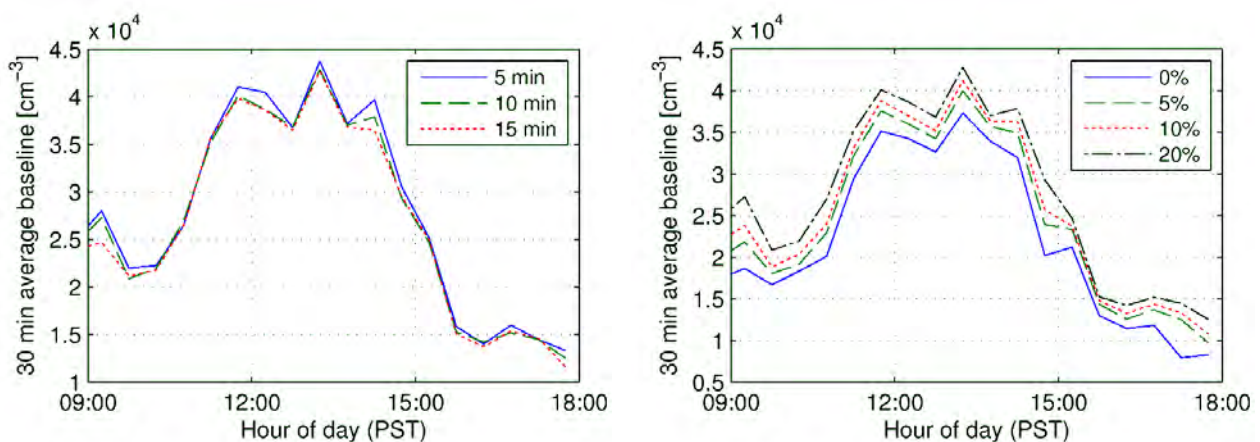
The UFP concentration time series contains information about the local vehicle emissions in the form of large amplitude short lived spikes superimposed on the slowly varying baseline. These local emission events from high emitting vehicles produce large concentration spikes that can be separated from the total concentration. We filtered the signal to separate the slowly varying component from the spikes, which contained information about local emissions. A moving average filter with a window size larger than the time scale of the spikes does not adequately separate the two components because the concentration distribution is highly skewed, making the average an inadequate measure of the baseline concentration. Instead of the moving average, we used a windowed percentile to separate the components. We defined the baseline as the concentration that is below a chosen percentile of the concentration distribution. Then, within each time window of a chosen length, each data point was classified as either baseline or spike if the concentration was below or above the percentile cutoff of the window. The baseline was then constructed by linearly interpolating between the points that are classified as baseline, and the spikes were separated by subtracting the baseline from the total. This type of analysis is common for analyzing UFP time series, especially in analysis of mobile monitoring data (Bukowiecki et al., 2002).

Figure 35 shows the result of this procedure with the baseline at the 10th percentile for several hours of data collected in 8th St on May 9th, 2014. The window size was taken to be 10 minutes to capture several spikes, each of which lasted for about a minute. This procedure resulted in a clear separation of the spikes and baseline concentrations.



**Figure 35. Baseline and total concentration.**

A windows size of 10 minutes resulted in an adequate separation of the concentration signals, but can be considered to be somewhat arbitrary. We calculated the 30-minute average of the baseline concentration for window sizes of 5, 10, and 15 minutes, and found no significant difference in the results. This is shown in Figure 36 for data collected at 8th St. Because the cutoff percentile is also an arbitrary choice we chose different cutoff percentiles and compared the resulting 30-minute average baselines. Figure 36 shows that the baseline is affected by the choice of cutoff, with larger cutoffs producing larger baselines. The spikes are also sensitive to the choice of cutoff. However, this does not affect the analysis significantly because different cutoffs only result in a shift of the concentrations by a constant amount. The important feature of this procedure is that it removes the variability caused by variation in the baseline.



**Figure 36. Sensitivity of calculated baseline to window size (left) and cutoff percentile (right).**

The VDM was applied to the data from the field studies using the best fit parameters  $h_0 = 2 \text{ m}$ ,  $\gamma = 1.0$ , and  $\beta = 1.0$ . The values of  $\beta$  and  $\gamma$  were determined by matching the observed and modeled concentrations from the Los Angeles data. The value of  $\beta = 1.0$  is smaller than the value of 1.7 that corresponds to the value determined from the best fit of equation (14) to the Göttinger Strasse data. This uncertainty in parameter values is acceptable in the light of the uncertainty in

NO<sub>x</sub> emission estimates, which are mostly within a factor of two of observations (Smit et al., 2010). This uncertainty range suggests that  $\beta$  lies between 0.85 and 3.4. We have chosen  $\beta = 1.0$  because this produces a UFP emission factor consistent with literature values. The value of  $\gamma = 1.0$  produces a good fit between the surface local contribution and Equation (14) and also produces the correct magnitude of the rooftop value of the local contribution through Equation (13).

Figure 37 indicates that the model provides a good description of the measured local contributions of UFP at most of the sites. This implies that local contributions are primarily governed by the ratio of equivalent building height to street width and the standard deviation of the vertical velocity fluctuations. The slope of the fit line is consistent with an emission factor of  $1 \times 10^{14} \text{ veh}^{-1} \text{ km}^{-1}$ , which is within the range reported by (Ketzel et al., 2003).

The observed local contribution at the 8th St open site is much larger than that predicted by the model. The emissions have to be approximately five times larger than that estimated based on the traffic flow rate on 8th St to account for the model underestimation. We suspect that emissions from adjacent streets influence the concentration at the open site, which implies that the VDM estimate represents the concentration averaged over an area larger than a single street, and the effective building height for the open site should encompass the buildings within a larger area than the region directly adjacent to the street. To examine this possibility, the building height of the 8th St open section was changed from its initial value of zero to the area weighted building height of the 8th St building section. The right panel of Figure 37 shows that now the model has almost no bias for the 8th St open site. Thus, the model underestimation for the open site is likely due to underestimation of the effective building height. This also means that concentrations in a relatively open site among buildings are affected by the presence of adjacent buildings.

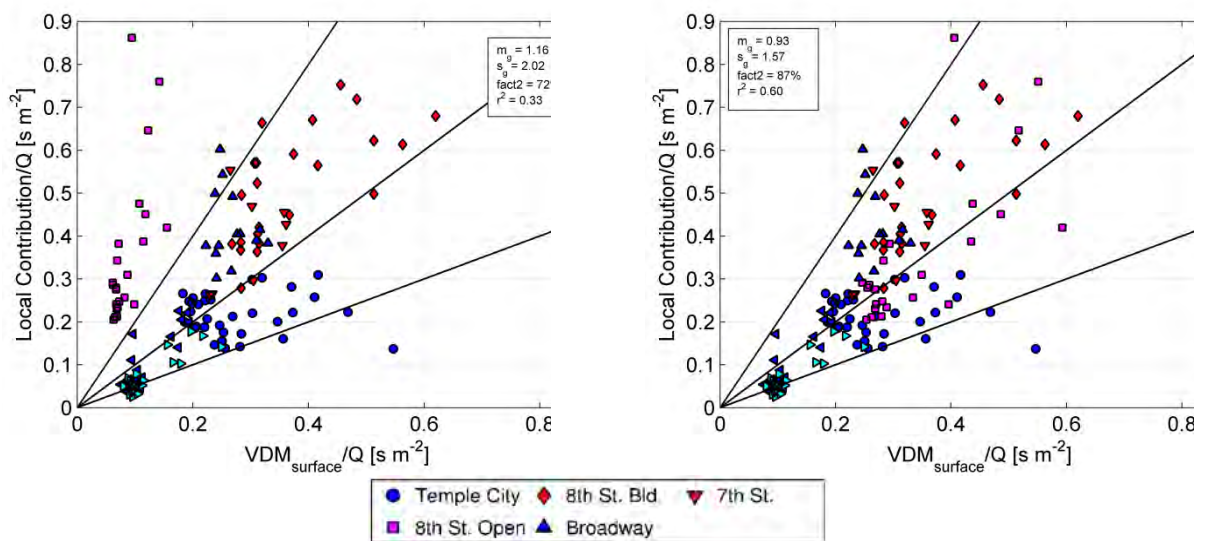


**Figure 37. Comparison of estimates from VDM with 30-minute averaged local contributions. Concentration is normalized by daily average emission rate, assuming an emission factor of  $10^{14} \text{ veh}^{-1} \text{ km}^{-1}$ . Left – The 8<sup>th</sup> St open section building height is zero. Right - The building height of the 8th St open section has been set equal to that of the 8th St building section.**

Our analysis of data from field studies conducted in urban areas suggests that vertical mixing governs near surface concentrations within the urban canopy. This conclusion is supported by observations analyzed in (Hanna et al., 2014), which show that data from field studies conducted in Manhattan, NY, indicate rapid vertical mixing in the presence of buildings. We show that modeling the air quality impact of vehicular emissions within cities with significant building height variability reduces to estimating the effective aspect ratio of the street, the ratio of the mean street width and the area weighted building height, and the roof level  $\sigma_w$ . The effective aspect ratio plays the major

role in magnifying concentrations relative to those that would have been measured in the absence of buildings. Concentrations are relatively insensitive to the mean wind speed at the rooftop or surface. This supports the conclusion that vertical turbulent transport rather than advection by the mean wind dominates dispersion in cities.

We have provided evidence to show that the simple vertical dispersion model provides an adequate description of the variation of local contributions within a street lined by buildings of varying heights. However, in order to estimate the impact of buildings on concentrations that would have been observed in the absence of buildings, we need to quantify the effects of buildings on the primary meteorological variable governing dispersion within the VDM, the standard deviation of the vertical velocity fluctuations,  $\sigma_w$ . This requires a model that will trace the evolution of the urban boundary layer as it travels from a rural area to the urban site of interest. This model needs to incorporate the morphology of buildings upwind of the urban site. While progress has been made (Luhar et al., 2006) in developing such a model, the model estimates are not yet reliable. However, we can obtain insight into the problem through empirical information from the field studies. This is addressed next.

*vi.4.2.5. Micro-meteorology*

The relationships among the  $\sigma_w$  measured on 8<sup>th</sup> street and those at the upwind LAX location are illustrated in Figure 38. The top left panel shows that the standard deviation of the vertical velocity fluctuations at roof level and at street level are highly correlated. The street level  $\sigma_w$  is about 0.67 of the roof level values, which is consistent with Equation (16). The observed ratio is similar to the ratios of 0.63 and 0.54 found in the MSG05 (Hanna et al., 2007) and MID05 (Hanna and Zhou, 2009) measurements in Manhattan. The top right panel justifies the assumption used to derive Equation (16): the shear production of turbulence at roof level,  $u_*^2 U_r$ , is proportional to  $\sigma_w^3$  at roof level.

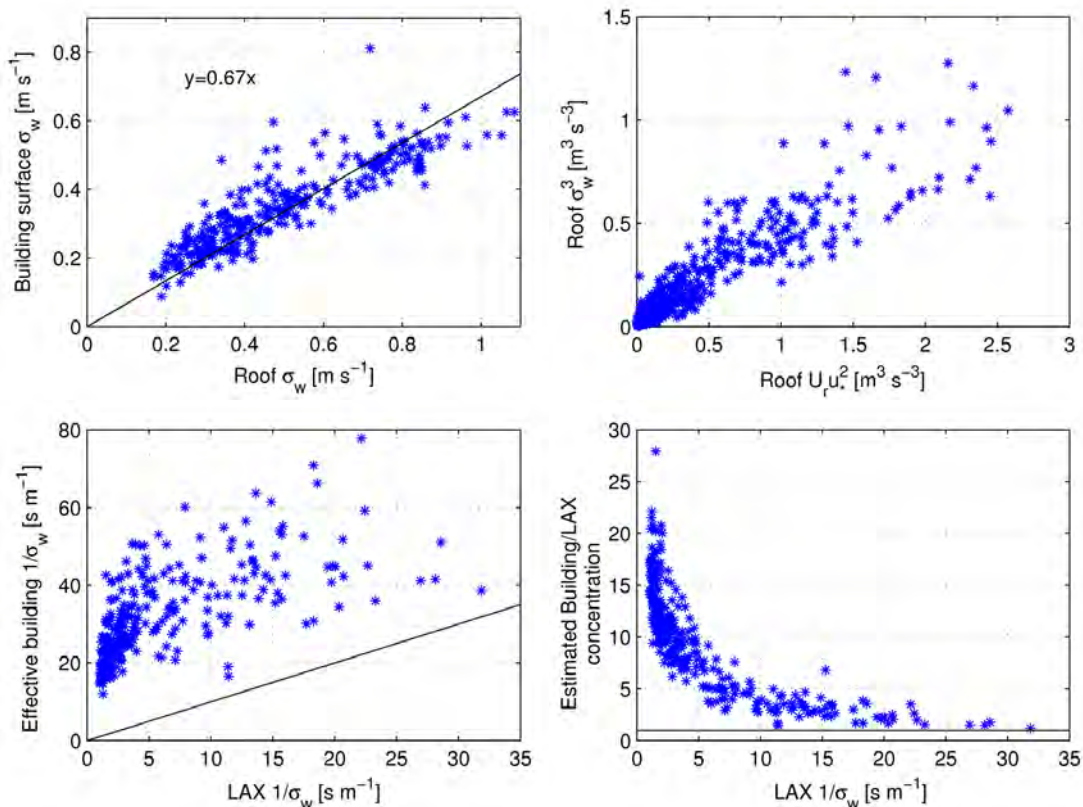


**Figure 38. Micrometeorology measured at Los Angeles 8<sup>th</sup> St. site. Micrometeorology is determined from the 8<sup>th</sup> St. “building” and “roof” sonic anemometers.**

The bottom two panels of Figure 38 illustrate the effect of the building aspect ratio on the effective  $\sigma_w$ . The bottom left panel compares  $1/\sigma_w$  measured at the upwind LAX site to the effective value at the building site,

$$\frac{1}{\sigma_{weff}} = \frac{1}{\sigma_{wr}} + \frac{1}{\sigma_w} \left( \frac{\gamma}{\beta} \frac{H(1+a_r)}{H+h_0(1+a_r)} \right) \quad (18)$$

derived from Equation (14). Notice the role of the aspect ratio in decreasing the effective  $\sigma_w$ . We see that the effective building values of  $1/\sigma_w$  (a measure of concentration) are always larger than those at the upwind LAX site, but they are not correlated for upwind values less than about 0.2 m/s; while the LAX  $\sigma_w$  decrease, the effective building  $\sigma_w$  values fluctuate around 0.03 m/s. The bottom right panel of Figure 38 shows that, based on the modeled concentrations, the building always magnifies concentrations relative to the open terrain at LAX, but the magnification decreases to unity when the  $\sigma_w$  at the LAX site is about 0.03 m/s.

By assuming that turbulent kinetic energy produced at roof level is dissipated inside the canyon, we have derived the tentative relationship given in Equation (16), with the best fit to the data when  $\eta = 0.4$ . Figure 39 shows that this equation provides a useful estimate of the near surface  $\sigma_w$  using the measured values at roof level at several sites in Los Angeles.

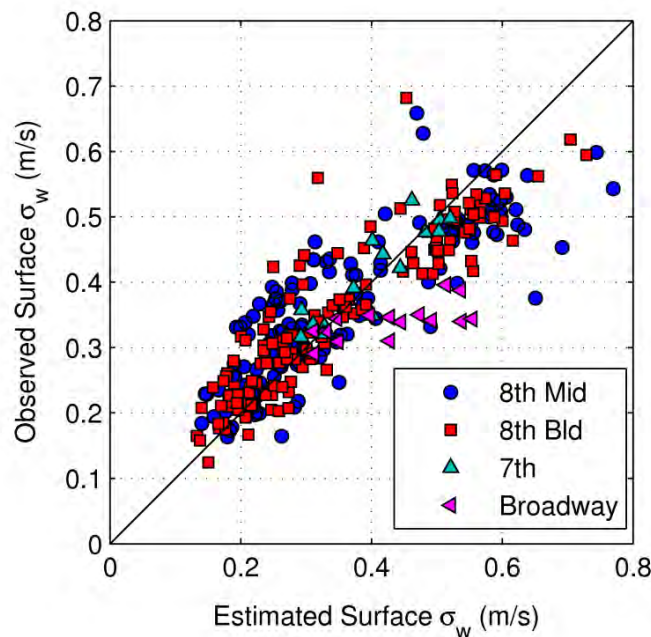


**Figure 39. Estimates of vertical velocity fluctuations measured at street level compared with measured values at several sites in Los Angeles. The black line is the 1 to 1 line.**

The relationship between the  $\sigma_w$  measured at the roof level and the upwind site can, in principle, be estimated using an internal boundary layer model (Luhar et al., 2006). Figure 40 compares the LAX and 8<sup>th</sup> St. roof values of  $\sigma_w$ . For wind blowing from LAX to 8<sup>th</sup> St., which occurs during daytime, the  $\sigma_w$  measured at the rooftop is about 1.2 times the LAX value. For other wind directions, the two values of  $\sigma_w$  are not well correlated, and during nighttime the roof  $\sigma_w$  can be much larger than that at LAX. This variability in relationships between the upwind  $\sigma_w$  and the roof top value suggests using measurements as a guide to specifying the value of  $\sigma_w$ .

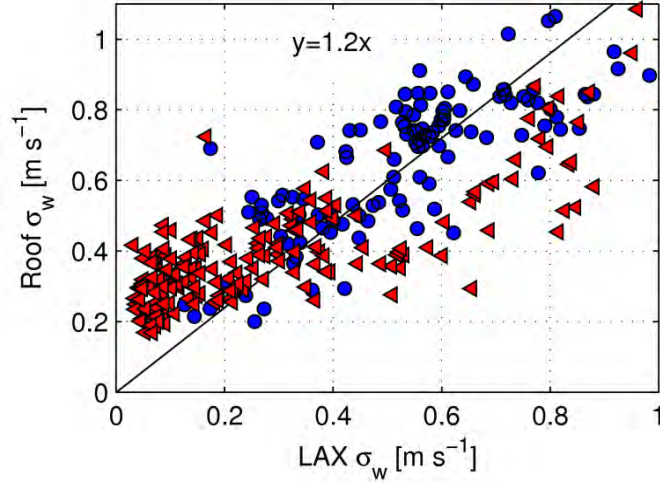


**Figure 40. Relationship between vertical velocity fluctuations measured at LAX and those at roof level on 8<sup>th</sup> St. ● - Data filtered so the roof site is downwind of the LAX site. (Wind direction at LAX within 20 degrees of the heading from LAX to 8<sup>th</sup> St.) ▶ - All other data.**

#### vi.4.2.6. Using VDM to Assess Exposure to Traffic Emissions in TODs

VDM provides city planners with the tools necessary to evaluate the impact of the built environment on exposure to traffic emissions in TODs. The model can be used in two ways: (1) to understand the effect of changing model input variables on the air pollution concentration (sensitivity analysis), and (2) to estimate the air pollution concentrations for real-world cities and alternative TOD designs using detailed emission and meteorological inputs and parameters. This section shows the results of the sensitivity analysis and describes how VDM can be used to generate detailed air pollution concentration estimates. For these purposes, the VDM equations have been translated into a tool that consists of a python code and an excel spreadsheet that provide the overall model formulation and an easy to use graphical interface. This spreadsheet tool allows city planners to use VDM to conduct sensitivity analysis and generate practical concentration estimates.

The spreadsheet tool uses readily available meteorological inputs and user specified traffic counts, emission factors, and building parameters. The process used by the tool to estimate concentrations of local traffic emissions is as follows:

- 1) Derive estimates of the surface roughness length of the city. This is done using methods of MacDonald et al. (1998) to convert the plan area fraction, frontal area fraction, and average building height into estimates of the zero plane displacement height and surface roughness length through equations (19) and (20):

$$\frac{d}{H} = 1 + 4.43^{-\lambda_p} (\lambda_p - 1) \quad (19)$$

$$\frac{z_{0urban}}{d} = \left(1 - \frac{d}{H}\right) \exp \left[ - \left(0.5 \frac{C_D}{\kappa^2} \left(1 - \frac{d}{H}\right) \lambda_f \right)^{-0.5} \right] \quad (20)$$

where  $z_{0urban}$  is the surface roughness length,  $d$  is the zero plane displacement height,  $\bar{H}$  is the average building height,  $\lambda_p$  and  $\lambda_f$  are the plan and frontal area fractions,  $C_D$  is the building drag coefficient that is taken to be 1.2, and  $\kappa$  is the Von Karman constant.

- 2) Estimate the urban rooftop standard deviation of vertical velocity fluctuations,  $\sigma_{wr}$ , from measurements at an upwind rural or airport reference location. We use a simplified form of the internal boundary layer model (Luhar et al., 2006) to convert the standard deviation of vertical velocity fluctuations from the rural area to the corresponding rooftop value:

$$\frac{\sigma_{wr}}{\sigma_{wrural}} = \left( \frac{z_{0urban}}{z_{0rural}} \right)^{0.14} \quad (21)$$

where  $\sigma_{wrural}$  is the standard deviation of vertical velocity fluctuations at the rural or airport reference location and  $z_{0rural}$  is the surface roughness length at the reference location.  $\sigma_{wrural}$  can be taken from standard AERMOD (Cimorelli et al., 2005) meteorological input files produced by the AERMET preprocessor. These input files are readily available for many meteorological measurement sites in California.

- 3) Compute the concentration of local traffic emissions (from within the TOD) at the building rooftop using equation (13). Alternatively, the rooftop concentration can be calculated using AERMOD and input into the spreadsheet. For this option, AERMOD is run without considering the buildings explicitly. The impact of buildings in AERMOD is only included through the standard AERMOD urban options.
- 4) Compute the surface concentration of local traffic emissions using equation (12) and equation (16) using the user-specified area-weighted building height and street width.

The user can specify emission inputs in the spreadsheet by providing traffic flow rates and emission factors. The tool includes built-in emission factors for  $PM_{2.5}$ , UFP, and  $NO_x$ .

The model calculated results are displayed in the spreadsheet using several figures. First, the diurnal variation of the concentrations is shown. Second, the variation of the concentration and the magnification, the ratio of air pollution concentration with and without buildings, with building height are shown. The user can also export data from the spreadsheet to conduct additional analysis.

We now provide some basic results that can be examined by planners using the spreadsheet tool. Figure 41 shows the sensitivity of the predicted magnification to changes in the area-weighted building height generated using the spreadsheet. The magnification increase quickly with building height at first and then increases linearly with the ratio of area-weighted building height to street width. This result provides insight into the effect of increasing building heights within a TOD.



**Figure 41: Sensitivity of magnification (ratio of concentration with buildings to that with no buildings) to the area-weighted building height. The street width is 30 m.**

Figure 42 shows the diurnal variation of the VDM-estimated PM<sub>2.5</sub> concentration for a typical urban area. These results can be incorporated into exposure estimates by city planners. They can, for example, be combined with time-activity patterns and building indoor/outdoor ratios to estimate exposure to local traffic emissions for residents who live in the TOD.

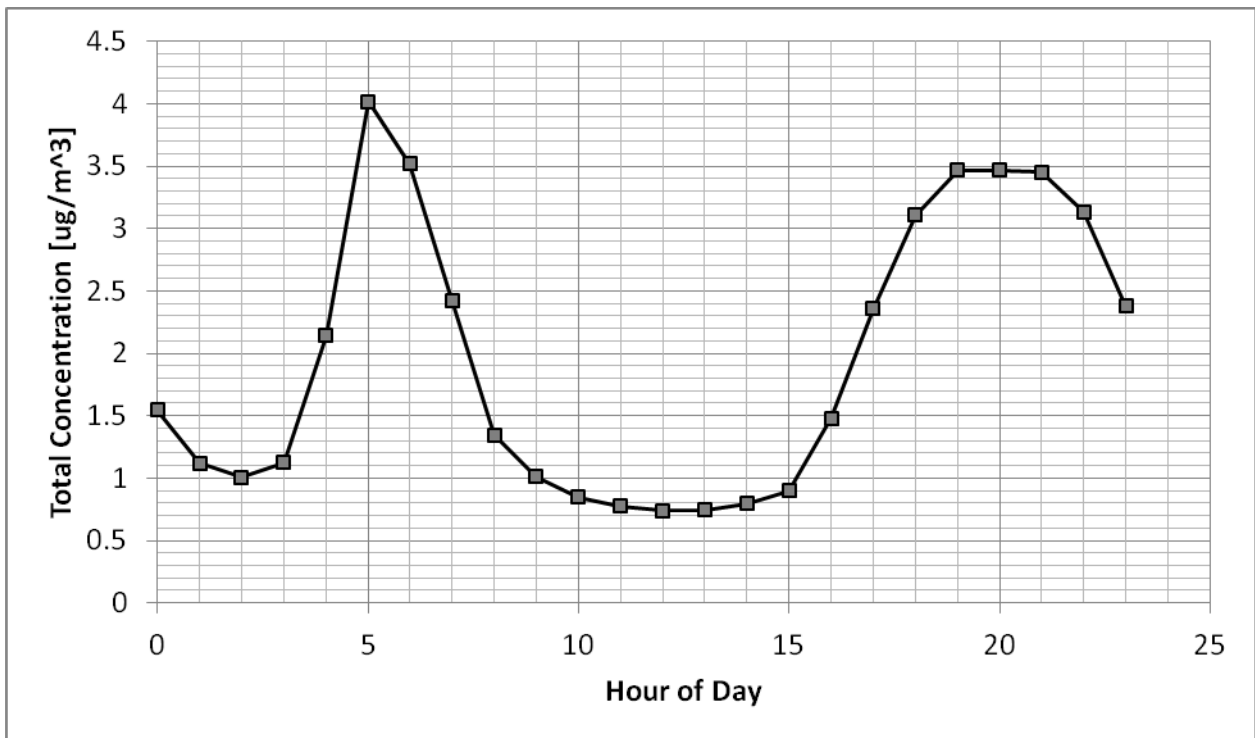


**Figure 42: Variation of PM<sub>2.5</sub> concentration with hour of day predicted by the VDM spreadsheet. The area-weighted building height is 28 m and street width is 30 m. Traffic is typical of “arterial” roads.**

*vi.4.2.7. Implications to pedestrian exposure and transit-oriented development*

The VDM indicates two general strategies that can be used to mitigate exposure to elevated concentrations of traffic emissions. First, methods can be implemented that limit the effective street aspect ratio; the ratio of the area-weighted building height to street width. The expected result of reducing the aspect ratio is a reduction in exposure to air pollution concentration as indicated in Figure 41. To reduce the aspect ratio, planners can set limits on building heights, require that buildings be spaced apart or include open areas in the TOD design, or increase the street width.

Second, the local traffic within the TOD can be limited to reduce traffic emissions and exposure to air pollution concentrations. Air pollution concentrations are directly proportional to traffic emission rate and so a given reduction in traffic corresponds to an equal reduction in air pollution concentration. The implementation of traffic management strategies can be designed by the planner based on the expected air pollution concentrations calculated by the VDM. Traffic management can also be combined with changes to building parameters that limit the effective aspect ratio.

Finally, conversion of streets within TODs into pedestrian zones completely removes the impact of local traffic on exposure to air pollution concentrations and may provide significant reductions in total exposures for TOD residents.

These strategies must be implemented by planners based on knowledge of the expected urban background air pollution concentrations. The magnitude of the reduction in concentrations of local traffic emissions that is expected due to implementation of mitigation strategies should be considered in context of the air pollution contribution from background sources.

## vii. Conclusions

California is on a path to transition towards more sustainable communities, and state, regional, and local governments are making important investments to support the future transportation needs of the growing population, including integrated transportation and land use planning, as well as providing accessibility to sustainable transportation choices and transit-oriented developments. However, these developments may also put public closer to traffic air pollution corridors, including heavily trafficked urban cores. Therefore, it is important to study and understand the potential air quality exposures experienced in these urban cores, and identify potential strategies in built-environment design, land use planning, and traffic management that can help reduce public exposure to traffic air pollutants in the transit-oriented developments.

Urban environments are very complex, especially the heterogeneous built environments typical of California. We have shown, however, that it is possible to isolate the impact of the many aspects of heterogeneous fleets, urban driving modes, and the built environment on air quality in these environments. Depending on the spatial and temporal scale that is relevant to the question being asked, different features of the urban environment play a larger or smaller role.

The project utilized two distinct data collection and analysis approaches to evaluate the design and operational considerations in Transit Oriented Developments using comprehensive air quality measurement studies in Los Angeles County, CA. One team collected and analyzed high frequency mobile measurements using statistical analysis and modeling. The other team collected comprehensive dataset using stationary air pollution and meteorological monitors to develop a dispersion model that can be used to estimate the impact of urban morphology on air pollution associated with traffic emissions.

The study highlights that although direct emissions from the fleet are of primary importance and dominate the concentrations at the 1-second time scale in micro dynamics models, built environment factors play a much larger role when averaged over longer time (minutes) and length scales (tens of meters). The results of this study can inform the design of transit-oriented developments to reduce exposure to traffic emissions.

Our research findings have important implications for urban planning, traffic management policies and air pollution exposure of pedestrians and vehicle occupants in urban centers. Broadly, our data provide quantitative insights into how the built environment and traffic flows influence pedestrian exposure to vehicle pollution, and offer urban planners and traffic managers strategies to reduce street-level pollutant concentrations.

Our findings that lower traffic flows and fewer stops reduce near-roadway pollution are consistent with earlier studies and shed light on the potentials of traffic management policies that may be employed to mitigate pedestrian exposure. In addition to the obvious dependence on traffic volumes, different built environment characteristics are important at different times of day, because atmospheric stability varies with time of day.

For calm mornings, the study found that the area aspect ratio ( $Ar_{area}$ ) is an important factor in controlling the block-scale vehicular pollutant concentrations. Higher values of  $Ar_{area}$ , correspond to more building volume and less open space, and limited mixing with the above ambient air. On the other hand, turbulence intensities played a major role in dispersing vehicular emissions in the afternoon. The built environment affects surface turbulence intensities, enhances vertical mixing and thus plays an indirect role in controlling block-scale [UFP concentration]. An isolated tall building surrounded by open space or short buildings is likely help to reduce the levels of vehicular pollution by up to a factor of two. Thus, urban planning focused on decreasing  $Ar_{area}$  and increasing

heterogeneity of building distributions is expected to substantially improve near-roadway air quality and reduce pedestrian exposure to vehicular emissions.

In general, the project suggests several broad mitigation methods to reduce exposures to pollutant concentrations:

- 1) Avoid creating street canyons by placing tall buildings next to one another, or reduce emissions most where building aspect ratios are large. Emissions can be reduced by reducing traffic flow or by regulating traffic in built up areas to avoid acceleration of vehicles, which produces high emissions.
- 2) Including open spaces among the buildings and building heterogeneity, not only in the center of the TOD but also within several surrounding blocks will also reduce exposures.
- 3) Separate pedestrian and heavy vehicle traffic into different streets.
- 4) Reduce traffic during early morning and late evening hours when turbulence levels are low.

Our results and recommendations on TOD design are consistent with the other studies on the impact of the built environment on air pollution (Klein et al., 2007: Driving physical mechanisms of flow and dispersion in urban canopies. *International Journal of Climatology*, 27, 1887-1907, P. Klein, B. Leitl, and M. Schatzmann; Yuan et al., 2014: Improving air quality in high-density cities by understanding the relationship between air pollutant dispersion and urban morphologies. *Building and Environment*, 71, 2014, 245-258. C. Yuan, E. Ng, and L.K. Norford). These studies also show that dispersion of vehicle emissions is governed by building aspect ratio and turbulence levels. We have contributed to advancing the state-of-the-science by developing methods that provide quantitative estimates of air pollution levels using these variables as inputs.

## vii.1. General Recommendations for TOD Design

Table 17 below summarizes the overall size of the effects of different features of the built environment investigated in this report.

### vii.1.1. Built Environment Considerations

#### *vii.1.1.1. Single street scale*

Analysis of data collected in Hannover and in the field studies conducted in this project show that near-road concentrations of vehicle related pollutants are governed by the ratio of frontal-area weighted building height to street width and the vertical average of the standard deviation of vertical velocity fluctuations primarily. These relationships are summarized in a dispersion model referred to as the Vertical Dispersion Model (VDM). We translated the VDM equations into an easy to use spreadsheet tool and python code that allows city planners to use VDM to conduct sensitivity analysis, generate concentration estimates, and develop mitigation strategies. The model provides understanding on the roles of the following features in governing air quality in built environments. This tool is made available through the California Air Resources Board.

Effective aspect ratio: Analysis using the VDM dispersion model indicates that the effective aspect ratio,  $a_r$ , plays a major role in determining the effect of buildings on the impact of vehicle emissions on street level concentrations. The aspect ratio is defined by the equations:

$$a_r = \frac{H}{W} ; H = \frac{\sum_i A_i}{2L}$$

where  $W$  is the width of the street,  $A_i$  is the area of a buildings facing the street on *both* sides projected on a vertical plane, and  $L$  is the length of the block. Thus, the effective height,  $H$ , of buildings on a street lined with buildings of uniform height with little space between them will be close to the actual height of buildings. On the other hand,  $H$  of a street lined with buildings with widely varying heights will weigh the buildings with the largest areas obstructing the flow across the street. Furthermore, open spaces between buildings, corresponding to zero frontal areas, will reduce the effective height and hence the aspect ratio,  $\alpha_r$ .

Street Canyons: Dispersion analysis in urban areas suggests that vertical mixing governs near surface concentrations within the urban canopy, consistent with observations analyzed in (Hanna et al., 2014), which show that data from field studies conducted in Manhattan, NY, indicate rapid vertical mixing in the presence of buildings. In the study at Los Angeles, 8th St, 50 m tall buildings next to the 20 m wide street are associated with a 50% increase in the UFP concentration due to local emissions relative to the section of the road, which had no buildings directly adjacent, resulting in a 25% increase in the total concentration.

Building Heterogeneity: The dispersion model shows that the presence of buildings lining a street decreases dispersion of local vehicle emissions relative to open terrain, and thus increases street-level concentrations by an increment that is proportional to  $(1 + \alpha_r)$ . The modeling results indicate that at the sites in Los Angeles where the field studies were conducted, the presence of buildings increases the concentration by a factor of 1.19 to 1.58 relative to the concentration that would be measured in the absence of buildings. This increase is related to the magnification of concentrations associated with local emissions: the presence of the buildings can potentially magnify street-level concentrations associated with local emissions by as much as a factor of 4 relative to those in the absence of buildings. This implies that built-up areas with large aspect ratios create local hot spots in the presence of local emissions.

#### *vii.1.1.2. Multi-block scale*

The built environment at the multi-block scale has a markedly larger influence than it does at the street scale, and further approaching TOD design from the point of view of several blocks rather than a single street or intersection offers more options to design for lower exposure in TODs. Concentrations are generally higher in the morning, a time when our results showed lower building volumes and/or interspersed open space can result in substantially lower pollutant concentrations. In the afternoons, more building heterogeneity is helpful. Thus, avoiding street canyons and designing heterogeneous built environments that include open space within a block or two of busy roadways or intersections may be the best overall approach. While our research at the multi-block scale is novel, it would benefit from additional study to verify and expand on these important findings.

#### *vii.1.2. Street design and land use considerations*

Intersection design: Analysis of mean cross-intersection [UFP] profiles suggests larger variability at and around the intersection peak locations than at distances farther away from the intersection. While comparing the concentration distributions profiles around traffic intersections, the overall [UFP] peak concentration was recorded at 10 m before the center of intersection. This implies that under some conditions (e.g., when traffic signal changes), pedestrian can possibly be exposed to more intensive and frequent excessive vehicular emissions near the intersections than mid-blocks.

Since the concentrations varied widely by sites as well as by traffic directions at the same site, the traffic patterns were related to the magnitude of UFP elevations at the peak locations. It was found that are UFP elevations at the intersections were affected by several important factors, including the traffic flow rates per traffic-signal cycle ( $\text{vehicles} \cdot \text{min}^{-1}$ ), the vehicle number waiting for green light at the moment the signal changed from red to green (queue length; Q-length), and the queue length

considering the proportion of high emitting vehicles (HEV; defined as heavy and medium duty diesel vehicles in this study). This is reasonable considering that heavy-duty diesel trucks emit much more UFP than gasoline-powered vehicles and a bigger group of vehicles accelerating simultaneously would emit more UFP.

**Transit Stop Siting:** The study analyzed the UFP concentrations experienced by transit users depending on the location of transit stops with respect to traffic intersections. The results suggest that pedestrian experiences more exposure when a bus-stop is located 20 m away from an intersection, when compared to 40 m distance. The total exposure levels were  $1.4 \times 10^7$  particles· $cm^{-3}$  vs.  $2.0 \times 10^7$  particles· $cm^{-3}$  at the 40 m and 20 m bus stop location, respectively. This corresponds to 38% reduction in UFP exposure when the bus stop is located at 40 m from the intersection. This result indicates that locating bus stops around 40 m and farther away from the center of intersections reduces transit user’s exposure to intersection emission events.

### vii.1.3. Other features of the built environment and other topics for future research

Several other aspects of urban design not investigated in this study clearly also have the potential to impact exposures of users in complex urban environments. These include street configurations such as “complete streets”, lane configurations (one way, configurations that reduce or create more stop/starts and accelerations), mode shifting, proximity to other major roadways, airports, freight movements, traffic management strategies and placement of vegetation. While some of these topics have been investigated to a sufficient level that the magnitude of the effects are understood fairly well, the potential gains from several of them are poorly understood and in need of additional research.

**Table 17. General recommendations to reduce pedestrian and residential air pollution exposure in built environment.**

Management	Suggested Direction	Approx. Size of Effect	Atmospheric Conditions & Notes
Areal aspect ratio ( $Ar_{area}$ ), which combines building area-weighted height, building footprint, and the amount of open space	Lower building volumes and more open space result in lower pollutant concentrations.	The difference between very dense and low density built environments is approximately a factor of three.	Important under calm conditions (in the mornings at our sites).
Building Heterogeneity	Isolated tall (high-rise) buildings result in lower concentrations than homogeneous shorter or many taller buildings with similar volume.	Highly heterogeneous built environments can decrease concentrations by up to approximately a factor of two relative to completely homogeneous built environments.	Important under unstable conditions with moderate winds (afternoons at our sites). Not critical when the atmosphere is stable.
Street Canyons (relatively contiguous walls of buildings)	Heterogeneous building forms avoid hotspots created by street canyons.	Tall street canyons (~50 m) can increase local traffic air pollution concentrations by up to about 50% relative to open space.	
Bus Stop Siting	Siting bus stops further from intersection will reduce exposures.	From no effect to more than a factor of two reduction from moving the site from 20 to 40 meters from the intersection on the “far” side.	Pollutant concentrations usually peak near the center of the intersection, although there is a high degree of variability.

## viii. Acknowledgement and References

### viii.1. Acknowledgements

The authors gratefully acknowledge additional support for some of the results presented here from the U.S. National Science Foundation, Contract No. CNS-1111971001. Dr. Wonsik Choi was partially funded by Korean Ministry of Environment through "Climate Change Correspondence Program". The authors also thank our colleagues Ms. Lisa Wu, Ms. Karen Bunavage, Ms. Michelle Kuang, Mr. Valentin Aniel, and Drs. Rodrigo Seguel and Brian Taylor for assistance in extensive field measurements and discussion. The mobile monitoring platform measurements were made possible with the assistance of Dr. Walter Ham and Mr. Steve Mara and Dr. Kathleen Kozawa and Dr. Toshihiro Kuwayama at CARB. The views and opinions in this study are those of the authors and do not reflect the official views of the NSF or CARB.

### viii.2. References

#### viii.2.1. References for Section II

- Adams, H. S., Nieuwenhuijsen, M. J. and Colville, R. N. (2001a). Determinants of fine particle (PM<sub>2.5</sub>) personal exposure levels in transport microenvironments, London, UK. *Atmos. Environ.* 35:4557-4566.
- Adams, H. S., Nieuwenhuijsen, M. J., Colville, R. N., McMullen, M. A. S. and Khandelwal, P. (2001b). Fine particle (PM<sub>2.5</sub>) personal exposure levels in transport microenvironments, London, UK. *Sci. Total Environ.* 279:29-44.
- Baldauf, R., Thoma, E., Khlystov, A., Isakov, V., Bowker, G., Long, T. and Snow, R. (2008). Impacts of noise barriers on near-road air quality. *Atmos. Environ.* 42:7502-7507.
- Bau, S., Zimmermann, B., Payet, R. and Witschger, O. (2015). A laboratory study of the performance of the handheld diffusion size classifier (DiSCmini) for various aerosols in the 15-400 nm range. *Environmental Science: Processes & Impacts*:Advance Article, DOI:10.1039/c1034em00491d.
- Behrentz, E., Sabin, L. D., Winer, A. M., Fitz, D. R., Pankratz, D. V., Colome, S. D. and Fruin, S. A. (2005). Relative importance of school bus-related microenvironments to children's pollutant exposure. *J. Air Waste Manage. Assoc.* 55:1418-1430.
- Birmili, W., Rehn, J., Vogel, A., Boehlke, C., Weber, K. and Rasch, F. (2013). Micro-scale variability of urban particle number and mass concentrations in Leipzig, Germany. *Meteorologische Zeitschrift* 22:155-165.
- Boarnet, M. G., Houston, D., Edwards, R., Princevac, M., Ferguson, G., Pan, H. S. and Bartolome, C. (2011). Fine particulate concentrations on sidewalks in five Southern California cities. *Atmos. Environ.* 45:4025-4033.
- Boogaard, H., Kos, G. P. A., Weijers, E. P., Janssen, N. A. H., Fischer, P. H., van der Zee, S. C., de Hartog, J. J. and Hoek, G. (2011). Contrast in air pollution components between major streets and background locations: Particulate matter mass, black carbon, elemental composition, nitrogen oxide and ultrafine particle number. *Atmos. Environ.* 45:650-658.
- Bowker, G. E., Baldauf, R., Isakov, V., Khlystov, A. and Petersen, W. (2007). The effects of roadside structures on the transport and dispersion of ultrafine particles from highways. *Atmos. Environ.* 41:8128-8139.
- Brugge, D., Durant, J. L. and Rioux, C. (2007). Near-highway pollutants in motor vehicle exhaust: A review of epidemiologic evidence of cardiac and pulmonary health risks. *Environ. Health* 6:12.
- Buonanno, G., Fuoco, F. C. and Stabile, L. (2011). Influential parameters on particle exposure of pedestrians in urban microenvironments. *Atmos. Environ.* 45:1434-1443.

- Canagaratna, M. R., Jayne, J. T., Ghertner, D. A., Herndon, S., Shi, Q., Jimenez, J. L., Silva, P. J., Williams, P., Lanni, T., Drewnick, F., Demerjian, K. L., Kolb, C. E. and Worsnop, D. R. (2004). Chase studies of particulate emissions from in-use New York City vehicles. *Aerosol Sci. Technol.* 38:555-573.
- Chan, T. L., Dong, G., Leung, C. W., Cheung, C. S. and Hung, W. T. (2002). Validation of a two-dimensional pollutant dispersion model in an isolated street canyon. *Atmos. Environ.* 36:861-872.
- Choi, W., Faloona, I. C., McKay, M., Goldstein, A. H. and Baker, B. (2011). Estimating the atmospheric boundary layer height over sloped, forested terrain from surface spectral analysis during BEARPEX. *Atmospheric Chemistry and Physics* 11:6837-6853.
- Choi, W., He, M., Barbesant, V., Kozawa, K. H., Mara, S., Winer, A. M. and Paulson, S. E. (2012a). Prevalence of wide area impacts downwind freeways under pre-sunrise stable atmospheric conditions. *Atmospheric Environment* 62:318-327.
- Choi, W., Hu, S. S., He, M., Kozawa, K. H., Mara, S., Winer, A. M. and Paulson, S. E. (2013a). Neighborhood-scale air quality impacts of emissions from motor vehicles and aircraft. *Atmospheric Environment* 80:310-321.
- Choi, W., Paulson, S. E., Cassmassi, J. and Winer, A. M. (2013b). Development of a classification system for air pollution meteorology applied to primary pollutants in the Los Angeles Air Basin. *Atmos. Environ.* 64:150-159.
- Choi, W. and Paulson, S. E. (2016). Closing the ultrafine particle number concentration budget at road-to-ambient scale: Implications for particle dynamics. *Aerosol Sci. Technol.* 50:448-461.
- Choi, W., Ranasinghe, D., Bunavage, K., DeShazo, J. R., Wu, L. S., Seguel, R., Winer, A. M. and Paulson, S. E. (2016). The effects of the built environment, traffic patterns, and micrometeorology on street level ultrafine particle concentrations at a block scale: Results from multiple urban sites. *Sci. Total Environ.* 553:474-485.
- Choi, W. S., He, M., Barbesant, V., Kozawa, K., Mara, S., Winer, A. M. and Paulson, S. E. (2012b). Prevalence of wide areas of air pollutant impact downwind of freeway during pre-sunrise at several locations in Southern California. *Atmos. Environ.* 62 318-327.
- Choi, W. S., He, M., Barbesant, V., Kozawa, K., Mara, S., Winer, A. M. and Paulson, S. E. (2013c). Neighborhoods, roadways, and airports: Air quality benefits of emissions reductions from mobile sources. *Atmos. Environ.* 80:300-321.
- Choi, W. S., Winer, A. M. and Paulson, S. E. (2014). Factors controlling pollutant plume length downwind of major roadways in nocturnal surface inversions. *Atmos. Chem. Phys.* 14:6925 - 6940.
- Finn, D., Clawson, K. L., Carter, R. G., Rich, J. D., Eckman, R. M., Perry, S. G., Isakov, V. and Heist, D. K. (2010). Tracer studies to characterize the effects of roadside noise barriers on near-road pollutant dispersion under varying atmospheric stability conditions. *Atmos. Environ.* 44:204-214.
- Fritsch, F. N. and Carlson, R. E. (1980). Monotone piecewise cubic interpolation. *SIAM Journal of Numerical Analysis* 17:238-246.
- Fruin, S. and Isakov, V. (2006). Ultrafine Particle Concentrations near Freeways at Night or Early Morning under Calm Conditions. , in *25th International Conference of the American Association for Aerosol Research*, , St. Paul, Minnesota.
- Fruin, S., Westerdaal, D., Sax, T., Sioutas, C. and Fine, P. M. (2008). Measurements and predictors of on-road ultrafine particle concentrations and associated pollutants in Los Angeles. *Atmos. Environ.* 42:207-219.
- Fruin, S. A., Winer, A. M. and Rodes, C. E. (2004). Black carbon concentrations in California vehicles and estimation of in-vehicle diesel exhaust particulate matter exposures. *Atmos. Environ.* 38:4123-4133.
- Goel, A. and Kumar, P. (2015). Zone of influence for particle number concentrations at signalised traffic intersections. *Atmospheric Environment* 123:25-38.

- Hagler, G. S. W., Lin, M. Y., Khlystov, A., Baldauf, R. W., Isakov, V., Faircloth, J. and Jackson, L. E. (2012). Field investigation of roadside vegetative and structural barrier impact on near-road ultrafine particle concentrations under a variety of wind conditions. *Sci. Total Environ.* 419:7-15.
- Haughey, R. and Sherriff, R. (2010). Challenges and Policy Options for Creating and Preserving Affordable Housing near Transit and Other Location-efficient Areas., in *Center for Housing Policy*.
- Hitchins, J., Morawska, L., Wolff, R. and Gilbert, D. (2000). Concentrations of submicrometre particles from vehicle emissions near a major road. *Atmos. Environ.* 34:51-59.
- Hoek, G., Brunekreef, B., Goldbohm, S., Fischer, P. and van den Brandt, P. A. (2002). Association between mortality and indicators of traffic-related air pollution in the Netherlands: a cohort study. *Lancet* 360:1203-1209.
- Hu, S., Fruin, S., Kozawa, K., Mara, S., Winer, A. M. and Paulson, S. E. (2009a). Characterization of aircraft emission impacts in a neighborhood adjacent to a general aviation airport in Southern California. *Env. Sci. Technol.* 43:8039-8045.
- Hu, S., Paulson, S. E., Fruin, S., Kozawa, K., Mara, S. and Winer, A. M. (2012). Observation of elevated air pollutant concentrations in a residential neighborhood of Los Angeles California using a mobile platform. *Atmospheric Environment* 51:311-319.
- Hu, S. S., Fruin, S., Kozawa, K., Mara, S., Paulson, S. E. and Winer, A. M. (2009b). A wide area of air pollutant impact downwind of a freeway during pre-sunrise hours. *Atmospheric Environment* 43:2541-2549.
- Hussein, T., Karppinen, A., Kukkonen, J., Harkonen, J., Aalto, P. P., Hameri, K., Kerminen, V. M. and Kulmala, M. (2006). Meteorological dependence of size-fractionated number concentrations of urban aerosol particles. *Atmospheric Environment* 40:1427-1440.
- Janssen, N. A. H., Brunekreef, B., van Vliet, P., Aarts, F., Meliefste, K., Harssema, H. and Fischer, P. (2003). The relationship between air pollution from heavy traffic and allergic sensitization, bronchial hyperresponsiveness, and respiratory symptoms in Dutch schoolchildren. *Environ. Health Perspect.* 111:1512-1518.
- Karra, S., Malki-Epshtein, L. and Neophytou (2011). The dispersion of traffic related pollutants across a non-homogeneous street canyon. *Procedia Environmental Sciences* 4.
- Kaur, S., Nieuwenhuijsen, M. J. and Colvile, R. N. (2007). Fine particulate matter and carbon monoxide exposure concentrations in urban street transport microenvironments. *Atmos. Environ.* 41:4781-4810.
- Kinney, P. L., Aggarwal, M., Northridge, M. E., Janssen, N. A. H. and Shepard, P. (2000). Airborne concentrations of PM<sub>2.5</sub> and diesel exhaust particles on Harlem sidewalks: A community-based pilot study. *Environ. Health Perspect.* 108:213-218.
- Kittelson, D. B., Watts, W. F. and Johnson, J. P. (2004a). Nanoparticle emissions on Minnesota highways. *Atmos. Environ.* 38:9-19.
- Kittelson, D. B., Watts, W. F., Johnson, J. P., Remerowki, M. L., Ische, E. E., Oberdorster, G., Gelein, R. A., Elder, A., Hopke, P. K., Kim, E., Zhao, W., Zhou, L. and Jeong, C. H. (2004b). On-road exposure to highway aerosols. 1. Aerosol and gas measurements. *Inhal. Toxicol.* 16:31-39.
- Klems, J. P., Pennington, M. R., Zordan, C. A. and Johnston, M. V. (2010). Ultrafine Particles Near a Roadway Intersection: Origin and Apportionment of Fast Changes in Concentration. *Environmental Science & Technology* 44:7903-7907.
- Knoblauch, R., Pietrucha, M. and Nitzburg, M. (1996). Field studies of pedestrian walking speed and start-up time. *Transportation Research Record: Journal of the Transportation Research Board* 1538:27-38.
- Kozawa, K. H., Fruin, S. A. and Winer, A. M. (2008). Using a Mobile Monitoring Platform to Characterize Pollution Concentrations On and Near Heavily-Traveled Roadways in Communities Adjacent to the Ports of Los Angeles and Long Beach. *Epidemiology* 19:S224-S225.

- Kozawa, K. H., Fruin, S. A. and Winer, A. M. (2009). Near-road air pollution impacts of goods movement in communities adjacent to the Ports of Los Angeles and Long Beach. *Atmos. Environ.* 43:2960-2970.
- Kumar, P., Ketzler, M., Vardoulakis, S., Pirjola, L. and Britter, R. (2011). Dynamics and dispersion modelling of nanoparticles from road traffic in the urban atmospheric environment-A review. *J. Aerosol. Sci.* 42:580-603.
- Liu, C.-H., Barth, M. C. and Leung, D. Y. C. (2004). Large-eddy simulation of flow and pollutant transport in street canyons of different building-height-street-width ratios *Journal of Applied Meteorology* 43:1410-1424.
- Marshall, J. D., McKone, T. E., Deakin, E. and Nazaroff, W. W. (2005). Inhalation of motor vehicle emissions: effects of urban population and land area. *Atmos. Environ.* 39:283-295.
- Mills, J. B., Park, J. H. and Peters, T. M. (2013). Comparison of the DiSCmini aerosol monitor to a handheld Condensation Particle Counter and a Scanning Mobility Particle Sizer for submicrometer sodium chloride and metal aerosols. *Journal of Occupational and Environmental Hygiene* 10:250-258.
- Misra, P. and Enge, P. (2006). *Global positioning system: signals, measurements, and performance*. Ganga-Jamuna Press, Lincoln, MA, U.S.A.
- Ning, Z., Geller, M. D., Moore, K. F., Sheesley, R., Schauer, J. J. and Sioutas, C. (2007). Daily variation in chemical characteristics of urban ultrafine aerosols and inference of their sources. *Environmental Science & Technology* 41:6000-6006.
- Ning, Z., Hudda, N., Daher, N., Kam, W., Herner, J., Kozawa, K., Mara, S. and Sioutas, C. (2010). Impact of roadside noise barriers on particle size distributions and pollutants concentrations near freeways. *Atmos. Environ.* 44:3118-3127.
- Parise, C., Sternfeld, B., Samuels, S. and Tager, I. B. (2004). Brisk walking speed in older adults who walk for exercise. *Journal of the American Geriatrics Society* 52(3):411-4116.
- Patel, M. M., Chillrud, S. N., Correa, J. C., Feinberg, M., Hazi, Y., Deepti, K. C., Prakash, S., Ross, J. M., Levy, D. and Kinney, P. L. (2009). Spatial and temporal variations in traffic-related particulate matter at New York City high schools. *Atmos. Environ.* 43:4975.
- Paulson, S. E., Winer, A. M., Choi, W. S., He, M., Barbesant, V., Hu, S., Kozawa, K. and Mara, S. (2012). Mobile Platform III: Characterizing Spatially Inhomogeneous Non-Criteria Pollutants in the Los Angeles Air Basin., California Air Resources Board Report, 110.
- Pearson, R. L., Wachtel, H. and Ebi, K. L. (2000). Distance-weighted traffic density in proximity to a home is a risk factor for leukemia and other childhood cancers. *J. Air Waste Manage. Assoc.* 50:175-180.
- Pirjola, L., Parviainen, H., Hussein, T., Valli, A., Hameri, K., Aalto, P., Virtanen, A., Keskinen, J., Pakkanen, T. A., Makela, T. and Hillamo, R. E. (2004). "Sniffer" - a novel tool for chasing vehicles and measuring traffic pollutants. *Atmos. Environ.* 38:3625-3635.
- Quiros, D. C., Zhang, Q., Choi, W. S., He, M., Paulson, S. E., Winer, A. M., Wang, R. and Zhu, Y. (2012). Near-Roadway Air Quality Impacts of a Scheduled 36-hour Closure of a Major Highway. *Atmos. Environ.* 67:404-414.
- Ranasinghe, D., Choi, W., Winer, A. M. and Paulson, S. E. (2015). Developing high spatial resolution concentration maps using mobile air quality measurements. *Aerosol and Air Quality Research* submitted.
- Ranasinghe, D., Choi, W., Winer, A. M. and Paulson, S. E. (2016). Developing high spatial resolution concentration maps using mobile air quality measurements. *Aerosol and Air Quality Research* under review.
- Ren, C., Wu, J., Chung, J. H., Delfino, R. J. and Ritz, B. (2008). Association Between Local Traffic-generated Air Pollution and Preterm Delivery in the South Coast Air Basin of California. *Epidemiology* 19:S158-S159.
- Rivera, M., Basagana, X., Aguilera, I., Agis, D., Bouso, L., Foraster, M., Medina-Ramon, M., Pey, J., Kunzli, N. and Hoek, G. (2012). Spatial distribution of ultrafine particles in urban settings: A land use regression model. *Atmos. Environ.* 54:657-666.

- Rodes, C. E. and Holland, D. M. (1981). Variations Of No, No<sub>2</sub> And O<sub>3</sub> Concentrations Downwind Of A Los-Angeles Freeway. *Atmos. Environ.* 15:243-250.
- Rodes, C. e. a. (1998). Measuring Concentrations of Selected Air Pollutants Inside California Vehicles.
- Ryan, P. H., LeMasters, G. K., Levin, L., Burkle, J., Biswas, P., Hu, S. H., Grinshpun, S. and Reponen, T. (2008). A land-use regression model for estimating microenvironmental diesel exposure given multiple addresses from birth through childhood. *Sci. Total Environ.* 404:139-147.
- Salmond, J. A., Pauscher, L., Pigeon, G., Masson, V. and Legain, D. (2010). Vertical transport of accumulation mode particles between two street canyons and the urban boundary layer. *Atmos. Environ.* 44:5139-5147.
- Seibert, P., Beyrich, F., Gryning, S. E., Joffre, S., Rasmussen, A. and Tercier, P. (2000). Review and intercomparison of operational methods for the determination of the mixing height. *Atmospheric Environment* 34:1001-1027.
- Shikiya, D. C., Liu, C. S., Hahn, M. I., Juarros, J. and Barcikowski, W. (1989a). In-Vehicle Air Toxics Characterization Study in the South Coast Air Basin. Final Report, , South Coast Air Quality Management District, El Monte, California.
- Shikiya, D. C., Liu, C. S., Hahn, M. I., Juarros, J. and Barcikowski, W. (1989b). In-Vehicle Air Toxics Characterization Study in the South Coast Air Basin.
- Steffens, J. T., Wang, Y. J. and Zhang, K. M. (2012). Exploration of effects of a vegetation barrier on particle size distributions in a near-road environment. *Atmos. Environ.* 50:120-128.
- Tong, Z. M., Wang, Y. J., Patel, M., Kinney, P., Chirud, S. and Zhang, K. M. (2012). Modeling Spatial Variations of Black Carbon Particles in an Urban Highway-Building Environment. *Environ. Sci. Technol.* 46:312-319.
- Tonne, C., Melly, S., Mittleman, M., Coull, B., Goldberg, R. and Schwartz, J. (2007). A case-control analysis of exposure to traffic and acute myocardial infarction. *Environ. Health Perspect.* 115:53-57.
- Vardoulakis, S., Fisher, B. E. A., Pericleous, K. and Gonzalez-Flesca, N. (2003). Modelling air quality in street canyons: a review. *Atmos. Environ.* 37:155-182.
- Volk, H. E., Hertz-Picciotto, I., Delwiche, L., Lurmann, F. and McConnell, R. (2011). Residential Proximity to Freeways and Autism in the CHARGE Study. *Environ. Health Perspect.* 119:873-877.
- Weijers, E. P., Khlystov, A. Y., Kos, G. P. A. and Erisman, J. W. (2004). Variability of particulate matter concentrations along roads and motorways determined by a moving measurement unit. *Atmos. Environ.* 38:2993-3002.
- Westerdahl, D., Fruin, S., Sax, T., Fine, P. M. and Sioutas, C. (2005). Mobile platform measurements of ultrafine particles and associated pollutant concentrations on freeways and residential streets in Los Angeles. *Atmos. Environ.* 39:3597-3610.
- Westerdahl, D., Fruin, S. A., Fine, P. L. and Sioutas, C. (2008). The Los Angeles International Airport as a source of ultrafine particles and other pollutants to nearby communities. *Atmos. Environ.* 42:3143-3155.
- Zhou, Y. and Levy, J. I. (2007). Factors influencing the spatial extent of mobile source air pollution impacts: a meta-analysis. *BMC Public Health* 7.
- Zhu, Y. F., Hinds, W. C., Kim, S., Shen, S. and Sioutas, C. (2002). Study of ultrafine particles near a major highway with heavy-duty diesel traffic. *Atmos. Environ.* 36:4323-4335.
- Zhu, Y. F., Hinds, W. C., Kim, S. and Sioutas, C. (2002a). Concentration and size distribution of ultrafine particles near a major highway. *J. Air Waste Manage. Assoc.* 52:1032-1042.
- Zhu, Y. F., Kuhn, T., Mayo, P. and Hinds, W. C. (2006). Comparison of daytime and nighttime concentration profiles and size distributions of ultrafine particles near a major highway. *Environ. Sci. Technol.* 40:2531-2536.
- Zhu, Y. F., Eiguren-Fernandez, A., Hinds, W. C. and Miguel, A. H. (2007). In-cabin commuter exposure to ultrafine particles on Los Angeles freeways. *Environ. Sci. Technol.* 41:2138-2145.

### viii.2.2. References for Section III

- Barlow, J.F., Belcher, S.E., 2002. A Wind Tunnel Model for Quantifying Fluxes In The Urban Boundary Layer. *Bound.-Layer Meteorol.* 104, 131–150.
- Belcher, S.E., 2005. Mixing and transport in urban areas. *Philos. Trans.* 363, 2947–2968. doi:10.1098/rsta.2005.1673
- Berkowicz, R., 2000. OSPM - A Parameterised Street Pollution Model. *Environ. Monit. Assess.* 65, 323–331.
- Berkowicz, R., Hertel, O., Larsen, S.E., Sørensen, N.N., Nielsen, M., 1997. Modelling traffic pollution in streets. Ministry of Environment and Energy, National Environmental Research Institute.
- Boarnet, M., Crane, R., 2007. L. A. Story, A Reality Check for Transit-Based Housing. *J. Am. Plann. Assoc.* 63, 189–204.
- Brixey, L. a, Heist, D.K., Richmond-Bryant, J., Bowker, G.E., Perry, S.G., Wiener, R.W., 2009. The effect of a tall tower on flow and dispersion through a model urban neighborhood: part 2. Pollutant dispersion. *J. Environ. Monit. JEM* 11, 2171–9. doi:10.1039/b907137g
- Bukowiecki, N., Dommen, J., Prevot, A.S.H., Richter, R., Weingartner, E., Baltensperger, U., 2002. A mobile pollutant measurement laboratory—measuring gas phase and aerosol ambient concentrations with high spatial and temporal resolution. *Atmos. Environ.* 36, 5569–5579.
- CARB, 2015. Mobile Source Emission Inventory [WWW Document]. URL <https://www.arb.ca.gov/msei/msei.htm>
- Cimorelli, A.J., Perry, S.G., Venkatram, A., Weil, J.C., Paine, R.J., Wilson, R.B., Lee, R.F., Peters, W.D., Brode, R.W., 2005. AERMOD: A dispersion model for industrial source applications. Part I: General model formulation and boundary layer characterization. *J. Appl. Meteorol.* 44, 682–693.
- Di Sabatino, S., Buccolieri, R., Pulvirenti, B., Britter, R., 2007. Simulations of pollutant dispersion within idealised urban-type geometries with CFD and integral models. *Atmos. Environ.* 41, 8316–8329. doi:10.1016/j.atmosenv.2007.06.052
- Grimmond, C.S.B., Oke, T.R., 1999. Aerodynamic Properties of Urban Areas Derived from Analysis of Surface Form. *J. Appl. Meteorol.* 38, 1262–1292.
- Hang, J., Li, Y., Buccolieri, R., Sandberg, M., Di Sabatino, S., 2012. On the contribution of mean flow and turbulence to city breathability: the case of long streets with tall buildings. *Sci. Total Environ.* 416, 362–73. doi:10.1016/j.scitotenv.2011.12.016
- Hanna, S., Chang, J.C., Flaherty, J., 2014. Observed Ratios of Rooftop to Surface Concentrations in Built-Up City Centers. Atlanta, Georgia. Available at [www.ametsoc.org](http://www.ametsoc.org).
- Hanna, S., White, J., Zhou, Y., 2007. Observed winds, turbulence, and dispersion in built-up downtown areas of Oklahoma City and Manhattan. *Bound.-Layer Meteorol.* 125, 441–468. doi:10.1007/s10546-007-9197-2
- Hanna, S.R., Zhou, Y., 2009. Space and Time Variations in Turbulence during the Manhattan Midtown 2005 Field Experiment. *J. Appl. Meteorol. Climatol.* 48, 2295–2304. doi:10.1175/2009JAMC2046.1
- Heist, D.K., Perry, S.G., Bowker, G.E., 2004. EVIDENCE OF ENHANCED VERTICAL DISPERSION IN THE WAKES OF TALL BUILDINGS IN WIND TUNNEL SIMULATIONS OF LOWER MANHATTAN. AMS 5th Conf. Urban Environ. Paper 7.5, Paper 7.5-Paper 7.5.
- Kaimal, C., Finnigan, J.J., 1994. Atmospheric boundary layer flows: their structure and measurement. Oxford University Press.
- Karra, S., Malki-Epshtein, L., Neophytou, M., 2011. The Dispersion of Traffic Related Pollutants Across a Non-Homogeneous Street Canyon. *Procedia Environ. Sci.* 4, 25–34. doi:10.1016/j.proenv.2011.03.004

- Ketzel, M., Berkowicz, R., 2004. Modelling the fate of ultrafine particles from exhaust pipe to rural background: an analysis of time scales for dilution, coagulation and deposition. *Atmos. Environ.* 38, 2639–2652. doi:10.1016/j.atmosenv.2004.02.020
- Ketzel, M., Berkowicz, R., Lohmeyer, A., 2000. Comparison of Numerical Street Dispersion Models with Results From Wind Tunnel and Field Measurements. *Environ. Monit. Assess.* 65, 363–370.
- Ketzel, M., Wåhlin, P., Berkowicz, R., Palmgren, F., 2003. Particle and trace gas emission factors under urban driving conditions in Copenhagen based on street and roof-level observations. *Atmos. Environ.* 37, 2735–2749. doi:10.1016/S1352-2310(03)00245-0
- Kittelson, D.B., Watts, W.F., Johnson, J.P., 2004. Nanoparticle emissions on Minnesota highways. *Atmos. Environ.* 38, 9–19. doi:10.1016/j.atmosenv.2003.09.037
- Knibbs, L.D., Cole-Hunter, T., Morawska, L., 2011. A review of commuter exposure to ultrafine particles and its health effects. *Atmos. Environ.* 45, 2611–2622. doi:10.1016/j.atmosenv.2011.02.065
- Kumar, P., Ketzel, M., Vardoulakis, S., Pirjola, L., Britter, R., 2011. Dynamics and dispersion modelling of nanoparticles from road traffic in the urban atmospheric environment—A review. *J. Aerosol Sci.* 42, 580–603. doi:10.1016/j.jaerosci.2011.06.001
- Los Angeles County, 2008. Countywide Building Outlines [WWW Document]. URL <http://egis3.lacounty.gov/dataportal/2011/04/28/countywide-building-outlines/>
- Louka, P., Belcher, S.E., Harrison, R.G., 2000. Coupling between air flow in streets and the well-developed boundary layer aloft. *Atmos. Environ.* 34, 2613–2621.
- Luhar, A.K., Venkatram, A., Lee, S.-M., 2006. On relationships between urban and rural near-surface meteorology for diffusion applications. *Atmos. Environ.* 40, 6541–6553.
- Macdonald, R.W., Griffiths, R.F., Hall, D.J., 1998. An improved method for the estimation of surface roughness of obstacle arrays. *Atmos. Environ.* 32, 1857–1864. doi:10.1016/S1352-2310(97)00403-2
- Nakamura, Y., Oke, T.R., 1988. Wind, temperature and stability conditions in an east-west oriented urban canyon. *Atmos. Environ.* 22, 2691–2700. doi:10.1016/0004-6981(88)90437-4
- Nelson, M.A., Pardyjak, E.R., Klewicki, J.C., Pol, S.U., Brown, M.J., 2007. Properties of the Wind Field within the Oklahoma City Park Avenue Street Canyon. Part I: Mean Flow and Turbulence Statistics. *J. Appl. Meteorol. Climatol.* 46, 2038–2054. doi:10.1175/2006JAMC1427.1
- Pournazeri, S., Tan, S., Schulte, N., Jing, Q., Venkatram, A., 2014. A computationally efficient model for estimating background concentrations of NO<sub>x</sub>, NO<sub>2</sub>, and O<sub>3</sub>. *Environ. Model. Softw.* 52, 19–37. doi:10.1016/j.envsoft.2013.10.018
- Smit, R., Brown, A.L., Chan, Y.C., 2008. Do air pollution emissions and fuel consumption models for roadways include the effects of congestion in the roadway traffic flow? *Environ. Model. Softw.* 23, 1262–1270.
- Smit, R., Ntziachristos, L., Boulter, P., 2010. Validation of road vehicle and traffic emission models – A review and meta-analysis. *Atmos. Environ.* 44, 2943–2953. doi:10.1016/j.atmosenv.2010.05.022
- Soulhac, L., Salizzoni, P., Cierco, F.-X., Perkins, R., 2011. The model SIRANE for atmospheric urban pollutant dispersion; part I, presentation of the model. *Atmos. Environ.* 45, 7379–7395. doi:10.1016/j.atmosenv.2011.07.008
- Tiwary, A., Robins, A., Namdeo, A., Bell, M., 2011. Air flow and concentration fields at urban road intersections for improved understanding of personal exposure. *Environ. Int.* 37, 1005–18. doi:10.1016/j.envint.2011.02.006
- Vardoulakis, S., Fisher, B.E., Pericleous, K., Gonzalez-Flesca, N., 2003. Modelling air quality in street canyons: a review. *Atmos. Environ.* 37, 155–182. doi:10.1016/S1352-2310(02)00857-9
- Venkatram, A., Isakov, V., Thoma, E., Baldauf, R., 2007. Analysis of air quality data near roadways using a dispersion model. *Atmos. Environ.* 41, 9481–9497. doi:10.1016/j.atmosenv.2007.08.045

Yamartino, R.J., Wiegand, G., 1986. Development and evaluation of simple models for the flow, turbulence and pollutant concentration fields within an urban street canyon. *Atmos. Environ.* 20, 2137–2156. doi:10.1016/0004-6981(86)90307-0

## ix. Appendix: Supporting information for Section vi.4

**Los Angeles Field Measurements.** Los Angeles - 8th St, April 23 - May 13 2014 measurements were made near the 8th and Hill St intersection in Los Angeles between April 23 and May 13, 2014. An overview of the experiment is shown in Figure A1. The site was chosen because 8th St has a section where there are no buildings next to the road, the “parking lot” site, and a section where there are tall buildings directly next to the road, the “building” site. This design helps remove the effect of emission variation: because the open and building sites have very similar traffic we can directly compare the concentrations at the site to determine the effect of the buildings at the “building” section on the concentration. Sonic anemometers were placed at an upwind rural location near LAX airport, at a rooftop location on the 50 m tall Union Lofts building, located at the 8th and Hill St intersection, at the parking lot and building sites, and at the mid-section between the two sites.

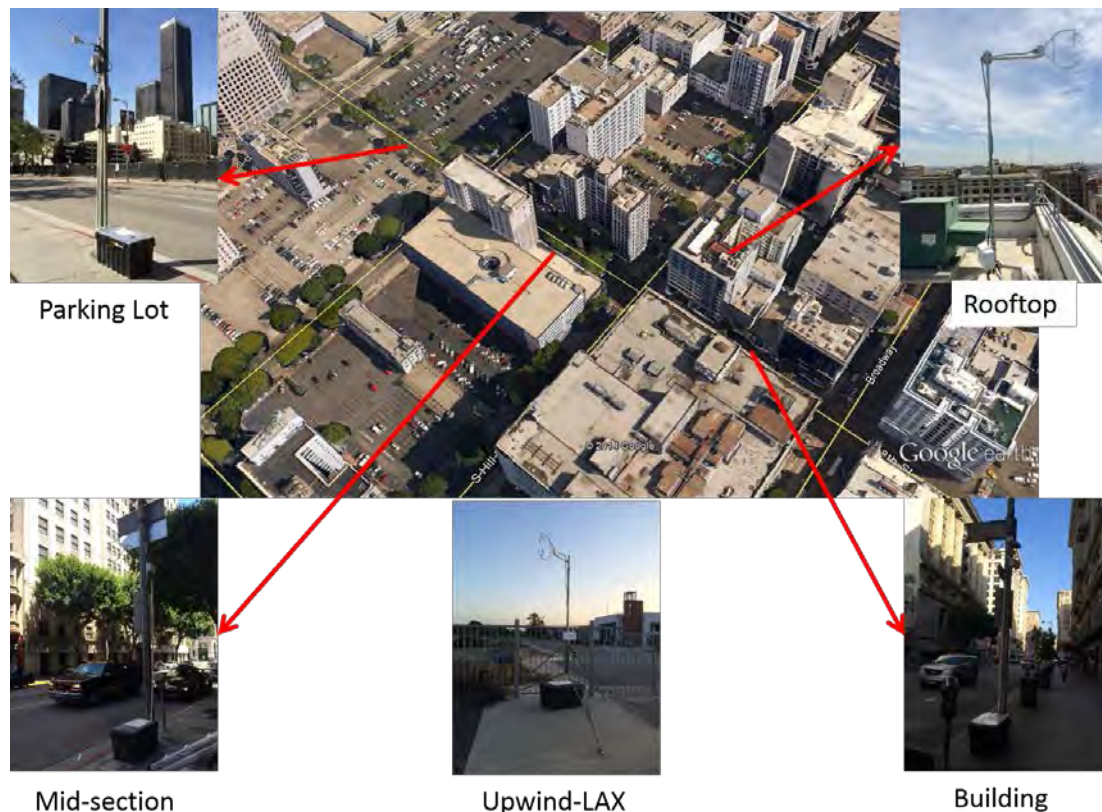


**Figure A1: Overview of 8th St field study.**

The upwind rural sonic anemometer was mounted on a tripod at 3.15 m above ground level (AGL). The bottom center picture in Figure A1 shows this anemometer, looking downwind. There were no buildings upwind of the sonic essentially all the way to the Pacific Ocean several kilometers to the west. The street level sonic anemometers were mounted to light poles next to 8th St at about 4 m AGL (Figure A1). See Figure A4 and Table A1 for detailed instrument locations. The anemometers were attached to 2 foot beams attached to the poles and oriented with the sensor pointed toward the street, except for the sonic next to the parking lot, which was oriented southwest because the predominant wind direction is southwesterly. We attempted to place the anemometers away from major obstructions. However, 8th St has several large trees next to the road, and the instrument at location 1 (Table A1) was placed about 10 m downwind of a tree, and instrument location 2 was at a section of road where there were trees upwind and downwind. Locations 3 and 4, the locations of the primary sonic anemometer measurements, were far from any trees or other obstacles.

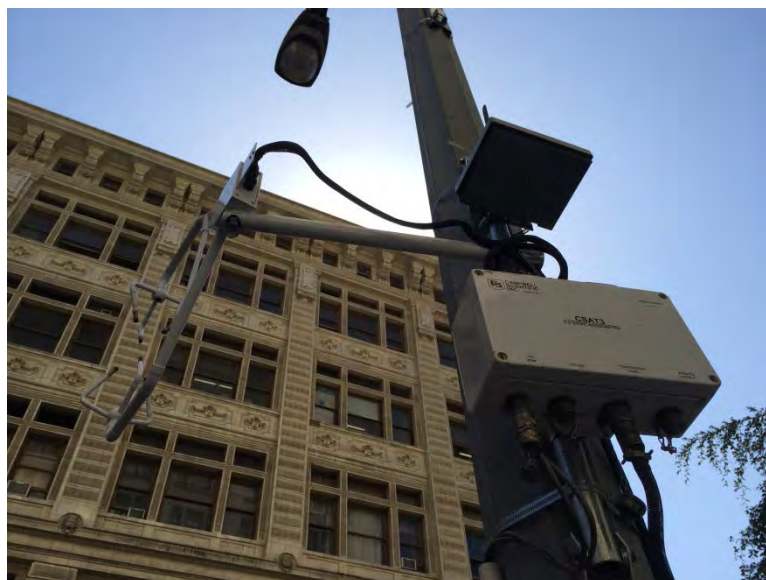


**Figure A2: Sonic anemometer and AQMesh monitor mounted to light pole next to 8th St.**

Condensation particle counters were placed at the locations shown in Figure A4. The CPCs were placed on May 7th and May 9th between about 8:00 and 18:00 PDT, but no rooftop CPC (number 360) was used on May 7th because the instrument was not available. The CPCs were co-located (Figure A3) for 30 minutes before the start of measurements on both May 7th and 9th to derive inter-instrument calibration factors used to adjust the data. The results of the calibration are shown in Appendix B.



**Figure A3: Co-location of CPCs before start of measurements on 8th St.**

Traffic data for 8th St was obtained from automatic traffic detectors run by city of LA. The traffic was recorded at the 8th St and Olive St intersection located midway between the open and building sites.

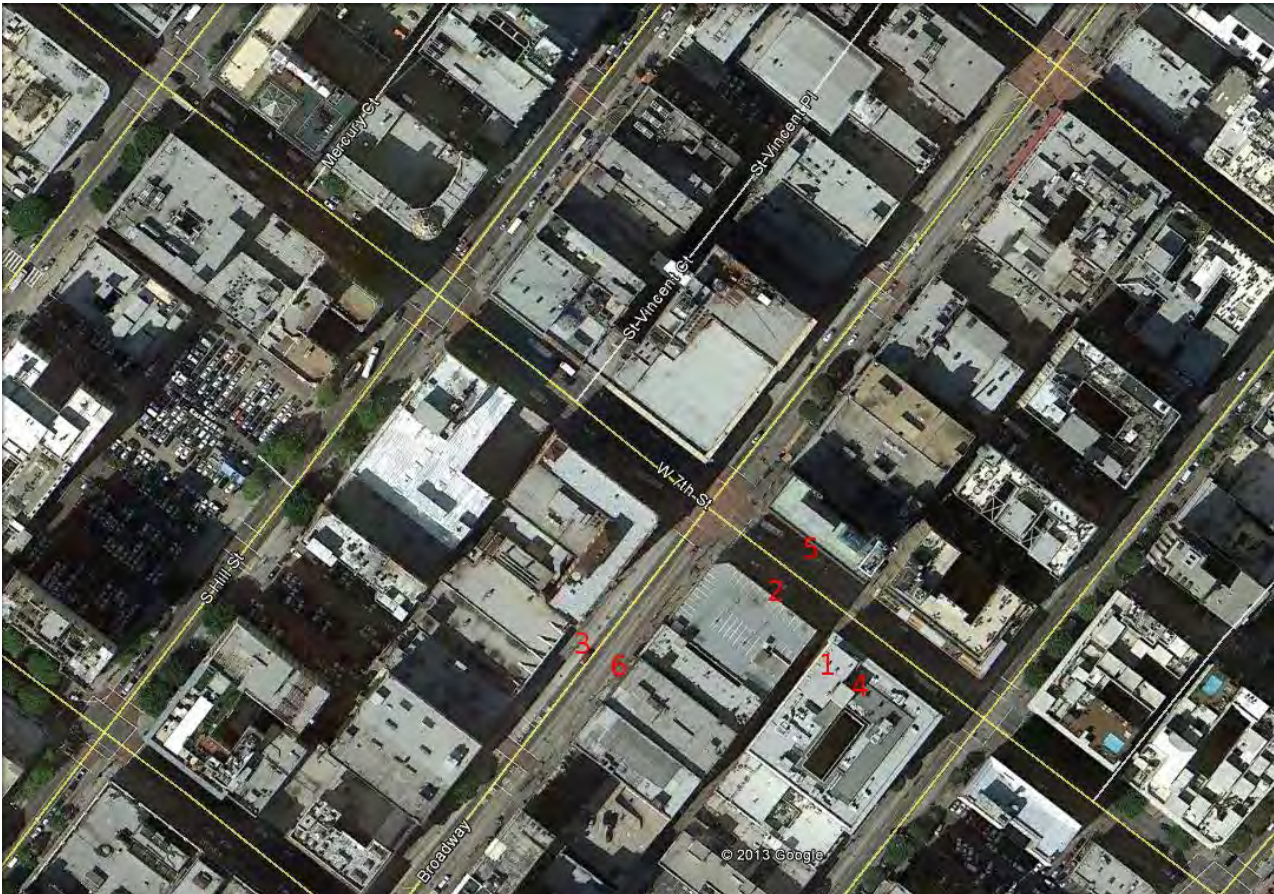


Figure A4: Instrument locations on 8th St. See Table A1 for symbol definitions.

**Table A1: Detailed instrument locations on 8th St.**

ID	Instrument	Location	Latitude	Longitude	Heading (° from north)	Height (inches)	Dates (month/day/year)
1	Sonic 0984	Building Region	34.04413	--118.25533	19	146	4/23-5/1
2	Sonic 0984	Middle region	34.04482	-118.25603	190	157	5/1-5/13
3	Sonic 0245	Building region	34.04403	-118.25541	204	160	4/23-5/13
4	Sonic 1055	Parking lot	34.04523	-118.25713	37	155	4/22-5/13
5	Sonic 2564	Upwind LAX airport	33.95494	-118.40472	36	124	5/7-5/13
6	Sonic	8th St. roof of union lofts	34.044285	-118.255326	18	95	5/1-5/13
1	AQMesh 82150	Building region				152	5/1-5/9
3	AQMesh 89150					166	5/1-5/9
A	CPC 483	Near sonic 0245	34.04403	-118.25541		59	5/7-5/9
B	CPC 498	ACross street from sonic 0245	34.044213	-118.255361		59	5/7-5/9
C	CPC 494	Near sonic 1055	34.045406	-118.25738		59	5/7 and 5/9
D	CPC 502	ACross street from sonic 1055	34.045506	-118.257285		59	5/7 and 5/9
E	CPC 360	Roof of union lofts building	34.044398	-118.255464		59	5/9

**Los Angeles - 7th St and Broadway, September 20, 2013.** Figure A5 shows an overhead view of the locations of measurements made in Los Angeles on September 20. Table A2 shows the detailed locations of the instruments. Four sonic anemometers were mounted on tripods at several locations: one on a tripod about 3 m above the top of the 55 m tall Van Nuys apartment building next to 7th St, one at 2.4 m AGL on the southwest side of 7th St, one at 2.4 m AGL on the northwest side of Broadway, and one at 2.4 m AGL at a park, Rancho Cienega Recreation center, approximately 10 km west (upwind) of the 7th St site. The upwind sonic was placed as far from buildings and trees as possible on a flat baseball field. The buildings surrounding the park were 1 or 2 stories tall. The rooftop sonic was placed on a section of the rooftop about 10 m higher than the rest of the roof near the edge of the building (Figure A6). A small structure stands about 7 m to the east of the sonic.



**Figure A5: Instrument locations at 7th St and Broadway field site. See Table 6 for symbol definitions.**

**Table A2: Detailed instrument locations at 7th St and Broadway.**

ID	Instrument	Location	Latitude	Longitude	Heading (° from north)	Height
1	Sonic	Roof	34.044645	-118.25297	83	57.4
2	Sonic	7th St	34.04495	-118.253129	210	2.4
3	Sonic	Broadway	34.044639	-118.253956	322	2.4
2	DiscMini 2	7th St South	34.044888	-118.253035		1
3	CPC 483	Broadway west	34.044719	-118.253955		1
4	CPC 481	Roof	34.044623	-118.252775		56
5	DiscMini 1	7th St North	34.045004	-118.252914		1
6	CPC 360	Broadway East	34.044634	-118.253786		1
	Sonic	Upwind Park	34.023285	-118.35091	75	2.4



**Figure A6:** Location of rooftop sonic anemometer near the edge of a section of roof about 10 m above the rest of the roof. A small structure sites about 7 m to the east of the sonic.

Three TSI 3022A CPCs and two Matter Aerosol DiSCminis were used to measure concentrations of ultrafine particle number. Two CPCs were placed on opposite sides of Broadway, and one on top of the 55 m tall Van Nuys apartment building. The two DiSCminis were placed on opposite sides of 7th St. The CPCs and DiSCminis were calibrated relative to each other by co-locating the instruments for about 30 minutes and adjusting the data using the resulting calibration factors. Appendix B shows the calibration plots along with the regression coefficients for each instrument. Traffic at the 7th St and Broadway intersection was recorded using a camera attached to a tripod on the roof of the Van Nuys building. Additionally, traffic data was obtained from the city of LA's automatic traffic counting system. The traffic data for 7th St was obtained from detectors located at 7th St and San Pedro intersection, and for Broadway from detectors at Broadway and Pico St. The manual and automatic counts were compared, and the automatic counts were adjusted to match the magnitude of the manual counts.

**Temple City - Las Tunas Dr and Temple City Blvd.** This site is characterized by fairly uniform single story buildings. Measurements of particle concentrations and turbulence were made between January 13 and February 13, 2014 in Temple City at the Las Tunas Dr and Temple City Blvd intersection. Figure A7 shows the locations of the CPCs and sonic anemometers at the site. One anemometer was placed on the roof of a 6.1 m tall building near the intersection and another was mounted to a light post at the south side of the street near mid-block. An additional sonic was placed at a rural upwind site at Rose Hill Park. CPCs were placed at the four corners of the block and on both sides of the street near mid-block on January 15, 16, and 17. The CPCs were co-located to derive calibration factors. Results are given in Appendix B. Traffic was counted using a video camera near mid-block. Table A3 gives a summary of the instrument locations.

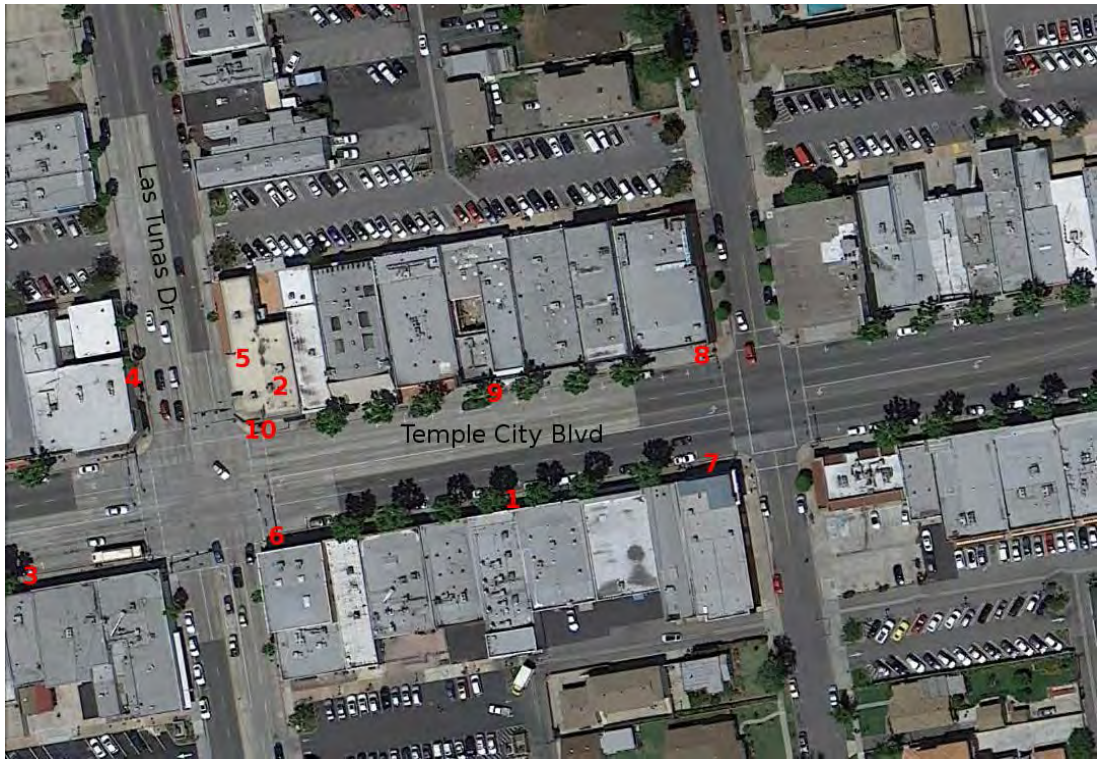


Figure A7: Temple City experiment site. For marker definitions see Table 7.

**Table A3: Detailed instrument locations at Temple City site.**

ID	Instrument	Location	Latitude	Longitude	Heading (° from north)	Height	Dates (month/day/year)
1	Sonic	South Center	34.106693	-118.060151	88	2.4	1/13/14-2/13/14
2	Sonic	Roof	34.1069	-118.060712	354	8.4	1/13/14-2/13/14
1	CPC 502	South Center	34.106693	-118.060151	322	1	1/15/14,1/16/14,1/17/14
2	CPC 498	Roof	34.106874	-118.060758		7	1/15/14,1/16/14,1/17/14
6	CPC 499	South West	34.10662	-118.060669		1	1/15/14,1/16/14,1/17/14
7	CPC 480	South East	34.106761	-118.059658		1	1/15/14,1/16/14,1/17/14
8	CPC 497	North East	34.106975	-118.059708		1	1/15/14,1/16/14,1/17/14
9	CPC 494	North Center	34.106903	-118.060259		1	1/15/14,1/16/14,1/17/14
10	CPC 483	North West	34.106834	-118.060711	75	1	1/15/14,1/16/14,1/17/14

**Beverly Hills - Wilshire Blvd.** The measurements on Wilshire Blvd, Beverly Hills were similar to those made on 8th St, except no rooftop measurements were made. Figure A8 shows an aerial view of the site, showing CPC locations near the “parking lot” and “building” locations, which have only short buildings and 50 m tall buildings directly next to the road, respectively. Sonic anemometers were placed next to the street at the "parking lot" and "building" locations, and at the same upwind LAX site used in the Los Angeles 8th St field study. Four CPCs were placed at the location shown in Figure A8. Table A4 gives details of the instrument locations.



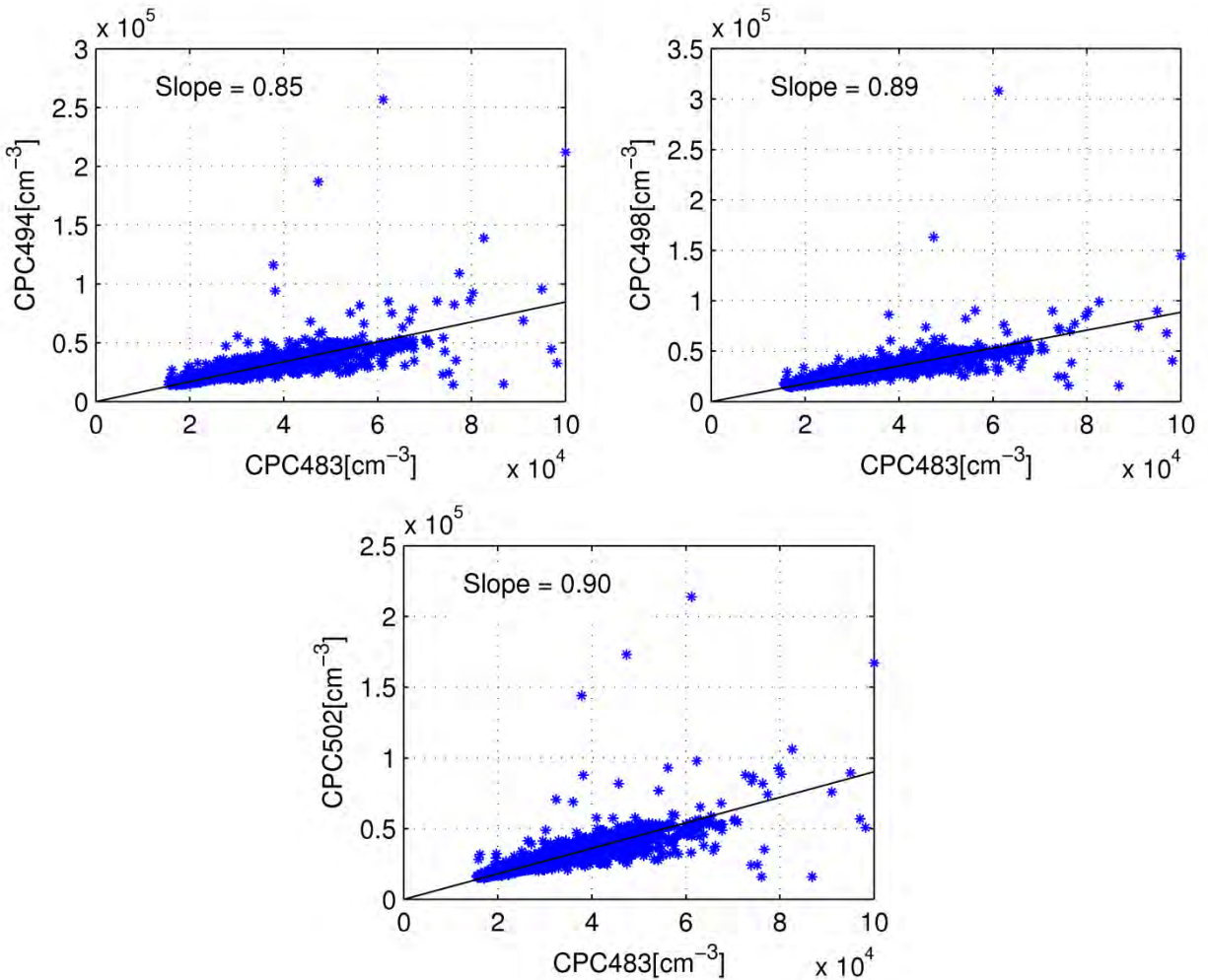
**Figure A8:** View of Wilshire Blvd field site. For marker definitions see Table 8.

**Table A4: Detailed instrument locations at Beverly Hills site.**

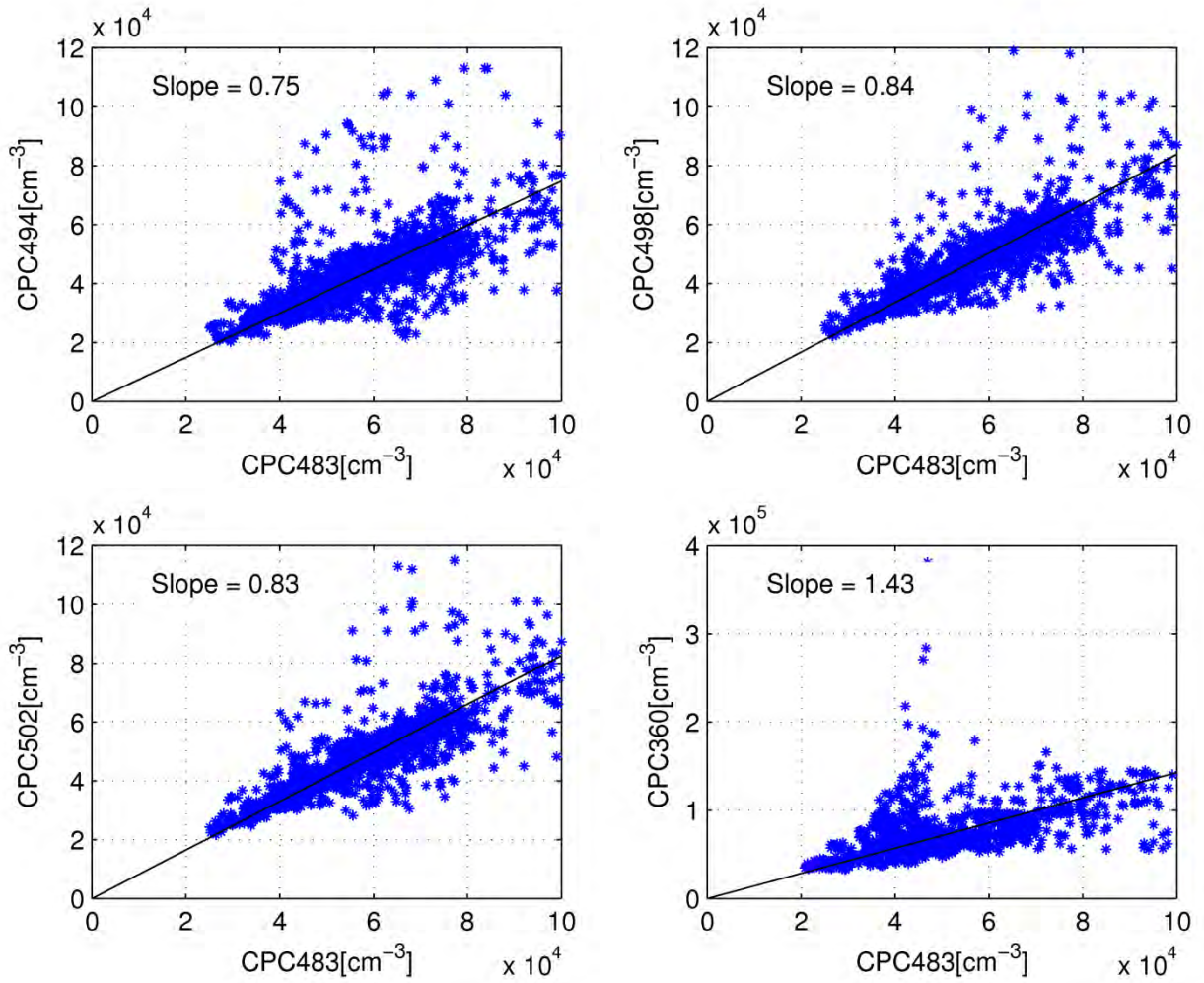
ID	Instrument	Location	Latitude	Longitude	Heading (° from north)	Height	Dates (month/day/year)
1	Sonic 0245	Building Region North	34.067162	-118.390488	50	4.14	5/19/14-7/1/14
3	Sonic 0984	Open Region South	34.06696	-118.3923	95	4.06	5/19/14-7/1/14
1	CPC 494	Building Region North	34.067162	-118.390488		1	5/30/14
2	CPC 483	Building Region South	34.066954	-118.390392		1	5/30/14
3	CPC 498	Open Region South	34.06696	-118.3923		1	5/30/14
4	CPC 502	Open Region North	34.067162	-118.392417		1	5/30/14
	Sonic 1055	Upwind near LAX	33.95494	-118.40472		3.15	5/19/14-7/1/14

**Calibration of Condensation Particle Counters.** On each day that measurements were made, prior to locating the TSI3022A condensation particle counters at field locations, the instruments were co-located at one location next to the street. The data collected during the co-location was used to derive inter-instrument calibration factors that were used to adjust the concentrations measured during the experiments.

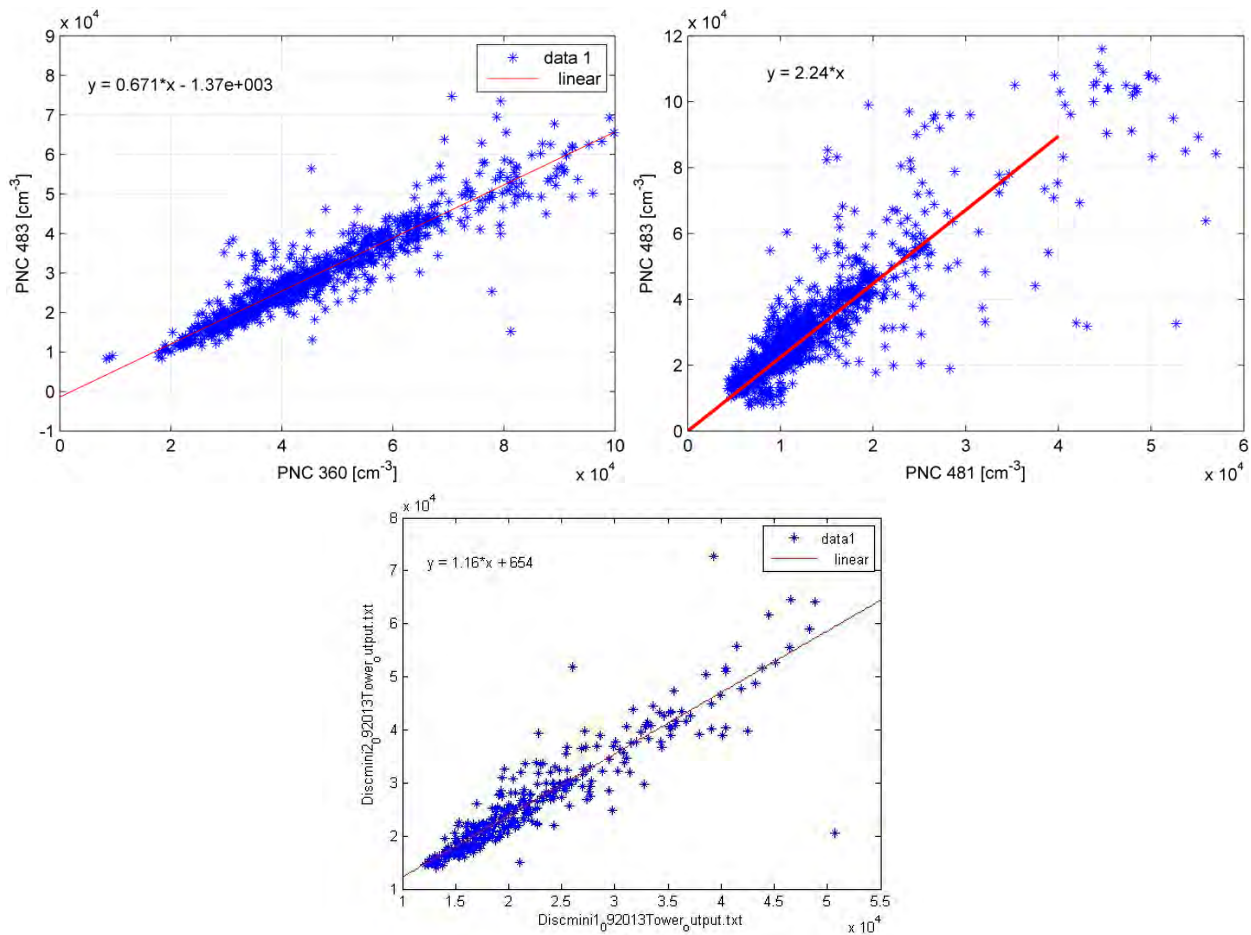
Figure B1 shows scatter plots comparing concentrations measured by three of the CPCs at the 8th St field site on May 7th, 2014 with one CPC used as the reference. Figure B2 shows a similar comparison for May 9th, 2014. Figure B3 shows scatter plots comparing concentrations measured by the four CPCs and one DiscMini at the Broadway field site on September 20, 2013. Figure B4 shows the calibration plots for the CPCs used at the Temple City field site on January 16, 2014. Calibration plots for the CPCs used at the Wilshire Blvd site are shown in Figure B5.



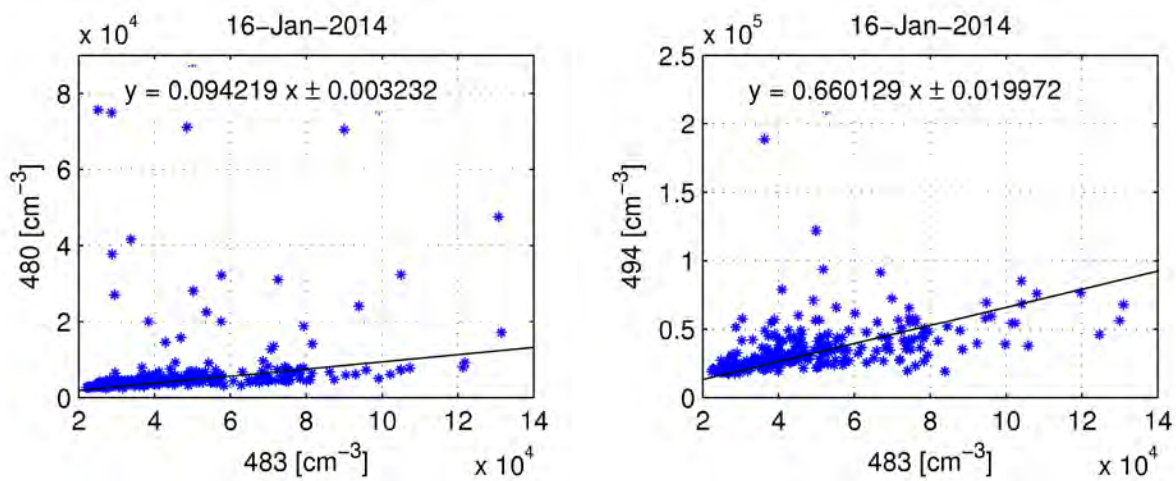
**Figure B1: Calibration derived from co-location of instruments next to 8th St on May 7<sup>th</sup>.**

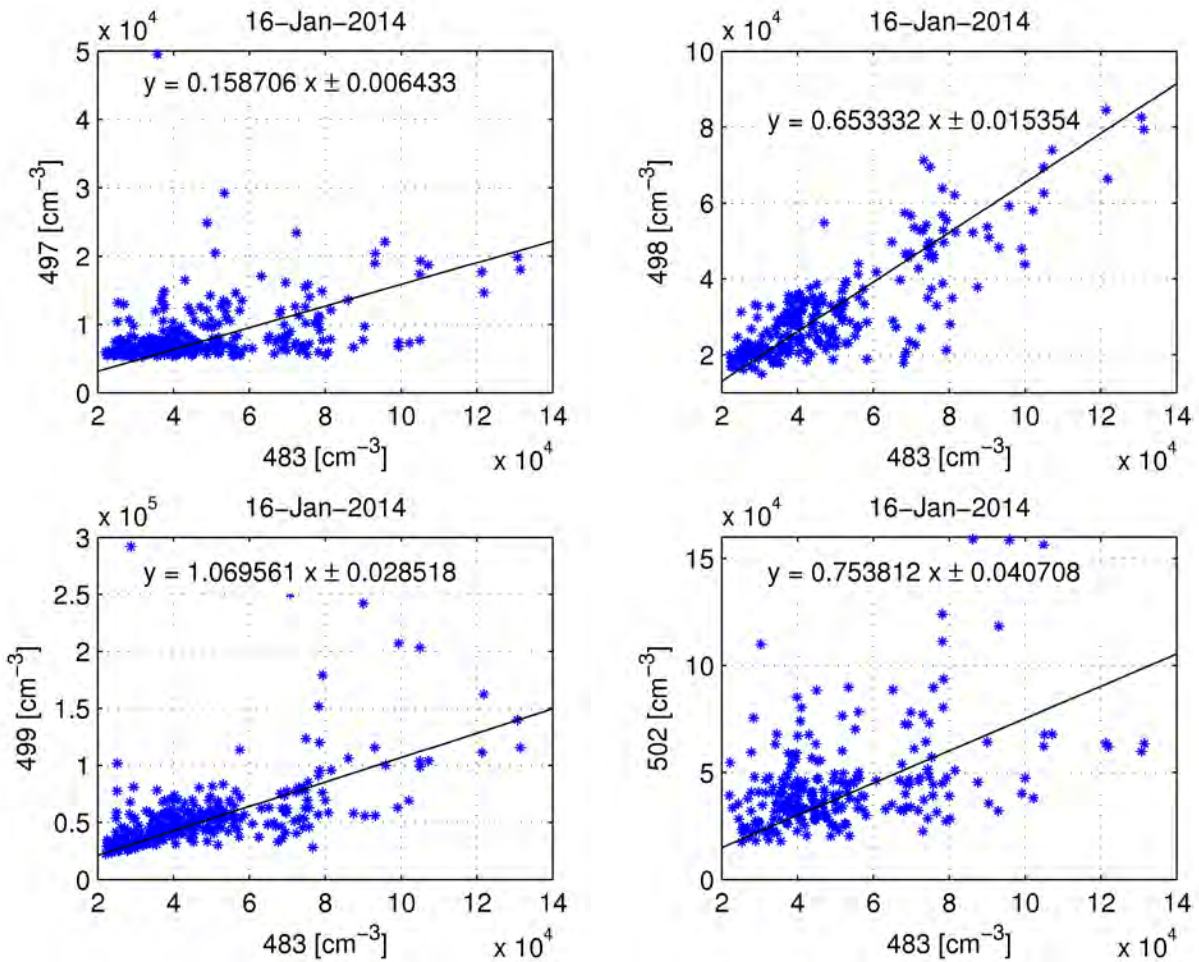


**Figure B2: Calibration derived from co-location of instruments next to 8th St on May 9<sup>th</sup>.**

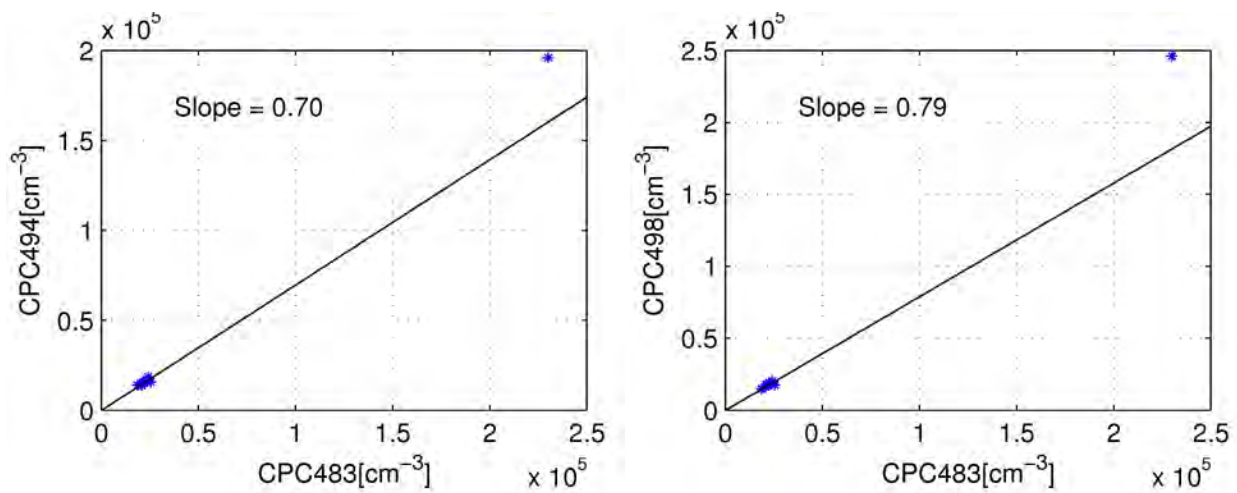


**Figure B3: Calibration derived from co-location of instruments next to Broadway on September 20th. The calibration factor between DiSCmini 2 and CPC 483 was 1.34 (not shown).**





**Figure B4: Calibration derived from co-location of instruments next to Temple City Blvd on January 16, 2014.**



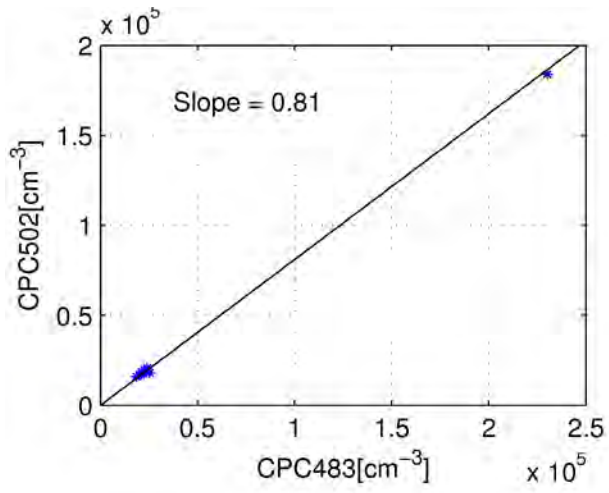


**Figure B5: Calibration derived from co-location of instruments next to Wilshire Blvd on May 30, 2014.**